UCRL-LR-125741

Inertial Fusion Energy: A Clearer View of the Environmental and Safety Perspectives

Jeffery F. Latkowski
(Ph.D Dissertation)

November 1996

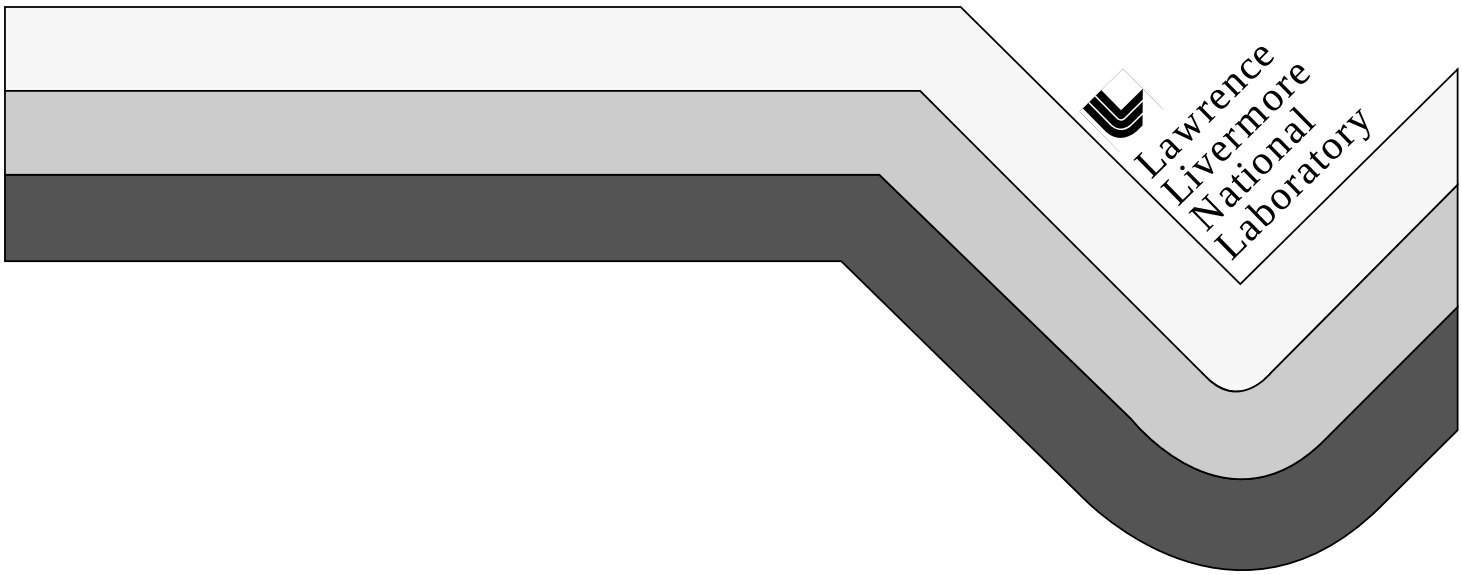

Work performed under the auspices of the U.S. Department of Energy by Lawrence Livermore National Laboratory under Contract W-7405-Eng-48.

UCRL-LR-125741
Distribution Category UC-700

Inertial Fusion Energy: A Clearer View of the Environmental and Safety Perspectives

Jeffery E. Latkowski
(Ph.D Dissertation)

November 1996

LAWRENCE LIVERMORE NATIONAL LABORATORY
University of California • Livermore, California • 94551

Inertial Fusion Energy:
A Clearer View of the
Environmental and Safety Perspectives

by

Jeffery Fredrick Latkowski

B.S. (University of Illinois at Urbana-Champaign) 1990

A dissertation submitted in partial satisfaction of the

requirements for the degree of

Doctor of Philosophy

in

Engineering–Nuclear Engineering

in the

GRADUATE DIVISION

of the

UNIVERSITY of CALIFORNIA, BERKELEY

Committee in charge:

Professor Jasmina L. Vujic, Chair
Professor T. Kenneth Fowler
Professor John P. Holdren

1996

The dissertation of Jeffery Fredrick Latkowski is approved:

Chair Date

Date

Date

University of California, Berkeley

1996

Abstract

Inertial Fusion Energy:
A Clearer View of the
Environmental and Safety Perspectives

by

Jeffery Fredrick Latkowski

Doctor of Philosophy in Nuclear Engineering

University of California, Berkeley

Professor Jasmina L. Vujic, Chair

Controlled thermonuclear fusion has the potential to provide future generations with virtually unlimited energy that is relatively clean, safe, and economic when compared with the alternatives that are available for long-term use. If fusion energy is to achieve its full potential for safety and environmental (S&E) advantages, the S&E characteristics of fusion power plant designs must be quantified and understood, and the resulting insights must be embodied in the ongoing process of development of fusion energy. As part of this task, the present work compares S&E characteristics of five inertial and two magnetic fusion power plant designs.

The inertial fusion energy (IFE) power plant designs include direct- and indirect-drive designs, thick-liquid and traditional first-wall protection schemes, and low-activation and traditional structural materials. IFE designs analyzed in the present work include Cascade, HYLIFE-II, Osiris, Prometheus-H, and SOMBRERO. The magnetic fusion energy (MFE) designs, silicon carbide and stainless steel tokamaks, likely represent the best and worst S&E characteristics, respectively, of MFE.

For each design, a set of radiological hazard indices has been calculated with a system of computer codes and data libraries assembled for this purpose. These indices quantify the radiological hazards associated with the operation of fusion power plants with respect to three classes of hazard: accidents, occupational exposures, and waste disposal. The three classes of hazard have been qualitatively integrated to rank the best and worst fusion power plant designs with respect to S&E characteristics. For example, because it poses the least hazard in each of the hazard categories, Osiris is the best overall IFE design. Prometheus-H was found to be the worst overall IFE design, due primarily to its liquid-lead first wall.

From these rankings, the specific designs, and other S&E trends, design features that result in S&E advantages have been identified. Specifically, the use of low-activation and high-damage materials and thick-liquid first-wall protection schemes produce designs with favorable S&E characteristics.

Additionally, key areas for future fusion research have been identified. Specific experiments needed include the investigation of elemental release rates (expanded to include many more materials) and the verification of sequential charged-particle reactions.

Finally, improvements to the calculational methodology are recommended to enable future comparative analyses to represent more accurately the radiological hazards presented by fusion power plants. The use of heat-transfer models and a chemical-reaction kinetics package would improve the reliability of release fraction calculations. The dose library should be expanded to ensure that all significant radionuclides have been included. Finally, future work must consider economic effects. Trade-offs among design features will be decided not by S&E characteristics alone, but also by cost-benefit analyses.

Table of contents

		Page
Table of contents		iii
List of figures		v
List of tables		vii
List of abbreviations and acronyms		viii
Acknowledgments		x
Chapter 1.	Introduction	1
	Background	
	Future energy demand	
	Future energy supply	
	Previous studies	
	Shortcomings of previous studies	
	Purpose, methodology, and strengths of this study	
	Organization of the present work	
Chapter 2.	Models	21
	Monte Carlo particle transport	
	Radiation damage	
	Matrix exponential method for activation	
	Radionuclide releases and health effects	
Chapter 3.	Indices of radiological hazard	63
	Accident hazards	
	Occupational and routine hazards	
	Waste-disposal hazards	
	Summary	

Chapter 4. The RADSAFE computer code system 80
Particle transport
Materials damage
Sequential charged-particle reactions
Radionuclide generation/depletion
Accident consequences
TARTREAD utility
Synthesis

Chapter 5. Effects of pulsed irradiation 99
Analytic relations for simple reaction chains
Calculations for complicated reaction chains
Routine and unplanned maintenance

Chapter 6. Effects of sequential charged-particle reactions 123

Chapter 7. Overview of fusion power plant designs 132
Inertial fusion energy designs
Magnetic fusion energy designs
Summary of designs

Chapter 8. Results 184
Accident hazards
Occupational and routine hazards
Waste-disposal hazards

Chapter 9. Synthesis 263
Summary of hazards by design
Integration of the classes of hazard
Recommended design features
Directions for future research
Improvements to the calculational methodology

Appendix A. Material compositions 292

List of figures

2.3.1	Isotopic daughters from a target nucleus	38
2.4.1	Elements assigned to release categories	42
4.7.1	RADSAFE computational system	94
5.1.1	SS and ESS approximations in MFE activation calculations	103
5.1.2	SS approximation as applied to an IFE power plant	104
5.1.3	ESS approximation as applied to an IFE power plant	105
5.2.1	Coolant activation with the ESS approximation	115
5.2.2	Target activation with the ESS approximation	117
6.1.1	Contact dose rate from pure Flibe with and without sequential charged-particle reactions	126
6.1.2	Contact dose rate from pure and impure Flibe	127
6.1.3	Impurities dominate the contact dose rate from Flibe	128
7.1.1	Major components of the reference IFE target design	136
7.1.2	Reference IFE capsule design	138
7.1.3	Artist's conception of the Cascade power plant	142
7.1.4	Artist's conception of the HYLIFE-II power plant	147
7.1.5	The HYLIFE-II first wall protected by a pocket of liquid Flibe from oscillating deflectors	148
7.1.6	Plan view of HYLIFE-II	150
7.1.7	Plan view of Osiris	154
7.1.8	Cross-sectional view of the Prometheus first wall	158
7.1.9	Schematic of Prometheus-H blanket module	159
7.1.10	Elevation view of the Prometheus-H reactor cavity	160
7.1.11	Cross section of the SOMBRERO chamber	165
7.1.12	Cross-sectional view of the SOMBRERO reactor building	166
8.1.1	Total activity, excluding tritium, for each power plant	191
8.1.2	Biological hazard potential in air for each design	193
8.1.3	Worst-case early doses to the bone marrow, lung, and gastrointestinal tract from each of the designs	200

8.1.4 Initial-case early doses to the bone marrow, lung, and gastrointestinal tract from each of the designs 201
8.1.5 Mechanistic-case early doses to the bone marrow, lung, and gastrointestinal tract from each of the designs 219
8.1.6 Chronic doses from each of the designs 221
8.1.7 Estimated number of early and cancer fatalities for the worst-case release fractions 226
8.1.8 Estimated number of early and cancer fatalities for the initial-case release fractions 228
8.1.9 Estimated number of early and cancer fatalities for the mechanistic-case release fractions 230
8.3.1 Life-cycle waste volume for each design 246
8.3.2 Biological hazard potential in water for each design 250
8.3.3 Total annualized intruder hazard potential for each design 256

List of tables

2.2.1	Maximum displacements-per-atom values for several materials	32
2.4.1	Parameters used with the Gaussian plume model	49
2.4.2	Acute-dose reduction factors	53
2.4.3	Parameters used with Weibull-type dose-response functions	55
3.2.1	Governmental regulations of public dose	74
5.2.1	Results of the irradiation of ^{56}Fe at 1 Hz for 1 hour	111
5.2.2	Results of the irradiation of ^{56}Fe at 1 Hz for 1 year	112
5.2.3	Results of the irradiation of natural iron at 5 Hz for 1 hour	114
5.2.4	Results of the irradiation of natural iron at 5 Hz for 1 year	115
7.1.1	Five IFE power plant designs	134
7.1.2	Estimate of total target factory tritium inventory	140
7.2.1	Basic design parameters for the PCA-Li/TOK design	171
7.2.2	Cylindrical approximation for the PCA-Li/TOK design	172
7.2.3	Basic design parameters for the SiC-He/TOK design	174
7.2.4	Cylindrical approximation for the SiC-He/TOK design	175
7.3.1	Summary of the main parameters for each design	178
8.1.1	Radioactive inventories for each design	187
8.1.2	Total critical threshold-dose release fractions by mobility category	195
8.1.3	Total chronic threshold-dose release fractions by mobility category	197
8.1.4.	Mobilization rates and mechanistic-case release fractions for the PCA-Li/TOK design	216
8.2.1	Contact dose rates from activated components	233
8.3.1	Waste-disposal indices from activated components	243

List of abbreviations and acronyms

AIHP	annualized intruder hazard potential
BCSS	Blanket Comparison and Selection Study
BHP	biological hazard potential
DDI	deep disposal limit
DOE	Department of Energy
DPA	displacements-per-atom
DT	deuterium–tritium
EAF	European Activation File
EPA	Environmental Protection Agency
ES&H	environment, safety, and health
ESECOM	Environment, Safety, and Economics Committee (Senior Committee on Environmental, Safety, and Economic Aspects of Magnetic Fusion Energy)
ESS	equivalent steady-state
FeCrV	iron–chromium–vanadium alloy
Flibe	fluorine–lithium–beryllium molten salt
GA	General Atomics
GI	gastrointestinal
GIMMs	grazing incidence metal mirrors
H3	tritium
HT	hydrogen–tritium
HTO	tritiated water
HYLIFE	High-Yield Lithium-Injection Fusion-Energy
IAEA	International Atomic Energy Agency
ICF	inertial confinement fusion
ICRP	International Commission on Radiological Protection
IFE	inertial fusion energy
ITER	International Thermonuclear Experimental Reactor
INEL	Idaho National Engineering Laboratory
LLI	lower large intestine
LLNL	Lawrence Livermore National Laboratory
LSA	level of safety assurance
MFE	magnetic fusion energy
MPD	maximum permissible dose
NIF	National Ignition Facility
NRC	Nuclear Regulatory Commission

PCA	primary candidate alloy
PKA	primary knock-on atoms
PRA	probabilistic risk assessment
R&D	research and development
RADSAFE	Radiological Safety Analysis of Fusion Environments
RCG	recommended concentration guide
S&E	safety and environmental
SAL	specific activity limit
SOMBRERO	Solid Moving Breeder Reactor
SS304	stainless steel type 304
SS	steady-state
TBR	tritium breeding ratio
TDRF	threshold-dose release fraction
WDR	waste-disposal rating

Acknowledgments

The full list of people who have had an impact upon this dissertation is too long to be given here. I wish to thank everyone who has helped me with gathering reports, assembling data, understanding physics, running computer codes, and improving grammar. In addition, there are a group of people who have had a special effect on this endeavor.

Ralph Moir has contributed to this work via many conversations regarding the HYLIFE-II design and IFE in general. Ralph's recent work on HYLIFE-II brought IFE to the point at which an analysis such as this was possible. His rapid response to my many questions ranging from details of the HYLIFE-II design to his thoughts on sequential charged-particle reactions and radionuclide release fractions have made the completion of this work easier.

Wayne Meier, formerly of W. J. Schafer Associates, has served a similar role for the Osiris and SOMBRERO designs. Wayne has tolerated my barrage of questions about many design details. When unable to answer my questions, he has rapidly put me in touch with those able to do so. Finally, Wayne read and commented upon virtually the entire text of this dissertation. Many thanks, Wayne.

Thanks to Robin Forrest of the United Kingdom Atomic Energy Agency for making both the European Activation File version 3.1 and the sequential charged-particle reactions codes and libraries available to me.

Many thanks to Wolfgang Raskob of Karlsruhe. Wolfgang generously offered to repeat some tritium dose calculations for the release parameters used in the present work. Without his help, the tritium results could not have included contributions from ingestion of contaminated food and water.

Steve Piet of the US ITER team and Kathy McCarthy of the Idaho National Engineering Laboratory have answered my many questions in the areas of radionuclide release fractions and oxidation-driven mobilization. Their suggestions and data have made me aware of the enormous challenges that must be overcome in order to estimate release fractions accurately.

Lawrence Greenwood of Pacific Northwest Laboratory provided me with the SPECTER code for the calculation of radiation damage. His explanations of the code's operation and use are appreciated.

Micah Lowenthal has been a constant source of knowledge throughout this work. It has been reassuring to be in contact with

another student, who is working on similar problems, at the same stage as I have been during a large portion of my thesis work. Micah has answered many questions pertaining to MFE, waste disposal, and ES&H issues as a whole. Thanks for your help and congratulations on your degree.

I thank Mike Tobin of LLNL for allowing me the time to complete this work while continuing with to work, half-time, in support of the National Ignition Facility. Over five years ago, Mike took me under his wing at Lawrence Livermore National Laboratory (LLNL). He accepted me as a member of his group and got me started using neutron transport and activation codes. It was also Mike who suggested that I consider the nuclear engineering department at Berkeley.

The Inertial Confinement Fusion Advanced Applications Chamber Dynamics (headed by Bill Hogan, John Woodworth, and Grant Logan during my dissertation work) and Target Area Technologies (headed by Tom Bernat) groups have generously provided my funding throughout this endeavor. I appreciate your confidence in me and your support of my work.

Many thanks to all of the members of the ESECOM committee. Without the existence of such a comparison for MFE, the likelihood of such an undertaking for IFE would be greatly diminished. I would also like to thank Steve Fetter. Not only did Steve help me with many suggestions and comments throughout this project, but he also laid much of the groundwork for the ESECOM study itself.

I would like to thank Grant Logan for his never ending support and enthusiasm for this project. The task surely would have been much more difficult without your valuable advice regarding my dissertation and other areas.

My orals and dissertation committees have provided continual support, comments, ideas, and suggestions. In particular, Ken Fowler has taken much time to answer my questions and make many suggestions that have improved this dissertation. John Holdren provided an interface between LLNL and Berkeley that has been quite valuable. As the chair of the ESECOM committee, he has been able to answer many questions and direct me to those that did much of the original work. His direction has ensured that my results are reasonably conservative yet still reasonable. The chair of my committee, Jasmina Vujic, has guided me through this entire

process. She recommended coursework and potential thesis topics and offered suggestions for handling the “crisis of the week.” Her assistance is much appreciated and was essential to the timely completion of this work.

Red Cullen provided me with the best Monte Carlo transport code that is currently available. Red often helped me by searching through my input files to find the errors that prevented my models from running properly. Without his help and his geometry plotting code, it would have been very difficult, if not impossible, to create detailed models of the various geometries. Red has also provided advice that helped me navigate the entire affair.

Javier Sanz has been absolutely essential to most facets of this work. Not only has Javier influenced every piece of this work -- from activation to sequential charged-particle reactions to accident consequences to radiological indices, but he has become my dear friend. His daily involvement in this dissertation made it possible. Grácias por todo Javier!

Without the support of my parents throughout my education, I may not have attended college let alone gone to graduate school. Although their love and guidance was the most important factor in

their support, the far-sighted purchase of a home computer many years ago surely played a major role in the development of my computer skills which have been absolutely essential to the completion of this work. I love you both.

If any single individual has made a defining contribution to this work, it is my wife, Gwen Loosmore. Gwen has had a major influence upon this entire work. She has listened to my problems and made concrete suggestions for their rapid solution. Whenever I would go astray or get down, she has been able to put me back on track. A wife with a technical mind has been a wonderful blessing. I love you, and I thank you for all of the help that you've given me during this adventure. I only hope that I can be as supportive of you as you have been of me.

1. Introduction

Controlled thermonuclear fusion has the potential to provide future generations with an energy source that is virtually unlimited and is relatively clean, safe, and economic when compared with the alternatives that are available for long-term use. If fusion's potential for environmental and safety advantages is to be fully realized, however, the environmental and safety characteristics of fusion power plant designs must be understood and quantified, and the resulting insights must be embodied in the ongoing process of development of fusion energy in commercializable forms. As part of that process, this dissertation quantifies the environmental and safety characteristics of inertial fusion energy (IFE). IFE, along with magnetic fusion energy (MFE), is one of the two principal approaches to fusion now being proposed by the U.S. Department of Energy (DOE).

1.1 Background

Fusion occurs when light nuclei, such as deuterium and tritium, are joined. The process can occur only under extreme temperatures that allow such nuclei to overcome the repulsive Coulomb forces

that keep them apart. The fusion of a single mole of deuterium with one of tritium (the easiest fusion reaction to produce in the laboratory) releases as much energy as the combustion of nearly 70 tons of bituminous coal. During normal operation of a fusion power plant, the fusion by-products would be nearly entirely contained; the combustion of the corresponding quantity of coal would release approximately 200 tons of CO_2 gas.

A 1000 MWe power plant would use 1 mole of deuterium-tritium (DT) fuel or 50 tons of coal every 10 minutes. Even if it were 30% efficient, a solar power plant would require a land area of more than 5 km^2 in order to provide the same power. Fusion power has clear advantages over coal and solar in resources used and by-products produced. Fusion power, if safe and economical, holds great promise for future societies.

Three different methods for confinement of a fusion plasma exist: gravitational, magnetic, and inertial. Gravitational confinement is used by the sun and all of the other stars in the universe. For obvious reasons, gravitationally confined fusion is not practical on a laboratory scale. Magnetic fusion has been researched for nearly four decades. Although magnetic fusion research has

progressed to the point at which energy break-even may soon be achieved in the laboratory, much more research will be required to reach the point of technological and economic feasibility.

IFE has not progressed as far as its magnetic fusion counterpart, due, at least in part, to historically smaller research budgets and classification issues which, until recently, precluded much international collaboration. There have been some milestones reached in the HALITE/CENTURION program; for example, energy from underground explosions at the Nevada Test Site was used to implode an inertial fusion capsule [1]. Such experiments put to rest fundamental questions about basic feasibility to achieve high gain [1]. Currently envisioned research projects, such as the National Ignition Facility (NIF), would bring inertial confinement fusion (ICF) beyond the point of energy break-even in the laboratory.

Despite fusion's potential to achieve a superior safety and environmental record, recent magnetic fusion energy (MFE) reports have shown that its full potential is not achieved automatically [2,3]. In addition to basic fusion research, safety studies must be performed in parallel. A high degree of safety (and a low degree of overall hazard) may be achieved only when intelligent design

decisions are made in areas such as materials selection and modes of operation. Where decisions cannot be made with today's level of knowledge, additional research is required.

Although past major studies have compared the environment, safety, and health (ES&H) characteristics of several MFE power plant designs, no comparably detailed work has been completed for IFE [2,3,4]. The main goal of this work is to compare several IFE power plant designs, on equal footing, and draw conclusions about their ES&H characteristics. Design trends which affect IFE's likelihood of achieving its full potential with respect to ES&H characteristics will be identified. A secondary goal of this work is to compare the IFE designs to two representative MFE designs. Such a comparison may reveal fundamental advantages of one technology over the other. Such advantages, if they become apparent, may serve to guide future research in fusion energy. Finally, this work seeks to identify high-leverage research areas: those which may result in the greatest benefit for a given amount of research.

1.2 Future energy demand

The great advances of the industrial and technological ages have been possible, in part, because of the availability of cheap fossil fuels [4]. Estimates of the global energy demand in the year 2030 range from about 10 TW•yr/yr, which actually represents a 25% decrease from the 1990 energy use, to more than 30 TW•yr/yr [2].

The World Energy Council estimates that the energy demand of developing countries will increase threefold by the year 2020. That of North America should increase by 13% [5]. In the developing countries, China and India are of particular concern. Even if these countries sustain their current annual rates of growth, their per-capita energy consumption would remain less than one-third of that of the United States (where demand is still growing). By 2010, developing countries should produce nearly one-half of the world's annual CO_2 emissions: both China and India plan to use their large coal reserves to support their growth [5]. China's current rate of growth, if sustained, will require the construction of a medium-sized power plant every week until the year 2000 and one every few days beyond 2000 [5].

Increased energy demand cannot be satisfied indefinitely with fossil fuels and other currently available energy resources. The effects of increased demand are exacerbated in developing countries in which modern pollution controls are not necessarily legislated or even available.

1.3 Future energy supply

No known energy source is totally safe or completely environmentally benign. The combustion of coal produces a large amount of CO_2 and its mining and transportation produce other environmental hazards [2]. Fission reactors produce large quantities of high-level radioactive waste for which there is currently no officially accepted method of disposal in the United States. Due to reactor accidents at Three-Mile Island and Chernobyl, fission reactors also have questionable safety records and suffer from a lack of public acceptance. Even wind power, which might appear to be totally environmentally benign, has environmental costs: during the past two years, nearly 8% of the western USA population of bald eagles have died in collisions with windmills in the Altamont Pass near San Francisco [4]. As sources of coal, natural gas, uranium, and

oil become depleted and favorable locations for hydroelectric and wind power become more scarce, environmental costs are likely to rise.

In the long-term, there appear to be only three options for sustainable energy sources: fission breeder reactors, solar energy, and energy from fusion [6]. Each of these potential sources has advantages, disadvantages, and economies. The composition of the mix of power plants used to meet future energy demand depends upon their relative safety, environmental effects, ease of development, and cost of electricity.

Fission breeder reactors could ultimately supply approximately 10^6 TW•yr of energy [2]. Unfortunately, the ultimate cost of electricity and the safety and environmental consequences of the widespread use of breeder reactors are uncertain. Additionally, the potential for proliferation of nuclear weapons resulting from global use of fission breeder reactors is not well understood.

Solar power has the potential to supply an immense amount of energy. About 88,000 TW•yr/yr of sunlight reaches the earth's surface [2]. Unfortunately, this energy is at a low concentration -- averaging 175 W/m^2 over the whole planet, all seasons, and night

and day -- and thus, it must be collected over a large area to be useful for large-scale electricity production [7]. Additionally, some approaches for the use of solar energy carry significant environmental costs [2].

Fusion energy, accomplished by either magnetic or inertial confinement schemes could provide about 10^8 TW•yr of energy, if limited by oceanic lithium used in the DT reaction [2]. While fusion energy has often been reported as “clean” in the popular press, its environmental effects would not be negligible. These effects, however, are likely to be significantly smaller than those of fission and fission breeder reactors and may be even smaller than those of large-scale solar technologies [2].

1.4 Previous studies

Nearly forty major conceptual IFE power plant designs have been published during the last 25 years [4]. Even more MFE designs have been published [2,3,8]. The ESECOM report sought to compare various MFE designs using a standardized set of assumptions and a single set of computer codes. Only thus can the characteristics of one design be compared to those of another in a meaningful way. Through the

use of a consistent methodology for analyzing safety, environmental, and economic characteristics, the ESECOM committee was able to make recommendations about the most promising directions for research and development (R&D) in MFE. The ESECOM committee identified key areas in which further research could “improve the prospects for achieving fusion’s full potential with respect to economics, environment, and safety” [2].

1.5 Shortcomings of previous studies

As mentioned above, the meaningful comparison of one design to another requires that both designs be evaluated with the same methods. To enable a complete comparison to occur, calculations should be performed with the same models and assumptions, the same data, and the same calculational tools (computer codes); and the same measurements should be made. Unfortunately, each design study tends to focus upon a different aspect of a design; thus, different measurements are made and presented. Additionally, no single set of validated nuclear data and computer codes is widely used in the fusion community. Finally, each design team brings a different set of assumptions about how a fusion power plant might

be operated and regarding the limitations and performance levels for various technologies and materials. Each of these factors tends to make comparisons of one design to another more difficult and less meaningful. Thus, this work compares several designs using a consistent set of assumptions, computer codes, and measurements.

Past IFE studies have been faced with additional obstacles in the form of classification. Until recently, many details of the ICF process were classified by the DOE; thus studies often were incomplete, used assumptions that were inaccurate, or did not consider all aspects of a design [8].

Past IFE studies have routinely performed neutronics calculations using one-dimensional approximations [9,10,11,12,13]. Such approximations tend to overestimate radionuclide inventories, as they underestimate effective shielding thicknesses and do not accurately account for geometric effects.

A recent study sponsored by the International Atomic Energy Agency (IAEA) sought to identify neutron activation codes that are able to read standard cross-section libraries, predict accurately the quantity of radionuclides produced in multi-step pathways, calculate accurately light nuclide production, and treat isomeric

states [14]. Other criteria which were not applied but were identified for their potential future importance include the abilities to utilize information about uncertainty, to treat actinide data, and to calculate the effects of sequential charged-particle reactions [14]. The IAEA study found that only the FISPACT and ACAB codes were “suitable and satisfactory” for detailed fusion calculations. Four other codes performed poorly in at least one of the areas, and five codes were found to be inadequate [14]. Additionally, the first IAEA benchmark study showed wide discrepancies among results when participants used their own transport codes and nuclear data [15]. It is likely that similar differences in realism exist among particle-transport, materials-damage, and accident-consequences codes.

1.6 Purpose, methodology, and strengths of this study

In order to facilitate comparisons of one IFE design to another, this study uses a consistent set of assumptions and a single set of computer codes and data libraries to calculate a large set of hazard indices for each design. The present work seeks to identify key areas

of research that may improve the prospects for achieving inertial fusion's full potential with respect to environment and safety.

This study assumes that each power plant is operated for thirty years at full capacity. Preliminary calculations were performed to establish the appropriateness of steady-state approximations to the actual, pulsed irradiation. Rather than assuming that each first-wall material can withstand the same energy flux during its lifetime, the present work uses material-damage calculations and estimated material-damage limits. Two-dimensional neutron-transport models have been created for each of the IFE power plant designs to account for geometric features and liabilities that may influence a design's overall hazard.

In order to allow comparisons to be made between designs on many different levels, this study calculates a large number of radiological indices. These indices are divided into three categories of hazard: accident, occupational/routine releases, and waste disposal. Accident indices include total activity, biological hazard potential in air, threshold-dose release fractions, early and chronic doses, and early and cancer fatalities. Occupational/routine exposure indices include contact dose rates, routine population

doses, and cancer fatalities from routine operation. Finally, waste-disposal indices include life-cycle waste volumes, biological hazard potential in water, waste-disposal rating/intruder dose, deep disposal index, and annualized intruder hazard potential. This assortment of indices will enable limited comparison to past studies.

An assortment of state-of-the-art computer codes has been assembled as a basis for this work. Calculations are performed with a well-established Monte Carlo transport code, an improved version of one of the activation codes deemed acceptable by the IAEA, and an extensive nuclear data library. Improvements to the activation code allow sequential charged-particle reactions to be considered for the first time in the analysis of any IFE power plant design. The activation code has also been modified to allow use of nuclear cross-section uncertainty data, although this refinement was not incorporated into the comparisons of IFE designs.

Rather than assuming that each material can withstand the same energy fluxes, calculations of material-damage rates have been performed. Organ-dependent early and chronic whole-body doses have been calculated using the best accident-consequences code

currently available. The chronic doses include contributions from ingestion of contaminated food and water to allow a full assessment of the consequences of an accident and of routine releases of tritium.

Although this study cannot address all issues or incorporate all facets of the radiological hazards posed by fusion power plants, it does advance the state-of-the-art in the field of radiological hazard estimation and allows more meaningful comparisons to be made than those previously available.

1.7 Organization of the present work

The following sections describe the tools used to make the design comparisons, the measures of comparison, and the assumptions that have been made. Chapter 2 of this report describes the models that have been used, ranging from Monte Carlo particle transport to the Gaussian plume model.

Chapter 3 explains each of the indices that have been calculated in the present work. The indices are divided into three categories of hazard: accidents, occupational and routine exposures, and waste

disposal. The calculation of each index is explained and comments about their relative usefulness and meaningfulness are made.

Chapter 4 gives a detailed explanation of each of the computer codes and data libraries that have been used in the present work.

Chapters 5 details the effects of pulsed irradiation upon activation calculations. Several different timescales are analyzed and recommendations for the approximation of pulsed irradiation conditions are made.

Chapter 6 demonstrates the potential importance of sequential charged-particle reactions upon radionuclide inventories and radiological hazard indices. Recommendations for the inclusion of sequential charged-particles are made.

Chapter 7 gives an overview of each of the inertial and magnetic fusion power plant designs that have been analyzed in the present work. In addition, the reference inertial fusion target and capsule design is presented.

Chapter 8 presents the results of the analyses for each design. The results are presented according to radiological hazard indices in the three hazard categories.

Chapter 9 summarizes the findings presented in Chapter 8, by design, and integrates the findings by hazard category. The designs are ranked qualitatively, advantageous design features are recommended, and directions for future fusion energy research are identified. Finally, improvements to the calculational methodology, which could increase the usefulness of future studies of this type, are suggested.

References for Chapter 1

1. “Inertial Fusion Fact Sheet,” U. S. Department of Energy, (September 30, 1988).
2. J. P. Holdren, D. H. Berwald, R. J. Budnitz, J. G. Crocker, J. G. Delene, R. D. Endicott, M. S. Kazimi, R. A. Krakowski, B. G. Logan, and K. R. Schultz, “Report of the Senior Committee on Environmental, Safety, and Economic Aspects of Magnetic Fusion Energy,” Lawrence Livermore National Laboratory, UCRL-53766, (September 1989).
3. A. P. Kinzig, J. P. Holdren, and P. J. Hibbard, “Safety and Environmental Comparisons of Stainless Steel with Alternative Structural Materials for Fusion Reactors,” *Fusion Technology*, **26**, 79-104, (August 1994).
4. W. J. Hogan, ed., *Energy from Inertial Fusion*, Vienna, Austria: International Atomic Energy Agency, (1995).
5. “Power to the People,” *The Economist*, (June 1994).
6. J. P. Holdren and P. Herrera, *Energy*, San Francisco: The Sierra Club, 101, (1971).
7. J. J. Lienhard, *A Heat Transfer Textbook*, Englewood Cliffs, New Jersey: Prentice-Hall, Inc., 506, (1987).

8. S. A. Fetter, “Radiological Hazards of Fusion Reactors: Models and Comparisons,” Doctoral Dissertation, University of California, Berkeley, Energy and Resources, (May 1985).
9. W. R. Meier, R. L. Bieri, M. J. Monsler, C. D. Hendricks, P. Laybourne, K. R. Shillito, S. K. Ghose, L. M. Goldman, K. D. Auclair, C. Y. Pang, R. F. Bourque, L. D. Stewart, E. E. Bowles, E. L. Hubbard, C. W. von Rosenberg, Jr., M. W. McGeoch, I. N. Sviatoslavsky, R. R. Peterson, M. E. Sawan, H. Y. Khater, L. J. Wittenberg, G. L. Kulcinski, G. A. Moses, E. A. Mogahed, J. J. MacFarlane, S. Rutledge, S. Humphries, Jr., and E. T. Cheng, “Osiris and SOMBRERO Inertial Confinement Fusion Power Plant Designs,” DOE/ER/54100-1, WJSA-92-01, W. J. Schafer Associates, Inc., Livermore, CA, (March 1992).
10. J. A. Blink, W. J. Hogan, J. Hovingh, W. R. Meier, and J. H. Pitts, “The High-Yield Lithium-Injection Fusion Energy (HYLIFE-I) Reactor,” Lawrence Livermore National Laboratory, UCID-53559, (1985).
11. R. W. Moir, “HYLIFE-II Inertial Fusion Energy Power Plant Design,” *Inertial Confinement Fusion: 1992 Annual Report*, Lawrence

Livermore National Laboratory, UCRL-LR-105820-92, 139, (June 1993).

12. R. W. Moir, R. L. Bieri, X. M. Chen, T. J. Dolan, M. A. Hoffman, P. A. House, R. L. Leber, J. D. Lee, Y. T. Lee, J. C. Liu,. R. Longhurst, W. R. Meier, P. F. Peterson, R. W. Petzoldt, V. E. Schrock, M. T. Tobin, and W. H. Williams, “HYLIFE-II: A Molten-Salt Inertial Fusion Energy Power Plant Design – Final Report,” *Fusion Technology*, **25**, (January 1994).
13. L. M. Waganer, D. E. Driemeyer, V. D. Lee, R. L. Calkins, H. B. Wald, F. R. Williams, R. S. Matsugu, O. K. Kveton, K. Kalyanam, S. K. Sood, S. L. Ostrow, S. F. Marschke, P. J. Estreich, M. J. Parnes, D. J. Drake, J. W. F. Millard, J. Ballantyne, T. Haines, D. Perrot, C. English, C. Holloway, A. Turner, G. J. Linford, S. W. Fornaca, A. W. Maschke, M. A. Abdou, N. M. Ghoniem, M. S. Tillack, J. E. Eggleston, F. Issacci, A. Y. Ying, A. El-Azab, A. R. Raffray, M. Z. Youssef, Z. R. Gorbis, S. Sharafat, L. Zhang, and I. Jun, “Inertial Fusion Energy Reactor Design Studies: Prometheus-L and Prometheus-H,” McDonnell-Douglas Aerospace, MDC 92E0008, DOE/ER-54101, (March 1992).

14. E. T. Cheng, R. A. Forrest, and A. Pashchenko, “Report on the Second International Activation Calculation Benchmark Comparison Study,” TSI Research Report, TSIR-21, (November 1993).
15. E. T. Cheng, K. M. Feng, R. Forrest, J. H. Huang, J. Kopecky, F. M. Mann, A. V. Kashirskij, D. V. Markovskij, O. Schipakin, M. Sawan, and Y. Seki, “International Fusion Activation Calculation Comparison Study,” TSI Research Report, TSIR-12, (January 1991).

2. Models

Each of the models used in this work is absolutely essential to the final product. Transport models are used to determine particle spectra in materials of interest; radiation-damage models are used to estimate a material's lifetime under irradiation; matrix exponential methods are used to calculate nuclide inventories during and after irradiation; plume models are used to predict radionuclide concentrations on the ground and in the air during and after the accidental release of radiation; and dose-effect relationships are used to estimate the effects of a given release of radioactivity. A detailed description of the operation and application of these models is given below.

2.1 Monte Carlo particle transport

The Monte Carlo method is used extensively throughout this work to calculate the energy-dependent neutron and/or photon pathlengths within certain materials in the various power plant designs. The pathlengths as a function of particle energy are used, in turn, to calculate the energy-dependent particle fluxes at these locations.

The fluxes are calculated from the pathlengths according to the relation:

$$\phi(E) = \frac{L(E) \times S}{V} \qquad (2.1.1)$$

where $\phi(E)$ is the energy-dependent particle flux, L(E) is the energy-dependent particle pathlength, S is the particle source term, and V is the volume of the material zone.

The Monte Carlo method provides statistical estimates for quantities of interest when applied to deterministic or statistical problems [1]. Monte Carlo particle transport is accomplished by simulating the life histories of individual particles. Specifically, a statistically significant number of particles are followed throughout their life history until their death. At its death, each of the particles is classified into one of several terminal categories (e.g., escaped, absorbed, and scattered) [2]. The Monte Carlo method may be applied to particle transport as long as the probabilities for particle characteristics and events in the life history of a particle are well-characterized [2]. Relevant probabilities are applied to such issues as: the initial kinetic energy that a particle has at birth;

the angle at which a particle is scattered in a collision; and the type of collision that a particle undergoes. Such a probabilistic description enables the prediction of particle behavior in all situations during its life history.

The Monte Carlo method, especially when applied to particle transport, breaks down naturally into a series of blocks or programming subroutines [2]. These blocks include source parameters, distance to boundary or collision, type of collision, parameters after collision, and classification of termination.

Source parameters include information such as the initial energy, direction, and spatial distribution. Each source parameter may be described by discrete or continuous distributions.

The physical concept required for evaluation of the distance to a collision is the mean free path [2]. The mean free path is a function of the particle type, its energy, and the medium. If the distance to an event is greater than the distance to the boundary in the current direction and zone, then the particle will escape from the current zone (and possibly from the entire problem). If not, then the particle will undergo a collision.

The type of collision is a function of the relevant cross sections. As for the mean free path, the cross sections are functions of the particle, its energy, and the medium. Possible collisions include elastic and inelastic scattering and capture. Some capture collisions result in the birth of one or more new particles, each of which must be followed until its own termination.

Once the type of collision is determined, the post-collision particle parameters, if any, must be determined. For example, if the collision results in a scattering event, for example, a scattering angle must be sampled. The scattering angle uniquely determines the energy and direction of a scattered particle.

The final subroutine needed for Monte Carlo calculations is the termination subroutine, in which particles are categorized according to their ultimate demise. Example terminal categories include escape and absorption. Escaping particles penetrate the outer boundary of the geometry being considered. In escape, a particle's energy, point of escape, and final direction may be of interest. Relevant information for particle absorption includes the type of absorption, the position of absorption, the energy absorbed, and the particles that are emitted following the absorption. All particles

must be followed until they escape from the problem, are absorbed, or are eliminated for other reasons (e.g., their energies fall below a predetermined level).

Each of the blocks requires both information about the probabilities which constrain the possible outcomes and random numbers. The latter will be addressed first.

All Monte Carlo calculations require the use of random numbers which are denoted here with the symbol ξ [3]. In this context, random numbers are real numbers that are uniformly distributed on the interval $0 \leq \xi \leq 1$. Random numbers are used so extensively in the Monte Carlo method that their generation has become a topic in its own right [4,5,6]. Suitable random numbers must be independent of one another, yet they should be repeatable in order to allow calculations to be repeatable as well [3]. These and other requirements are not easily met. The reader is directed to references 4-6 for more information on the generation of random number sequences.

The probabilities that determine possible events may be described in terms of a probability density function, p(x). Suppose that E_1, ..., E_n are n independent, mutually exclusive events with

probabilities p_1, ..., p_n, respectively, where $p_1 + ... + p_n = 1$. If the random number ξ, $(0 \leq \xi \leq 1)$, is such that:

$$p_1+\cdots+p_{i-1} \leq \xi < p_1+\cdots+p_i \qquad (2.1.2)$$

then ξ determines the event E_i [2]. Equation 2.1.3 gives the relation for a discrete probability density function.

$$p(x) = p_i \qquad \text{where } i-1 \leq x < i \text{ for } i=1,2,...,n \qquad (2.1.3)$$

The cumulative probability distribution function for the inequality $x' \leq x$ for $x=i$, $i=1,2,...,n$ may be written as $P(x)$, where:

$$\xi = P(x) = \int_0^x p(t)\, dt = \sum_{k < (x)}^{n} p_k \qquad (2.1.4)$$

Equation 2.1.4 uniquely determines x as a function of ξ in such a way that x falls on the interval $i-1 \leq x < i$ with frequency p_i, thereby determining the event E_i [3].

For a continuous probability density function, $p(x)$, $a \leq x < b$, integration of Equation 2.1.4 over the interval [a,b) yields the

cumulative probability distribution function, P(x), where x falls with frequency p(x)•dx in the interval (x, x+dx) [3].

Once the cumulative probability distribution function has been determined, random numbers may be generated and used to solve for specific parameters. Such parameters include the particle energy, direction, and distance to collision. As an example, the calculation of the distance to a collision is shown below.

The probability that a particle of energy E has not yet had a collision after travelling through a distance s in a given medium is simply:

$$e^{-\Sigma_t s} \qquad (2.1.5)$$

where Σ_t is the total macroscopic cross section of the particle at its current energy in the current medium. The total macroscopic cross section may be interpreted as the probability of a collision per unit length [3]. Thus, the probability of a particle undergoing a collision during the distance ds is simply $\Sigma_t ds$. The overall probability of a particle having its first collision between s and (s+ds) is given by the probability density function:

$$p(s)ds = \Sigma_t e^{-\Sigma_t s} ds \qquad (2.1.6)$$

Integration of Equation 2.1.6 from 0 to s yields the cumulative probability distribution function:

$$P(s) = 1 - e^{-\Sigma_t s} \qquad (2.1.7)$$

Equation 2.1.7 is used by setting the right-hand side equal to the random number ξ and solving for the distance, s:

$$s = -\frac{1}{\Sigma_t} ln(1-\xi) \qquad (2.1.8)$$

Since the distribution of $ln(\xi)$ is the same as that of $ln(1-\xi)$, we may simplify Equation 2.1.8 to obtain:

$$s = -\frac{1}{\Sigma_t} ln(\xi) \qquad (2.1.9)$$

Thus, a particle of a given total macroscopic cross section will travel a distance s before undergoing a collision. Once the particle collides, other probability density functions are used to determine

the type of collision, the energy lost in the collision, and the particle direction after the collision. Using the above methods, particles are followed until they are absorbed or they escape from the problem.

The sampling method used in the above example is known as direct inversion. Direct inversion is possible only when the cumulative probability distribution function is in a simple form that can be solved analytically. Complicated cumulative probability distribution functions are often sampled using the rejection method. The rejection method is analogous to determination of the area under a given curve by counting squares -- coordinates are chosen at random, and they are accepted if they are located under the curve. Coordinates that are above the curve are rejected. Direct inversion is almost always more efficient and faster than the rejection method.

Calculations in which individual particles are followed until their termination are referred to as analog Monte Carlo calculations. Analog Monte Carlo calculations are used extensively in the present work to determine energy-dependent particle pathlengths and

particle fluxes. The particle fluxes are used in subsequent activation calculations.

2.2 Radiation damage

Exposure to radiation can change the properties of most materials. These changes arise primarily from the displacement of atoms from with the material's lattice structure [7]. Previous studies such as ESECOM have assumed that a material's maximum lifetime is only a function of the first-wall neutron loading [8]. Since ESECOM analyzed only MFE designs, which all would have nearly the same neutron spectrum, this approximation was reasonable. Among IFE designs, the neutron spectrum at the first wall and within the blanket may be quite different from one design to another. Thus, the present work uses radiation-damage calculations to determine the maximum lifetime of structural materials.

Radiation damage results from the collision of neutrons with the atoms of a given material. These collisions produce primary knock-on atoms (PKA) which move through the material and cause secondary atom displacements. Neutron reactions may result in the production of secondary particles, which themselves may act as PKA

and cause additional displacements [7]. Radiation damage is often expressed in units of displacements–per–atom (DPA). DPA calculations remove the spectral dependence that must be considered when examining the neutron wall loading or fluence. The IAEA has recommended that DPA be accepted as the preferred method to characterize neutron irradiations [9].

The probability of displacing an atom from its lattice site depends upon several factors: the neutron energy, the neutron cross sections, the energy of the recoil atom, and the probability of inducing secondary recoils. The overall probability of creating a displacement may be expressed as:

$$\sigma_{dis}(E) = \sum_{i} \sigma_i(E) \times \int_{T_1}^{T_2} K(E,T)_i \times \nu(T)\, dT \qquad (2.2.1)$$

where E is the energy of the incident neutron, T is the energy of the recoil nucleus, $\sigma_i(E)$ is the cross section for the i^{th} channel at energy E, $K(E,T)_i$ is the neutron–atom energy transfer kernel for the i^{th} channel, and $\nu(T)$ is the secondary displacement function [7]. The energy transfer kernel gives the probability that a neutron of a given energy will produce a recoil atom of a given energy. The secondary

displacement function gives the quantity of secondary atomic displacements that occur due to stopping of the PKA [7].

Maximum allowable DPA values for a given material are not well-characterized. Nevertheless, recommended values do exist for some structural materials of interest to this study. Table 2.2.1 gives recommended maximum DPA values for several materials that are included in the designs analyzed in the present work. The lifetime of a given material, and thus, the irradiation duration used in activation calculations, is the shorter of the power plant lifetime and the DPA limit divided by the annual DPA rate. The limits shown in Table 2.2.1 are values based upon knowledge of existing materials and reasonable extrapolation of existing materials to ones that might be available for use in a power plant of the future.

Table 2.2.1. Maximum DPA values have been estimated for some materials of interest.

Material	Damage limit (DPA)	Source(s)
PCA steel (austenitic)	100 (500 °C)	BCSS[10]
HT-9 steel (ferritic)	200, 150	BCSS, IAEA[11]
V-15Cr-5Ti	> 200	BCSS
SiC	20	Cascade report[12]
C composite	75	Osiris/SOMBRERO report[13]

2.3 Matrix exponential method for activation

Nuclide inventories are determined from activation calculations. Activation calculations involve the solution of a system of first-order ordinary homogeneous or inhomogeneous differential equations [14]. Specifically, the rate at which a nuclide is generated or destroyed by nuclear transmutation may be written as:

$$\frac{dX_i}{dt} = \sum_{j=1}^{N} l_{ij}\lambda_j X_j + \phi \sum_{k=1}^{N} f_{ik}\sigma_k X_k - (\lambda_i + \phi\sigma_i + r_i)X_i + F_i, \quad i=1,...,N \qquad (2.3.1)$$

where:

- X_i = atom density of nuclide i;
- N = number of nuclides;
- l_{ij} = fraction of radioactive disintegration by other nuclides that leads to formation of species i;
- λ_i = radioactive decay constant;
- ϕ = spatially- and energy-averaged neutron flux;
- f_{ik} = fraction of neutron absorption by other nuclides that leads to formation of species i;
- σ_k = spectrum-averaged neutron absorption cross section of nuclide k;
- r_i = continuous removal rate of nuclide i from the system; and
- F_i = continuous feed rate of nuclide i.

The system of N inhomogeneous differential equations described by Equation 2.3.1 may be solved to yield quantities of each nuclide

present at the end of each timestep [14]. Neglecting the continuous removal and feed rates and noting that the neutron flux varies only slowly with time (actually with the composition, which varies slowly with time), the system may be treated as a set of linear simultaneous first-order ordinary differential equations [15]. This set has constant coefficients and may be written in matrix form as:

$$\dot{\mathbf{X}} = \mathbf{A}\mathbf{X} \qquad (2.3.2)$$

where:

- $\dot{\mathbf{X}}$ = time derivative of the nuclide concentrations (a column vector);
- $\mathbf{A}$ = transition matrix containing the rate coefficients for radioactive decay and neutron capture (an N $\times$ N matrix filled with mostly zeros); and
- $\mathbf{X}$ = nuclide concentrations (a column vector).

Equation 2.3.2 has the known solution:

$$\mathbf{X}(t) = e^{\mathbf{A}t}\mathbf{X}(0) \qquad (2.3.3)$$

where:

- $\mathbf{X}(t)$ = concentration of each nuclide at time t;
- $\mathbf{X}(0)$ = vector of initial nuclide concentrations; and
- t = time at end of timestep.

The function $e^{\mathbf{A}t}$, the matrix exponential function, may be written as a truncated series with enough terms to be sufficiently accurate. This series is written as:

$$e^{\mathbf{A}t} = \mathbf{I} + \mathbf{A}t + \frac{(\mathbf{A}t)^2}{2!} + \ldots = \sum_{m=0}^{\infty} \frac{(\mathbf{A}t)^m}{m!} \qquad (2.3.4)$$

where $\mathbf{I}$ is the identity matrix [15]. Rather than store the entire matrix (most of which is filled with zeros), an expression for a single nuclide in Equation 2.3.3 may be derived:

$$X_i(t) = \sum_{n=0}^{\infty} c_i^n \qquad (2.3.5)$$

where c_i^n is generated through the use of a recursion relation:

$$c_i^0 = X_i(0), \qquad (2.3.6)$$

$$c_i^{n+1} = \frac{t}{n+1} \sum_{j=1}^{N} a_{ij} c_j^n \qquad (2.3.7)$$

where a_{ij} is an element in the transition matrix that gives the rate constant for the formation of nuclide i from nuclide j. Use of this

recursion relation makes solution of Equation 2.3.2 possible and requires the storage of only a single vector (c^n) in addition to the current solution [15].

Solution of Equations 2.3.1 and 2.3.2 in this manner is known as the matrix exponential method. This method has been used and benchmarked extensively in both fission and fusion neutronics calculations [14,15,16,17]. All activation calculations performed in this work rely upon the matrix exponential method.

2.3.1 Neutron activation calculations

Traditionally, only neutron reactions have been considered in MFE and IFE power plant studies [8,10,12,13,17,18,19]. Activation calculations use the time-dependent nuclide concentrations, calculated with the matrix exponential or some other suitable method, to determine other quantities of interest such as radionuclide activities and dose rates.

The present work considers twenty different neutron reactions [20]. These reactions include: (n,γ), (n,2n), (n,3n), (n,4n), (n,p), (n,d), (n,n'p), (n,t), (n,n'd), (n,2np), (n,n't), (n,2p), (n,^{3}He), (n,pd), (n,α), (n,n'^{3}He), (n,n'α), (n,2nα), (n,2α), and (n,n'2α). Although all neutron

activation calculations performed for the present work allow each of the above reactions, not all reactions on all target nuclides are energetically possible in a DT fusion spectrum. Each of the neutron reactions may proceed from a target nuclide that is in the ground, first, or second isomeric state and may result in a product that is in the ground, first, or second isomeric state [20].

Radionuclide decay may proceed from ground, first, and second isomeric states and may result in nuclides that are in the ground and first isomeric states. Decay modes that are considered in the present work include β^-, β^+, electron capture, and neutron and alpha emission [20].

2.3.2 Sequential charged-particle activation calculations

The concept of sequential charged-particle reactions ((x,n) reactions) was first introduced by Cierjacks and Hino [21]. These “reactions” consist of a two-step process. In the first step, a neutron interacts with an atom, and a charged particle is created. In the second step, the charged particle reacts with another atom. Often, the nuclide that is created in the second step may be produced only via complicated reaction/decay chains if only neutron reactions

are allowed. Figure 2.3.1 highlights the additional daughter radionuclides which may be produced directly when (x,n) reactions are considered.

Figure 2.3.1. Isotopic daughters that require multi-step neutron reaction and decay chains may be created directly in (x,n) reactions (shaded).

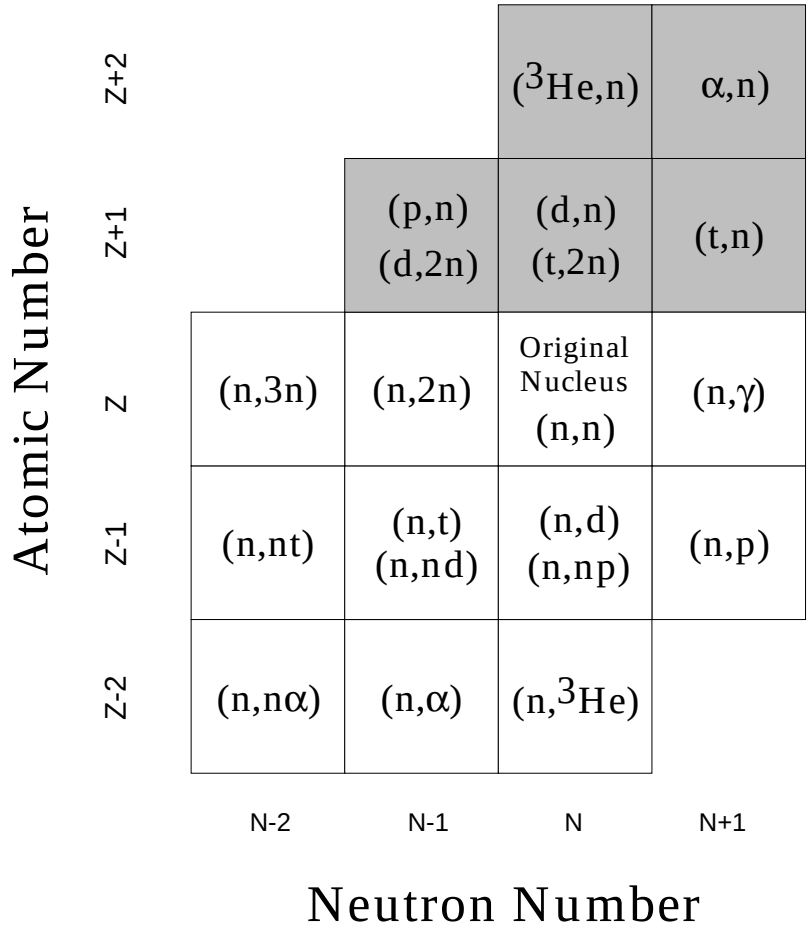

The first step of the (x,n) reaction process may be written as A(n,x)B. The second step may be written as C(x,n)D where C may or

may not be the same as A (charged particles may be created by one isotope in a material and then react with another isotope). The number of atoms of isotope D that are created during irradiation is given by Equation 2.3.8 [22].

$$N_D(t) = t_{eff} \sum_{A} \sum_{i=1}^{175} \phi_n(E_{n_i}) \sigma_{n,x}(E_{n_i}) N_A \Delta E_{n_i} \times \sum_{j=1}^{24} f_{n,x}(E_{n_i}, E_{x_j}) \Delta E_{x_j} \sum_{k=j}^{1} \sigma_{x,D}(E_{x_k}) N_C \Delta R_x(\Delta E_{x_k}) \quad (2.3.8)$$

where:

$N_D(t)$	=	number of atoms of nuclide D (cm^{-3});
t_{eff}	=	effective irradiation time;
$\phi_n(E_{n_i})$	=	neutron flux in the i^{th} energy group ($cm^{-2}s^{-1}MeV^{-1}$);
ΔE_n	=	neutron energy lethargy bin (175 bins are considered);
$\sigma_{n,x}(E_{n_i})$	=	cross section for the production of charged particle x in the i^{th} neutron energy group (cm^2);
N_A	=	number of atoms of target nuclide A (cm^{-3});
$f_{n,x}(E_{n_i}, E_{x_j})$	=	normalized charged-particle spectrum in uniform energy steps of ΔE_{x_k} = 1 MeV; refers to the i^{th} neutron energy group and charged-particle energy of E_{x_j} = 0.5, 1.5, ..., 23.5 MeV (24 groups);
$\sigma_{x,D}(E_{x_k})$	=	cross section for production of nucleus D via the charged-particle reaction C(x,n)D; and
$\Delta R_x(\Delta E_{x_k})$	=	differential thickness of the material that corresponds to 1 MeV energy losses for charged particles of energy E_{x_k}.

The effective irradiation time is given by:

$$t_{eff} = \frac{1 - e^{-\lambda t}}{\lambda} \tag{2.3.9}$$

where λ is the radioactive decay constant. The first two summations in Equation 2.3.8 deal with the production of charged particles. The other summations cover the stopping of the charged particles and the production of nucleus D [22]. Rearrangement and simplification of Equation 2.3.8 yields Equation 2.3.10 [22].

$$N_D(t) = t_{eff}\, \phi_n^{int}\, N_C\, \sigma_{x,D}^{pseudo} \tag{2.3.10}$$

where:

$$\phi_n^{int} = \sum_{i=1}^{175} \phi_n(E_{n_i}) \Delta E_{n_i} \tag{2.3.11}$$

and:

$$\sigma_{x,D}^{pseudo} = \frac{1}{\phi_n^{int}} \sum_{A} \sum_{i=1}^{175} \phi_n(E_{n_i}) \sigma_{n,x}(E_{n_i}) N_A \Delta E_{n_i} \times \sum_{j=1}^{24} f_{n,x}(E_{n_i}, E_{x_j}) \Delta E_{x_j} \sum_{k=j}^{1} \sigma_{x,D}(E_{x_k}) N_C \Delta R_x(\Delta E_{x_k}) \tag{2.3.12}$$

Determination of the number of atoms of nuclide D that are produced requires that “pseudo” cross sections be produced. Equation 2.3.12 defines the pseudo cross section as a cross section

for the reaction C(x,n)D per one nucleus C per initial neutron [22]. It is important to note that the pseudo cross sections are used in conjunction with the *neutron* flux and are applied to the target nucleus C. Since the pseudo cross sections actually account for a two-step process, they tend to have values a few orders of magnitude lower than typical nuclear cross sections.

2.4 Radionuclide releases and health effects

Radionuclide inventories are the source term for subsequent accident consequence calculations. The radionuclide inventories are used with estimated release fractions, the Gaussian plume model, and dose conversion factors to estimate radiation doses that would be received by the surrounding population in the event of an accident. In addition, estimates of the number of early and cancer fatalities are made using dose-effect relationships.

2.4.1 Release fractions

The task of calculating release fractions is difficult and controversial. Past studies, such as ESECOM, developed simple, generic heat-transfer models in order to calculate time-

temperature distributions within the various power plant components [8]. Piet, Cheng, and Porter defined elemental mobility categories to account for the fact that some elements (or their oxides) have a greater likelihood of mobilization than do others [23]. Categorization of elements is made according to the lower boiling point of the pure element or its oxide. Figure 2.4.1 shows the mobility categories and the corresponding assumed release fractions on the periodic table.

Figure 2.4.1. Elements assigned to release categories [23].

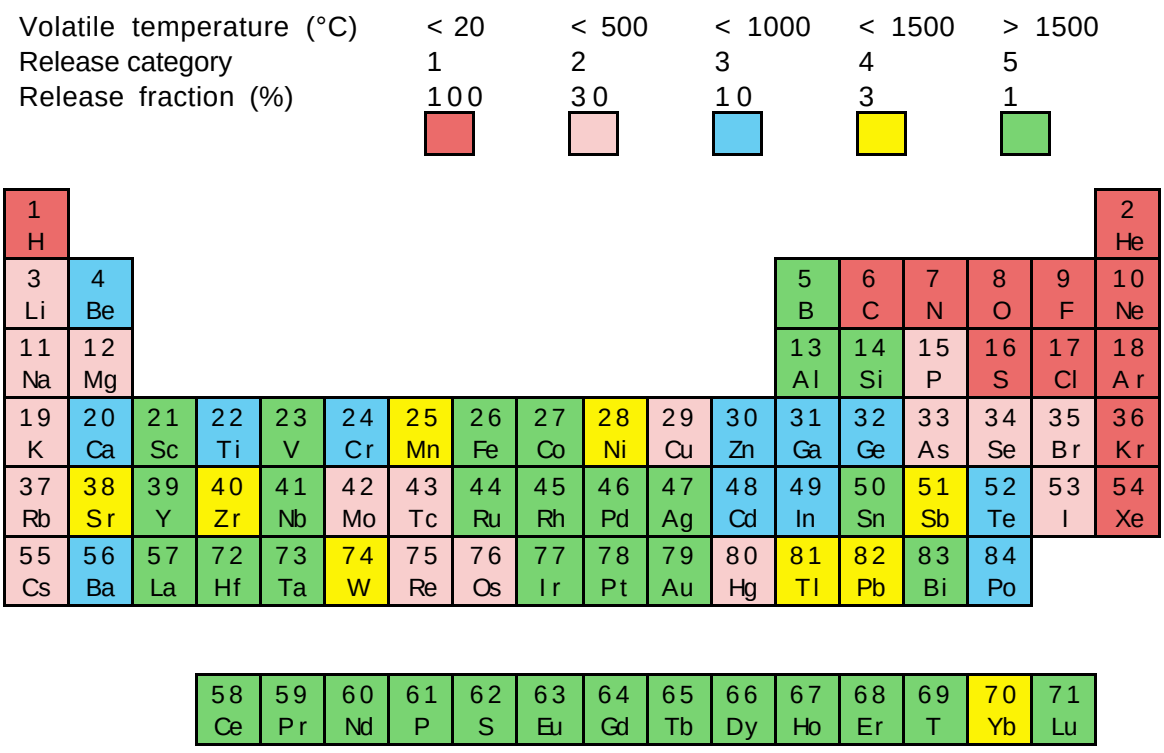

The ESECOM report used the time-temperature profiles along with limited mobilization data and these mobility category assignments to estimate mobilization rates for each of a series of blanket designs [8]. In subsequent work, Kinzig, Holdren, and Hibbard abandoned the use of heat-transfer models "in favor of consistent application of a single, pessimistic release envelope" [24]. They cited the requirement for many models and databases, the need for much committee discussion, and the lack of available data as reasons for doing away with such models [24]. In lieu of detailed analyses of mobilization rates, they opted to use the previously mentioned mobility categories upon which they superimposed multipliers that served as location-based release fractions. The multipliers were intended to loosely account for the fact that the radioactive afterheat should decrease with distance from the fusion source. (Less afterheat suggests a lower likelihood of mobilization.) The values used were 1.0 for the first wall, 0.5 for the blanket and manifold, and 0.1 for the shield [24].

One unfortunate drawback to this method is its failure to consider afterheat as a function of material. Two first-wall materials, such as PCA and SiC, may have drastically different

afterheat resulting from the same irradiation. While the afterheat would only increase the SiC first-wall temperature by about 1300 °C within one week, it would increase the temperature of the PCA first wall by nearly 70,000 °C in the same time. (It is worth noting that Kinzig, Holdren, and Hibbard calculate the temperature increase in SiC to be just over 100 °C, using the ACTL cross-section library, which has a very low value for the $^{28}Si(n,n'p)^{27}Al$ cross section [25]. The ^{27}Al, produced in this reaction undergoes an (n,α) reaction to produce the ^{24}Na that is responsible for the additional afterheat and temperature rise.)

Despite the fact that the afterheat would be much greater in the PCA than in the SiC, the Kinzig method assigns both materials location-based release fractions of 1.0. Although the mobility-category portion of the overall release fraction does account for differences in a given material's mobilization characteristics, it does not account for differences in a material's afterheat.

The Kinzig method is more difficult to apply to IFE power plants. Perhaps the HYLIFE-II liquid-Flibe blanket, which lies in front of the first wall, could be assigned a location-based release fraction of 1.0, (ordinarily assigned to the first wall). Despite being exposed to

large fluxes, the Flibe would never attain an adiabatic temperature rise of even 100 °C. Although the Flibe would be essentially at normal operating temperatures, it would receive a location-based multiplier equal to that used for a PCA first wall, which would experience a large temperature rise. Thus, use of a location-based multiplier would significantly overestimate the afterheat of the Flibe. Such inconsistencies preclude the use of location-based multipliers with IFE designs.

The present work will calculate doses for three different sets of radionuclide release fractions. The first two sets of doses do not consider the energy available (or lack thereof) to cause such large radionuclide releases. The final set of doses places an upper bound on possible releases by considering the energy available and likely release mechanisms.

The first set of release fractions is denoted the “worst-case” release fractions. It assumes that all materials react chemically to form the most mobile chemical species between the pure element and its possible oxides. Thus, the worst-case release fractions and mobility categories are exactly those shown in Table 2.4.1. Examples include carbon, which is assumed to be present as CO_2 gas, and the

fluorine in LiF, which is assumed to be present as F_2 gas. Due to their low boiling points, 100% of the carbon and fluorine are assumed to be released in an accident.

The second set of release fractions -- the “initial-case” release fractions -- also utilize the concept of mobility categories, but they account for the initial chemical composition of a given material. For example, Flibe is no longer treated as lithium, beryllium, and fluorine in elemental or oxide forms. Instead, Flibe is treated for what it is -- a mixture of LiF and BeF_2. Such treatment results in a 1% release fraction for LiF (based upon its 1670 °C boiling point) and a 10% release fraction for BeF_2 (conservatively chosen due to the 800 °C sublimation point of solid BeF_2).

The initial-case release fractions use the same mobility categories but for chemical compounds rather than pure elements. The mobility category of a particular compound is determined by its boiling point. The elements within a given compound are assumed to be released at the fraction assigned to the appropriate mobility category. Since it is not obvious what chemical form impurities and transmutation products would take, the initial-case results continue

to assume that they are released according to the worst-case release fractions.

The initial-case release fractions introduce one possible nonconservatism in that they do not account for oxidation or other possible chemical reactions. A more appropriate method would be to calculate exactly what chemical reactions occur (as a function of time) and then to determine the release fractions according to the mobility categorization of the reaction products. This task, however, would require detailed heat-transfer and chemical-reaction kinetics calculations. It would also require an enormous quantity of materials data. Finally, it would require accident information that could be obtained only through detailed assumptions about the type of accident. In the end, there would be no guarantee that the worst possible accident had been characterized.

The final set of release fractions includes an analysis of likely energy sources to establish an upper limit to the radionuclide inventories that might be released in an actual accident. These release fractions, dubbed the “mechanistic-case” release fractions, assume that all available energy is channeled into the mobilization of the largest contributing radionuclide(s) identified in the worst-

case and initial-case analyses. The mechanistic-case release fractions consider energy provided by fusion yield (a capsule is ignited just as the accident begins), radioactive afterheat, and obvious chemical sources.

2.4.2 Gaussian plume model

The best model for the dispersion of radionuclides is the Gaussian plume diffusion model [26]. Equation 2.4.1 gives the general form of the Gaussian plume model.

$$\chi = \frac{Q'}{2\pi\sigma_y\sigma_z u} \times \exp\left[-\frac{y^2}{2\sigma_y^2}\right] \times \left\{\exp\left[-\frac{(z-h)^2}{2\sigma_z^2}\right] + \exp\left[-\frac{(z+h)^2}{2\sigma_z^2}\right]\right\} \quad (2.4.1)$$

where:

- χ = radionuclide concentration (Bq/m^3);
- Q' = source strength (Bq/s);
- z = vertical distance from the plume centerline (m);
- y = lateral distance from the plume centerline (m);
- σ_z = vertical diffusion (m);
- σ_y = lateral diffusion (m);
- u = windspeed (m/s); and
- h = release height (m).

In the present work, the Gaussian plume model is used with release and atmospheric parameters consistent with those used in

the ESECOM study. These parameters are believed to result in conservative doses and are given in Table 2.4.1 [8].

Table 2.4.1. Parameters used with the Gaussian plume model lead to the conservative estimation of accident doses.

Parameter	**Value**
Atmospheric stability class	Pasquill-Gifford Class F
Wind speed	1 m/s
Inversion layer height	250 m
Release height	0 m - ground–level
Thermal plume rise	None
Initial building wake	100 m wide × 50 m high
Deposition velocities	0.002 m/s for particulates 0.010 m/s for halogens 0 m/s for other gases

When calculated on the plume centerline (y=0 and z=0) and for a ground–level release (h=0), Equation 2.4.1 reduces to:

$$\chi = \frac{Q'}{\pi \sigma_y \sigma_z u} \qquad (2.4.2)$$

Values for σ_y and σ_z are functions of the atmospheric stability and downwind distance. The parameterization provided by Tadmor and Gur has been used in this report [27].

For radioactive effluents, decay during plume transport must be considered, which may be done by replacing the source strength in

Equation 2.4.2 with the quantity $Q'_0 \exp(-\lambda t)$, where Q'_0 is the rate of emission of the given radionuclide [28]. Neglecting plume meander, Equation 2.4.2 becomes:

$$\chi = \frac{Q'_0}{\pi \sigma_y \sigma_z u} \times \exp\left(\frac{-\lambda x}{u}\right) \qquad (2.4.3)$$

where x is the downwind distance in meters. Accounting for dry deposition of the radioactivity, Equation 2.4.3 becomes:

$$\chi = \frac{Q'_0}{\pi \sigma_y \sigma_z u} \times \exp\left[-\left(\sqrt{\frac{2}{\pi}} \frac{u_d}{u \sigma_z} + \frac{\lambda x}{u}\right)\right] \qquad (2.4.4)$$

where u_d is the dry deposition velocity in m/s [28].

Using Equation 2.4.4 in conjunction with the radionuclide decay constants, release rates, values for σ_y and σ_z, and parameters found in Table 2.4.1, it is a straightforward task to obtain radionuclide concentrations and deposition rates. The radionuclide concentrations are used to obtain cloudshine and inhalation doses, and the deposition rates are used for the calculation of groundshine, ingestion, and resuspension doses.

2.4.3 Doses and health effects

When radionuclides are released into the atmosphere, they may result in radiation doses to the surrounding population. When delivered to humans, the most useful unit of dose is the dose equivalent [28]. Dose equivalents may result in injuries such as radiation sickness and erythema. Large dose equivalents, if delivered in a short period of time, may cause death. Dose equivalents may also result in latent cancers.

The doses delivered to the population from various pathways may be determined using the radionuclide concentrations, calculated with the Gaussian plume model and dose conversion factors, along with parameters such as respiration and food consumption rates. Estimates of the effects resulting from radiation doses may be made using risk analysis and epidemiological data from the irradiation of humans and animals. Acute and somatic effects have been estimated using the results presented in NUREG/CR-4214, Rev. 1 [29].

The effective acute dose (early dose) is a dose equivalent that is defined as “that dose which if delivered entirely in one day would induce the same health effects as the actual dose that was delivered over many days” [31]. The early dose is obtained by applying

effective acute dose reduction factors to the dose received during the various time intervals following the radiation exposure. These are not only time-dependent, they are organ-dependent. Table 2.4.2 gives effective acute dose reduction factors for the bone marrow, the GI tract, and the lungs. The values shown in Table 2.4.2 are used throughout this work to calculate early doses. For example, the early dose to the bone marrow is equal to 100% of the first day's dose plus 50% of the next 13 days' doses plus 25% of the next 16 days' doses.

Table 2.4.2. Acute dose reduction factors [31].

Organ of interest	**Time period after exposure (days)**					
	0-1	1-7	7-14	14-30	30-200	200-365
Red bone marrow	1.0	0.5	0.5	0.25		
Lungs	1.0	0.0625	0.0625	0.0270	0.0270	0.0109
GI tract	1.0	0.43				

Early doses have been calculated for the bone marrow, the gastrointestinal (GI) tract, and the lungs. For acute exposures, the small intestine is the critical organ for injury to the GI tract [29]. Early doses have been calculated for the lower large intestine (LLI), because data for the small intestine was not available and use of the LLI provides a conservative result [30].

Early doses include contributions from inhalation, cloudshine, and groundshine. Inhalation and cloudshine are assumed to occur only during plume passage. Groundshine occurs for the entire seven day period during which the affected population is relocated. To be conservative, no corrections have been made for evacuation or sheltering. Corrections have been made for added shielding during time spent indoors. Early doses do not include contributions from the ingestion of contaminated food or water.

The chronic effective dose equivalent (chronic dose) is a 50-year dose commitment. It includes contributions from inhalation and cloudshine during plume passage, groundshine after plume passage, and cloudshine and inhalation from resuspended material. The chronic dose also includes contributions from the ingestion of contaminated food and water. Corrections are made to the chronic dose to account for surface roughness and for added shielding during time spent indoors.

Radionuclide inventories are multiplied by release fractions to obtain a release inventory, in Bq, for each radionuclide. The release inventories are then multiplied by the early and chronic dose factors (expressed in Sv/Bq released) to obtain both centerline early doses

to the bone marrow, the GI tract, and the lungs and a chronic dose. Results are obtained for many radial intervals, and adjustments are made to correct for population residing away from the plume centerline. The doses are summed over all radionuclides to obtain both chronic and early doses for each of the three organs.

Early doses are used in a set of two-parameter Weibull functions to obtain cumulative hazards for death associated with injury to the bone marrow, the GI tract, and the lungs [29]. The cumulative hazard from each effect is modeled as:

$$H = \ln(2) \times \left(\frac{D}{D_{50}}\right)^{\nu} \qquad (2.4.5)$$

where H is the cumulative hazard from the effect, D is the early dose, D_{50} is the early dose that would result in death in 50% of the population, and ν is the shape parameter of the dose-effect relationship [29]. The cumulative hazard is defined to be zero for an early dose of less than the threshold dose, D_{thresh}. Values for D_{50}, ν, and D_{thresh} are given in Table 2.4.3.

The values of D_{50} and D_{thresh} are given by NUREG/CR-4214 in units of grays. This report assumes a Q-value of one, and thus, the values have been converted to sieverts. This assumption is conservative,

because Q-values greater than one would yield higher values of D_{50} and D_{thresh} than those reported. Larger values of D_{50} and D_{thresh} would result in a decrease in the effects noted for a particular dose. This assumption is also accurate, because the vast majority of the dose delivered by the release of radionuclides from a fusion power plant would likely come from γ-rays and high-energy betas [32]. Both forms of radiation have Q-values of one.

Table 2.4.3. Parameters used with Weibull-type dose-response functions [29].

Organ or Tissue	D_{50} (Sv)	Shape Factor, ν	D_{thresh} (Sv)
Red bone marrow	3.0	6	1.5
GI Tract	15.0	10	7.5
Lungs	10.0	12	5.0

The cumulative hazard from the three early effects is simply the sum of the individual cumulative hazards [29].

$$H_{early} = H_{bone} + H_{gi} + H_{lung} \qquad (2.4.6)$$

where H_{early} is the total cumulative hazard and H_{bone}, H_{gi}, and H_{lung} are the cumulative hazards associated with injury to the respective organs. The total risk of lethality from the three effects is calculated using Equation 2.4.7.

$$\text{Risk} = 1 - e^{-H_{early}} \qquad (2.4.7)$$

The number of early deaths may be estimated by multiplying the risk by the total population subject to that risk. The population within each interval is calculated assuming a constant population density of 100 people per square kilometer (equal to the population density of Ohio). The population is assumed to begin at a distance of 1 km from the point of release. The number of early fatalities is calculated by summing over all intervals.

Conservative assessments of induced cancer fatalities assume a linear method without a threshold dose. The rate constant for cancer fatalities resulting from the irradiation of humans is approximately 3×10^{-2}/person–Gy [29]. It should be noted that this value is the mean of the predicted range of 10^{-2}/person–Gy to 10^{-1}/person–Gy that is reported in the literature [29]. Again, the present work conservatively assumes a Q-value of one and obtains a rate constant of 3×10^{-2} cancer fatalities/person–Sv. The total number of cancer fatalities is estimated.

References for Chapter 2

1. M. Clark, Jr. and K. F. Hansen, *Numerical Methods of Reactor Analysis*, New York: Academic Press, (1964).
2. E. D. Cashwell and C. J. Everett, *A Practical Manual on the Monte Carlo Method for random walk problems*, Los Angeles: Pergamon Press, (1959).
3. L. L. Carter and E. D. Cashwell, "Particle-Transport Simulation with the Monte Carlo Method," Los Alamos Scientific Laboratory, TID-26607, (1975).
4. M. D. MacLaren and G. Marsaglia, "Uniform Random Generators," *J. Ass. Comput. Mach.*, **12**, 83-89, (1965).
5. G. Marsaglia, "Random Numbers Fall Mainly in the Planes," *Proc. Nat. Acad. Sci.*, **61**, 25-28, (1968).
6. J. Moshman, "The Generation of Pseudorandom Numbers on a Decimal Calculator," *J. Ass. Comput. Mach.*, **1**, 88.
7. L. R. Greenwood and R. K. Smither, "SPECTER: Neutron Damage Calculations for Materials Irradiations," Fusion Power Program - Argonne National Laboratory, ANL/FPP/TM-197, (January 1985).
8. J. P. Holdren, D. H. Berwald, R. J. Budnitz, J. G. Crocker, J. G. Delene, R. D. Endicott, M. S. Kazimi, R. A. Krakowski, B. G. Logan,

and K. R. Schultz, “Report of the Senior Committee on Environmental, Safety, and Economic Aspects of Magnetic Fusion Energy,” Lawrence Livermore National Laboratory, UCRL-53766, (September 1989).

9. Recommendation of the IAEA Working Group on Reactor Radiation Measurements, *Nuc. Eng. Des.*, **33**, 92, (1975).

10. D. L. Smith, C. C. Baker, D. K. Sze, G. D. Morgan, M. A. Abdou, S. J. Piet, K. R. Schultz, R. W. Moir, and J. D. Gordon, “Overview of the Blanket Comparison and Selection Study,” *Fusion Technology*, **8**, 10, (1985).

11. W. J. Hogan, ed., *Energy from Inertial Fusion*, Vienna, Austria: International Atomic Energy Agency, (1995).

12. J. H. Pitts, R. F. Bourque, W. J. Hogan, W. R. Meier, and M. T. Tobin, “The Cascade Inertial Confinement Fusion Reactor Concept,” Lawrence Livermore National Laboratory, UCRL-LR-104546, (December 1990).

13. W. R. Meier, R. L. Bieri, M. J. Monsler, C. D. Hendricks, P. Laybourne, K. R. Shillito, S. K. Ghose, L. M. Goldman, K. D. Auclair, C. Y. Pang, R. F. Bourque, L. D. Stewart, E. E. Bowles, E. L. Hubbard, C. W. von Rosenberg, Jr., M. W. McGeoch, I. N. Sviatoslavsky, R. R.

Peterson, M. E. Sawan, H. Y. Khater, L. J. Wittenberg, G. L. Kulcinski, G. A. Moses, E. A. Mogahed, J. J. MacFarlane, S. Rutledge, S. Humphries, Jr., and E. T. Cheng, “Osiris and SOMBRERO Inertial Confinement Fusion Power Plant Designs,” DOE/ER/54100-1, WJSA-92-01, W. J. Schafer Associates, Inc., Livermore, CA, (March 1992).

14. A. G. Croff, “ORIGEN2: A Versatile Computer Code for Calculating the Nuclide Compositions and Characteristics of Nuclear Materials,” *Nuclear Technology*, **62**, 335-352, (September 1983).
15. M. J. Bell, “ORIGEN: The ORNL Isotope Generation and Depletion Code,” Oak Ridge National Laboratory, ORNL-4628, (May 1973).
16. J. A. Blink, “FORIG: A Modification of the ORIGEN2 Isotope-Generation and Depletion Code for Fusion Problems,” Lawrence Livermore National Laboratory, UCRL-53263, (1982).
17. E. T. Cheng, R. A. Forrest, and A. Pashchenko, Report on the Second International Activation Calculation Benchmark Comparison Study, TSI Research Report TSIR-21 FINAL Draft, (November 1993).
18. J. D. Lee, ed., “TIBER II/ETR: Final Design Report,” Lawrence Livermore National Laboratory, UCID-21150, (September 1987).

19. R. W. Moir, M. G. Adamson, R. O. Bangter, R. L. Bieri, R. H. Condit, C. W. Hartman, P. A. House, A. B. Langdon, B. G. Logan, C. D. Orth, R. W. Petzoldt, J. H. Pitts, R. F. Post, R. A. Sacks, M. T. Tobin, W. H. Williams, T. J. Dolan, G. R. Longhurst, M. A. Hoffman, V. E. Schrock, P. F. Peterson, R. Y. Bai, X. M. Chen, J. C. Liu, D.-K. Sze, and W. R. Meier, “HYLIFE-II Progress Report,” Lawrence Livermore National Laboratory, UCID-21816, (December 1991).
20. J. Sanz, J. F. Latkowski, M. T. Tobin, J. M. Perlado, D. Guerra, and A. S. Pérez, “ACAB: Activation Code for Fusion Applications User’s Manual V2.0,” Lawrence Livermore National Laboratory, UCRL-MA-122002, (September 1995).
21. S. Cierjacks and Y. Hino, “The Importance of Sequential (x,n) Reactions on Element Activation of Fusion Reactor Materials,” *Journal of Nuclear Materials*, **170**, 134-139, (February 1990).
22. S. Cierjacks, P. Oblozinsky, and B. Rzehorz, “Nuclear Data Libraries for the Treatment of Sequential (x,n) Reactions in Fusion Materials Activation Calculations,” KfK 4867, Institute for Materials, Kernforschungszentrum Karlsruhe, (July 1991).

23. S. J. Piet, E. T. Cheng, and L. J. Porter, “Accident Safety Comparison of Elements to Define Low-Activation Materials,” *Fusion Technology*, **17**, 636-657, (July 1990).

24. A. P. Kinzig, J. P. Holdren, and P. J. Hibbard, “Safety and Environmental Comparisons of Stainless Steel with Alternative Structural Materials for Fusion Reactors,” *Fusion Technology*, **26**, 79-104, (August 1994).

25. M. A. Gardner and R. J. Howerton, “ACTL: Evaluated Neutron Activation Cross Section Library -- Evaluation Techniques and Reaction Index,” Lawrence Livermore National Laboratory, UCRL-50400, vol. 18, (1978).

26. D. H. Slade, ed., *Meteorology and Atomic Energy–1968*, Washington, D. C.: U. S. Atomic Energy Commission, 97-103, (1968).

27. J. Tadmur and Y. Gur, “Analytical Expressions for the Vertical and Lateral Dispersion Coefficients in Atmospheric Diffusion,” *Atmospheric Environment*, **3**, 688-689, (1969).

28. J. R. Lamarsh, *Introduction to Nuclear Engineering, 2nd Edition*, Menlo Park, California: Addison–Wesley Publishing Company, 556-564, (1983).

29. S. Abrahamson, M. Bender, S. Book, C. Buncher, C. Denniston, E. Gilbert, F. Hahn, V. Hertzberg, H. Maxon, B. Scott, W. Schull, and S. Thomas, “Health Effects Models for Nuclear Power Plant Accident Consequence Analysis, Low LET Radiation, Part II: Scientific Bases for Health Effects Models,” Sandia National Laboratories, NUREG/CR-4214, Rev. 1, Part II, (May 1989).
30. D. Chanin, Sandia National Laboratory, private communication, (October 1995).
31. D. Chanin and M. Young, “Code Manual for MACCS2: Volume 1, User’s Guide (Draft),” SANDXX-XXXX, (May 1995).
32. G. M. Smith and G. J. Butterworth, “Neutron Activation of Elements and the Radiological Implications for Development and Use of Low Activation Materials,” *Journal of Nuclear Materials*, **191**, 1455-1460, (September 1992).

3. Indices of radiological hazard

An understanding of the risks involved in the operation of a technology often can be obtained through the use of probabilistic risk assessment (PRA). The use of PRA, however, fundamentally requires operational experience at least on a component if not on an integrated system level. Because there are not, as of yet, any existing operating fusion power plants, no operational experience is available. Thus, an understanding of the risks involved in the operation of a fusion power plant cannot be obtained at this time. The hazards posed by the operation and existence of fusion power plants can be estimated. A useful tool in estimating these hazards is the radiological hazard index.

Fetter gives four qualities that an ideal hazard index should possess: (1) intuitive meaning, (2) amenability to computation, (3) generality, and (4) compatibility with past and future studies [1]. The radiological hazard indices possess each of these qualities to a varying degree. The present work considers indices from three classes of hazard. These include power plant accidents, routine and occupational exposures, and waste disposal. Each of these areas will affect the overall acceptability of a particular design. Through

examination of the three classes of hazard, trade-offs between the classes may become apparent. The identification of such trade-offs would help guide future design decisions. A description of each of the classes of hazard and of the indices within each class is given in the following sections.

3.1 Accident hazards

The hazards posed by the potential for the accidental release of radioactivity into the atmosphere can be quantified with several different indices. These indices vary widely in both their meaningfulness and their ease of calculation. They range from activity, which is the least meaningful but easiest to calculate, to early and cancer fatalities, which are quite meaningful but quite difficult to calculate accurately.

3.1.1 Activity

Activity is a measure of the decay rate of a radioactive material. Quantitatively, activity is calculated as:

$$A_i = \lambda_i N_i \qquad (3.1.1)$$

where A_i is the activity of the i^{th} radionuclide, λ_i is its decay constant, and N_i is the number of atoms of the i^{th} radionuclide. The decay constant is given by:

$$\lambda_i = \ln(2)/t_{1/2} \qquad (3.1.2)$$

where $t_{1/2}$ is the radioactive half-life of the i^{th} radionuclide. Activity is often expressed in units of Bq. One Bq is equal to one disintegration per second.

Typically, the total activity (the activity of each radionuclide summed over all those that are present) is reported in most studies. Unfortunately, activity tells very little about the actual hazard posed by a material. The total disintegration rate of a material, without essential information such as the mode of radioactive decay, the decay energies, or the radioactive half-life, does not convey much information about the hazard. For a fixed activity, the hazard posed by two radionuclides may vary by several orders of magnitude or more.

3.1.2 Biological hazard potential

The biological hazard potential (BHP) is better than activity as a measure of the hazard posed by a material or power plant that contains and/or produces the material. As shown in Equation 3.1.3, BHP is the activity of a particular radionuclide divided by its recommended concentration guide (RCG), which was previously known as the maximum permissible concentration. A total BHP is obtained by summing over all radionuclides.

$$BHP = \sum_i \frac{A_i}{RCG_i} \qquad (3.1.3)$$

The RCG is calculated for each radionuclide such that an individual continuously breathing the air or drinking the water would receive the maximum permissible dose (MPD) of 5 mSv/yr [2]. When the chemical form of a radionuclide in uncertain, it is common practice to assume that it is in its most restrictive form [1].

Because the RCG values are derived in units of Bq/m^3, the BHP is expressed in units of m^3. The BHP may be thought of as the volume necessary to dilute the radioactivity to the concentration that would result in attainment of the MPD. Since the dispersion of

radionuclides occurs most rapidly via their transport in the atmosphere, the BHP in air is usually used in analysis of power plant accidents.

Since BHP considers radioactive half-life, decay mode, decay energies, and uptake by the body, it is better than activity as a measure of accident hazard. There are, however, several limitations to the usefulness of BHP. For example, the RCGs used in the calculation of BHP are based upon continuous exposure and thus do not convey information about transient exposures that would be expected during an accidental release of radioactivity [2]. In addition, BHP is not an easily understood measure of hazard. Fetter points out that “it is difficult for the average person to interpret the meaning of a dilution volume of 10^{18} m^3 of air” [1].

The International Commission on Radiological Protection (ICRP) is the official source for RCG values. Unfortunately, values are published for only about 240 radionuclides, and many of these are of interest for fission, not fusion, power plants [3]. Despite this, RCG values for radionuclides of interest may be calculated using the ICRP models. In this work, all BHP calculations utilize RCG values calculated using the 1990 ICRP model [3].

3.1.3 Doses

The concept of dose has been used in many studies in both the fission and fusion communities. Dose-response relationships have been established for many different health effects. There are many assumptions that must be made in the calculation of doses, which can produce large variations in the results. Doses may be calculated at many different times and distances and for many organs, weather conditions, and release scenarios. As described in Chapter 2, the present work uses two types of doses: early and chronic.

Early doses have been calculated for three organs that may make a significant contribution to the overall probability of early fatality [4]. Doses have been calculated using three sets of radionuclide release fractions. All dose calculations have been performed using a consistent set of parameters that define the weather conditions at the time of release. These parameters were given in Table 2.4.1.

3.1.4 Threshold-dose release fractions

The ESECOM report introduced the concept of threshold-dose release fractions (TDRFs) [5]. A TDRF is simply the fraction of a given element, isotope, or group thereof which, if released, would

result in a threshold dose being achieved at a defined distance from the release [5]. ESECOM defined two TDRFs. The first, the critical TDRF, corresponds to a 2 Sv early (whole-body) dose received by the maximally exposed individual located 1 km from the point of release. The second, the chronic TDRF, uses a 0.25 Sv chronic dose threshold and a distance of 10 km. Although ESECOM did not include the ingestion pathway for the chronic TDRF, it will be included in the chronic dose results presented in this report.

ESECOM selected the 2 Sv critical TDRF threshold dose, because it approximates the smallest dose that has an appreciable chance of causing an early fatality in a sensitive individual [5]. Since the present work calculates early doses to three organs in lieu of a single, whole-body dose, three different critical TDRFs are calculated. The critical threshold doses are equal to the threshold doses presented in Table 2.4.3. For example, the threshold dose for death associated with injury to the bone marrow is 1.5 Sv. Thus, the critical TDRF for the bone marrow uses 1.5 Sv as the threshold dose.

ESECOM selected the 0.25 Sv chronic TDRF threshold dose, because current regulatory standards call for either evacuation or extensive cleanup procedures if a 0.25 Sv chronic dose could result

[5]. The chronic TDRF demonstrates the possible accident cleanup and/or evacuation that might be required following an accident [5].

As in the ESECOM report, the present study will calculate TDRFs according to the mobility categories proposed by Piet, Cheng, and Porter [6]. TDRFs will be given for radionuclides in each mobility category and for all radionuclides that are more mobile than the current category. That is, results are given for category 1, for category 2 plus category 1, and so on. The most restrictive TDRF includes radionuclides from all five mobility categories. TDRFs are given for each component in each design, and the dominant radionuclides are identified. Note that TDRFs greater than unity are desirable as they indicate that the entire radionuclide inventory may be released without causing early doses in excess of the threshold doses.

3.1.5 Early and cancer fatalities

The number of early and cancer fatalities caused by an accident are meaningful and understandable as hazard indices. These two indices not only allow one fusion power plant to be compared to another, but they also enable comparison to technologies and power

plant designs that preclude the use of radioactive materials [1]. The use of early and cancer fatalities as a measure of hazard would allow the consideration of mining accidents for coal, refinery accidents for petroleum, and dam breaks for hydroelectric power, for example. A description of the methods used to estimate the number of early and cancer fatalities that might result from the accidental release of radioactivity was given in Chapter 2.

3.2 Occupational and routine hazards

The evaluation of routine exposure requires that one understand the routine operation of a technology. Since fusion power plants have never been constructed, this understanding is not available. Thus, the results presented in the present work must be considered preliminary. It is likely that fusion power plants will have to meet regulations similar to those that are currently applied to the fission power industry. Rather than giving an absolute measure of the hazard posed by the routine operation of fusion facilities, the results are indicative of the relative difficulty of meeting these regulations.

3.2.1 Contact dose rates

Occupational exposures are analyzed using contact dose rates for the various power plant components. Contact dose rates are given as a function of time after shutdown. They are calculated using a semi-infinite medium approximation, which assumes that the radionuclides are present at a constant concentration (calculated for the finite component). In general, this approximation leads to the conservative estimation of the actual dose rates that would be presented by a finite component.

3.2.2 Dose and cancer fatalities

During routine operation, public exposure to radiation is strictly limited by several governmental agencies [7,8,9]. Table 3.2.1 gives dose limits for routine releases to the public. The dose resulting from routine releases includes contributions from activation products and tritium. Since the doses should be very low, there is no risk of early fatalities from routine exposures. Thus, only the number of cancer fatalities has been calculated for each design.

Table 3.2.1. Several governmental agencies regulate routine doses to the public. Table adapted from reference 5.

Dose description	NRC[a]	EPA
Airborne effluents from single facility:		
• Total body	50 μSv/yr	250 μSv/yr[b]
• Skin	150 μSv/yr	
Aqueous effluents from a single facility (total body or any organ)	5 μSv/yr	4 μSv/yr[c]
All causes		1 mSv/yr[b]

[a] See reference 7.
[b] See reference 8.
[c] See reference 9.

3.3 Waste-disposal hazards

The waste-disposal indices estimate quantities ranging from the volume of waste that must be disposed of to the dose that an intruder at the disposal site might receive 100–1000 years after disposal. Since data regarding the condition of the disposal site, of the waste, or even of the government hundreds of years after disposal cannot be predicted reliably, waste-disposal indices attempt to estimate conservatively the maximum hazard the waste might present.

3.3.1 Life-cycle waste volume

The life-cycle waste volume is easily calculated. It is simply the total volume of radioactive waste generated over the 30 full-power-year lifetime of the power plant. The life-cycle waste volume includes components that are changed-out during the plant lifetime as well as materials that are ultimately disposed of when plant operation ceases.

3.3.2 Biological hazard potential

Because the long-term dispersion of radionuclides is probably dominated by groundwater transport processes, the BHP in water is most often used as a waste-disposal index. Once again, BHP is calculated using the RCGs given in the 1990 ICRP report [3]. The BHP in water has the same advantages and disadvantages as the BHP in air.

3.3.3 Waste-disposal rating/intruder dose

The waste-disposal rating (WDR) is given by:

$$WDR = \sum_i \frac{A_i / V}{SAL_i} \qquad (3.3.1)$$

where A_i is the activity of the i^{th} radionuclide, SAL_i is its specific activity limit given by Fetter, Cheng, and Mann, and V is the component volume in m^3 [10]. Summation over all radionuclides provides a single value that allows one component to be compared to another. A WDR less than unity indicates that a component would qualify for disposal via shallow land burial.

The SALs are based upon a 50-year dose commitment limit of 5 mSv consistent with the MPD for members of the public [10]. Since the numerator of Equation 3.3.1 is equivalent to the concentration of the i^{th} radionuclide, and the SALs are also concentrations, the WDR is a dimensionless index. The intruder dose is obtained by multiplying the WDR by the MPD. It is expressed in units of Sv/yr.

It is worth noting that the use of waste-disposal ratings and intruder dose in the present work is not intended to indicate that shallow land burial will be an available method for waste disposal nor that it will necessarily be the best method of waste disposal. These indices are used merely to quantify relative hazards that might be presented by the various designs.

3.3.4 Deep disposal index

For components that fail to meet the criteria for disposal via shallow land burial, the deep disposal index (DDI) has been calculated. The DDI is simply the product of the WDR and the life-cycle volume of a given component [2]. The DDI quantifies the volume and intensity of waste that is unable to qualify for disposal via shallow land burial.

3.3.5 Annualized intruder hazard potential

The annualized intruder hazard potential (AIHP) is the product of the intruder dose and the average annual waste volume for each power plant component [2]. In addition to calculating the AIHP for each component, a total AIHP has been calculated for each power plant design. The AIHP provides a relative comparison for components within a design and among different designs. It is a meaningful measure of the relative magnitude of the waste-management task. The AIHP is given in units of $Sv \cdot m^3/year$.

3.4 Summary

The models described in Chapter 2 are used to obtain the information required for the calculation of the various radiological indices described within this chapter. The radiological indices span three classes of hazard: accidents, occupational and routine exposures, and waste disposal. The individual indices vary widely with regard to their meaningfulness and ease of calculation. To ensure compatibility with past studies, results are presented for a large number of radiological indices.

References for Chapter 3

1. S. A. Fetter, “Radiological Hazards of Fusion Reactors: Models and Comparisons,” Doctoral Dissertation, University of California, Berkeley, Energy and Resources, (May 1985).
2. A. P. Kinzig, J. P. Holdren, and P. J. Hibbard, “Safety and Environmental Comparisons of Stainless Steel with Alternative Structural Materials for Fusion Reactors,” *Fusion Technology*, **26**, 79-104, (August 1994).
3. International Commission on Radiological Protection, “Limits for Intakes of Radionuclides by Workers,” ICRP Publication 30, Pergamon Press, (1990).
4. S. Abrahamson, M. Bender, S. Book, C. Buncher, C. Denniston, E. Gilbert, F. Hahn, V. Hertzberg, H. Maxon, B. Scott, W. Schull, and S. Thomas, “Health Effects Models for Nuclear Power Plant Accident Consequence Analysis, Low LET Radiation, Part II: Scientific Bases for Health Effects Models,” Sandia National Laboratories, NUREG/CR-4214, Rev. 1, Part II, (May 1989).
5. J. P. Holdren, D. H. Berwald, R. J. Budnitz, J. G. Crocker, J. G. Delene, R. D. Endicott, M. S. Kazimi, R. A. Krakowski, B. G. Logan, and K. R. Schultz, “Report of the Senior Committee on

Environmental, Safety, and Economic Aspects of Magnetic Fusion Energy," Lawrence Livermore National Laboratory, UCRL-53766, (September 1989).

6. S. J. Piet, E. T. Cheng, and L. J. Porter, "Accident Safety Comparison of Elements to Define Low-Activation Materials," *Fusion Technology*, **17**, 636-657, (July 1990).

7. "Exposures to Members of the Public," *Code of Federal Regulations*, ch. 20, pt. 50, U. S. Nuclear Regulatory Commission, Washington, D. C., (1985).

8. "National Emissions Standards for Hazardous Air Pollutants: Standards for Radionuclides," *Code of Federal Regulations*, ch. 40, pt. 61, U. S. Environmental Protection Agency, Washington, D. C., (1985).

9. "Emissions Standards for Hazardous Water Pollutants," *Code of Federal Regulations*, ch. 40, pt. 141, U. S. Environmental Protection Agency, Washington, D. C., (1985).

10. S. A. Fetter, E. T. Cheng, and F. M. Mann, "Long-term radioactive waste from fusion reactors: Part II," *Fusion Engineering and Design*, **13**, 239-246, (November 1990).

4. The RADSAFE computer code system

The calculation of a large number of radiological indices, such as those described in Chapter 3, requires a complex system of computer codes. The system of codes that work together to produce the radiological indices has been named RADSAFE (**RAD**iological **S**afety **A**nalysis of **F**usion **E**nvironments).

The main components of the RADSAFE system are particle transport, materials damage, sequential charged-particle reactions, radionuclide generation and depletion, radionuclide release models, and accident consequences. Each of these components requires interaction among two or more codes and their respective data libraries. Much of the interaction between codes and libraries is automated through the use of the TARTREAD utility [1].

4.1 Particle transport

A calculation begins with the creation of a particle-transport model for use with the TART95 Monte Carlo neutron and photon particle-transport code [2]. The creation of such a model has several distinct steps. These steps include the specification of a geometric

model, the definition of the particle source, the assumptions that are made during particle transport, the choice of nuclear data and cross-section libraries, and the selection of the types of output. Each of these steps are described in the following sections.

4.1.1 Creation of a geometric model

Models are created in TART95 through the use of a set of geometric surfaces. Commonly used surfaces include spheres, planes, cylinders, and cones. Interactions among these surfaces are declared and are used to define zones. Each zone must be assigned a material. Capture and reflecting zones are also available. The input and output of the TART95 code are quite similar to those of the more widely distributed MCNP.

The more complicated the geometry is, the more likely it is that the TARTCHEK code will be required [2]. TARTCHEK is an interactive code that graphically displays cross sections and surfaces of TART95 geometries. TARTCHEK offers features such as particle flooding and tracking, zone overlap, and location of holes. These features are invaluable for the rapid debugging of TART95

geometries. A second interactive code is available for the rapid creation of TART95 input files, but it has not been used in this work.

4.1.2 Definition of the particle source

A source region is defined in terms of its physical location and its particle characteristics. Example sources include points, lines, disks, spheres, and cylinders. Some source-particle characteristics are type (neutron or photon), energy distribution, and angular distribution. One or more sources may be defined in each problem.

4.1.3 Control over particle transport

TART95 gives the user a great deal of control over the physics of how a calculation proceeds, accomplished primarily through the use of ”sentinel” cards. Sentinel card inputs determine such parameters as how many particles are followed, what the minimum particle energies will be (and what to do when a particle’s energy drops below the minimum value), whether corrections are made for resonance self-shielding, and whether thermal scattering effects are considered.

4.1.4 Choice of nuclear data and cross-section libraries

TART95 uses nuclear data available in the ENDL library [3]. This library contains neutron-interaction and neutron-induced photon-production data. Photon-interaction data is provided by the ENGL library [4]. These libraries include multi-group cross sections rather than continuous energy cross sections like those used by codes such as MCNP. The use of multi-group cross sections results in a large time savings in TART95 calculations without introducing any significant deviations in the results. TART95 may also be executed using a non-standard data library based upon ENDF/B-VI.

4.1.5 Selection of output type

Sentinel cards not only allow the user to select which assumptions are made during particle transport, but they also give the user much control over what type of output tallies are generated. TART95 can provide output in terms of the number of particles, particle energy and angular distributions, particle absorption, and energy deposition. When needed, TART95 can generate time-dependent output (using temporal bins). TART95 also allows various response functions (results that are a function of particle energy,

such as dose rates) to be calculated directly. Estimates of neutron reaction rates can be obtained as well.

For this work, the most important output from TART95 is the energy-dependent particle distribution in each zone of interest. TART95 calculates neutron pathlengths in a 175-group energy structure. These pathlengths are converted by the TARTREAD utility into 175-group neutron fluxes for use in subsequent neutron activation calculations. The fluxes also may be collapsed down into 100 groups for use in the calculation of pseudo cross sections or into a single group for subsequent neutron and (x,n) reaction activation calculations.

4.2 Materials damage

The SPECTER code calculates the DPA and gas production rates for a material that experiences a given neutron spectrum and total flux [5]. The 175-group neutron flux is calculated by TART95 and TARTREAD. TARTREAD then collapses the 175-group neutron flux down to a 100-point energy grid used by SPECTER. SPECTER uses cross sections from the ENDF/B-V library and from the DISCS computer code [5]. SPECTER is able to treat both elastic and

inelastic scattering as well as (n,xn), (n,d), (n,t), (n,p), (n,^{3}He), (n,α), and (n,γ) reactions. (Some of these reactions are treated in an approximate manner.)

SPECTER output is given for many different elements and materials. TARTREAD converts SPECTER output into an easy-to-read table so that the user may quickly ascertain total DPA and gas production rates.

4.3 Sequential charged-particle reactions

The PCROSS code permits consideration of the effects of (x,n) reactions through the use of pseudo cross sections [6]. PCROSS calculates the 1-group pseudo cross sections for a particular neutron spectrum and an initial material composition. Charged-particle reactions that are currently considered by PCROSS are (p,n), (d,n), (t,n), (^{3}He,n), (α,n), (d,2n), and (t,2n).

The PCROSS code uses three different data libraries: KFKSPEC, KFKSTOP, and KFKXN. The PCROSS development team at Karlsruhe, Germany chose to develop the KFKSPEC library due to the lack of available charged-particle spectra data [7]. This library was generated using the ALICE code, which makes use of the pre-

equilibrium hybrid model and the evaporation statistical model for compound nuclei [8]. ALICE is limited to n, p, d, α, and γ exit particles. The KFKSTOP library contains stopping powers and ranges of the various charged particles and was created from an updated version of the PRAL code [9]. The KFKXN library contains the charged-particle reaction cross sections and was generated with the ALICE code as well [7].

Starting with the incident neutron spectrum, PCROSS uses the KFKSPEC library to calculate the normalized charged-particle spectra that result from neutron interactions in the specified medium. PCROSS then uses the charged-particle spectra along with the stopping powers from the KFKSTOP library and charged-particle reaction cross sections found in the KFKXN library to calculate the pseudo cross sections [7].

TARTREAD combines the 1-group pseudo cross sections with 1-group neutron cross sections, which are generated using the neutron spectrum as a weighting function. The combined 1-group cross-section library is used as an input to subsequent activation calculations.

4.4 Radionuclide generation/depletion

The ACAB code performs the nuclide generation and depletion calculations [10,11]. The ACAB input file specifies the material volume and composition, the neutron spectrum and flux, and the irradiation/cooling temporal history. The primary results generated by ACAB are the isotopic concentrations as a function of time for each spatial interval and/or zone within the TART95 geometric model. ACAB also generates many of the radiological indices that are based upon isotopic concentrations and/or radionuclide activities.

ACAB was one of only two activation codes that satisfied all four criteria set by the IAEA in its 1993 activation code benchmark study [12]. The criteria were intended to judge the suitability of an inventory code for application to fusion problems.

Since the completion of the IAEA study, major improvements have been made to ACAB by code author Javier Sanz. Most of these improvements occurred during a one-year sabbatical spent at LLNL and resulted in the creation of ACAB V2.0 [11]. ACAB V2.0 improvements include coupling to Monte Carlo transport codes, treatment of pulsed/intermittent irradiation, treatment of sequential charged-particle reactions, addition of decay photons

from second isomeric states, calculation of contact dose rate contributions from high-energy Bremsstrahlung radiation and from a thin layer of material, coupling to the CHAINS code for pathway analyses, and provision for specifying the neutron flux in an arbitrary group structure [11].

ACAB uses the European Activation File version 3.1 (EAF3.1) neutron cross-section library [13]. A pointwise version of the EAF3.1 library was converted into the standard ENDF/B-VI format and collapsed into the TART95 175-group structure by Red Cullen using the LINEAR and GROUPIE codes [14]. The 175-group constants were converted by the author back into the EAF3.1 format for use with ACAB.

The ACAB decay library is largely based upon the UKDECAY3 data available with the FISPACT code [15]. (Incidentally, FISPACT is the other activation code that the IAEA benchmark study found suitable for application to fusion problems.) The photon library consists of data from UKDECAY3 and the Erdtmann and Soyka photon library [16]. ACAB uses mass attenuation coefficients that have been recompiled and calculated by Hubbell [17]. These are given for 40 elements in 35 energy groups that range from 1.0 keV to 20 MeV. SALs for waste

disposal via shallow land burial are taken from Fetter, Cheng, and Mann [18]. These limits are used with the radionuclide inventories to estimate the waste-disposal rating and the intruder dose.

Subsequent spreadsheet calculations use the intruder dose and life-cycle waste volumes to generate the DDI and AIHP indices.

4.5 Accident consequences

Accident-consequence calculations are performed with the ACCON code [19]. ACCON reads radionuclide inventories from processed ACAB output. ACCON automatically uses the worst-case radionuclide release fractions, but the user may elect to alter the assumed set of release fractions. This option is used to obtain results for the initial-case and mechanistic-case release fractions.

ACCON calculates the doses and estimates the health effects resulting from a particular radionuclide release using the MAXDOSE data library [19]. This library was created with the MACCS2 accident-consequence code system [20]. It includes four different doses in each of twenty spatial intervals. In generating the MAXDOSE library, results could be obtained only for radionuclides that were included in the DECAYLIB.DAT, DOE-EH70, and INDEXR.DAT libraries.

(The first two libraries are used by one code in the MACCS2 code system, and the last library is used by another.) The intersection of the three data libraries results in the MAXDOSE library having data for about 250 radionuclides [19]. A complete list of radionuclides available in the MAXDOSE library is given in reference 19.

Each of the doses computed for the MAXDOSE library is given on a per-unit-activity basis. When doses per quantity released are multiplied by release inventories, dose estimates are obtained. These doses are used to estimate the number of early and cancer fatalities that would result from a particular release of radioactivity.

4.6 TARTREAD utility

The TARTREAD code has been developed to expedite the calculation of a large number of radiological indices. TARTREAD is an interactive code that walks the user through the process of interpreting TART95 output files, generating ACAB input files, generating pseudo cross sections for (x,n) reactions, and calculating materials-damage information [1].

TARTREAD begins by prompting the user for the name of a TART95 output file from which spectral information is to be obtained. In order for TARTREAD to create an ACAB input file, TART95 must have been executed in the 175-energy group mode. TARTREAD allows the user to select one or more zones from the TART95 geometry. Once the selection of zones has been completed, the user enters a source term, which is used to convert the energy-dependent neutron pathlengths into neutron fluxes. The user may then simply output the energy-dependent neutron fluxes or may continue to create an ACAB input file, calculate DPA and gas production rates with the SPECTER code, or calculate pseudo cross sections with the PCROSS code.

If the user chooses to create an ACAB input file, he or she is prompted for a title card, materials to be irradiated, irradiation and cooling histories, and desired output tables. If materials-damage information is desired, the user is prompted for a total irradiation time, and the SPECTER calculation proceeds. Upon completion, TARTREAD interprets the SPECTER results and converts them into tabular form.

If pseudo cross sections are to be calculated, the user is prompted to enter the initial materials, and PCROSS is executed. The 175-group neutron fluxes are collapsed into 1-group fluxes and are combined with the 1-group pseudo cross sections to form a single library, which is used by ACAB. The user is then prompted to enter information needed to create an ACAB input file. After TARTREAD execution, the user is left with two files: an ACAB input file and a 1-group neutron and pseudo cross section library that must be used with ACAB and the input file.

When creation of an ACAB input file is selected, TARTREAD creates a file, with the name indicated, within the current directory. If a file with that name already exists in the current directory, it will be overwritten. Thus, use of the TARTREAD default file names is not recommended. The ACAB input file may be moved to another directory and immediately executed with ACAB and its standard libraries. If a combined neutron and pseudo cross-section library was created, it must be used with the ACAB input file that was created at the same time.

Use of TARTREAD makes calculation of many radiological indices a much simpler and more efficient process. TARTREAD quickly

generates input files that can be used immediately with ACAB. Much time that otherwise might be wasted debugging manually-written input files is saved through use of TARTREAD. TARTREAD currently operates only with the TART95 transport code, but conversion to allow operation with other transport codes (MCNP, ONEDANT, ANISN, etc.) would not be difficult.

4.7 Synthesis

All calculations performed for the present work use the RADSAFE system. A flowchart that describes the calculational process followed by the RADSAFE system is given in Figure 4.7.1. The RADSAFE system currently operates only on an HP/735 workstation, but it may be converted quite easily for use on other Unix-based workstations and Crays. Requests for copies of the complete RADSAFE system or for portions of the system should be directed to the author.

5. Effects of pulsed irradiation

IFE power plants will probably operate in a pulsed mode, whereas MFE power plants will operate nearly continuously. MFE power plants will probably ramp up their current for a time period on the order of one hour, shut down for several minutes, and repeat the process. Typical repetition rates for IFE power plants will be around 5 Hz. Thus, neither IFE nor MFE operations will be truly steady-state.

Traditionally, activation calculations are performed assuming steady-state operation, using a scaled neutron flux [1,2,3,4,5,6]. Recently, however, it has been suggested that this assumption may not yield accurate results for all radionuclides of concern [7].

5.1 Analytic relations for simple reaction chains

IFE and MFE each have two different pulse durations of interest. The first, the interstage pulse duration, is the time between shots in IFE and the time between current ramp-ups in MFE. This interstage pulse duration, also known as the dwell time, is about 200 ms in IFE and about 5 minutes in MFE. The second pulse duration of interest consists of shutdown time for routine and unplanned maintenance

operations. Unfortunately, neither the routine nor the unplanned maintenance are well enough understood to allow accurate calculations to be performed.

Sisolak, Spangler, and Henderson have expressed concerns regarding the use of steady-state approximations for the calculation of activation products resulting from pulsed irradiation [7]. They define two methods for the approximation of pulsed irradiation: the Steady-State (SS) and Equivalent Steady-State (ESS) methods. Both methods conserve the total fluence. The SS method also conserves the total irradiation time, while the ESS method conserves the total operation time. In order to conserve both the total fluence and the total operation time, the ESS method scales the flux by the ratio of the irradiation time to the operation time.

For a single, stable isotope that reacts to form a second, radioactive isotope, Sisolak, Spangler, and Henderson developed analytic expressions for the ratio of the approximate inventory, computed with steady-state assumptions, to the actual inventory of the second isotope. Equations 5.1.1 and 5.1.2 give the ratios for the SS and ESS methods, respectively [7]. An ideal approximation to the actual, pulsed irradiation history would yield a ratio of one.

$$\frac{N_{2_{ss}}}{N_{2_p}} = \left[\frac{e^{-n\sigma\phi_p\theta} - e^{-n\lambda\theta}}{e^{-\sigma\phi_p\theta} - e^{-\lambda\theta}}\right] \times \left[\frac{e^{-\sigma\phi_p\theta} - e^{-\lambda(\theta+\Delta)}}{e^{-n\sigma\phi_p\theta} - e^{-n\lambda(\theta+\Delta)}}\right] \qquad (5.1.1)$$

$$\frac{N_{2_{ess}}}{N_{2_p}} \approx \frac{(\lambda - \sigma\phi_p)\theta}{(\theta+\Delta)\lambda - \sigma\phi_p\theta} \times \left[\frac{e^{-\sigma\phi_p\theta} - e^{-\lambda(\theta+\Delta)}}{e^{-\sigma\phi_p\theta} - e^{-\lambda\theta}}\right] \qquad (5.1.2)$$

where:

λ = decay constant (s^{-1});

σ = cross section (cm^{-2});

ϕ_p = pulsed neutron flux (n/cm^2–s);

θ = irradiation time (s);

Δ = time between pulses (s); and

n = number of pulses (dimensionless).

Sisolak, Spangler, and Henderson applied Equations 5.1.1 and 5.1.2 to estimates of the conditions likely to be encountered in future MFE and IFE *experimental facilities*. Here, the parameters used are different because the equations are applied to MFE and IFE *power plants*, using reasonable estimates of the operating conditions that might be experienced.

For an MFE tokamak power plant operating at 3000 MW of fusion power with a 5 m major radius and a 2 m minor radius, the neutron flux incident upon the first wall would be about 3×10^{14} n/cm^2–s. For an IFE power plant with a 3-m-radius spherical chamber and a 1 μs

pulse length, the first-wall flux would be 1.9×10^{20} n/cm^2–s for an IFE power plant. These fluxes may be used in Equations 5.1.1 and 5.1.2 to determine the suitability of the SS and ESS methods when applied to IFE and MFE power plants.

Figure 5.1.1 shows that both the SS and ESS approximations yield acceptable results when used to calculate activation for MFE power plant conditions. The ESS approximation does not perform as well as the SS method. The ESS method underestimates the activities of radionuclides with half-lives less than several times the dwell time of 5 minutes. The SS method slightly overestimates the activities of radionuclides with half-lives between several hours and several years.

Figure 5.1.2 indicates that the SS method is ill-suited for use in IFE calculations. This method leads to large overestimation of the activities of radionuclides with half-lives between 1 μs and several years. Because the SS method conserves the total irradiation time, and a typical IFE power plant would experience only 80 minutes of irradiation time during 30 years of operation, the failure of the SS method under IFE power plant conditions is not surprising.

Figure 5.1.1. Both the SS and ESS approximations are sufficiently accurate for use in MFE activation calculations.

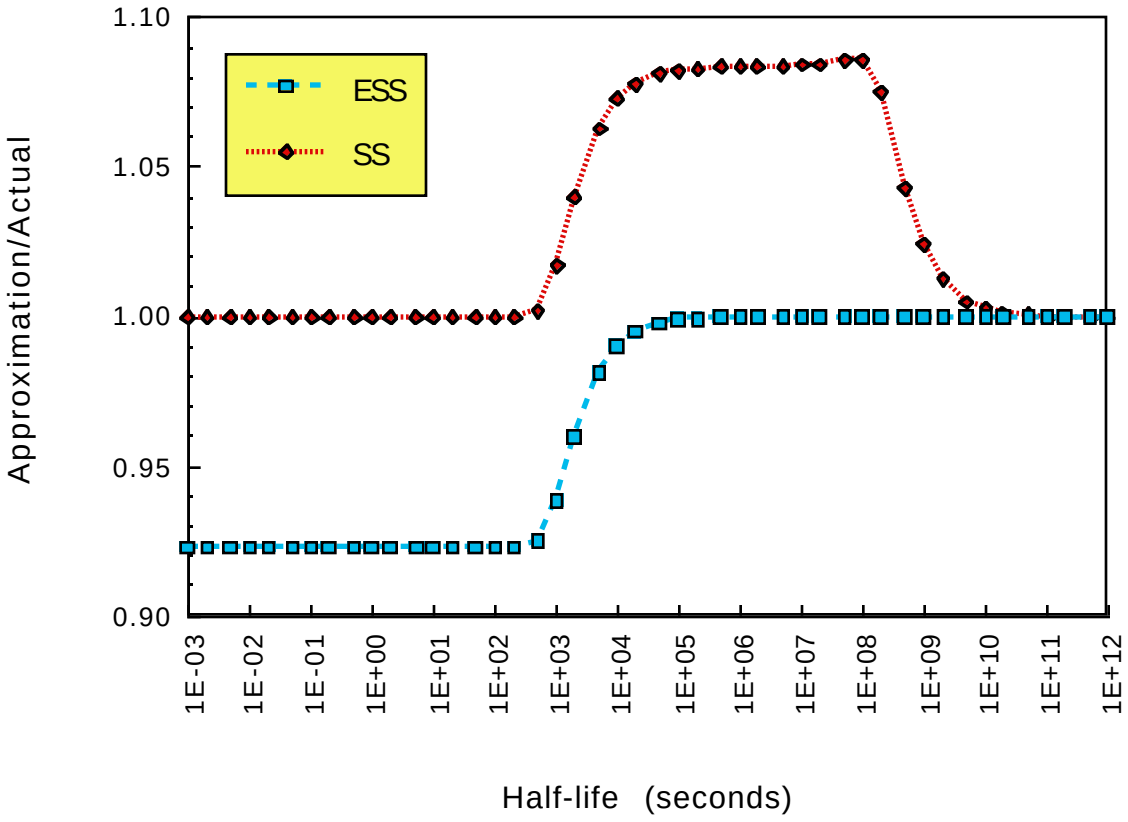

Figure 5.1.3 shows results of the application of the ESS method to conditions which might be experienced in an IFE power plant. The ESS method yields accurate results for radionuclides with half-lives greater than several times the dwell time of 200 ms. Fortunately, it is only these radionuclides that are of concern for occupational and accident analyses.

Figure 5.1.2. The SS approximation yields unacceptably inaccurate results when used to calculate the activation in an IFE power plant.

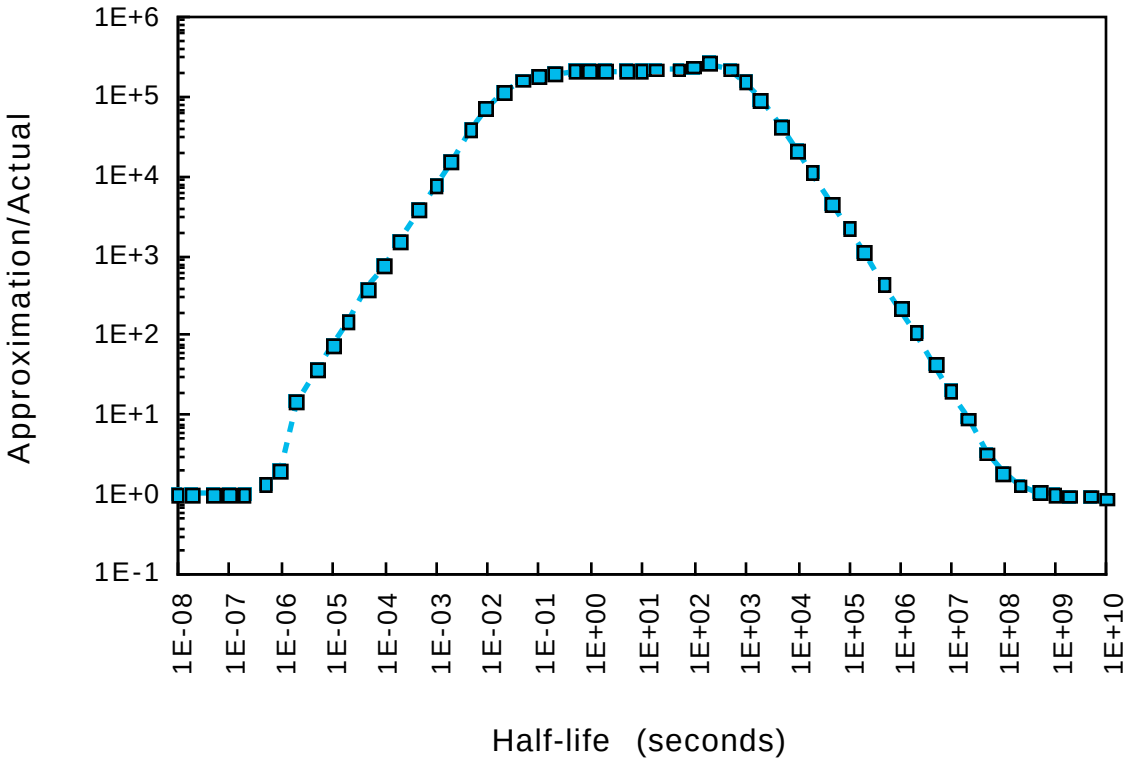

It should be noted, however, that it is possible for the ESS method to underestimate key radionuclides in situations in which a short-lived intermediate radionuclide reacts to form a longer-lived "bad actor" radionuclide. Since the ESS approximation, as previously shown, underestimates short-lived radionuclides, it would effectively truncate the multi-step reaction chain and, as a result, would lead to underestimation of the longer-lived radionuclide. As of yet, no reaction chains of this type have been identified.

Figure 5.1.3. When applied to conditions that might be found in an IFE power plant, the ESS approximation gives reasonable results for radionuclides with half-lives greater than 1 second.

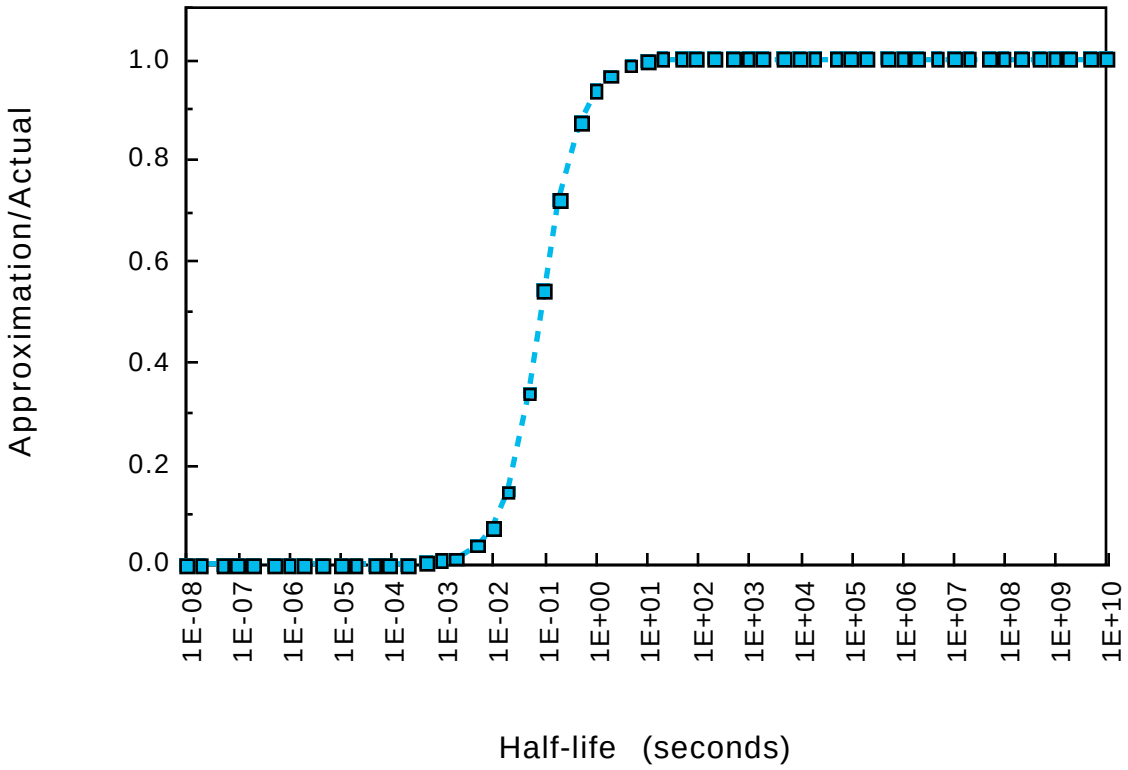

5.2 Calculations for complicated reaction chains

The equations derived by Sisolak, Spangler, and Henderson apply only to a single, stable nuclide that reacts to a single, radioactive daughter. Unfortunately, complicated reaction and decay schemes cannot be analyzed so easily. In order to address more complicated reaction chains and determine the suitability of the ESS method for real activation problems, four example calculations have been

performed with the ACAB activation code. The first two calculations were performed for fixed components such as the first wall or other structural materials that would be irradiated at repetition rates of between 1 Hz and 5 Hz. The final two calculations were performed for coolant and target materials. Circulating coolant would probably be irradiated at a repetition rate near 0.05 Hz. High-Z target materials, if recycled on a weekly basis (as recommended in several IFE power plant design studies), would be irradiated at approximately 1.7×10^{-6} Hz [4,6,8].

5.2.1 Irradiation of fixed components

First-wall structural activation calculations have been performed for several operation times ranging from 1 hour to 1 year. For each operation time, calculations were performed for 1 Hz and 5 Hz irradiation. At each frequency, two calculations have been completed. The first used the ESS method, and the second modeled the pulsed irradiation exactly. A comparison of the results has been made to determine whether or not use of the ESS method is justified under IFE irradiation conditions.

Modeling the exact irradiation history would be prohibitively expensive for most production calculations. Computing times for the exact pulsed irradiation at 1 Hz operation are approximately 5% of the operation time that is to be modeled. That is, in order to simulate 1 hour of pulsed irradiation, about 3 minutes of CPU time was required. The simulation of 1 year of operation for 5 Hz irradiation required nearly 2000 hours of CPU time. The computing times for the ESS approximation, on the other hand, are short -- less than 10 seconds for all cases. Thus, there is a clear rationale for use of the ESS method.

Table 5.2.1 gives results for the 1 Hz irradiation of pure ^{56}Fe for an operation time of 1 hour (3600 pulses). Table 5.2.2 gives the results for an operation time of 1 year (3.2×10^7 pulses). Both tables list all radionuclides with half-lives greater than 1 second and shutdown activities (in the pulsed irradiation case) in excess of 3.7×10^4 Bq (1 μCi). Radionuclides whose ESS and pulsed activities differ by more than 5% are highlighted in bold print. These tables show that the ESS approximation provides a very good estimate of the radionuclide inventories. In fact, only a single radionuclide, ^{50}Sc, was not estimated to within 5% after 1 hour of operation. The ESS

Table 5.2.1. Activities after 1 hour of pulsed irradiation of ^{56}Fe at a repetition rate of 1 Hz. Radionuclides with half-lives ≥ 1 s and shutdown activities ≥ 3.7×10^4 Bq are included. Results that differ by more than 5% are highlighted in bold print.

Nuclide	Half-life (s)	Pulsed Activity (Bq)	Ratio: ESS/Pulsed SHUTDOWN	1 hour
H 3	3.88E+08	4.01E+12	1.0000	1.0000
SC 47	2.89E+05	3.78E+04	1.0000	1.0000
SC 49	3.44E+03	3.85E+05	1.0000	1.0000
SC 50	**1.03E+02**	**2.85E+05**	**1.0840**	**1.0840**
TI 51	3.46E+02	2.67E+12	0.9989	0.9990
TI 52	1.02E+02	2.30E+07	1.0395	1.0395
V 52	2.26E+02	8.90E+10	0.9985	0.9985
V 53	9.66E+01	7.39E+11	1.0367	1.0365
V 54	4.98E+01	1.42E+12	1.0133	1.0138
CR 51	2.39E+06	1.06E+08	1.0000	1.0000
CR 55	2.10E+02	3.25E+18	0.9985	0.9981
MN 52M	1.27E+03	1.87E+06	0.9995	0.9996
MN 54	2.70E+07	4.43E+14	1.0000	1.0000
MN 56	9.28E+03	1.55E+16	1.0000	1.0000
FE 55	8.61E+07	2.47E+12	1.0000	1.0000

method calculated the shutdown activities of all radionuclides (with half-lives greater than 1 second and shutdown activities greater than 3.7×10^4 Bq) to within 5% of the pulsed results for 1 year of operation.

Tables 5.2.3 and 5.2.4 give similar results for the 5 Hz irradiation of natural iron. Once again, the ratios of the ESS-calculated shutdown activity to the actual, pulsed activity are given for all radionuclides with half-lives greater than 1 second and shutdown activities greater than 3.7×10^4 Bq (1 μCi). The ESS method again yields excellent results. The results of these

Table 5.2.2. Activities after 1 year of pulsed irradiation of ^{56}Fe at a repetition rate of 1 Hz. Radionuclides with half-lives ≥ 1 s and shutdown activities ≥ 3.7×10^4 Bq are included. The ESS and pulsed results agree to within 5% for all radionuclides.

Nuclide	Half-life (s)	Pulsed Activity (Bq)	Ratio: ESS/Pulsed	
			SHUTDOWN	1 hour
H 3	3.88E+08	3.41E+16	1.0000	1.0000
S 37	3.03E+02	1.39E+06	1.0022	1.0021
CL 38	2.23E+03	5.88E+07	1.0010	1.0010
CL 39	3.34E+03	1.66E+06	1.0084	1.0087
CL 40	8.28E+01	2.48E+06	0.9996	0.9990
AR 37	3.02E+06	4.43E+04	1.0032	1.0032
AR 39	8.48E+09	1.82E+05	1.0225	1.0225
AR 41	6.55E+03	2.37E+11	1.0008	1.0006
AR 42	1.04E+09	2.29E+06	1.0092	1.0092
AR 43	3.24E+02	4.50E+07	1.0300	1.0299
AR 44	7.12E+02	9.70E+07	1.0355	1.0360
AR 45	2.15E+01	1.44E+06	0.9840	N/A
K 42	4.45E+04	1.83E+10	1.0066	1.0069
K 43	8.03E+04	2.53E+11	1.0107	1.0106
K 44	1.33E+03	4.14E+11	1.0002	1.0003
K 45	1.07E+03	8.04E+09	0.9999	1.0000
K 46	1.08E+02	1.28E+08	1.0305	1.0299
K 47	1.75E+01	1.42E+08	1.0162	N/A
K 48	6.80E+00	2.19E+06	0.9508	N/A
CA 45	1.41E+07	1.66E+12	1.0000	1.0000
CA 47	3.92E+05	8.78E+13	1.0362	1.0363
CA 49	5.23E+02	6.20E+09	0.9994	0.9994
SC 43	1.40E+04	3.37E+05	1.0416	1.0415
SC 44	1.41E+04	3.47E+10	1.0104	1.0116
SC 44M	2.11E+05	6.95E+09	1.0391	1.0392
SC 46	7.24E+06	6.86E+14	1.0000	1.0001
SC 46M	1.87E+01	2.23E+12	0.9861	N/A
SC 47	2.89E+05	1.14E+15	1.0299	1.0302
SC 48	1.57E+05	2.46E+12	1.0155	1.0153
SC 49	3.44E+03	1.23E+14	1.0000	1.0002
SC 50	1.03E+02	2.51E+13	0.9964	0.9966
TI 45	1.11E+04	6.38E+10	1.0017	1.0018
TI 51	3.46E+02	2.68E+16	0.9993	0.9990
TI 52	1.02E+02	1.67E+13	0.9964	0.9967
V 48	1.38E+06	2.52E+10	1.1952	1.1951
V 49	2.91E+07	5.96E+13	1.0000	1.0000
V 52	2.26E+02	1.40E+15	0.9986	0.9986
V 53	9.66E+01	5.47E+15	0.9963	0.9964
V 54	4.98E+01	1.28E+16	0.9929	0.9932

Table 5.2.2. (Continued.)

CR 51	2.39E+06	1.90E+15	1.0000	1.0000
CR 55	2.10E+02	3.20E+18	0.9984	0.9981
MN 51	2.77E+03	3.55E+07	1.0448	1.0451
MN 52	4.83E+05	5.81E+12	1.0449	1.0449
MN 52M	1.27E+03	3.44E+14	0.9997	0.9998
MN 53	1.17E+14	2.92E+10	1.0000	1.0000
MN 54	2.70E+07	2.61E+18	1.0000	1.0000
MN 56	9.28E+03	6.48E+16	1.0000	1.0000
FE 53	5.11E+02	2.76E+06	1.0004	0.9997
FE 53M	1.56E+02	2.77E+06	0.9978	0.9976
FE 55	8.61E+07	1.87E+16	1.0000	1.0000

calculations confirm that the ESS approximation, when applied to typical IFE power plant conditions, gives a very good estimate of the radionuclide activities after irradiation.

The ESS approximation appears to give sufficiently accurate results for the irradiation of fixed materials under typical IFE conditions. Pulsed irradiation from 1 to 5 Hz was modeled, but the results suggest that the observed trends would continue to repetition rates of 10 Hz or more, which might be experienced in some IFE power plant designs. Example calculations for 10 Hz pulsed irradiation have not been performed due to their prohibitively large computation times and expense.

Analysis of the SS approximation as it might be applied under typical MFE conditions yielded accurate, yet conservative results. Therefore, the radionuclide inventories for all fixed components will

be calculated using the ESS approximation for IFE power plants and the SS approximation for MFE power plants. The suitability of the ESS method for activation calculations of non-fixed components is explored in the following section.

Table 5.2.3. Activities after 1 hour of pulsed irradiation of natural iron at a repetition rate of 5 Hz. Radionuclides with half-lives ≥ 1 s and shutdown activities ≥ 3.7×10^4 Bq are included. Results that differ by more than 5% are highlighted in bold print.

Nuclide	Half-life (s)	Pulsed Activity (Bq)	Ratio: ESS/Pulsed	
			SHUTDOWN	1 hour
H 3	3.88E+08	3.04E+12	0.9989	0.9989
SC 49	3.44E+03	2.30E+05	0.9966	0.9966
SC 50	**1.03E+02**	**1.85E+05**	**1.0830**	**1.0830**
TI 51	3.46E+02	1.69E+12	0.9976	0.9975
TI 52	1.02E+02	4.24E+10	1.0396	1.0396
V 48	1.38E+06	6.20E+08	0.9977	0.9977
V 49	2.91E+07	1.10E+07	0.9979	0.9979
V 52	2.26E+02	4.89E+11	0.9939	0.9970
V 53	9.66E+01	4.69E+11	1.0372	1.0372
V 54	4.98E+01	8.99E+11	1.0171	1.0171
CR 51	2.39E+06	1.03E+10	0.9986	0.9986
CR 55	2.10E+02	2.20E+18	0.9985	0.9986
CR 56	3.54E+02	4.33E+16	0.9987	0.9987
CR 57	2.10E+01	3.87E+15	0.9956	N/A
MN 51	2.77E+03	2.28E+10	0.9977	0.9977
MN 52	4.83E+05	1.16E+16	0.9989	0.9989
MN 52M	1.27E+03	3.32E+11	0.9983	0.9983
MN 53	1.17E+14	2.87E+07	0.9990	0.9990
MN 54	2.70E+07	3.00E+14	0.9989	0.9989
MN 56	9.28E+03	3.99E+16	0.9989	0.9989
MN 57	8.70E+01	5.60E+15	0.9987	0.9982
MN 58	6.50E+01	1.54E+14	0.9978	0.9978
MN 58M	3.00E+00	1.38E+15	0.9761	N/A
FE 53	**5.11E+02**	**4.98E+15**	**0.9261**	**0.9477**
FE 53M	1.56E+02	5.04E+15	0.9992	0.9992
FE 55	8.61E+07	3.06E+13	0.9989	0.9989

Table 5.2.4. Results for 1 hour irradiation of natural iron at 5 Hz. Radionuclides with half-lives ≥ 1 s and activities ≥ 3.7×10^4 Bq (1 μCi) are included. The ESS and pulsed results lie within 5% for all radionuclides.

Nuclide	Half-life (s)	Pulsed Activity (Bq)	Ratio: ESS/Pulsed	
			SHUTDOWN	1 hour
H 3	3.88E+08	2.59E+16	0.9989	0.9989
S 37	3.03E+02	8.01E+05	1.0005	1.0005
S 39	1.15E+01	1.22E+05	0.9888	N/A
CL 38	2.23E+03	3.43E+07	0.9984	0.9984
CL 39	3.34E+03	1.10E+06	1.0044	1.0044
CL 40	8.28E+01	1.42E+06	1.0004	1.0004
CL 41	3.40E+01	1.05E+05	0.9931	0.9931
CL 42	6.80E+00	1.49E+05	0.9847	N/A
AR 39	8.48E+09	1.13E+05	1.0195	1.0195
AR 41	6.59E+03	1.46E+11	0.9989	0.9989
AR 42	1.04E+09	3.47E+07	0.9959	0.9959
AR 43	3.24E+02	2.75E+07	1.0291	1.0291
AR 44	7.12E+02	5.98E+07	1.0335	1.0335
AR 45	2.15E+01	2.71E+07	0.9923	N/A
K 42	4.45E+04	2.64E+10	1.0031	1.0031
K 43	8.03E+04	1.51E+11	1.0080	1.0080
K 44	1.33E+03	2.58E+11	0.9986	0.9986
K 45	1.07E+03	1.24E+10	0.9960	0.9960
K 46	1.08E+02	7.85E+07	1.0307	1.0307
K 47	1.75E+01	1.00E+08	1.0240	N/A
K 48	6.80E+00	4.02E+07	0.9854	N/A
CA 45	1.41E+07	2.95E+13	0.9967	0.9966
CA 47	3.92E+05	5.77E+13	1.0347	1.0347
CA 49	5.23E+02	4.43E+09	0.9981	0.9981
SC 44	1.41E+04	1.27E+11	0.9932	0.9951
SC 44M	2.11E+05	3.80E+10	1.0283	1.0283
SC 46	7.24E+06	4.28E+14	0.9977	0.9977
SC 46M	1.87E+01	1.95E+12	0.9968	N/A
SC 47	2.89E+05	8.20E+14	1.0282	1.0282
SC 48	1.57E+05	5.68E+12	1.0119	1.0119
SC 49	3.44E+03	7.69E+13	0.9977	0.9977
SC 50	1.03E+02	1.87E+13	0.9977	0.9977
TI 45	1.11E+04	3.73E+10	0.9986	0.9986
TI 51	3.46E+02	1.87E+16	0.9976	0.9976
TI 52	1.02E+02	3.86E+14	0.9971	0.9971
V 48	1.38E+06	1.32E+14	0.9368	0.9368
V 49	2.91E+07	6.90E+14	0.9977	0.9977
V 52	2.26E+02	5.02E+15	0.9974	0.9974
V 53	9.66E+01	3.48E+15	0.9971	0.9971

Table 5.2.4. (Continued.)

V 54	4.98E+01	8.16E+15	0.9964	0.9964
CR 51	2.39E+06	1.33E+16	0.9960	0.9960
CR 55	2.10E+02	2.16E+18	0.9986	0.9986
CR 56	3.54E+02	4.24E+16	0.9987	0.9987
CR 57	2.10E+01	3.79E+15	0.9956	N/A
MN 51	2.77E+03	1.26E+13	0.9978	0.9978
MN 52	4.83E+05	2.20E+18	0.9989	0.9989
MN 52M	1.27E+03	2.93E+15	0.9977	0.9977
MN 53	1.17E+14	2.65E+11	0.9988	0.9988
MN 54	2.70E+07	1.77E+18	0.9989	0.9989
MN 56	9.28E+03	1.71E+17	0.9989	0.9989
MN 57	8.70E+01	5.49E+15	0.9987	0.9982
MN 58	6.50E+01	1.51E+14	0.9978	0.9978
MN 58M	3.00E+00	1.35E+15	0.9762	N/A
FE 53	5.11E+02	4.90E+15	0.9989	0.9988
FE 53M	1.56E+02	4.90E+15	0.9984	0.9984
FE 55	8.61E+07	2.32E+17	0.9989	0.9989

5.2.2 Irradiation of mobile components

The final two sets of calculations were performed to determine whether or not the ESS approximation yields satisfactory results when applied to materials that are irradiated on a less-frequent basis. Examples of such materials include the coolant and the high-Z hohlraum. These materials might be irradiated at repetition rates on the order of 0.05 and 1.7×10^{-6} Hz, respectively. The repetition rate is low for the coolant because it circulates throughout the primary heat-transfer loop. About every 20 seconds, the coolant returns to the target chamber and is reirradiated. For the high-Z target materials, many IFE power plant designs plan only weekly

irradiation [4,6,8]. Each plant would have a single week's worth of target materials. This weekly inventory would be continuously refabricated into the next batch of targets. Thus, an average control volume of high-Z target material would be irradiated once per week.

Two calculations were performed to analyze the impact of using the ESS approximation to obtain the radionuclide inventories in the coolant. The first calculation used the actual, pulsed irradiation history in which a control volume of coolant was irradiated for 1 μs every 20 seconds. The second calculation assumed that the coolant was irradiated continuously at a scaled flux.

The ratio of the two results is presented in Figure 5.2.1 as a function of radionuclide half-life. These results suggest that the ESS method provides a reasonable estimate of the induced activity in a material that is irradiated at 0.05 Hz. When calculated with the ESS method, the inventories of radionuclides with half-lives greater than two to three times the 20-second dwell time are within 5 to 10% of the actual inventories. While the inventories of shorter-lived radionuclides are not calculated accurately (nor conservatively) with the ESS method, such short-lived isotopes do not make a significant contribution to accident doses. It should be noted,

however, that some of these radionuclides may, in fact, make a significant contribution to the occupational dose rates experienced during routine plant operations. Despite this possible disadvantage, the ESS approximation will be used for all coolant activation calculations.

Figure 5.2.1. As was seen for fixed components, the ESS method provides an accurate estimate of the activity for radionuclides with half-lives greater than two to three times the dwell time.

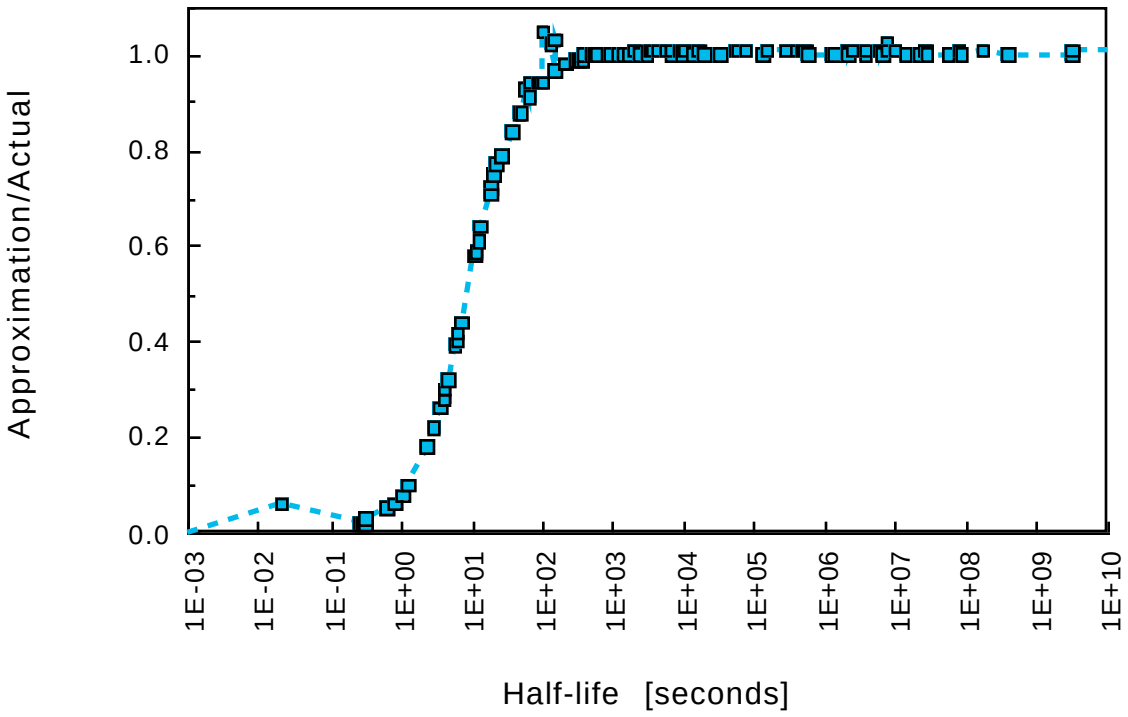

The final calculations were performed to evaluate the application of the ESS method to high-Z target materials that are

irradiated only once per week throughout the lifetime of the power plant. In the first calculation, activation products for tantalum, tungsten, mercury, and lead hohlraums were calculated using the actual, pulsed irradiation history (one irradiation per week for 30 years). The second calculation assumed continuous irradiation with a flux that was scaled by the ratio of the actual irradiation time (assumed at 1 μs per shot) to the operation time -- a factor of 1.7×10^{-12}.

The ratio of the ESS activity to the actual activity is plotted in Figure 5.2.2 as a function of radionuclide half-life. Once again, activities of radionuclides with half-lives more than two to three times greater than the dwell time are accurately estimated when the ESS method is used. Unfortunately, since the dwell time is one week, the inventories of radionuclides with half-lives of minutes, hours, and days are not accurately estimated. Since these are the very radionuclides that ordinarily dominate accident and routine exposures, the ESS method should not be used for high-Z target material activation. Fortunately, since target material would be irradiated only once per week, pulsed irradiation calculations require only 1560 individual pulses. Such a small number of pulses

can be easily modeled with current computing systems. All activation calculations performed for the high-Z target materials will use the actual, pulsed irradiation history.

Figure 5.2.2. Calculation of the activation of high-Z target materials using the ESS approximation gives accurate results for radionuclides with half-lives that are two to three times that of the dwell time. With a dwell time of 1 week, however, the ESS approximation cannot be used for high-Z target activation.

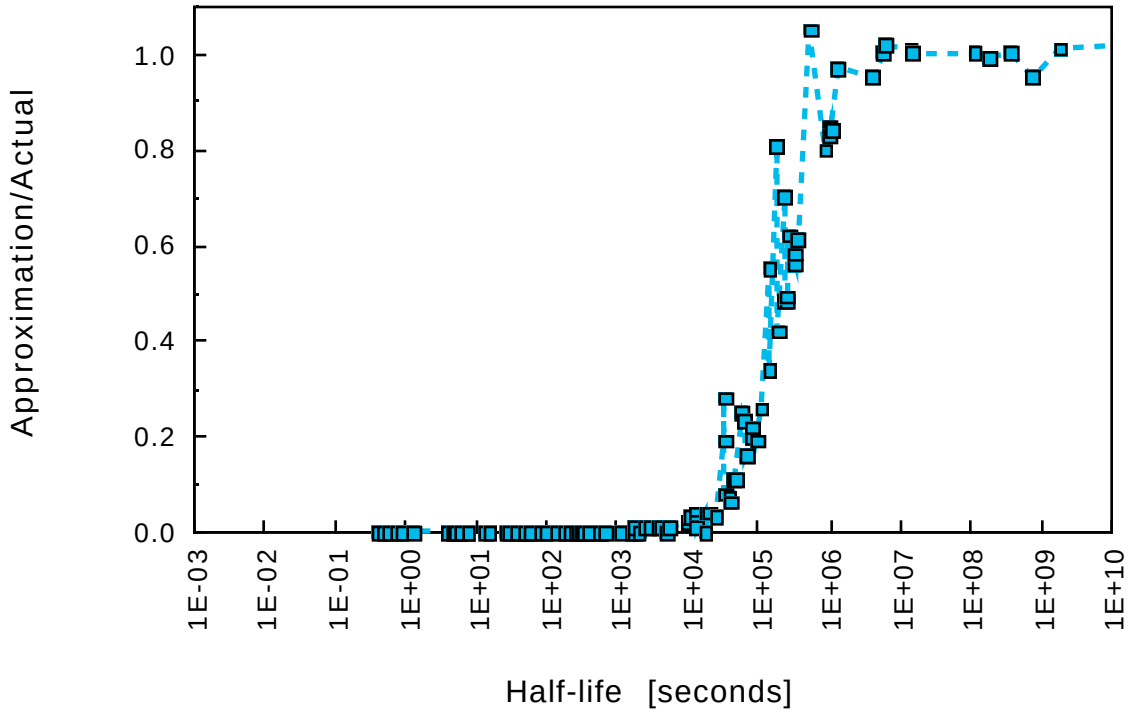

5.3 Routine and unplanned maintenance

The above analyses have shown that the ESS method is sufficiently accurate for modeling the pulsed irradiation inherent to

IFE power plants. Similarly, the SS approximation is useful in activation calculations under likely MFE conditions. Power plants, however, will often be brought down for periods of planned and unplanned maintenance. Neither approximation can account for these extended times during which no irradiation occurs. In addition, it is difficult to accurately predict the frequency or duration of maintenance operations for fusion power plant systems when many of these systems have never been constructed.

Two methods for compensating for shutdown periods have been used in the past. The first method, used traditionally, is simply to scale the neutron flux by the expected power plant capacity factor. This approach, however, underestimates short-lived radionuclides, which tend to dominate the doses in most accident scenarios. This approach would be nonconservative, and thus, will not be used in the present work.

The second approach uses a combination of the ESS method and pulsed irradiation. It was first used in activation calculations performed for the SOMBRERO and Osiris IFE power plant designs [8]. In the Osiris/SOMBRERO calculations, the predicted power plant availability of 75% was modeled using an assumption that the power

plant would operate continuously (100% capacity) for 25 days each month. At the end of each month, it was assumed that the plant would be shutdown for 5 days for routine maintenance. This sequence was repeated for 11 months, after which the plant was assumed to be shutdown for an additional 35 days for extended annual maintenance. During times of continuous operation, the ESS method was employed.

It is the author's opinion that little can be gained from this mixed approach. The combination of the ESS method with pulsed irradiation requires critical assumptions about the operation of fusion power plants that cannot be made at this time.

All activation calculations performed for this work assume that irradiation occurs at 100% capacity for either the component life-time or for 30 full–power–years of operation.

References for Chapter 5

1. E. T. Cheng, R. A. Forrest, and A. Pashchenko, “Report on the Second International Activation Calculation Benchmark Comparison Study,” TSI Research Report TSIR-21 FINAL Draft, (November 1993).
2. D. L. Smith, C. C. Baker, D. K. Sze, G. D. Morgan, M. A. Abdou, S. J. Piet, K. R. Schultz, R. W. Moir, and J. D. Gordon, “Overview of the Blanket Comparison and Selection Study,” *Fusion Technology*, **8**, 10, (1985).
3. J. P. Holdren, D. H. Berwald, R. J. Budnitz, J. G. Crocker, J. G. Delene, R. D. Endicott, M. S. Kazimi, R. A. Krakowski, B. G. Logan, and K. R. Schultz, “Report of the Senior Committee on Environmental, Safety, and Economic Aspects of Magnetic Fusion Energy,” Lawrence Livermore National Laboratory, UCRL-53766, (September 1989).
4. J. H. Pitts, R. F. Bourque, W. J. Hogan, W. R. Meier, and M. T. Tobin, “The Cascade Inertial Confinement Fusion Reactor Concept,” Lawrence Livermore National Laboratory, UCRL-LR-104546, (December 1990).

5. J. D. Lee, ed., “TIBER II/ETR: Final Design Report,” Lawrence Livermore National Laboratory, UCID-21150, (September 1987).

6. R. W. Moir, M. G. Adamson, R. O. Bangter, R. L. Bieri, R. H. Condit, C. W. Hartman, P. A. House, A. B. Langdon, B. G. Logan, C. D. Orth, R. W. Petzoldt, J. H. Pitts, R. F. Post, R. A. Sacks, M. T. Tobin, W. H. Williams, T. J. Dolan, G. R. Longhurst, M. A. Hoffman, V. E. Schrock, P. F. Peterson, R. Y. Bai, X. M. Chen, J. C. Liu, D.-K. Sze, and W. R. Meier, “HYLIFE-II Progress Report,” Lawrence Livermore National Laboratory, UCID-21816, (December 1991).

7. J. E. Sisolak, S. E. Spangler, and D. L. Henderson, “Pulsed/ Intermittent Activation in Fusion Energy Reactor Systems,” *Fusion Technology*, **21**, 2145, (May 1992).

8. W. R. Meier, R. L. Bieri, M. J. Monsler, C. D. Hendricks, P. Laybourne, K. R. Shillito, S. K. Ghose, L. M. Goldman, K. D. Auclair, C. Y. Pang, R. F. Bourque, L. D. Stewart, E. E. Bowles, E. L. Hubbard, C. W. von Rosenberg, Jr., M. W. McGeoch, I. N. Sviatoslavsky, R. R. Peterson, M. E. Sawan, H. Y. Khater, L. J. Wittenberg, G. L. Kulcinski, G. A. Moses, E. A. Mogahed, J. J. MacFarlane, S. Rutledge, S. Humphries, Jr., and E. T. Cheng, “Osiris and SOMBRERO Inertial

Confinement Fusion Power Plant Designs," DOE/ER/54100-1, WJSA-92-01, W. J. Schafer Associates, Inc., Livermore, CA, (March 1992).

6. Effects of sequential charged-particle reactions

For fusion power plants, (x,n) reactions may be of particular importance in tritium-breeding materials. By design, such materials must produce, on the average, more than one triton and one alpha particle per fusion reaction (a breeding ratio in excess of one is required to compensate for losses). Due to the large charged-particle fluxes generated in tritium-breeding materials, it seems likely that sequential charged-particle reactions may have a significant effect upon isotopic inventories.

In the HYLIFE-II and Osiris power plant designs, liquid Flibe is used as the coolant, the first-wall protection scheme, and tritium breeding material [1,2]. Flibe is typically considered a low- to medium-activation material [1,2,3,4]. This is because the only radiologically significant radionuclide produced from pure Flibe is ^{18}F, which decays with a 110 minute half-life. The only long-lived radioisotope produced in pure Flibe has been thought to be ^{10}Be. With a half-life of 1.6 million years, no energetic decay radiation, and a low production cross section, ^{10}Be does not present a significant radiological hazard. Previous studies, however, did not consider (x,n) reactions in their analyses.

Since Flibe is used for tritium breeding, many tritons and alpha particles will be generated. The alpha particles, although they stop in the remaining Flibe, have an opportunity to react with fluorine via the $^{19}F(\alpha,n)^{22}Na$ reaction (the reaction has a 2.36 MeV threshold). Since ^{22}Na has a 2.6 year half-life and emits 1.3 MeV γ-rays, the production of large amounts of ^{22}Na could significantly affect the radiological hazard posed by Flibe.

For clarity, it should be noted that ^{22}Na may, in fact, be produced in pure Flibe. Production in pure Flibe, however, is possible only via a multi-step reaction/decay chain. The dominant chain for the neutron reaction production of ^{22}Na is:

$$^{19}F(n,\gamma)^{20}F\ (\beta^-)\ ^{20}Ne(n,\gamma)^{21}Ne(n,\gamma)^{22}Ne(n,\gamma)^{23}Ne\ (\beta^-)\ ^{23}Na(n,2n)^{22}Na$$

Two calculations have been performed to demonstrate the importance of sequential charged-particle reactions in the activation of Flibe. The first calculation was performed for pure Flibe. The second calculation included Flibe's likely impurities. Each calculation was performed with and without (x,n) reactions. Both calculations utilized neutron spectra generated for the Flibe in a one-dimensional model of the HYLIFE-II power plant. The neutron

flux was scaled by a factor of 2.15×10^{-2} (using the ESS method) to account for the fraction of the total Flibe inventory (1240 m^3) that would be in the chamber at any given time. A 30-year operation time was used.

Figure 6.1.1 gives the contact dose rate as a function of time after shutdown resulting from a semi-infinite media that contains radionuclides at the concentrations calculated for the finite medium. The figure shows that neglect of potential (x,n) reactions can lead to severe underestimation of contact dose rates at shutdown times when maintenance and decommissioning would most likely be performed.

The large difference in the contact dose rates is due mostly to direct production of ^{22}Na via the $^{19}F(\alpha,n)$ reaction rather than by the 7-step neutron chain. Despite the small pseudo cross section (only 1.7×10^{-7} barns integrated over the neutron spectrum), ^{22}Na is much more likely to be produced directly than by the 7-step neutron chain. Consideration of the (x,n) reaction leads to a factor of 1.4×10^{14} more ^{22}Na being produced than by the 7-step neutron chain alone. When the (x,n) reaction is included, ^{22}Na reaches an equilibrium

concentration of 1.3 × 10^4 Bq/cc (due to a large ^{22}Na (n,p) ^{22}Ne cross section, ^{22}Na reaches equilibrium rapidly).

Figure 6.1.1. Without consideration of sequential charged-particle reactions, the contact dose rate from a semi-infinite medium of Flibe is severely underestimated at times when maintenance would likely take place (days to years). The production of ^{22}Na from ^{19}F(α,n) dominates the difference.

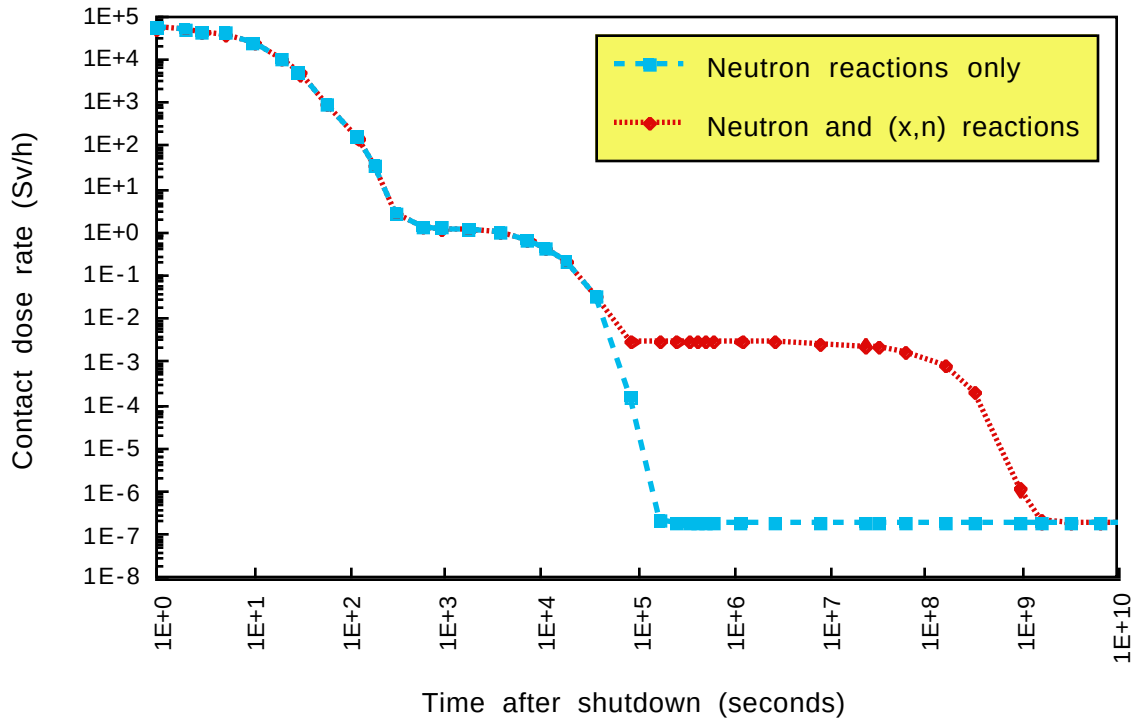

The second set of calculations was done for impure Flibe. The composition used was that suggested by Toma (see Appendix A) with 10 wppm tantalum added (to account for the high-Z target material that becomes an impurity in the Flibe) [5]. As above, the first calculation considered only neutron reactions, while the second also

considered (x,n) reactions. For impure Flibe, the addition of (x,n) reactions makes no difference in the resulting contact dose rate, because the contact dose rate is dominated by radionuclides produced in neutron reactions with Flibe impurities. Figure 6.1.2 shows the contact dose rates predicted from activated pure and impure Flibe, calculated including (x,n) reactions.

Figure 6.1.2. Calculations of the activation of pure and impure Flibe show that the Flibe impurities dominate the contact dose rate from minutes until hundreds of years after irradiation. Both calculations included (x,n) reactions.

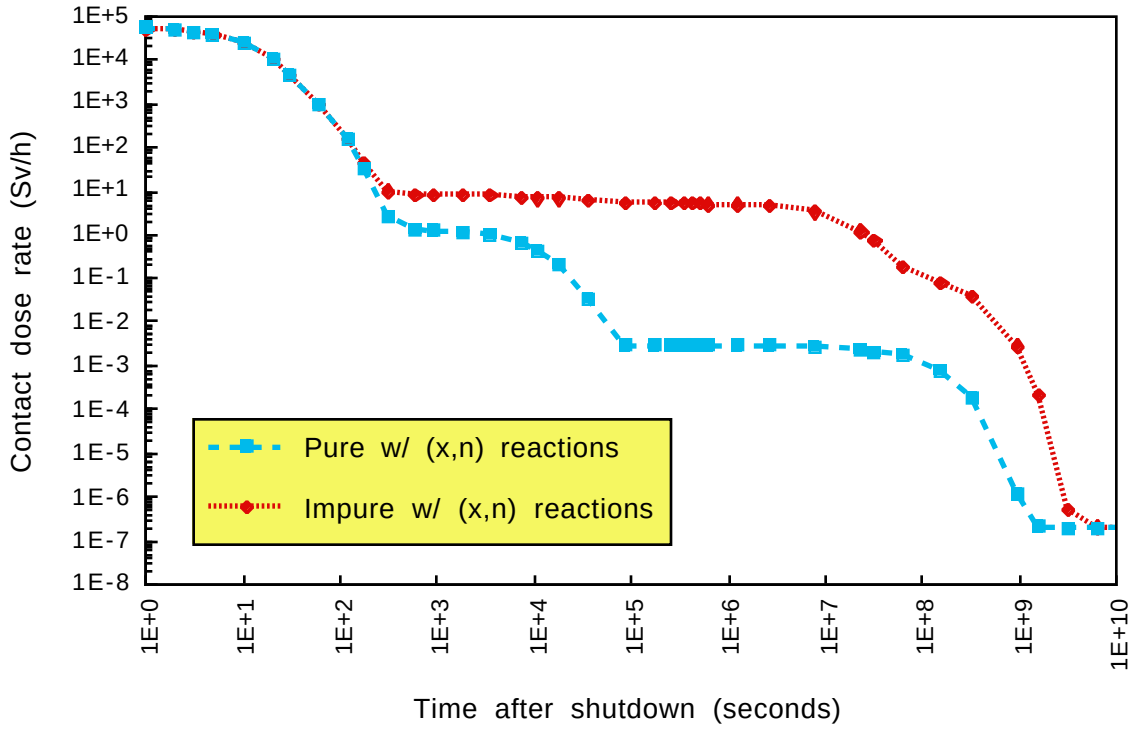

Figure 6.1.3 shows the contact dose rate as a function of time after irradiation for radionuclides that make a significant contribution to the total contact dose rate from impure Flibe. Note that in impure Flibe, ^{22}Na never accounts for more than about 1% of the total contact dose rate. Radionuclides such as ^{182}Ta and ^{60}Co dominate the dose rate at times of more than a few days after shutdown. The ^{24}Na and ^{56}Mn are both larger contributors to the total contact dose rate than is ^{22}Na. The ^{182}Ta is produced from the tantalum target material, and ^{60}Co, ^{24}Na, and ^{56}Mn are produced from the nickel, sodium, and iron impurities, respectively.

Figure 6.1.3. Radionuclides produced in neutron reactions with tantalum, nickel, sodium, and iron impurities dominate the contact dose rate from Flibe.

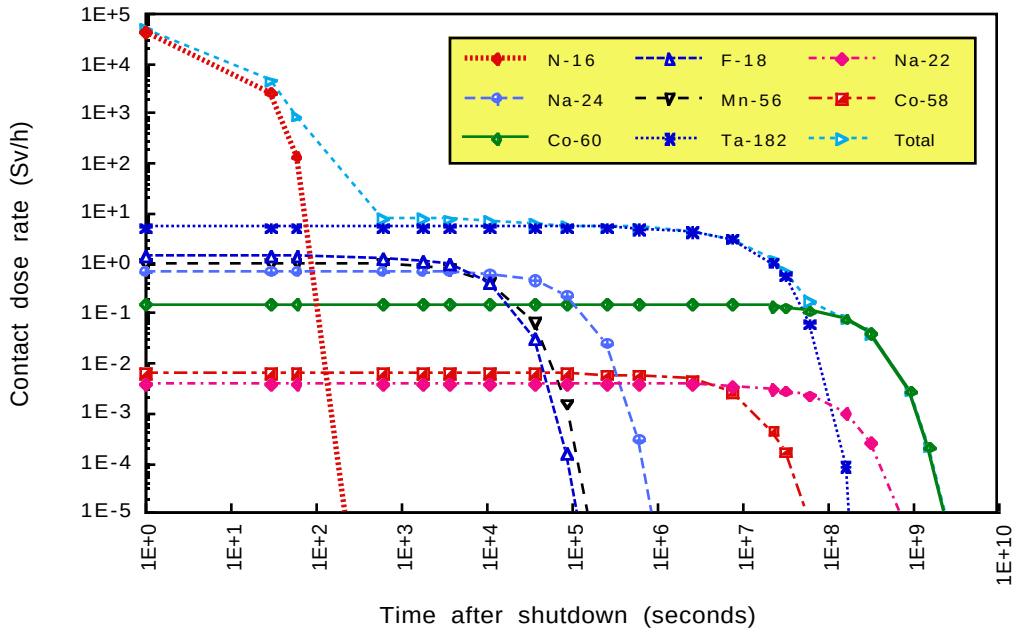

These example calculations show that the relative importance of (x,n) reactions may vary strongly with the composition of materials considered. Recent publications indicate that the importance of (x,n) reactions is not limited to breeding materials [6,7]. It is appropriate to include (x,n) reactions in every calculation until it is possible to identify materials and/or situations in which they are not important. Therefore, all calculations described in the remainder of the present work include contributions from (x,n) reactions.

References for Chapter 6

1. R. W. Moir, “A Review of Inertial Confinement Fusion (ICF), ICF Reactors, and the HYLIFE-II Concept Using Liquid FLiBe,” UCID-21748, Lawrence Livermore National Laboratory, (September 1989).
2. W. R. Meier, R. L. Bieri, M. J. Monsler, C. D. Hendricks, P. Laybourne, K. R. Shillito, S. K. Ghose, L. M. Goldman, K. D. Auclair, C. Y. Pang, R. F. Bourque, L. D. Stewart, E. E. Bowles, E. L. Hubbard, C. W. von Rosenberg, Jr., M. W. McGeoch, I. N. Sviatoslavsky, R. R. Peterson, M. E. Sawan, H. Y. Khater, L. J. Wittenberg, G. L. Kulcinski, G. A. Moses, E. A. Mogahed, J. J. MacFarlane, S. Rutledge, S. Humphries, Jr., and E. T. Cheng, “Osiris and SOMBRERO Inertial Confinement Fusion Power Plant Designs,” DOE/ER/54100-1, WJSA-92-01, W. J. Schafer Associates, Inc., Livermore, CA, (March 1992).
3. J. P. Holdren, D. H. Berwald, R. J. Budnitz, J. G. Crocker, J. G. Delene, R. D. Endicott, M. S. Kazimi, R. A. Krakowski, B. G. Logan, and K. R. Schultz, “Report of the Senior Committee on Environmental, Safety, and Economic Aspects of Magnetic Fusion

Energy," Lawrence Livermore National Laboratory, UCRL-53766, (September 1989).

4. W. J. Hogan, ed., *Energy from Inertial Fusion*, Vienna, Austria: International Atomic Energy Agency, 372, (1995).
5. R. W. Moir, Lawrence Livermore National Laboratory, private communication, (November 1995).
6. S. W. Cierjacks, P. Oblozinsky, S. Kelzenberg, and B. Rzehorz, "Development of a Novel Algorithm and Production of New Nuclear Data Libraries for the Treatment of Sequential (x,n) Reactions in Fusion Material Activation Calculations," *Fusion Technology*, **24**, 277-287, (November 1993).
7. K. Ehrlich, S. W. Cierjacks, S. Kelzenberg, and A. Moslang, "The Development of Structural Materials for Reduced Long-term Activation," *Journal of Nuclear Materials*, **215**, 678-683, (September 1994).

7. Overview of fusion power plant designs

No single design has been, or probably ever will be, universally accepted as the best fusion energy power plant (nor should one necessarily be so accepted). Since one of the purposes of this work is to learn something of the possibilities in the safety and environmental characteristics of IFE, it is prudent to consider a wide variety of design choices. This report makes comparisons not only among the various IFE designs but also between IFE and MFE designs.

The number of designs for which detailed design information is readily available is limited (even the most complete design reports usually fail to give sufficient information to allow repetition of results to take place). Designs published within the last decade are more likely to utilize assumptions consistent with modern target physics. Such designs are also more likely to contain target designs that could not be published previously due to their classification by the DOE. Additionally, more detailed analyses are possible for recent designs due to the relative ease of locating personnel who are familiar with such designs. Thus, the selection of IFE designs is biased towards the more recent undertakings.

In this report, five different IFE designs are analyzed. These designs include a wide variety of possible design features. They include indirect- and direct-drive targets, solid and liquid first-walls, and traditional and advanced structural materials. Although all possible design features and concepts are not represented, many of the most probable features are investigated. It should be noted, however, that the failure to include a particular design concept or feature is not intended to reflect negatively upon the possibility or probability of its future use. The simple fact is that not all possibilities could be considered.

To allow comparisons between IFE and MFE power plant designs to be done on equal footing (a relative comparison can be made only if each design is evaluated in the same manner and to the same degree), two MFE designs have been analyzed using the same methodology used for analysis of the IFE designs. Due to the limited background knowledge of the author, the MFE designs are not presented in as much detail as are their IFE counterparts. Additional details for several MFE designs are given in the ESECOM report and in a subsequent journal article by Kinzig, Holdren, and Hibbard [1,2]. Inclusion of the two MFE cases is intended to highlight key ES&H

advantages and/or disadvantages that are introduced by differences between the two technologies.

7.1 Inertial fusion energy designs

Five different IFE power plant designs have been analyzed. These designs are listed in Table 7.1.1 along with the organization which created the design and the year of initial publication. Descriptions of the major features of each of the designs are given in the sections that follow.

Table 7.1.1 Five IFE power plant designs have been analyzed.

Design name	Principal authoring organization	Date
Cascade	Lawrence Livermore National Laboratory	1983
HYLIFE-II	Lawrence Livermore National Laboratory	1991
Osiris	W. J. Schafer Associates	1992
Prometheus	McDonnell-Douglas Aerospace	1992
SOMBRERO	W. J. Schafer Associates	1992

As previously mentioned, the selection of IFE designs for this report is biased towards more recent designs. The reasons for this include updated target physics understanding and predictions, the recent declassification of many details of the ICF process, and the relative ease of tracking down information and personnel involved

with the various studies. It must be stressed, however, that those designs which have been selected do not necessarily represent all designs which are worthy of further pursuit. The recent IAEA book, *Energy from Inertial Fusion*, gives a comprehensive listing of major IFE power plant studies along with many operational parameters for each design [3]. The reader is encouraged to refer to Table 3.4.1 in the IAEA book.

7.1.1 Reference target design

All but one of the IFE power plant designs that are analyzed would use indirect-drive targets. Indirect-drive targets would rely upon high-Z materials such as tantalum or gold to convert laser or ion energy into x-rays that, in turn, ablate the outer shell of the capsule and cause the implosion to occur. Activation of the high-Z materials can be an significant factor in the safety and environmental characteristics of an IFE power plant design.

For purposes of analysis, a reference indirect-drive target design has been selected. This reference design, with minor modifications, is used for all of the indirect-drive IFE designs that are evaluated in this report. Only the high-Z target material and the

fusion yield are varied from one design to another. The reference target design is a slightly modified version of that presented by Woodworth and Meier and is shown in Figure 7.1.1 [4].

Figure 7.1.1. The major components of the reference IFE target design include the hohlraum, capsule, shield, and radiator [4].

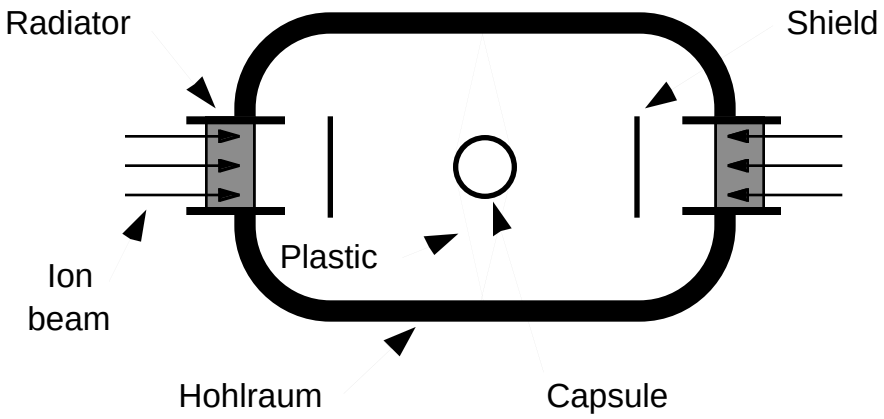

Components of the reference target design include the hohlraum casing, the high-Z hohlraum lining and shields, the helium fill gas, the capsule support system (thin plastic sheets), the radiation converters (for ion drivers only), and the actual capsule. The bulk of the hohlraum would be 1-mm-thick and would most likely be made of a material such as Flibe or metallic lithium. The high-Z hohlraum lining and shields would need to be about 40-μm-thick [5]. Several candidate high-Z materials include tantalum, tungsten, mercury, and

lead [3,4]. The helium fill gas would provide a back pressure, which would slow the migration of high-Z material from the hohlraum walls [5]. The capsule would be supported within the hohlraum by thin plastic sheets, which would need to be strong enough to withstand the large accelerations encountered during target injection [4].

The radiation converters, which would be used only with ion beam drivers, would be encased in high-Z material (20-μm-thick) and would be made of relatively low-Z materials such as beryllium, lithium, or Flibe. The converters would contain a small quantity of high-Z material (approximately 4×10^{-4} atom fraction) [6]. The low-Z material would stop the incident ions, which have energies as high as 10 GeV, and the high-Z material would efficiently reirradiate the absorbed energy as x-rays [6].

Figure 7.1.2 shows the design of a typical fuel capsule. The capsule would consist of three distinct regions: an ablator, the solid DT fuel, and a central region filled with DT gas. The ablator would be vaporized by the energy deposited by x-rays. Because the ablator would be blown away from the fuel surface, it would push against the fuel, causing the fuel to implode. The ablator would be made of

low-Z materials such as plastic or beryllium [4]. A typical IFE capsule would contain approximately 3.9 mg of fuel, of which 2.4 mg would be tritium (assuming that a fifty-fifty mix of deuterium and tritium would be used) [4].

Figure 7.1.2. The reference IFE capsule design would contain approximately 3.9 mg of DT fuel, of which 2.4 mg is tritium [4].

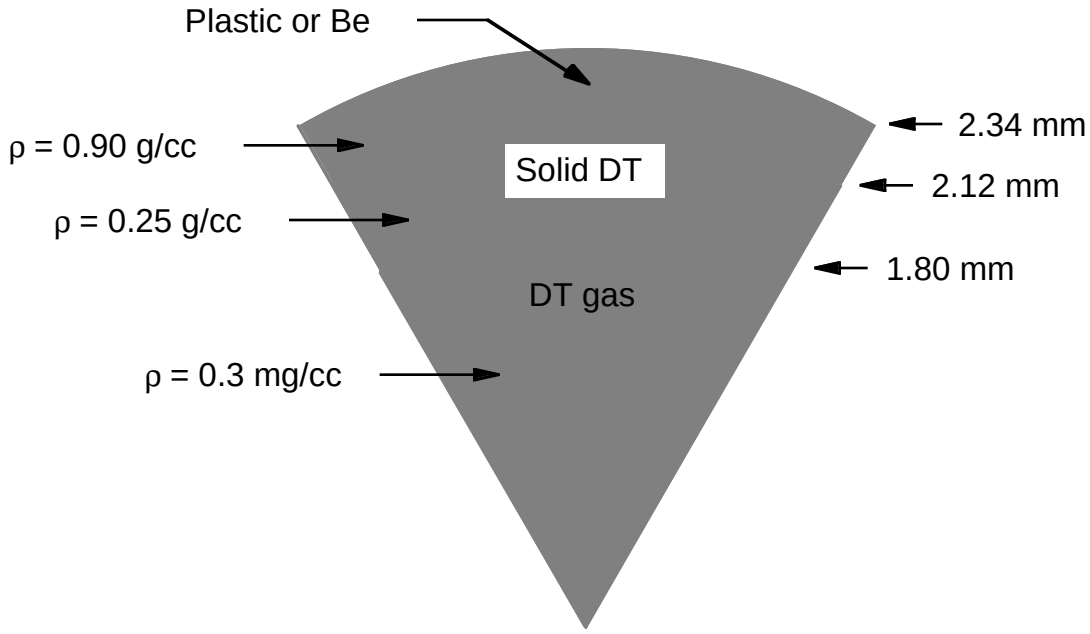

7.1.2 Reference target factory

Early IFE power plant designs will require DT, and thus, each will require an on-site target factory. (Later IFE power plants may not be based upon the DT fuel cycle.) The target factory is a major source

of tritium and activated target material, both of which may be susceptible to accidental release.

To analyze the hazards presented by the continual production of IFE targets, this report assumes a reference target factory. Such a target factory might consist of two separate target production lines, each of which ordinarily would be operated at 50% of its full capacity [7]. In the event of a failure on one of the production lines, the second line could be brought up to full capacity rapidly, and the power plant would avert a shutdown due to a lack of targets [7]. Such a design would reduce on-site tritium inventories by reducing the number of targets that would have to be stored to avoid frequent plant shutdowns.

Hazard analyses have been performed for both the tritium that is continually moving through the various target-production processes and the activated high-Z target material. Estimated tritium inventories for each of the target-factory processes are given in Table 7.1.2 [7]. The total target-factory tritium inventory is estimated at 300 g. This estimate is based upon assumptions of two production lines, a 6.7 Hz repetition rate, and a 30 minute supply of surplus targets [7]. Actual tritium inventories will vary from one

design to another due to differences in target yield, tritium per target, and repetition rates. Inventories may also vary according to target-production methods such as fuel-layering techniques and the types of quality-control systems used.

Table 7.1.2. Estimate of total target factory tritium inventory [4].

Process step	Tritium inventory (g)
Injection: 2 tritium reservoirs @ 100 g each 2 trays of capsules @ 5 g each	 200 10
Layering and quality assurance: 2 trays of capsules @ 5 g each	10
Sabot loading: 2 trays of capsules @ 5 g each	10
Storage of complete targets: 12,000 @ 2.4 mg each	29
Transport chain to target chamber: 50 m @ 1 m/s = 50 s 50 s of targets @ 6.7 Hz = 335 targets 335 targets @ 2.4 mg/target = 0.8 g	1
Allowance for tritium in piping and purge lines	40
Total target-factory tritium inventory	300

For an IFE plant operating at a 6.7 Hz repetition rate, the annual throughput of high-Z material would be more than 50 metric tons. The total inventory of activated high-Z target material can be greatly reduced through recycling on a weekly basis. That is, a used target and its high-Z material, vaporized during the shot, would be

recovered, held and allowed to cool for one week, and then reused in another target. Recycling would reduce the quantity of high-Z material required during the lifetime of a plant from more than 1500 tons to less than a single ton [4]. The obvious drawback of this practice is the required handling, fabrication, and storage of activated high-Z material. This material becomes an additional source of hazard. Calculations of the hazards presented by the target factory include contributions from activated high-Z target materials.

7.1.3 Cascade design

The Cascade design was first published in a 1983 paper by Lawrence Livermore National Laboratory (LLNL) [8]. The design represents one of the more unusual ones presented by the IFE community. Cascade would consist of a double-coned reaction chamber, which would rotate about its horizontal axis at a rate of 50 revolutions per minute [9]. The rotation might be similar to that of a cement mixer. The chamber rotation is such that ceramic granules may be injected near the ends and suspended against the first-wall. Figure 7.1.3 is an artist's conception of Cascade. The

figure is a cut-away view that shows the reaction chamber, the entry points for the heavy ion beams and the target, and the ceramic granules [9]. The figure also indicates the axis of rotation and shows the granule scoops and the support rails with rollers.

Figure 7.1.3. An artist's conception of the Cascade IFE power plant design shows the double-coned geometry, the SiC panels, the SiC-fiber/aluminum tendons, and the ceramic-granule blanket. Cascade would rotate about its horizontal axis in a manner similar to that of a cement mixer. Targets would be irradiated by either heavy ion or laser beams [9].

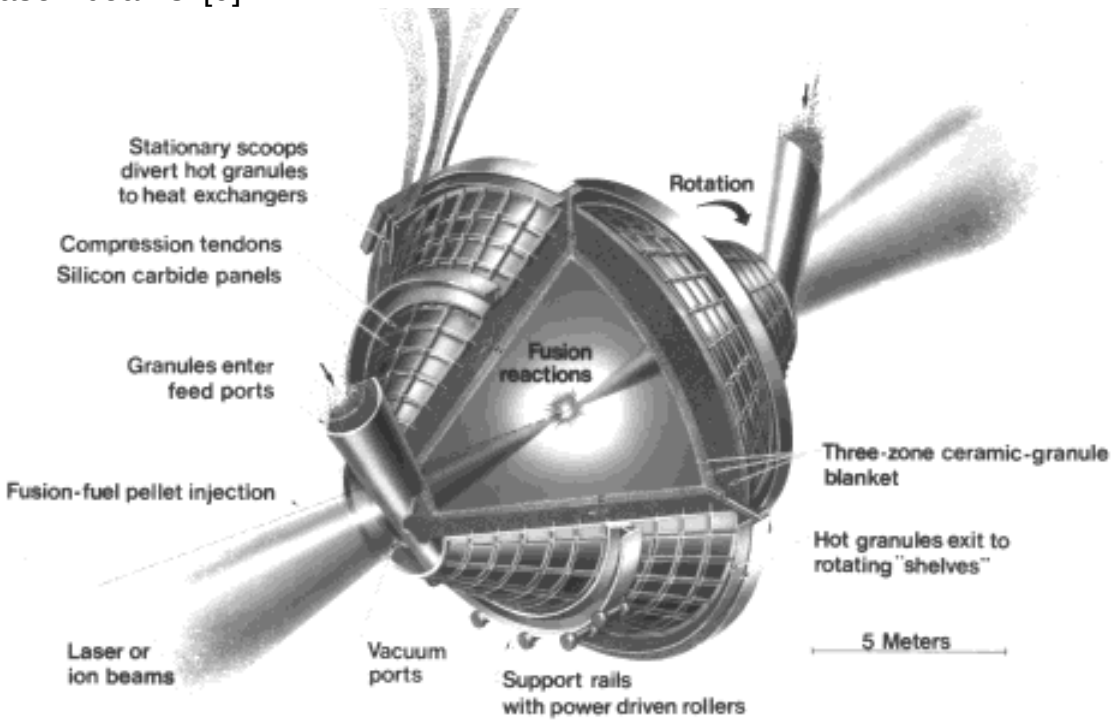

Targets would be injected into the Cascade chamber at a rate of 5 Hz and irradiated by 5 MJ of heavy ions. The targets would reach a peak areal density of 3 g/cm^2, and each target would yield 375 MJ of

fusion energy [9]. In addition to the hohlraum and capsule, each Cascade target would include a solid lithium x-ray and debris shield. The shield would have a total mass of 1 kg and would protect the front layer of ceramic granules against shocks, x-rays, and target debris. Openings at both ends would allow the heavy ion beams to enter the inner potion of the target. The shield would be mostly ^{7}Li to increase the overall tritium breeding ratio (TBR) [10].

The ceramic-granule blanket would be made of two different materials, which would be separated into three distinct regions. The total blanket thickness would be one meter. The first blanket region, closest to the chamber center, would consist of a 1-cm-thick layer of high-temperature carbon granules. This region would have unrestricted flow, which would result in good mixing throughout the layer. The granules in the first blanket region would absorb a large fraction of the fusion yield and would leave the chamber at a high temperature of approximately 1715 K. This region would lie just over three meters from the target chamber center [9].

The second blanket region also would consist of a 1 cm thickness of carbon granules. This region would be largely held in place by the innermost region, so there would be little radial mixing within the

layer. The flow rate of granules in the second region would be nearly ten times less than that of the first region. The granules in the second region would exit the chamber at a temperature of about 1500 K [9].

The final blanket region would consist of 98 cm of $LiAlO_2$ granules which would be enriched to 15% ^6Li. The $LiAlO_2$, in conjunction with the ^7Li x-ray and debris shield, would be responsible for all tritium production. This final region, like the second one, would undergo little radial mixing. The maximum exit temperature for $LiAlO_2$ granules would be around 1500 K, but the average exit temperature would be only 1425 K [9].

Granules would exit the Cascade reaction chamber at the maximum radius, at the mid-plane where the two cones connect. The different velocities of the granules would make separation upon exit rather simple -- the various exit velocities would be sufficient to carry the granules to the top of their respective heat-exchanger chutes. Once inside the chutes, the granules would flow down through the heat exchangers via gravity. Each heat exchanger would include horizontal SiC tubes which would contain flowing high-pressure (50 atm) helium gas. The granules would transfer their

energy to the helium, which, in turn, would be used in a once-through, regenerative Brayton-cycle turbine. The high temperatures would result in a net plant efficiency of 47% (assuming a 20%-efficient heavy-ion driver) [9].

The Cascade reaction chamber would be made from 5-cm-thick SiC tiles which would be “held in compression by composite SiC-fiber/aluminum tendons that [would] gird the reactor both circumferentially and axially” [9]. The thick blanket region would not only provide sufficient tritium production but would also shield the first wall from neutrons. The flux in the first wall would be nearly thirty times lower than that in the carbon granules. Nonetheless, the Cascade reports suggest that the SiC first wall would not be a lifetime component, due to excessive radiation damage [9,10]. The maximum DPA for SiC is not known at this time. It should be noted that the Cascade authors have assumed a conservative value of only 20 DPA.

The Cascade design, as presented in references 8-10, would generate a net power of 890 MWe. To enable comparisons among the various designs, each has been scaled to yield a net electric power of 1000 MWe. Cascade has been scaled by assuming a repetition rate

of 5.6 Hz rather than the reported value of 5 Hz. This modification may change some of the calculated efficiencies and costs slightly, but it should have only a minor effect upon the radiological indices.

7.1.4 HYLIFE-II design

The HYLIFE-II design is a modified version of the original HYLIFE design that was published in 1985 [11]. Although the more recent design still features a neutronically thick liquid between the target and the chamber walls, HYLIFE-II would use liquid Flibe rather than liquid lithium. Flibe would be used as the first-wall protection scheme, coolant, and breeding material. The switch from liquid lithium to Flibe eliminates the risk of fire inherent to lithium systems [12]. An additional benefit is the remarkably low solubility of tritium in Flibe [13]. Figure 7.1.4 shows an artist's conception of the HYLIFE-II design.

The HYLIFE-II design assumes a relatively modest gain of 70 for an indirect-drive target and a driver energy of 5 MJ (HYLIFE assumed a gain of 400 for a driver energy of 4.5 MJ). In order to maintain a net electric power output close to 1000 MWe, the HYLIFE repetition rate would have to be increased from 1.5 Hz to 6 Hz [12]. Such high

repetition rates would require the use of either pulsed or oscillating flow to ensure that the beam paths would be cleared between shots [12]. The oscillating flow would be accomplished through the use of two deflectors, which would need to move ±2.5° to create a “pocket” of Flibe to protect the first wall from x-rays, debris, and neutrons [13]. This inner pocket of Flibe would flow at a rate of approximately 12 m/s [14]. Figure 7.1.5 shows four stages of the formation of a Flibe pocket.

Figure 7.1.4. An artist’s conception of the HYLIFE-II power plant design shows the oscillating Flibe jets, a rotating shutter, and two sets of bypass pumps [13].

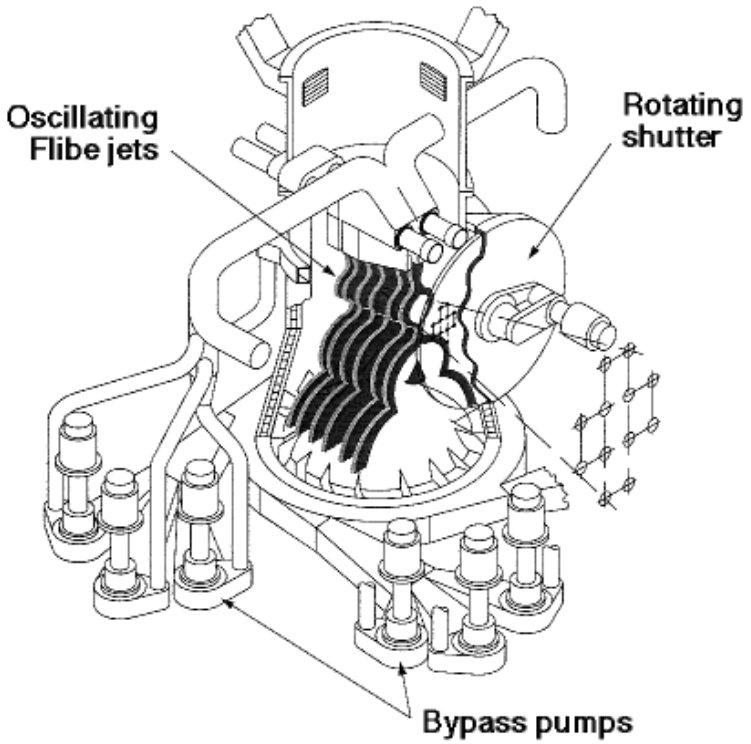

Figure 7.1.5. The HYLIFE-II first wall is protected by a “pocket” of Flibe coolant, which is created through the use of oscillating deflectors [15].

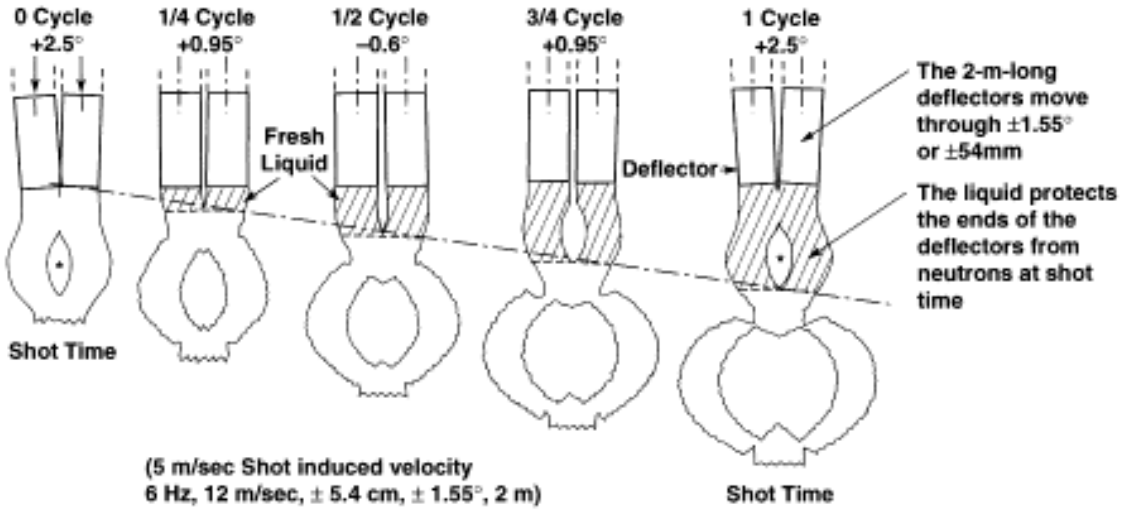

The HYLIFE-II first-wall and blanket system would have to satisfy several requirements, including serving as the vacuum and tritium barrier; transferring heat to the coolant; and withstanding severe cyclic pressure loadings [14]. As a result, the construction would be quite complicated. The first-wall and blanket system would consist of four distinct shells. The innermost shell would be made of 5-cm-radius tubes, separated by 2.5-cm-long plates.

Both the tubes and the plates would be 1.2-mm-thick stainless steel type 304 (SS304). SS304 is the primary candidate structural material for HYLIFE-II (the original design specified stainless steel type 316, prior to identification of an incompatibility between Flibe

and the manganese in the steel) [16]. Flibe coolant would flow through the steel tubes at a velocity of 1 m/s. In addition, Flibe would be sprayed on the inner side of the innermost shell [14].

The second shell would be separated from the first by 50 cm of Flibe. The two shells would be interconnected via a series of perforated rings, which would provide additional strength to the structure. The Flibe between the first and second shells would be used primarily for neutron shielding, although it would also transfer heat from the structure. Because the Flibe would not be essential for heat transfer, a low flow rate of 0.25 m/s would be sufficient.

Both the second and third shells would be made of 2.5-cm-thick SS304 [14]. They would be separated by a 2.5-cm-thick region of Flibe, flowing at 1 m/s.

The region between the third and fourth shells would be 10.2-cm-thick. It would consist mostly of permeable insulation and would include a slowly flowing purge gas. As for the outer shells, support rings would be used to provide the needed strength. The fourth shell would be a 1.6-mm-thick SS304 container that would surround the entire first-wall and blanket system [14]. Figure 7.1.6 is a plan view

of the HYLIFE-II design, including a cut-away view of the structure for the first-wall and blanket system.

Figure 7.1.6. A plan view of the HYLIFE-II design shows many of the key components. Liquid Flibe, formed into a “pocket” by oscillating nozzles, protects the chamber walls. View (b) is rotated 90° from view (a) [13].

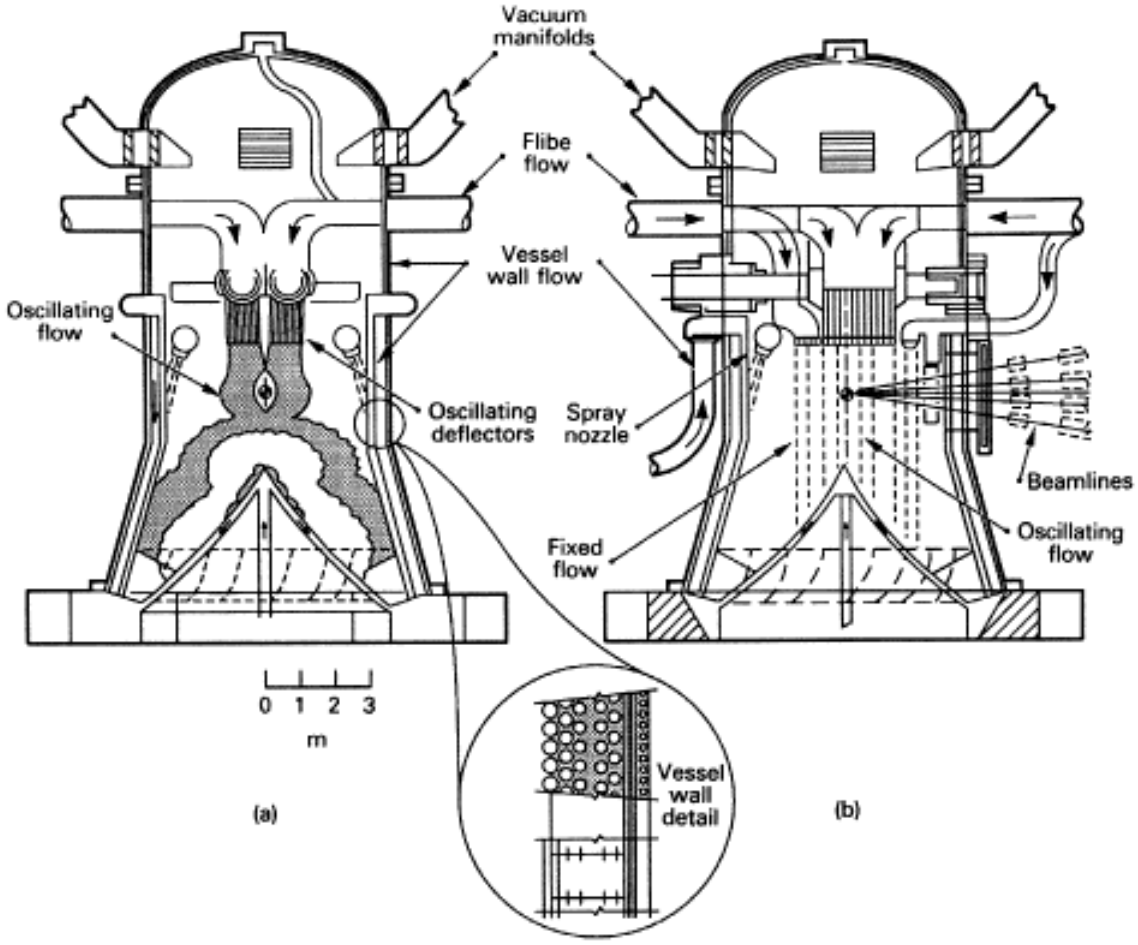

HYLIFE-II would include a head recovery system which would prevent Flibe from splashing upwards. Through use of turning vanes and diffusers, approximately 50% of the dynamic head would be

recovered. Liquid Flibe would travel through the four diffusers on its way to the twelve bypass pumps [14].

If built as designed, HYLIFE-II would have a net electric output of only 940 MWe [13]. Again, to facilitate comparisons among designs, the present work assumes that the HYLIFE-II repetition rate is increased from 6 Hz to 6.4 Hz, which would, to first order, increase the electrical output to 1000 MWe.

Although the other IFE designs are frozen, HYLIFE-II research continues. At least nine new HYLIFE-II papers have been published during 1994 and 1995. The author has attempted to obtain the most up-to-date design information possible but apologizes for any details that have changed and were overlooked.

7.1.5 Osiris design

The Osiris and SOMBRERO IFE design studies were commissioned in 1990 by the DOE Office of Fusion Energy. A research team was assembled by W. J. Schafer Associates. This team consisted of Bechtel, General Atomics, Textron Defense Systems, and the University of Wisconsin [7].

Osiris would use heavy-ion beams to drive an indirect fusion target. Like the HYLIFE-II design, Osiris would use liquid Flibe as the first-wall protection, coolant, and tritium breeding material. Osiris would use a flexible, porous carbon fabric as the structural material in the first-wall and blanket [7].

The assumptions made about driver energy, target gain, and repetition rate are consistent with those used in the HYLIFE-II design. Osiris would use 5 MJ of driver energy to release 432 MJ of fusion energy -- a fusion gain of 86. Targets would be imploded at 4.6 Hz.

While HYLIFE-II would rely upon oscillating jets of Flibe to ensure that the beampaths would be cleared of vaporized Flibe, Osiris would use geometry to ensure that the beams are able to propagate to the target. The chamber geometry would direct vaporized Flibe down towards a pool of liquid Flibe. Additionally, Flibe spray would be injected near the bottom of the chamber to accelerate Flibe condensation [7].

The first-wall and blanket system would consist of multiple layers of structural material and coolant. The Osiris reference design begins with a 2-mm-thick layer of Flibe on the first-wall

surface. Flibe would ooze through the porous carbon fabric and protect the first wall from x-rays and target debris. The shortest distance between the first wall and the target would be 3.5 m. The first wall itself would be 5-mm-thick. The coolant region behind the first wall would be 5-cm-thick. The inner and outer blanket walls each would be 5-mm-thick layers of carbon fabric. The blanket itself would be a 55-cm-thick region of Flibe [17].

Flibe coolant would make a circuitous path through the first wall and blanket. Flibe, at a temperature of 500 °C, would enter the first wall from an inlet at the top of the chamber. Most of the Flibe would flow down through the first-wall channel, while a small quantity would flow through the porous first wall to protect its surface. At the bottom of the chamber structure, Flibe would be redirected upwards through the bulk of the blanket, and from the top of the chamber the Flibe would cascade back down the outside of the blanket structure. This cascading layer would be about 10-cm-thick and would enter the Flibe pool at a temperature of 650 °C [18].

The blanket and first wall would be supported from the vacuum vessel by a series of carbon composite struts. The vacuum vessel itself also would be made from a carbon or silicon carbide

composite material and would be 20-cm-thick. The porosity of the vacuum vessel would be mitigated through the use of additional Flibe, which would be allowed to infuse into the composite structure. Because the melting point of Flibe is 460 °C, Flibe near the outside of the vessel would be solid and would effectively seal the vacuum vessel [7]. Figure 7.1.7 shows the Osiris design and identifies many of the main components.

Figure 7.1.7. A plan view of the Osiris power plant design shows details of the structure of the first wall and blanket [7].

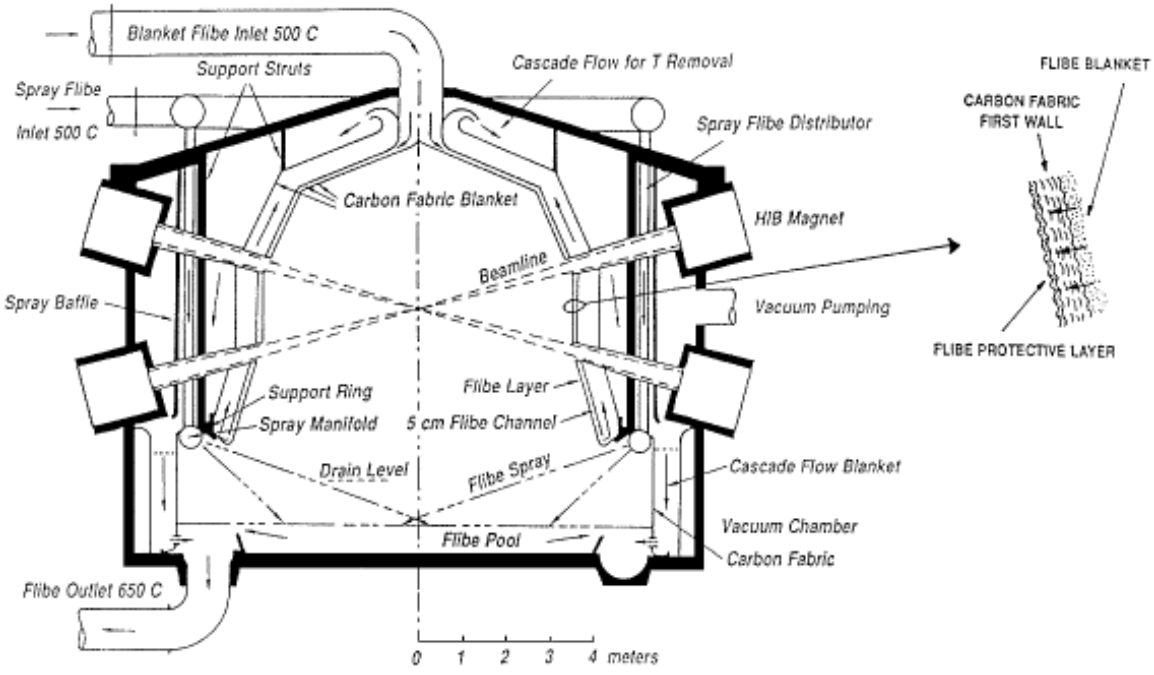

The Osiris vacuum vessel would be placed within a concrete reactor building with 3.2-m-thick concrete walls. The building

would confine tritium and protect the public from fusion neutrons. The reactor building would be large enough that the first-wall and blanket system could be drained of Flibe and hoisted out of the vacuum vessel as a single component, using an overhead crane [7].

The Osiris first-wall and blanket design would be made entirely of low-activation composite materials in a flexible, leak-tolerant configuration. Osiris would make good use of geometry to direct vaporized Flibe down towards the pool and low-temperature Flibe spray. The net electric output from Osiris would be 1000 MWe, so the repetition rate does not need to be adjusted to allow comparison to the other designs.

7.1.6 Prometheus design

The Prometheus-L and Prometheus-H IFE power plant designs were the result of another study commissioned by DOE in late 1990 and completed in early 1992. The design team was lead by McDonnell-Douglas Aerospace; other members were: the Canadian Fusion Fuels Technology Project; Ebasco Services, Inc.; KMS Fusion, Inc.; SPAR Aerospace, Ltd.; TRW Space and Electronics Group; and the University of California at Los Angeles [19].

The Prometheus-L design would use a direct-drive target, driven by a KrF laser, while the Prometheus-H design would use an indirect-drive target, driven by 4 GeV lead ions. From the standpoint of target chambers, the two designs are nearly identical. The major differences between the two designs include the need for high-Z material in the indirect-drive target and the dimensions of the target chamber. The heavy-ion-driven chamber would be only about nine-tenths the size of the laser-driven design. While the smaller size means that less material would be required for the first-wall and blanket system, it also would result in a higher neutron flux at the first wall. The higher first-wall neutron loading and the need for high-Z material suggest that the hazards of the heavy-ion-driven design may be greater than those of the laser-driven design. Thus, only the heavy-ion-driven design, Prometheus-H, is analyzed in this report.

The Prometheus-H design would use a single-beam linear accelerator to accelerate Pb^{+2} ions to energies of 4 GeV. A total of 7.0 MJ would be delivered to the target, and 719 MJ of fusion energy would be released for a target gain of 103. The repetition rate would be 3.54 Hz [20]. Since the heavy-ion design would deliver 999 MWe to

the grid, the repetition rate does not need to be adjusted for comparison with the other designs.

Unlike the other IFE designs, the Prometheus first wall would be separate from the blanket. The Prometheus first wall would include a 0.5-mm-thick film of liquid lead for first-wall protection and a 6-cm-thick structure that would contain lead coolant channels. The lead coolant would provide the neutron multiplication needed to obtain an adequate tritium breeding ratio.

The first-wall structural material would be SiC, which would range from 10% porosity at the front face to zero porosity at the back face. The lead coolant would flow at nearly 55,000 kg/s and would have inlet and outlet temperatures of 375 °C and 525 °C, respectively. The lead would leak through the porous front surface of the wall to wet its surface and protect it from damaging x-rays and target debris [20]. Figure 7.1.8 shows the design for the Prometheus first wall.

The Prometheus blanket design “builds on the existing data and design base developed by MFE” [20]. It is largely based upon the blanket design of the ARIES-I MFE power plant [21]. The blanket structural material would be a SiC composite, and the tritium

breeding material would be Li_2O pebbles, which would be cooled by helium gas. Lithium enriched to 25% ^6Li would be used. A low helium pressure of 15 MPa would be possible, as nearly 40% of the thermal power would be deposited within the thick first wall. Helium gas would enter the blanket modules at a temperature of 400 °C and would leave at 650 °C [20].

Figure 7.1.8. A cross-sectional view of the Prometheus first wall shows the liquid-lead protective layer, the SiC structure, and the lead-coolant channels [20].

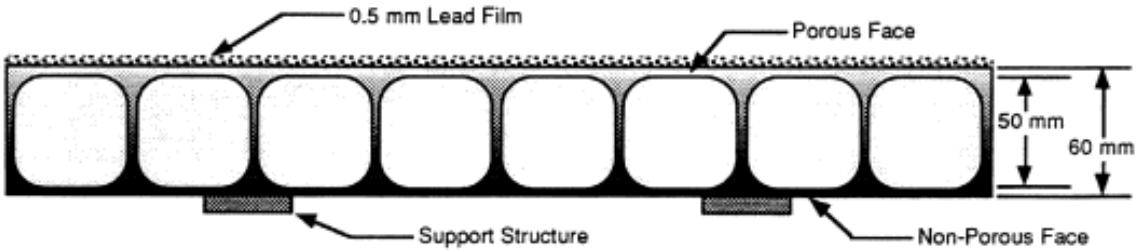

Each blanket module would consist of a layered configuration of SiC sheets which would be U-bend woven. The Li_2O would be packed between the SiC sheets and would be purged by the flowing helium gas. A 20-cm-thick SiC reflector would be included at the back end of the blanket modules [19]. Figure 7.1.9 shows the blanket module design.

Figure 7.1.9. Prometheus would feature blanket modules similar to those designed for the ARIES-I MFE power plant [20].

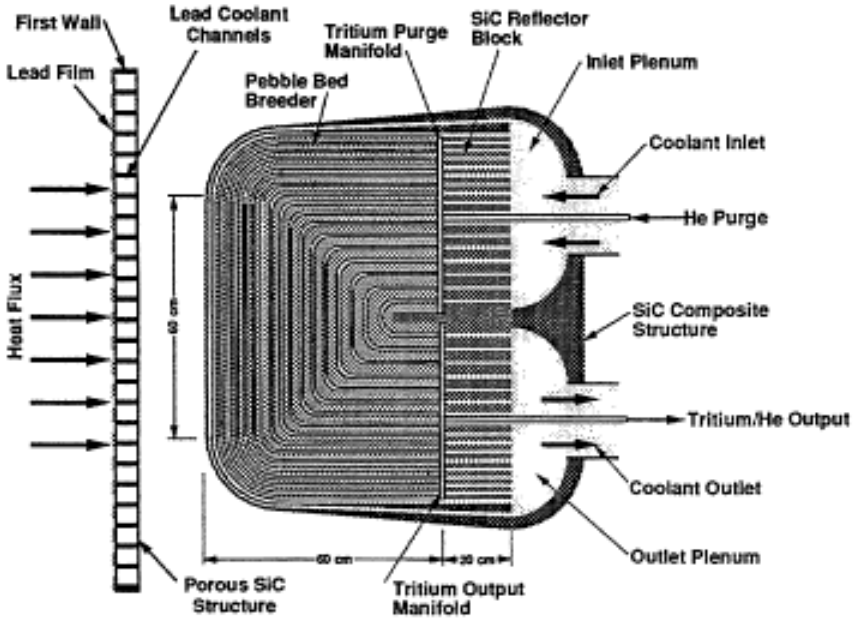

The blanket region would be followed by a vacuum vessel made of ferritic steel. The vacuum vessel would be 2-cm-thick at a distance of just over 8 m from the target chamber center. The vacuum vessel would be followed by the 1.3-m-thick bulk shield. The shield would be composed of 20% Pb, 20% B_4C, 25% SiC, 30% water, and 5% Al structure. The shield combines both superior γ-ray shielding and lower activation when compared with the more traditional concrete shields [20]. Figure 7.1.10 shows the Prometheus-H reactor building including the target chamber, blanket, vacuum vessel, bulk shield,

and vacuum pumps. The reactor cavity would be a cylinder with hemispherical end caps and a low aspect ratio [20].

The Prometheus designs combine low activation SiC structures with Li_2O breeders, a low-pressure helium coolant, and a lead first-wall protection system.

Figure 7.1.10. An elevation view of the Prometheus-H central reactor cavity region shows the vessel, blanket, shielding, and vacuum pumps [19].

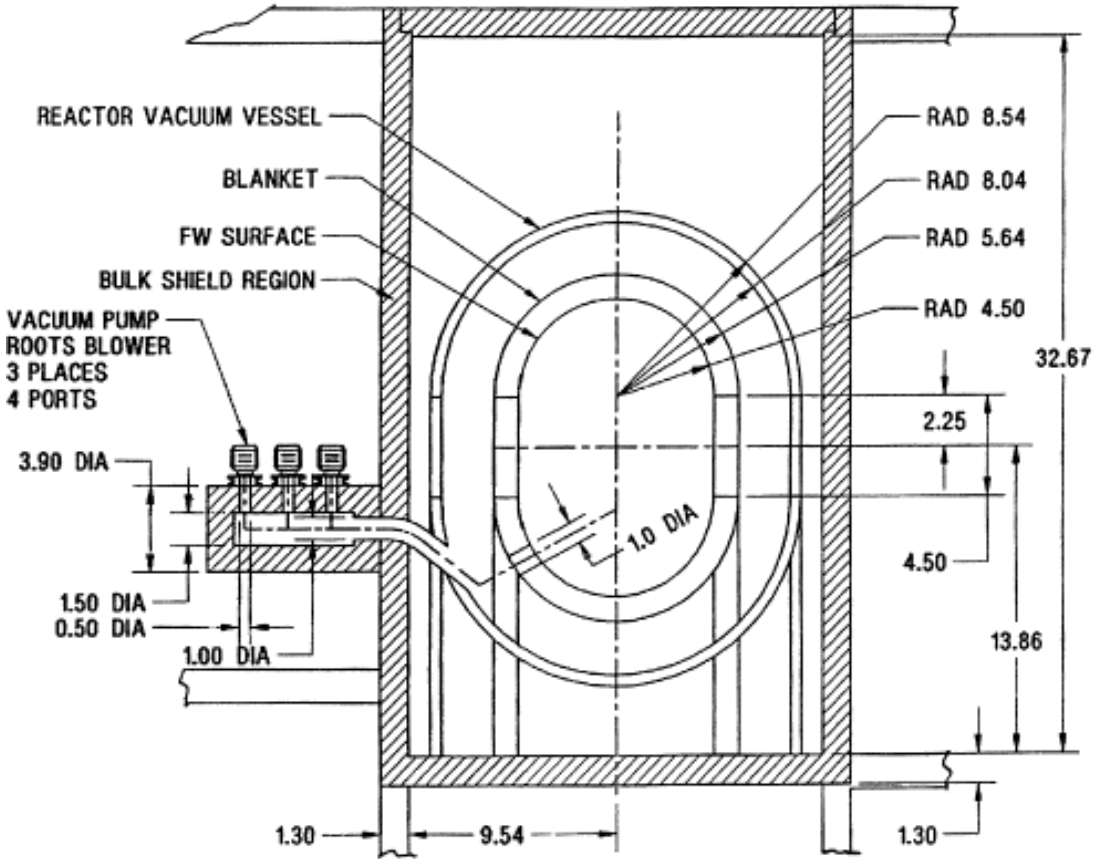

7.1.7 SOMBRERO design

As mentioned in section 7.1.5, the Osiris and SOMBRERO designs were developed by a team lead by W. J. Schafer Associates. The studies began in late 1990, and the reports were published in early 1992. While Osiris would be driven by heavy ions and would use an indirect-drive target, SOMBRERO would be laser-driven and would use a direct-drive target. SOMBRERO is an acronym for **SO**lid **M**oving **BRE**eder **R**eactor [7].

SOMBRERO targets would be imploded by a KrF-laser driver, and SOMBRERO is the only direct-drive design considered in the present work. The sixty beams of the KrF laser would deliver a total energy of 3.4 MJ to the target. The target yield would be 400 MJ for a gain of about 118, higher than that currently anticipated for indirect-drive targets. The repetition rate would be 6.7 Hz [7]. Since direct-drive targets do not require a hohlraum or high-Z materials, only the unburned DT fuel and the vaporized plastic shell need to be considered in target activation. SOMBRERO would use a target similar to the reference capsule design described in section 7.1.1.

Like Osiris, SOMBRERO would have a first wall and blanket made from carbon composite. The SOMBRERO first wall, however, would be

protected by 0.5 torr of xenon gas. Xenon is chemically inert and has a high x-ray absorption cross section, yet it would not absorb the KrF laser energy. Xenon would absorb energy from target x-rays and debris ions and reirradiate it to the first wall over a timescale long enough for conduction to prevent the extreme temperatures that would damage the wall [7].

The SOMBRERO chamber would consist of a central, cylindrical section and conical upper and lower sections. The cylindrical section would have a 6.5-m-radius and would be 5.2 m in height. The conical sections would make an angle of 135° with the cylindrical section, so their vertices would be 9.1 m from the center of the chamber. The sixty beams would fit in five cones above and below the chamber mid-plane. These cones would be at angles of 25.8°, 45.6°, 60.0°, 72.5°, and 84.3°. The SOMBRERO chamber would be divided into twelve modules, separated by vertical planes that would intersect the chamber axis. Due to symmetry of the beam ports, only two sets of chamber modules would be required, and the modules within each set would be identical in all respects [7].

SOMBRERO would use solid Li_2O particles as coolant and tritium breeding material. Solid breeding materials offer the possibility of

high-temperature, corrosion-free operation and low activation, and they have an established database of materials information. SOMBRERO would use Li_2O particles of 300-500 μm in diameter. These Li_2O particles would move through the blanket from top to bottom, driven by gravity as a fluidized bed, using helium gas as the carrier [7].

The SOMBRERO blanket would be 1.0-m-thick at the mid-plane. The blanket would reach a maximum thickness of 1.75 m at the top of the conical sections. Throughout the blanket, the Li_2O flow rate remains constant at 1.15 m/s.

The first wall would be a 1.0-cm-thick carbon composite. The blanket would be divided into three sections. At the mid-plane, the innermost section would be 19-cm-thick and would consist of 3% carbon composite and 97% Li_2O particles. The second and third sections each would be 40-cm-thick, and the Li_2O fractions in these sections would be 80% and 50%, respectively. The increasing carbon fraction would act as a neutron reflector and would enhance energy absorption and tritium breeding within the blanket [7].

The SOMBRERO chamber would be placed within a concrete shield that would be 1.7-m-thick with an inner radius of 10 meters. The

shield would enable components located outside to be accessed for hands-on maintenance within 24 hours of shutdown. The shield also would provide the structural support for the chamber [7]. Figure 7.1.11 shows the SOMBRERO chamber and its primary shield.

The grazing incidence metal mirrors (GIMMs) would be 30 m from chamber center through penetrations in the shield. The GIMMs would be in the line-of-sight of fusion neutrons, and would be susceptible to significant radiation damage. There is an unexplored potential for increasing the lifetime of the GIMMs though annealing. The use of GIMMs would allow the final focus mirrors to be located out of the line-of-sight of neutrons. These final focus mirrors would be located 50 m from the chamber center and their dielectric coatings would be quite sensitive to radiation damage. The final focus mirrors could not be annealed, and thus, their protection would be essential to the economical operation of the facility [7].

The SOMBRERO reactor building would be approximately 115 m in height and 110 m in diameter. Since SOMBRERO would not use beamtubes for laser transport, the entire building would have to serve as a vacuum vessel. The building would be maintained at an atmosphere of 0.5 torr of xenon gas and would be connected to a

vacuum system that would recover unburned tritium and target debris.

Figure 7.1.11. A cross section of the SOMBRERO chamber shows details of the first-wall and blanket design [17].

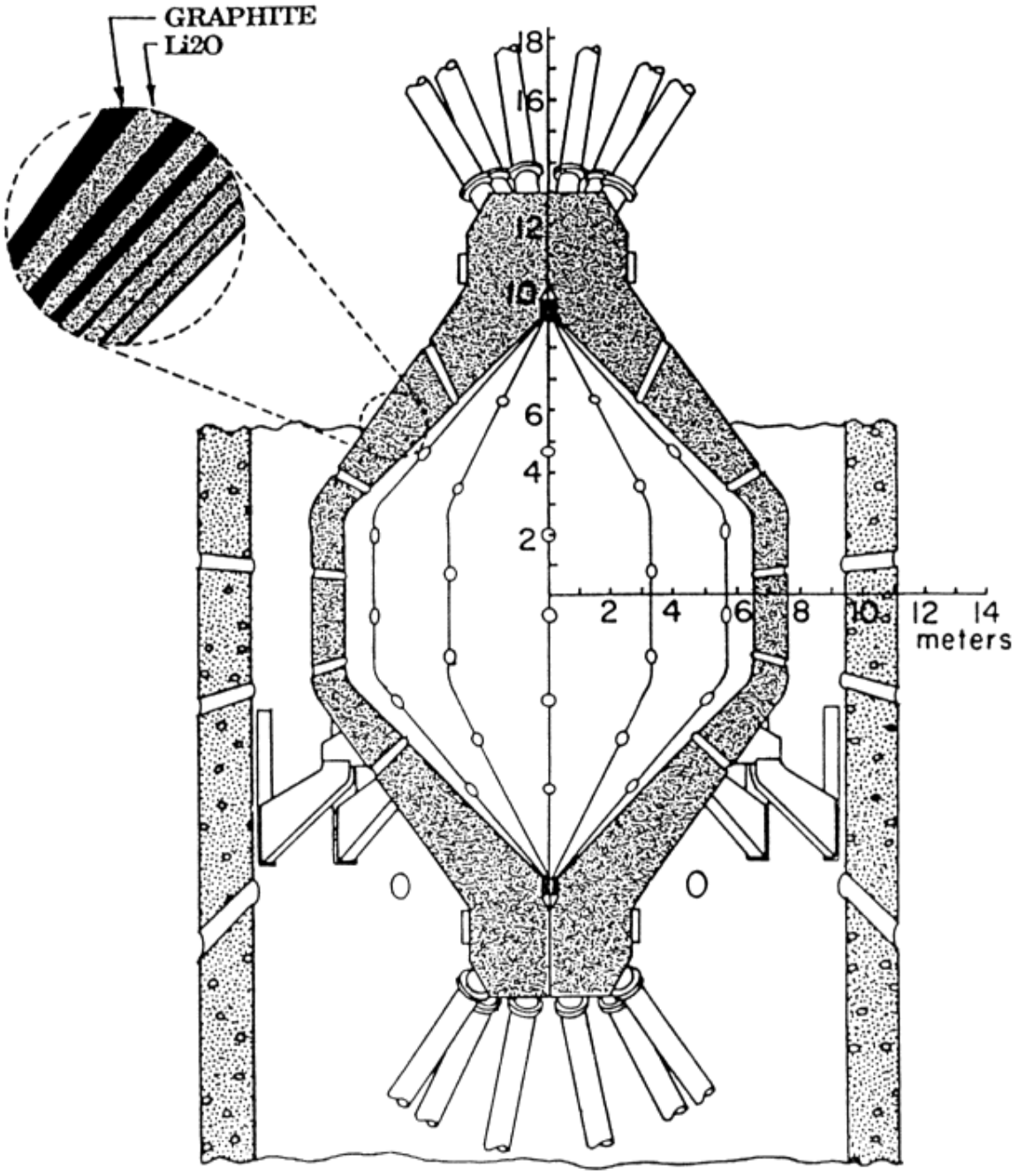

The reactor-building walls would be 1.2-m-thick concrete and would include neutron traps for neutrons that stream through the GIMMs. The minimum concrete thickness in any direction from the target would be 2.9 m reducing prompt doses outside the reactor building to acceptable levels [7]. Figure 7.1.12 shows the SOMBRERO reactor building along with the target chamber, shield, and one set of GIMMs.

Figure 7.1.12. A cross-sectional view of the SOMBRERO reactor building shows the location of the chamber, primary shield, one set of GIMMs, neutron traps, and other major components [17].

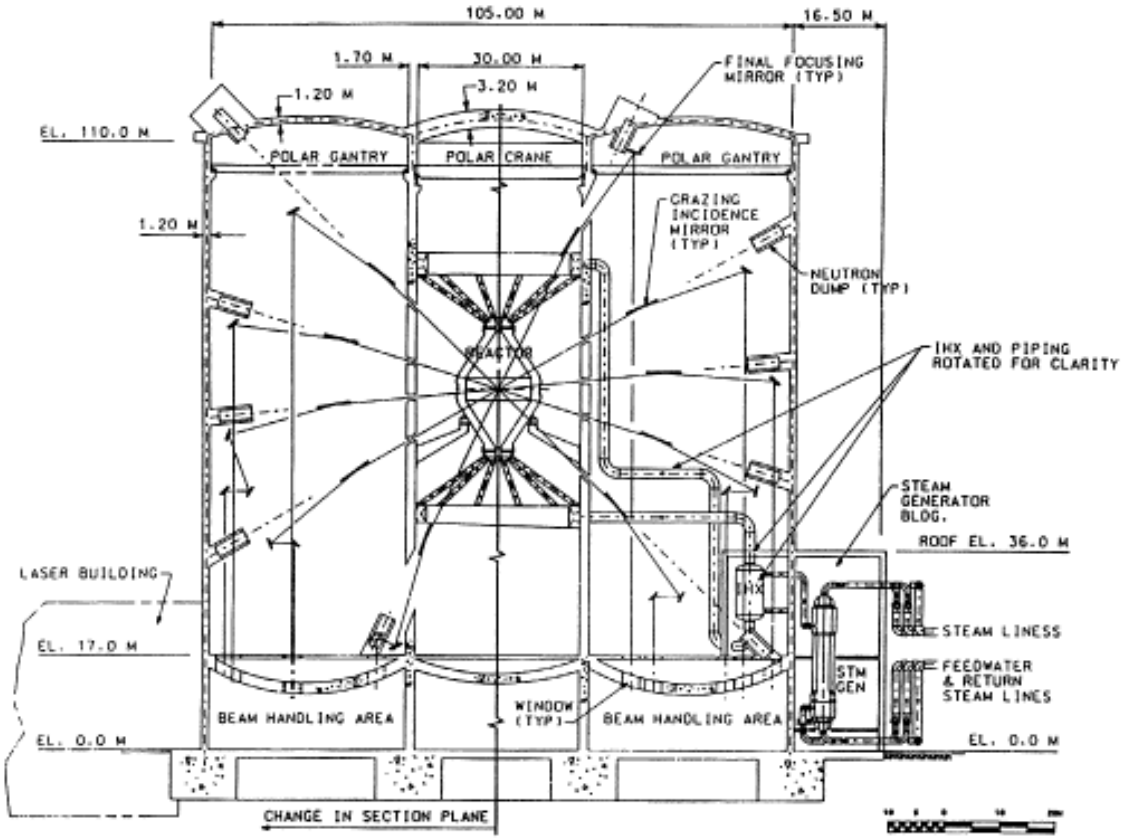

SOMBRERO is the only IFE power plant design being considered that would use a direct-drive target. It is also the only design that would use a laser driver. (The Cascade design could be used with either heavy-ion or laser-beam drivers, but the design was optimized for use with a heavy-ion-beam driver.) Although the lack of a need for high-Z target material would be a significant advantage over the other IFE power plant designs, the large number of laser beams required to provide adequate symmetry for target illumination would result in a large open solid-angle fraction, which could cause significant activation of components located outside the target chamber. Clever design of the reactor building, however, would mitigate most of the negative impact of this large open solid-angle fraction.

The SOMBRERO power plant, as designed, would generate a net electric power of 1000 MWe. Thus, its repetition rate does not need to be adjusted to allow comparison to the other designs.

7.2 Magnetic fusion energy designs

ESECOM did not consider a stainless steel tokamak, as the committee felt that “work in the early 1980’s had so convincingly

demonstrated the S&E liabilities of stainless steel as a fusion-reactor structural material" that this material would not be chosen for use in commercial reactors [2]. Kinzig, Holdren, and Hibbard note that this perception is at least questionable given that stainless steel was subsequently selected as the primary structural material for ITER. In this report, a stainless steel version of the ESECOM V-Li tokamak case is analyzed. Although this procedure is not as rigorous as developing a new design would be, it provides an easy way to generate a first-order analysis of such a system. It is the author's belief that this case represents something close to the worst-case tokamak design with respect to ES&H characteristics.

On the other end of the ES&H spectrum, the SiC-He tokamak design is analyzed. The low-activation properties of a silicon carbide structure, combined with inert helium coolant, are likely to result in a design that is close to the best-case tokamak in terms of ES&H characteristics.

The analysis of the PCA-Li and SiC-He tokamak designs should identify the range of MFE designs. It is not possible, of course, to guarantee that these designs represent the worst- and best-case

tokamaks, respectively, but their use should give some indication of where the “bookends” might be found.

Since the PCA-Li and SiC-He tokamak designs, as they were presented in the ESECOM report, are generalized tokamak designs, large amounts of detail are not available. The details that are available are given in the following sections.

In the ESECOM analyses, all tokamak designs were modeled using one-dimensional, cylindrical approximations, including reflecting planes at the ends to ensure that particles did not escape [1]. The simple, one-dimensional treatment of the MFE designs, used in the ESECOM study, is used here.

The cylindrical approximation scales a cylinder length and radius from actual design parameters. The cylinder length is equal to the circumference of the toroid at its major radius. The cylinder radius is selected such that the correct first-wall area is obtained [2].

7.2.1 PCA-Li tokamak design

As previously mentioned, the stainless steel tokamak modeled here, denoted PCA-Li/TOK, is only an approximation to an actual design. In fact, since the stainless steel replaced the vanadium alloy

in an already approximate design, the PCA-Li/TOK design is even more of an approximation. Nevertheless, this design is likely to provide insight into what is probably the worst-case tokamak design with respect to S&E characteristics.

The PCA-Li/TOK is modeled by simply replacing all vanadium alloy components in the ESECOM V-Li/TOK case with PCA on a one-for-one volumetric basis [2]. PCA-Li/TOK would have a major radius of 5.89 m, an aspect ratio of 4.0, and a plasma standoff of 1.1 [1]. The plasma elongation factor would be 2.5, resulting in a first-wall area of 716 m^2. The equivalent cylinder length would be 37.0 m, and the equivalent cylinder radius would be 3.08 m [1].

The steady-state fusion power would be 2862 MW, which would give an average first-wall neutron loading of 3.20 MW/m^2. The average blanket thickness would be 0.71 m [1]. The basic parameters for the PCA-Li/TOK design are summarized in Table 7.2.1.

The net electric power output would be 1200 MWe. In order to allow comparison with the IFE power plant designs, most of which provide electric outputs close to 1000 MWe, the PCA-Li/TOK source term is adjusted to yield 1000 MWe.

Table 7.2.1. The basic design parameters for the PCA-Li/TOK design are taken from the V-Li/TOK design as it was analyzed in the ESECOM report [1].

Design parameter	Value
Major radius	5.89 m
Aspect ratio	4.0
Plasma elongation	2.5
Plasma standoff	1.1
First-wall area	716 m^2
Average blanket thickness	0.71 m
Average shield thickness	0.83 m
Maximum toroidal field at coil	10.0 T
Plasma current	15.8 MA
Total plasma beta	0.1
Toroidal field in plasma	4.29 T
Fusion power	2862 MW
Neutron power	2289 MW
Neutron wall loading	3.20 MW/m^2
Neutron energy multiplication	1.27
Total thermal power	3563 MW
Tritium breeding ratio	1.28
Primary coolant inlet temperature	300 °C
Primary coolant outlet temperature	550 °C

Table 7.2.2 lists the inner radii and thicknesses of the various components included in transport and activation calculations. The inner radii, and thus, the solid volumes differ somewhat from those presented in the ESECOM report. These differences result from greater accuracy in the calculation of the cylindrical approximation parameters.

The volumetric percentages of liquid lithium and PCA in the first wall would be 80.0 and 20.0, respectively. The corresponding blanket percentages would be 92.5 and 7.5. The manifold would be composed

of FeCrV, liquid lithium, and PCA in volume percentages of 80.0, 10.0, and 10.0, respectively [1]. The manifold would be followed by a 10-cm-thick vacuum gap, followed by the shield of 80% FeCrV and 20% water.

Table 7.2.2. The PCA-Li/TOK design is modeled using a cylindrical approximation that gives the correct first-wall neutron loading [1].

Zone description	Inner radius (cm)	Thickness (cm)	Composition (volume %)	Solid volume (m^3)
Plasma	0	280	100 plasma	0
Vacuum gap	280	28	100 vacuum	0
First wall	308	5	80 Li, 20 PCA	7.2
Inner blanket	313	35	92.5 Li, 7.5 PCA	20.2
Manifold	348	35	80 FeCrV, 10 Li, 10 PCA	268
Gap	383	10	100 vacuum	0
Shield	393	30	80 FeCrV, 20 H_2O	228

While the ESECOM analyses assumed a first-wall lifetime corresponding to a constant neutron fluence limit of 20 MW–yr/m^2 at the first-wall, the present work relies upon calculations of first-wall spectra and DPA rates and estimates of maximum allowable DPA for each material, consistent with that used for analysis of the IFE designs.

The V-Li/TOK design, analyzed in ESECOM and upon which the PCA-Li/TOK design is based, was intended to serve as the point-of-

departure design [1]. While the original design used a vanadium alloy to minimize corrosion of the blanket structure, PCA may experience significant corrosion problems when used with liquid lithium. The design is also constrained in that all water, air, and concrete must be kept away from the liquid lithium due to its high chemical reactivity [1].

7.2.2 SiC-He tokamak design

The silicon carbide tokamak, SiC-He/TOK, is based upon work completed by General Atomics (GA) [22]. GA began its analysis with the STARFIRE tokamak design and redesigned each of the components to incorporate low-activation materials [22,23].

With a major radius of 7.02 m, the SiC-He/TOK design would be quite large. Other design parameters are summarized in Table 7.2.3 and are quite similar to those of the PCA-Li/TOK design. The equivalent cylindrical length and radius would be 44.1 m and 3.69 m, respectively. These values would give the correct first-wall area of 1020 m^2. The equivalent cylinder radius of 3.0 m and equivalent cylinder length of 46.4 m, used by ESECOM, give an incorrect first-wall area of only 875 m^2.

Table 7.2.3. The basic design parameters for the SiC-He/TOK design are taken from the ESECOM report [1]. They are based upon the STARFIRE design, which was modified to use only low-activation materials [22,23].

Design parameter	Value
Major radius	7.02 m
Aspect ratio	4.0
Plasma elongation	2.5
Plasma standoff	1.1
First-wall area	1020 m^2
Average blanket thickness	0.79 m
Average shield thickness	1.08 m
Maximum toroidal field at coil	10.0 T
Plasma current	17.0 MA
Total plasma beta	0.1
Toroidal field in plasma	3.88 T
Fusion power	3226 MW
Neutron power	2581 MW
Neutron wall loading	2.53 MW/m^2
Neutron energy multiplication	1.20
Total thermal power	3827 MW
Tritium breeding ratio	1.06
Primary coolant inlet temperature	250 °C
Primary coolant outlet temperature	500 °C

The SiC-He/TOK fusion power would be 3226 MW, and the neutron power would be 2581 MW. Thus, the first-wall neutron loading would be 2.53 MW/m^2 [1]. As for the PCA-Li/TOK design, the net electric power output for SiC-He/TOK would be 1200 MWe. Once again, for comparison purposes, the source is adjusted to yield a net electric power of 1000 MWe.

The thicknesses of the various zones in the SiC-He/TOK design are summarized in Table 7.2.4. The first wall would be 1-cm-thick

SiC. Li_2O would be used for breeding, and the blanket would be cooled by high-pressure helium gas which would run through SiC tubes. The blanket would be 49.1-cm-thick and would have a volumetric composition of 16% SiC, 64% Li2O, and 20% He [1].

Table 7.2.4. The SiC-He/TOK design is modeled using a cylindrical approximation that gives the correct first-wall neutron loading [1]. Note that values differ from those presented in the ESECOM report due to the different first-wall radii.

Zone description	Inner radius (cm)	Thickness (cm)	Composition (volume %)	Solid volume (m^3)
Plasma	0	335	100 plasma	0
Vacuum gap	335	34	100 vacuum	0
First wall	369	1	100 SiC	10.2
Inner blanket	370	49.1	64 Li_2O, 20 He, 16 SiC	429
Manifold	419.1	28.9	48 He, 32.3 C, 13.4 SiC, 6.3 BeO	181
Gap	448	40	100 vacuum	0
Shield	488	108	42.5 SiC, 18.4 B_4C, 12.4 Al, 10.9 H_2O, 10.3 W, 5.9 Pb	1445

The manifold region is modeled as a homogeneous mixture with volumetric percentages of 13.4% SiC, 32.3% graphite, 6.3% BeO, and 48% He. It would be 28.9-cm-thick and would be followed by a 40-cm-thick vacuum gap. The 108-cm-thick shield would follow the gap

and would be a composite material with volumetric percentages of 42.5% SiC, 18% B_4C, 12.4% Al, 10.3% W, 5.9% Pb, and 10.9% H_2O [1].

The low-activation SiC-He/TOK design offers a sharp contrast to the PCA-Li/TOK design. The SiC-He/TOK design was given a nominal level of safety assurance (LSA) rating of one by the ESECOM committee. Although subsequent analysis of the PCA-Li/TOK design did not include an LSA rating, it probably would have been assigned a value of four based upon the fact that “the PCA first-wall fares dismally when compared with dose potentials from other first-wall materials” [2]. The other materials to which PCA was compared in the Kinzig, Holdren, and Hibbard paper include SiC, VCrTi, and RAF to which ESECOM assigned nominal LSA ratings of one, three, and two, respectively [2]. Therefore, it is reasonable to expect that analyses of the SiC-He/TOK and PCA-Li/TOK designs will be representative of the safety range of MFE designs.

7.3 Summary of designs

In all, seven different fusion power plant designs are analyzed for their accident, occupational, and waste-disposal hazards. Five of these are IFE designs; two are MFE designs. The IFE designs are

intended to represent a wide range of possible design alternatives. They do not, of course, constitute a complete list of possible designs. Nor do they necessarily include the best possible design. The two MFE designs are intended to be representative of the range of hazards posed by MFE power plants but do not necessarily encompass the full range that is possible. Many design parameters for the various IFE and MFE designs are summarized in Table 7.3.1.

Table 7.3.1. Summary of the main parameters of the design analyzed in the present work.

Parameter	Cascade	HYLIFE-II	Osiris	Prometheus	SOMBRERO	SiC-He/TOK	PCA-Li/TOK
Driver	Heavy ion preferred	Heavy ion	Heavy ion	Heavy ion	Laser	N/A	N/A
First-wall description	5-cm-thick SiC tiles with composite SiC/Al tendons	SS316 tubes coated and filled with flowing Flibe	0.5-cm-thick C composite coated with 0.2 cm Flibe	6-cm-thick SiC structure filled with flowing Pb	1-cm-thick C composite	SiC tubes filled with high-pressure He	PCA structure with flowing Li
First-wall x-ray/debris protection	100 cm blanket of C and $LiAlO_2$ granules	55 cm inner pocket of liquid Flibe	0.2 cm of liquid Flibe	0.05 cm of liquid Pb	0.5 torr of Xe gas	None	None
Breeding material	$LiAlO_2$ granules	liquid Flibe	liquid Flibe	Li_2O pebbles	Li_2O granules	Li_2O pebbles	liquid Li
Blanket heat-transfer media	Granules radiating heat to He in SiC tubes	Flibe	Flibe	He	He	He	liquid Li
Blanket thickness	1.00 m	1.28 m (Flibe pocket and first wall)	0.71 m	1.04 m	1.00 m	0.78 m	0.70 m
Repetition rate	5.6 Hz*	6.4 Hz*	4.6 Hz	3.54 Hz	6.7 Hz	N/A	N/A
Target yield	375 MJ	350 MJ	432 MJ	719 MJ	400 MJ	N/A	N/A
Fusion power	2100 MW	2240 MW	1987 MW	2545 MW	2680 MW	2385 MW*	2688 MW*
Tritium breeding ratio	1.01	1.18	1.24	1.20	1.25	1.06	1.28
Net electric output	1000 MWe	1000 MWe	1000 MWe	1000 MWe	1000 MWe	1000 MWe	1000 MWe

* Adjusted to yield 1000 MWe.

References for Chapter 7

1. J. P. Holdren, D. H. Berwald, R. J. Budnitz, J. G. Crocker, J. G. Delene, R. D. Endicott, M. S. Kazimi, R. A. Krakowski, B. G. Logan, and K. R. Schultz, "Report of the Senior Committee on Environmental, Safety, and Economic Aspects of Magnetic Fusion Energy," Lawrence Livermore National Laboratory, UCRL-53766, (September 1989).
2. A. P. Kinzig, J. P. Holdren, and P. J. Hibbard, "Safety and Environmental Comparisons of Stainless Steel with Alternative Structural Materials for Fusion Reactors," *Fusion Technology*, **26**, 79-104, (August 1994).
3. W. J. Hogan, ed., *Energy from Inertial Fusion*, Vienna, Austria: International Atomic Energy Agency, (1995).
4. J. G. Woodworth and W. R. Meier, "Target Production for Inertial Fusion Energy," Lawrence Livermore National Laboratory, UCRL-JC-117396, L-19153-1, (March 1995).
5. D. D.-M. Ho, private communication, (October 27, 1995).
6. D. D.-M. Ho, J. D. Lindl, and M. Tabak, "Radiation Converter Physics and a Method for Obtaining the Upper Limit for Gain in Heavy Ion Fusion," *Nuclear Fusion*, **34**, 1081, (1994).

7. W. R. Meier, R. L. Bieri, M. J. Monsler, C. D. Hendricks, P. Laybourne, K. R. Shillito, S. K. Ghose, L. M. Goldman, K. D. Auclair, C. Y. Pang, R. F. Bourque, L. D. Stewart, E. E. Bowles, E. L. Hubbard, C. W. von Rosenberg, Jr., M. W. McGeoch, I. N. Sviatoslavsky, R. R. Peterson, M. E. Sawan, H. Y. Khater, L. J. Wittenberg, G. L. Kulcinski, G. A. Moses, E. A. Mogahed, J. J. MacFarlane, S. Rutledge, S. Humphries, Jr., and E. T. Cheng, "Osiris and SOMBRERO Inertial Confinement Fusion Power Plant Designs," DOE/ER/54100-1, WJSA-92-01, W. J. Schafer Associates, Inc., Livermore, CA, (March 1992).

8. J. H. Pitts, "Cascade: A Centrifugal-Action Solid-Breeder Reaction Chamber," *Nuclear Technology of Fusion*, **8**, 717, (1985).

9. D. R. Gardner, ed., "The Cascade Inertial Confinement Fusion Reactor Concept," Lawrence Livermore National Laboratory, UCRL-LR-104546, (December 1990).

10. M. T. Tobin, "Adapting an X-Ray/Debris Shield to the Cascade ICF Power Plant: Neutronics Issues," *Fusion Technology*, **19**, 679, (May 1991).

11. J. A. Blink, W. J. Hogan, J. Hovingh, W. R. Meier, and J. H. Pitts, "The High-Yield Lithium-Injection Fusion Energy (HYLIFE-I)

Reactor," Lawrence Livermore National Laboratory, UCID-53559, (1985).

12. R. W. Moir, "HYLIFE-II Inertial Fusion Energy Power Plant Design," *Inertial Confinement Fusion: 1992 Annual Report*, Lawrence Livermore National Laboratory, UCRL-LR-105820-92, 139, (June 1993).

13. R. W. Moir, R. L. Bieri, X. M. Chen, T. J. Dolan, M. A. Hoffman, P. A. House, R. L. Leber, J. D. Lee, Y. T. Lee, J. C. Liu,. R. Longhurst, W. R. Meier, P. F. Peterson, R. W. Petzoldt, V. E. Schrock, M. T. Tobin, and W. H. Williams, "HYLIFE-II: A Molten-Salt Inertial Fusion Energy Power Plant Design – Final Report," *Fusion Technology*, **25**, (January 1994).

14. P. A. House, "HYLIFE-II Reactor Chamber Mechanical Design: Update," Lawrence Livermore National Laboratory, UCRL-ID-109429, (October 1992).

15. R. W. Moir, "The Logic Behind Thick, Liquid–Walled, Fusion Concepts," *Fusion Engineering and Design*, **29**, 34, (March 1995).

16. R. W. Moir, M. G. Adamson, R. O. Bangter, R. L. Bieri, R. H. Condit, C. W. Hartman, P. A. House, A. B. Langdon, B. G. Logan, C. D. Orth, R. W. Petzoldt, J. H. Pitts, R. F. Post, R. A. Sacks, M. T. Tobin, W. H.

Williams, T. J. Dolan, G. R. Longhurst, M. A. Hoffman, V. E. Schrock, P. F. Peterson, R. Y. Bai, X. M. Chen, J. C. Liu, D.-K. Sze, and W. R. Meier, "HYLIFE-II Progress Report," Lawrence Livermore National Laboratory, UCID-21816, (December 1991).

17. W. R. Meier, "Osiris and SOMBRERO Inertial Fusion Power Plant Designs – Summary, Conclusions, and Recommendations," *Fusion Engineering and Design*, **25**, 145, (August 1994).

18. R. F. Bourque, W. R. Meier, and M. J. Monsler, "Overview of the Osiris IFE Reactor Conceptual Design," *Fusion Technology*, **21**, 1465, (May 1992).

19. L. M. Waganer, D. E. Driemeyer, V. D. Lee, R. L. Calkins, H. B. Wald, F. R. Williams, R. S. Matsugu, O. K. Kveton, K. Kalyanam, S. K. Sood, S. L. Ostrow, S. F. Marschke, P. J. Estreich, M. J. Parnes, D. J. Drake, J. W. F. Millard, J. Ballantyne, T. Haines, D. Perrot, C. English, C. Holloway, A. Turner, G. J. Linford, S. W. Fornaca, A. W. Maschke, M. A. Abdou, N. M. Ghoniem, M. S. Tillack, J. E. Eggleston, F. Issacci, A. Y. Ying, A. El-Azab, A. R. Raffray, M. Z. Youssef, Z. R. Gorbis, S. Sharafat, L. Zhang, and I. Jun, "Inertial Fusion Energy Reactor Design Studies: Prometheus-L and Prometheus-H,"

McDonnell Douglas Aerospace, MDC 92E0008, DOE/ER-54101, (March 1992).

20. L. M. Waganer, "Innovation Leads the Way to Attractive Inertial Fusion Energy Reactors – Prometheus-L and Prometheus-H," *Fusion Engineering and Design*, **25**, 125, (August 1994).

21. F. Najmabadi, R. W. Conn, and the ARIES Team, "The ARIES-1 Tokamak Reactor Study," 16th Symposium on Fusion Technology, London, UK, (September 3-7, 1990).

22. G. R. Hopkins, E. T. Cheng, R. L. Creedon, I. Maya, K. R. Schultz, P. Trester, and C. P. C. Wong, "Low-Activation Fusion Reactor Design Studies," *Nucl. Technol./Fusion*, **4**, 1251, (1985).

23. Argonne National Laboratory, McDonnell-Douglas Astronautics Co., General Atomics Co., and The Ralph M. Parsons Co., "STARFIRE: A Commercial Tokamak Fusion Power Plant Study," Argonne National Laboratory, Argonne, IL, ANL/FPP-80-1, (1980).

8. Results

In this section, results of the previously described analyses are given for each of the power plant designs. The methods and techniques that have been used are described in Chapter 2. The various radiological indices are defined and described in Chapter 3. These results are divided into three categories of radiological hazard: accident, occupational/routine, and waste disposal.

While the results for each of the classes of hazard are given independently, they are inexorably linked. That is, it is highly likely that changing a design detail in an effort to alter a result in one hazard category will also alter results not only in the same hazard category but also in the other two categories. For example, a new material might be selected to replace one that poses a significant accident risk due to its early dose. Although the new material may decrease the overall early dose, it may also have a negative effect upon other indices such as the intruder dose. When modifications are made to a point design, one must consider not only the implications for the hazard index that guided the design change but for the entire set of radiological indices as well.

8.1 Accident hazards

The indices that relate to the accident hazard posed by a particular design range from the relatively uninformative activity to the useful and intuitive estimates for the number of early and cancer fatalities. Results for each of the indices calculated in this study are given, along with some explanation of dominant pathways and contributors. In some cases, the implications of a particular result are discussed briefly.

8.1.1 Activity

As mentioned in Chapter 3, the use of activity as a measure of accident hazard has little value. Nonetheless, activity is often used due to its ease of calculation. In order to allow comparison to past studies which have given activity results and future studies which will inevitably give more activity results, such results are given here. Table 8.1.1 lists the activities found at shutdown for the major components in each power plant design. The results are given by mobility category with and without tritium activities. A total shutdown activity is also given for each power plant with and without its estimated tritium inventory. A dominant radionuclide is

identified for each component and mobility category. Finally, the shutdown activities for four pure and one impure candidate high-Z target materials are given. Figure 8.1.1 shows the total activity, excluding tritium, for each power plant as a function of time after shutdown.

The HYLIFE-II and Osiris designs would have the highest initial total activity due to the production of large quantities of ^{16}N and ^{8}Be via the $^{19}F(n,\alpha)$ and $^{9}Be(n,2n)$ reactions, respectively, on liquid Flibe. Both isotopes, however, have half-lives significantly shorter than one minute, so the total activities fall quickly.

The PCA-Li/TOK design would have the highest activity during most of the first 1000 years of decay. At times of less than several years, its activity would be dominated by ^{51}Cr and ^{55}Fe. SOMBRERO would have the lowest total activity during the first year of decay. The seven designs would differ in total activity by about a factor of fifty out to 1000 years of decay. None of the candidate target materials would make a significant contribution to the total activity of an IFE target factory or of any of the power plant designs.

Table 8.1.1. Radioactive inventories at shutdown for each of the power plant designs by component and mobility category.[a]

Component	Mobility category I Activity (Bq)	I Main Isotope	II Activity (Bq)	II Main Isotope	III Activity (Bq)	III Main Isotope	IV Activity (Bq)	IV Main Isotope	V Activity (Bq)	V Main Isotope
Cascade										
C granules	1.5E+16	^{6}He	7.9E+13	^{32}P	1.3E+17	^{8}Be	4.1E+14	^{207m}Pb	7.3E+13	^{55}Fe
$LiAlO_2$ granules w/o T	1.2E+19	^{16}N	1.5E+18	^{76}As	3.6E+17	^{8}Be	2.2E+17	^{122}Sb	1.2E+17	^{60m}Fe
$LiAlO_2$ granules w/ 1 kg T	1.3E+19	^{16}N	1.5E+18	^{76}As	3.6E+17	^{8}Be	2.2E+17	^{122}Sb	1.2E+17	^{60m}Fe
SiC first wall	1.7E+12	^{16}N	2.1E+15	^{27}Mg	1.6E+11	^{8}Be	8.6E+11	^{56}Mn	5.1E+17	^{28}Al
SiC/Al tendons	8.1E+13	^{23}Ne	6.2E+16	^{27}Mg	7.1E+15	^{65}Zn	2.0E+17	^{56}Mn	1.3E+18	^{28}Al
Water shield	7.5E+16	^{16}N	3.2E+17	^{27}Mg	4.4E+16	^{51}Cr	1.5E+18	^{56}Mn	8.5E+18	^{28}Al
Al-5083 vacuum vessel	2.7E+14	^{23}Ne	1.5E+17	^{24}Na	3.4E+15	^{51}Cr	1.2E+17	^{56}Mn	5.2E+17	^{28}Al
Concrete shield	6.0E+16	^{16}N	1.8E+17	^{24}Na	9.4E+15	^{45}Ca	3.6E+16	^{56}Mn	7.1E+17	^{28}Al
Total w/o T	1.2E+19	^{16}N	2.2E+18	^{76}As	5.5E+17	^{8}Be	2.1E+18	^{56}Mn	1.2E+19	^{28}Al
Total w/ 1 kg T	1.3E+19	^{16}N	2.2E+18	^{76}As	5.5E+17	^{8}Be	2.1E+18	^{56}Mn	1.2E+19	^{28}Al
HYLIFE-II										
SS304 first wall w/o T	2.9E+14	^{83m}Kr	1.0E+17	^{76}As	3.8E+17	^{51}Cr	7.5E+17	^{56}Mn	1.6E+18	^{55}Fe
SS304 first wall w/ 140 g T	5.2E+16	^{3}H	1.0E+17	^{76}As	3.8E+17	^{51}Cr	7.5E+17	^{56}Mn	1.6E+18	^{55}Fe
SS304 blanket	1.6E+12	^{14}C	3.5E+15	^{76}As	6.9E+15	^{51}Cr	4.1E+15	^{56}Mn	1.8E+16	^{55}Fe
SS304 assorted	8.3E+13	^{14}C	6.4E+16	^{76}As	1.9E+17	^{51}Cr	9.4E+16	^{56}Mn	3.7E+17	^{55}Fe
SS304 vacuum vessel	6.1E+11	^{14}C	5.2E+14	^{76}As	2.6E+15	^{51}Cr	7.7E+14	^{56}Mn	3.8E+15	^{55}Fe
Flibe w/o T	1.0E+20	^{16}N	5.4E+17	^{8}Li	1.3E+20	^{8}Be	1.5E+16	^{183m}W	7.6E+16	^{182}Ta
Flibe w/ 0.5 g T	1.0E+20	^{16}N	5.4E+17	^{8}Li	1.3E+20	^{8}Be	1.5E+16	^{183m}W	7.6E+16	^{182}Ta
Concrete shield	1.9E+15	^{37}Ar	9.5E+15	^{24}Na	8.8E+14	^{45}Ca	2.5E+16	^{56}Mn	4.2E+16	^{55}Fe
Total w/o T	1.0E+20	^{16}N	7.2E+17	^{8}Li	1.3E+20	^{8}Be	8.8E+17	^{56}Mn	2.1E+18	^{55}Fe
Total w/ 140 g T	1.0E+20	^{16}N	7.2E+17	^{8}Li	1.3E+20	^{8}Be	8.8E+17	^{56}Mn	2.1E+18	^{55}Fe

Table 8.1.1. (Continued.)

Component	Mobility category I Activity (Bq)	I Main Isotope	II Activity (Bq)	II Main Isotope	III Activity (Bq)	III Main Isotope	IV Activity (Bq)	IV Main Isotope	V Activity (Bq)	V Main Isotope
Osiris										
C/C first wall w/o T	5.6E+15	^{6}He	2.6E+13	^{24}Na	6.0E+16	^{8}Be	1.0E+13	^{207m}Pb	6.2E+13	^{28}Al
C/C first wall w/ 10.5 g T	9.5E+15	^{6}He	2.6E+13	^{24}Na	6.0E+16	^{8}Be	1.0E+13	^{207m}Pb	6.2E+13	^{28}Al
C/C blanket	1.6E+15	^{6}He	2.1E+13	^{24}Na	1.5E+16	^{8}Be	7.2E+12	^{207m}Pb	4.7E+13	^{28}Al
C/C vacuum vessel	1.0E+15	^{6}He	1.7E+15	^{24}Na	6.0E+15	^{8}Be	2.8E+13	^{56}Mn	1.1E+15	^{52}V
Flibe w/o T	8.4E+19	^{16}N	4.3E+17	^{8}Li	1.0E+20	^{8}Be	1.4E+16	^{183m}W	6.4E+16	^{12}B
Flibe w/ 1 g T	8.4E+19	^{16}N	4.3E+17	^{8}Li	1.0E+20	^{8}Be	1.4E+16	^{183m}W	6.4E+16	^{12}B
Concrete shield	1.7E+17	^{37}Ar	6.7E+17	^{24}Na	6.2E+16	^{45}Ca	1.6E+18	^{56}Mn	2.8E+18	^{55}Fe
Total w/o T	8.4E+19	^{16}N	1.1E+18	^{8}Li	1.0E+20	^{8}Be	1.6E+18	^{56}Mn	2.8E+18	^{55}Fe
Total w/ 11.5 g T	8.4E+19	^{16}N	1.1E+18	^{8}Li	1.0E+20	^{8}Be	1.6E+18	^{56}Mn	2.8E+18	^{55}Fe
PCA-Li/TOK										
PCA first wall	1.8E+14	^{13}N	3.3E+17	^{99}Mo	2.0E+18	^{51}Cr	8.8E+18	^{56}Mn	2.2E+19	^{55}Fe
PCA blanket	2.1E+14	^{13}N	4.1E+17	^{99}Mo	2.5E+18	^{51}Cr	1.1E+19	^{56}Mn	2.7E+19	^{55}Fe
PCA manifold	1.1E+13	^{13}N	9.6E+16	^{99}Mo	1.5E+17	^{51}Cr	8.7E+17	^{56}Mn	1.9E+18	^{58}Co
FeCrV manifold	1.3E+14	^{13}N	5.2E+16	^{64}Cu	4.8E+17	^{51}Cr	8.3E+18	^{56}Mn	5.7E+18	^{55}Fe
Li coolant w/o T	1.2E+19	^{6}He	2.5E+16	^{8}Li	2.3E+16	^{8}Be	1.7E+14	^{56}Mn	4.9E+15	^{28}Al
Li coolant w/ 700 g T	1.3E+19	^{6}He	2.5E+16	^{8}Li	2.3E+16	^{8}Be	1.7E+14	^{56}Mn	4.9E+15	^{28}Al
FeCrV shield	9.9E+14	^{16}N	1.8E+16	^{64}Cu	1.4E+17	^{51}Cr	4.8E+17	^{56}Mn	1.7E+18	^{55}Fe
Total w/o T	1.2E+19	^{6}He	9.2E+17	^{99}Mo	5.3E+18	^{51}Cr	2.9E+19	^{56}Mn	5.7E+19	^{55}Fe
Total w/ 700 g T	1.3E+19	^{6}He	9.2E+17	^{99}Mo	5.3E+18	^{51}Cr	2.9E+19	^{56}Mn	5.7E+19	^{55}Fe

Table 8.1.1. (Continued.)

Component	Mobility category I Activity (Bq)	I Main Isotope	II Activity (Bq)	II Main Isotope	III Activity (Bq)	III Main Isotope	IV Activity (Bq)	IV Main Isotope	V Activity (Bq)	V Main Isotope
Prometheus-H										
SiC first wall w/o T	8.4E+15	^{6}He	3.0E+17	^{27}Mg	6.0E+16	^{8}Be	5.5E+13	^{56}Mn	1.3E+19	^{28}Al
Pb first wall coolant	4.5E+10	^{127}Xe	9.5E+16	^{203}Pb	9.0E+15	^{210}Po	8.7E+19	^{207m}Pb	2.3E+16	^{110}Ag
SiC blanket	9.3E+15	^{6}He	5.6E+17	^{27}Mg	6.6E+16	^{8}Be	1.6E+14	^{56}Mn	3.8E+19	^{28}Al
Li_2O blanket w/o T	4.7E+18	^{16}N	9.0E+16	^{8}Li	8.5E+16	^{8}Be	4.5E+15	^{56}Mn	2.7E+15	^{58}Co
Li_2O blanket w/ 100 g T	4.7E+18	^{16}N	9.0E+16	^{8}Li	8.5E+16	^{8}Be	4.5E+15	^{56}Mn	2.7E+15	^{58}Co
HT-9 vacuum vessel	1.4E+12	^{14}C	7.2E+16	^{188}Re	5.7E+16	^{51}Cr	3.9E+17	^{187}W	1.1E+17	^{55}Fe
Prometheus shield	4.6E+15	^{16}N	5.2E+16	^{8}Li	1.2E+18	^{8}Be	7.3E+16	^{207m}Pb	2.0E+17	^{31}Si
Total w/o T	4.7E+18	^{16}N	1.2E+18	^{27}Mg	1.5E+18	^{8}Be	8.7E+19	^{207m}Pb	5.1E+19	^{28}Al
Total w/ 100 g T	4.7E+18	^{16}N	1.2E+18	^{27}Mg	1.5E+18	^{8}Be	8.7E+19	^{207m}Pb	5.1E+19	^{28}Al
SiC-He/TOK										
SiC first wall	2.4E+15	^{6}He	5.4E+17	^{27}Mg	2.8E+16	^{8}Be	8.2E+13	^{56}Mn	2.0E+19	^{28}Al
SiC blanket	1.1E+15	^{6}He	4.5E+17	^{27}Mg	7.2E+15	^{8}Be	1.1E+14	^{56}Mn	2.7E+19	^{28}Al
Li_2O blanket w/o T	1.9E+19	^{16}N	5.2E+17	^{8}Li	5.0E+17	^{8}Be	1.5E+16	^{56}Mn	6.3E+15	^{58}Co
Li_2O blanket w/ 360 g T	1.9E+19	^{16}N	5.2E+17	^{8}Li	5.0E+17	^{8}Be	1.5E+16	^{56}Mn	6.3E+15	^{58}Co
C+ manifold	1.5E+17	^{6}He	1.8E+15	^{27}Mg	8.0E+17	^{8}Be	2.6E+12	^{207m}Pb	4.1E+17	^{28}Al
SiC+ shield	1.6E+15	^{16}N	4.8E+16	^{27}Mg	5.5E+16	^{8}Be	4.9E+18	^{187}W	1.3E+17	^{28}Al
Total w/o T	1.9E+19	^{16}N	1.6E+18	^{27}Mg	1.4E+18	^{8}Be	4.9E+18	^{187}W	4.8E+19	^{28}Al
Total w/ 360 g T	1.9E+19	^{16}N	1.6E+18	^{27}Mg	1.4E+18	^{8}Be	4.9E+18	^{187}W	4.8E+19	^{28}Al

Table 8.1.1. (Continued.)

Component	Mobility category I Activity (Bq)	I Main Isotope	II Activity (Bq)	II Main Isotope	III Activity (Bq)	III Main Isotope	IV Activity (Bq)	IV Main Isotope	V Activity (Bq)	V Main Isotope
SOMBRERO										
C/C first wall w/o T	1.5E+16	^{6}He	6.8E+13	^{24}Na	1.5E+17	^{8}Be	2.8E+13	^{207m}Pb	1.7E+14	^{28}Al
C/C first wall w/ 10 g T	1.9E+16	^{6}He	6.8E+13	^{24}Na	1.5E+17	^{8}Be	2.8E+13	^{207m}Pb	1.7E+14	^{28}Al
C/C blanket	7.7E+15	^{6}He	2.0E+14	^{24}Na	6.4E+16	^{8}Be	5.0E+13	^{207m}Pb	3.8E+14	^{28}Al
Li_2O blanket w/o T	1.8E+19	^{16}N	7.0E+17	^{8}Li	6.8E+17	^{8}Be	2.1E+16	^{56}Mn	9.2E+15	^{55}Fe
Li_2O blanket w/ 167 g T	1.8E+19	^{16}N	7.0E+17	^{8}Li	6.8E+17	^{8}Be	2.1E+16	^{56}Mn	9.2E+15	^{55}Fe
Xe gas w/o T	4.9E+16	^{131m}Xe	3.8E+14	^{125}I	5.3E+13	^{137m}Ba	4.0E+09	^{124}Sb	5.1E+07	^{123}Sn
Xe gas w/ 4.6 g T	5.1E+16	^{131m}Xe	3.8E+14	^{125}I	5.3E+13	^{137m}Ba	4.0E+09	^{124}Sb	5.1E+07	^{123}Sn
Ba-concrete shield	2.5E+16	^{37}Ar	5.5E+16	^{32}P	2.0E+17	^{136m}Ba	5.8E+16	^{56}Mn	3.7E+16	^{55}Fe
Total w/o T	1.8E+19	^{16}N	7.6E+18	^{8}Li	1.1E+18	^{8}Be	7.9E+16	^{56}Mn	4.7E+16	^{55}Fe
Total w/ 182 g T	1.8E+19	^{16}N	7.6E+18	^{8}Li	1.1E+18	^{8}Be	7.9E+16	^{56}Mn	4.7E+16	^{55}Fe
High-Z Target Materials										
Tantalum	0.0E+00	N/A	2.9E+06	^{184}Re	0.0E+00	N/A	2.0E+15	^{181}W	3.7E+16	^{182}Ta
Tungsten	0.0E+00	N/A	5.5E+15	^{184}Re	0.0E+00	N/A	1.6E+17	^{185}W	1.2E+15	^{182}Ta
Mercury	0.0E+00	N/A	2.1E+16	^{203}Hg	0.0E+00	N/A	6.8E+14	^{202}Tl	1.2E+15	^{196}Au
Lead	0.0E+00	N/A	3.1E+13	^{203}Hg	4.1E+09	^{210}Po	6.0E+14	^{203}Pb	3.8E+10	^{207}Bi
Impure lead	0.0E+00	N/A	3.1E+13	^{203}Hg	9.5E+12	^{121}Te	6.8E+14	^{203}Pb	3.4E+13	^{106m}Ag

[a] Radionuclide activities are at shutdown after maximum irradiation of the indicated components (set according to radiation damage limit for the given material). Main isotope means largest single contributor to the total activity. Al-5083 denotes the ASTM 5083 aluminum alloy; Flibe denotes a molten salt of two parts LiF and one part BeF_2; C/C denotes carbon-carbon composite; Prometheus shield denotes a combination of SiC plus B_4C, Pb, H_2O, and Al; C+ means C plus SiC and BeO; SiC+ means SiC plus B_4C, Al, H_2o, W, and Pb. Impure lead includes 0.01 wt% Cu, 0.05 wt% Ag, 0.15 wt% Sb, and 0.20 wt% Bi.

Figure 8.1.1. Total activity, excluding tritium, for each power plant.

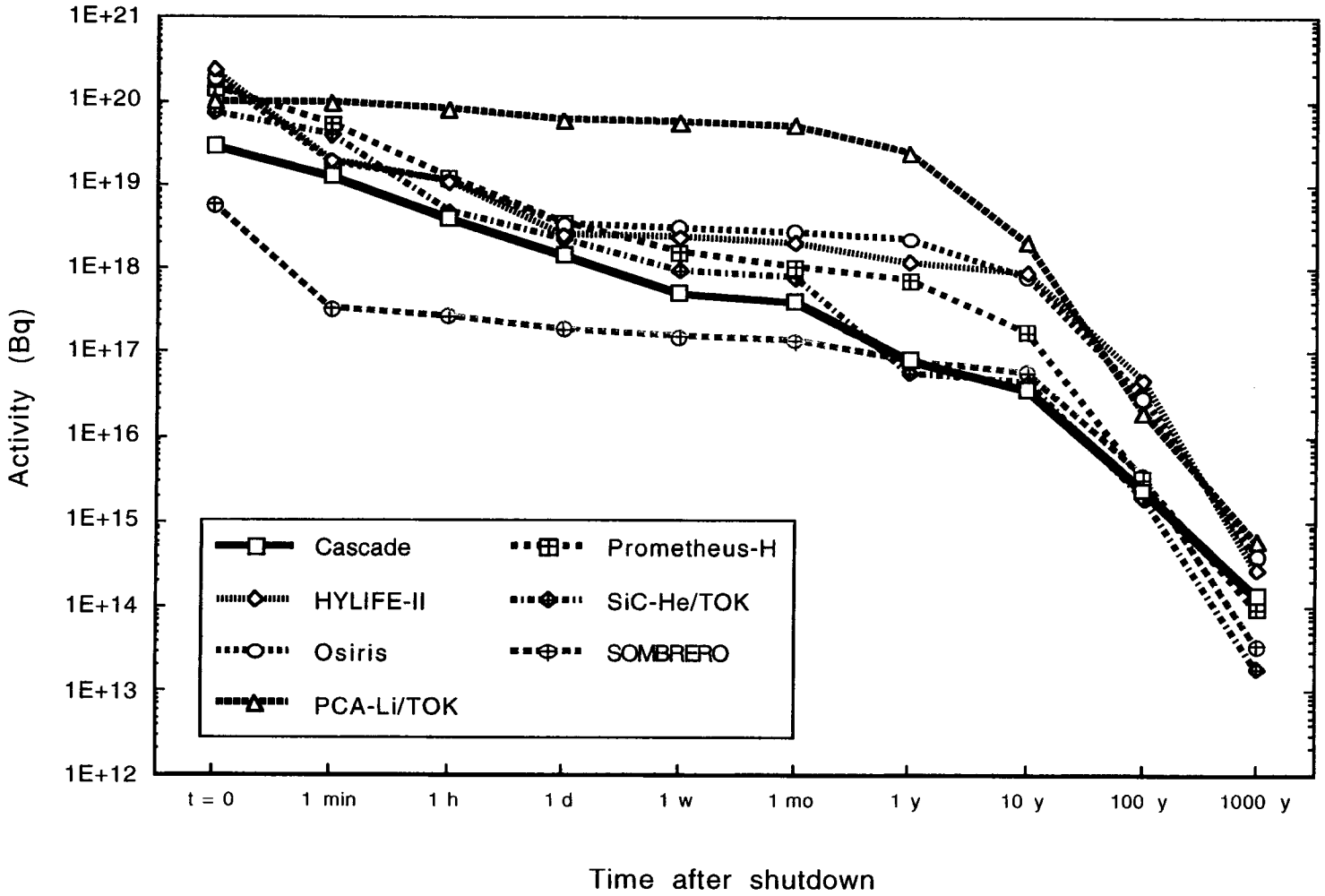

8.1.2 Biological hazard potential in air

The total biological hazard potential (BHP) in air (sum of the BHPs of all components) is given in Figure 8.1.2 for each power plant. Contributions from tritium are not included in the totals, but the BHP in air for 1 kg of tritium is shown for reference. From shutdown out to 10 years after shutdown, the SiC-He/TOK is better than the PCA-Li/TOK by two to three orders of magnitude. After 10 years, SiC-He/TOK is better than PCA-Li/TOK by about a factor of ten.

The BHPs for the IFE designs fall between the two MFE designs at most times. Just before 1000 years, however, Osiris moves into the highest position. Its BHP is dominated by ^{41}Ca. The BHP for HYLIFE-II falls below that for SiC-He/TOK just before 1000 years. Cascade, HYLIFE-II, and Prometheus-H, have the highest BHP at early times, and HYLIFE-II and SOMBRERO have BHPs that are five to ten times lower than those of the other IFE designs at 1000 years after shutdown.

Figure 8.1.2. The biological hazard potential in air is the volume of air which would be contaminated to maximum acceptable levels if the entire radioactive inventory of each design was released to the environment. Results for each design do not include contributions from tritium, but values for 1 kg of tritium are given for reference.

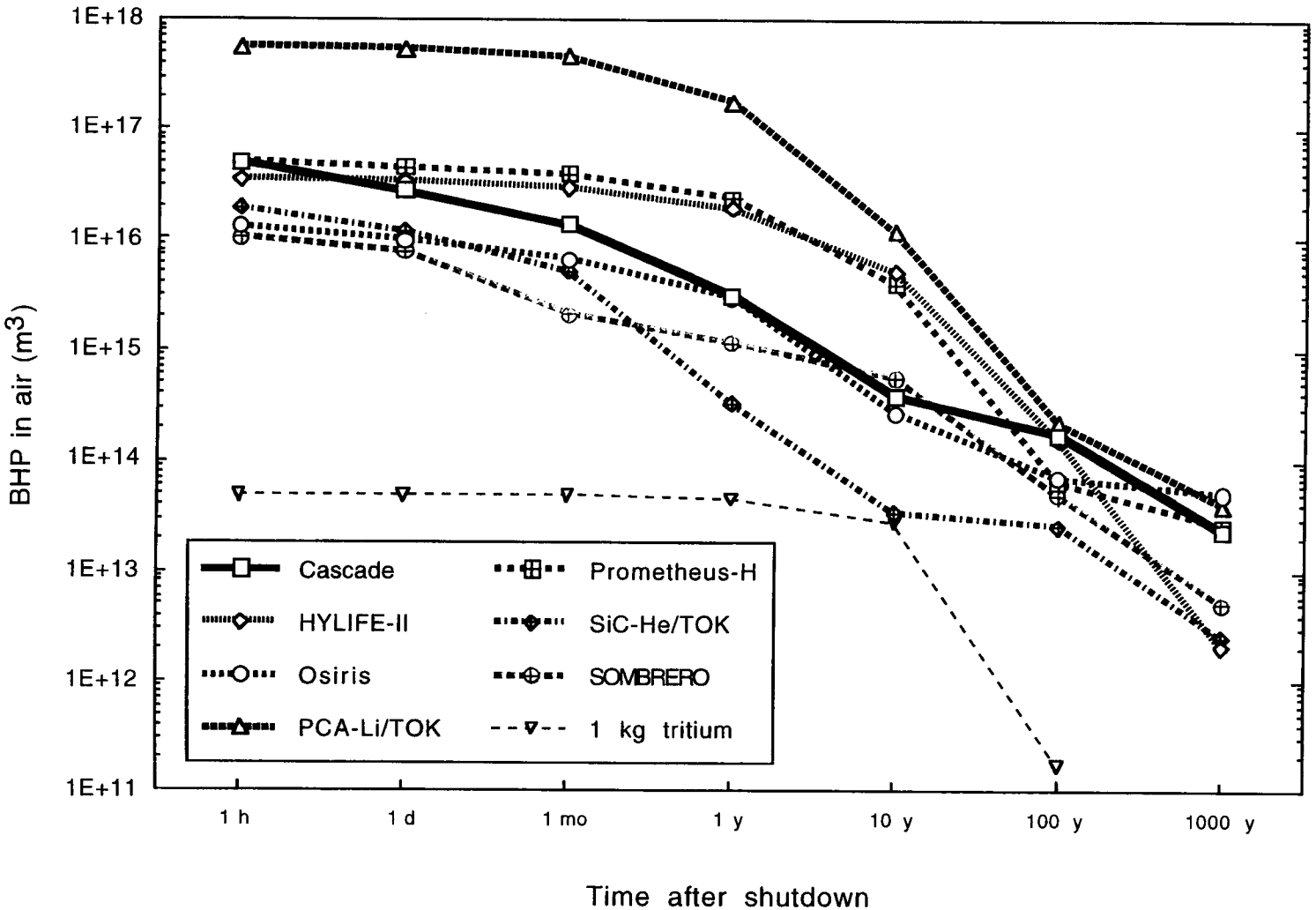

8.1.3 Threshold-dose release fractions

As mentioned in Chapter 3, this work uses organ-specific doses, so critical, whole-body, threshold-dose release fractions (TDRFs) have not been calculated. Instead, three separate critical TDRFs have been calculated. These TDRFs are for the bone marrow, lung, and gastrointestinal tract. Table 8.1.2 gives the total critical TDRFs for each design according to a range of mobility classes. The threshold doses used are 1.5 Sv for the bone marrow, 5.0 Sv for the lung, and 7.5 Sv for the gastrointestinal tract. Critical TDRFs are calculated for a downwind distance of 1 km using pessimistic release and weather assumptions.

Only the SOMBRERO design would have any critical TDRFs in excess of one. The entire SOMBRERO inventory may be released without the risk of causing early fatalities from doses associated with the lung or gastrointestinal tract. Such a release, however, would cause early fatalities due to bone marrow syndrome.

Chronic TDRFs have been calculated for a downwind distance of 10 km and use a threshold dose of 0.25 Sv. Table 8.1.3 gives the chronic TDRFs for each design and identifies the dominant radionuclides. SOMBRERO comes closest to attaining a chronic TDRF

Table 8.1.2. Total critical threshold-dose release fractions by mobility category.[a]

Mobility category	Bone marrow TDRF	Bone marrow Dominant radionuclides	Lung TDRF	Lung Dominant radionuclides	Gastrointestinal tract TDRF	Gastrointestinal tract Dominant radionuclides
Cascade						
I	1.7E+2	^{38}Cl	5.2E+2	^{38}Cl	6.1E+2	^{38}Cl
I-II	4.3E-2	^{24}Na, ^{76}As	4.6E-2	^{76}As	6.7E-2	^{76}As, ^{24}Na
I-III	3.9E-2	^{24}Na, ^{76}As	4.4E-2	^{76}As	6.3E-2	^{76}As, ^{24}Na
I-IV	2.6E-2	^{24}Na, ^{56}Mn, ^{76}As	3.2E-2	^{76}As, ^{56}Mn	4.7E-2	^{76}As, ^{24}Na
I-V	1.5E-2	^{46}Sc, ^{24}Na	2.6E-2	^{76}As, ^{56}Mn, ^{46}Sc	3.3E-2	^{76}As, ^{46}Sc, ^{24}Na
HYLIFE-II						
I	1.9E-2	^{18}F	7.5E-2	^{18}F	7.2E-2	^{18}F
I-II	1.8E-2	^{18}F	6.9E-2	^{18}F	6.9E-2	^{18}F
I-III	1.8E-2	^{18}F	6.7E-2	^{18}F	6.7E-2	^{18}F
I-IV	1.5E-2	^{18}F	5.2E-2	^{18}F	5.4E-2	^{18}F
I-V	8.2E-3	^{18}F, ^{58}Co, ^{60}Co	2.9E-2	^{18}F, ^{60}Co	2.7E-2	^{18}F, ^{58}Co, ^{60}Co
Osiris						
I	2.3E-2	^{18}F	9.1E-2	^{18}F	8.8E-2	^{18}F
I-II	1.6E-2	^{18}F	6.3E-2	^{18}F	6.3E-2	^{18}F
I-III	1.6E-2	^{18}F	6.3E-2	^{18}F	6.3E-2	^{18}F
I-IV	1.4E-2	^{18}F	4.5E-2	^{18}F	5.3E-2	^{18}F
I-V	1.3E-2	^{18}F	4.2E-2	^{18}F	4.7E-2	^{18}F
PCA-Li/TOK						
I	6.9E+2	^{38}Cl, ^{41}Ar	2.2E+3	^{38}Cl	2.5E+3	^{38}Cl, ^{41}Ar
I-II	1.9E-1	^{99}Mo	2.6E-1	^{99}Mo	1.8E-1	^{99}Mo
I-III	7.1E-2	^{51}Cr	1.6E-1	^{99}Mo, ^{51}Cr	1.1E-1	^{99}Mo, ^{51}Cr
I-IV	1.9E-3	^{54}Mn	5.9E-3	^{54}Mn, ^{56}Mn	6.3E-3	^{54}Mn
I-V	6.9E-4	^{58}Co, ^{54}Mn	2.4E-3	^{58}Co, ^{54}Mn, ^{56}Mn	2.1E-3	^{58}Co
Prometheus-H						
I	4.0E+2	^{13}N, ^{38}Cl	1.3E+3	^{38}Cl, ^{13}N	1.5E+3	^{13}N, ^{38}Cl
I-II	2.5E-1	^{24}Na	5.9E-1	^{24}Na, ^{28}Mg, ^{203}Hg	6.3E-1	^{24}Na, ^{203}Hg
I-III	1.9E-1	^{24}Na, ^{210}Po	4.4E-1	^{24}Na, ^{210}Po	4.3E-1	^{210}Po, ^{24}Na, ^{203}Hg
I-IV	2.5E-2	^{203}Pb	8.6E-2	^{203}Pb	7.8E-2	^{203}Pb
I-V	2.4E-2	^{203}Pb	5.4E-2	^{203}Pb	7.2E-2	^{203}Pb
SiC-He/TOK						
I	2.4E+2	^{38}Cl	7.3E+2	^{38}Cl	8.6E+2	^{38}Cl
I-II	3.8E-1	^{24}Na, ^{28}Mg	9.7E-1	^{24}Na, ^{28}Mg	1.2E+0	^{24}Na, ^{28}Mg
I-III	3.8E-1	^{24}Na, ^{28}Mg	9.6E-1	^{24}Na, ^{28}Mg	1.2E+0	^{24}Na, ^{28}Mg
I-IV	5.5E-2	^{187}W	1.1E-1	^{187}W	8.9E-2	^{187}W
I-V	5.3E-2	^{187}W	8.1E-2	^{187}W	8.5E-2	^{187}W

Table 8.1.2. (Continued.)

Mobility category	Bone marrow TDRF	Bone marrow Dominant radionuclides	Lung TDRF	Lung Dominant radionuclides	Gastrointestinal tract TDRF	Gastrointestinal tract Dominant radionuclides
			SOMBRERO			
I	1.5E+2	^{38}Cl, ^{135}Xe	5.0E+2	^{38}Cl, ^{135}Xe	4.2E+1	^{127}Xe
I-II	7.1E-1	^{32}P	3.4E+0	^{32}P	4.9E+0	^{32}P
I-III	5.4E-1	^{32}P	2.4E+0	^{32}P	2.0E+0	^{131}Ba, ^{32}P
I-IV	3.4E-1	^{32}P	1.2E+0	^{56}Mn, ^{32}P, ^{54}Mn	1.2E+0	^{54}Mn, ^{131}Ba, ^{32}P
I-V	3.2E-1	^{32}P	1.2E+0	^{56}Mn, ^{32}P, ^{54}Mn	1.1E+0	^{54}Mn, ^{131}Ba, ^{32}P

[a] TDRFs (threshold-dose release fractions) shown are the fraction (or multiple) of the radioactive inventory within each mobility category range that would produce early fatalities at 1 km from the release under pessimistic assumptions. The TDRF for each organ assumes that the dose received is entirely to that single organ. The lowest doses at which early fatalities would be expected are 1.5 Sv to the bone marrow, 5.0 Sv to the lung, and 7.5 Sv to the gastrointestinal tract.

Table 8.1.3. Total chronic threshold-dose release fractions by mobility category.[a]

Mobility category	TDRF	Dominant radionuclides
	Cascade	
I	1.4E+3	^{41}Ar
I-II	5.8E-2	^{76}As, ^{24}Na
I-III	3.7E-2	^{76}As, ^{65}Zn, ^{24}Na
I-IV	2.6E-2	^{76}As, ^{65}Zn, ^{24}Na
I-V	8.6E-3	^{46}Sc, ^{60}Co
	HYLIFE-II	
I	3.1E-1	^{18}F
I-II	2.5E-1	^{18}F
I-III	1.9E-1	^{18}F
I-IV	1.9E-2	^{54}Mn
I-V	1.1E-3	^{60}Co
	Osiris	
I	3.8E-1	^{18}F
I-II	9.9E-2	^{24}Na, ^{18}F
I-III	9.5E-2	^{24}Na, ^{18}F
I-IV	3.6E-2	^{54}Mn, ^{24}Na
I-V	2.3E-2	^{54}Mn, ^{24}Na, ^{59}Fe
	PCA-Li/TOK	
I	6.6E+3	^{41}Ar
I-II	1.9E-1	^{99}Mo
I-III	6.9E-2	^{51}Cr, ^{99}Mo
I-IV	4.8E-4	^{54}Mn
I-V	1.8E-4	^{54}Mn, ^{60}Co, ^{58}Co
	Prometheus-H	
I	7.0E+3	^{18}F
I-II	3.7E-1	^{203}Hg, ^{24}Na
I-III	1.2E-1	^{210}Po
I-IV	3.3E-2	^{203}Pb, ^{210}Po, ^{204}Tl
I-V	1.6E-2	^{207}Bi, ^{203}Pb
	SiC-He/TOK	
I	2.4E+3	^{41}Ar
I-II	9.6E-1	^{24}Na, ^{28}Mg
I-III	9.4E-1	^{24}Na, ^{28}Mg
I-IV	9.0E-2	^{187}W
I-V	8.0E-2	^{187}W

Table 8.1.3. (Continued.)

Mobility category	TDRF	Dominant radionuclides
	SOMBRERO	
I	2.8E+2	^{135}Xe
I-II	2.1E+0	^{32}P
I-III	1.8E-1	^{133}Ba
I-IV	1.0E-1	^{133}Ba, ^{54}Mn
I-V	9.6E-2	^{133}Ba, ^{54}Mn

[a] TDRFs (threshold-dose release fractions) shown are the fraction (or multiple) of the radioactive inventory within each mobility category range that would produce a 50-year effective whole-body dose of 0.25 Sv (including food and water ingestion) at 10 km from the release under pessimistic assumptions.

greater than one, but it still falls short by more than an order of magnitude. The PCA-Li/TOK design must, on the average, release less than one part in 10,000 of its entire inventory in order to fall below the 0.25 Sv threshold.

8.1.4 Worst- and initial-case early doses

Figures 8.1.3 and 8.1.4 give early doses, corresponding to the worst- and initial-cases, respectively, for each design at the site boundary distance of 1 km. The doses are given by organ and mobility category.

Each figure also gives a whole-body early dose resulting from the release of 1 kg of tritium (as oxide). The early dose at a distance of 1 km from the release is approximately 0.8 Sv/kg. This value is nearly seven times larger than estimated doses published in ESECOM and subsequent work [1,2]. The results vary due to the different assumptions made with regard to the time over which the dose would be received. ESECOM and Kinzig, Holdren, and Hibbard calculated a 50-year dose commitment resulting only from the inhalation that occurs during plume passage. The present work, however, assumes a 7-day residence time prior to evacuation and

Figure 8.1.3. Early doses to the three organs are shown for each of the power plant designs. These results use the worst-case release fractions, which assume that all materials react to form their most mobile compounds. The early dose (whole body) is also given for the release of 1 kg of tritium (as oxide).

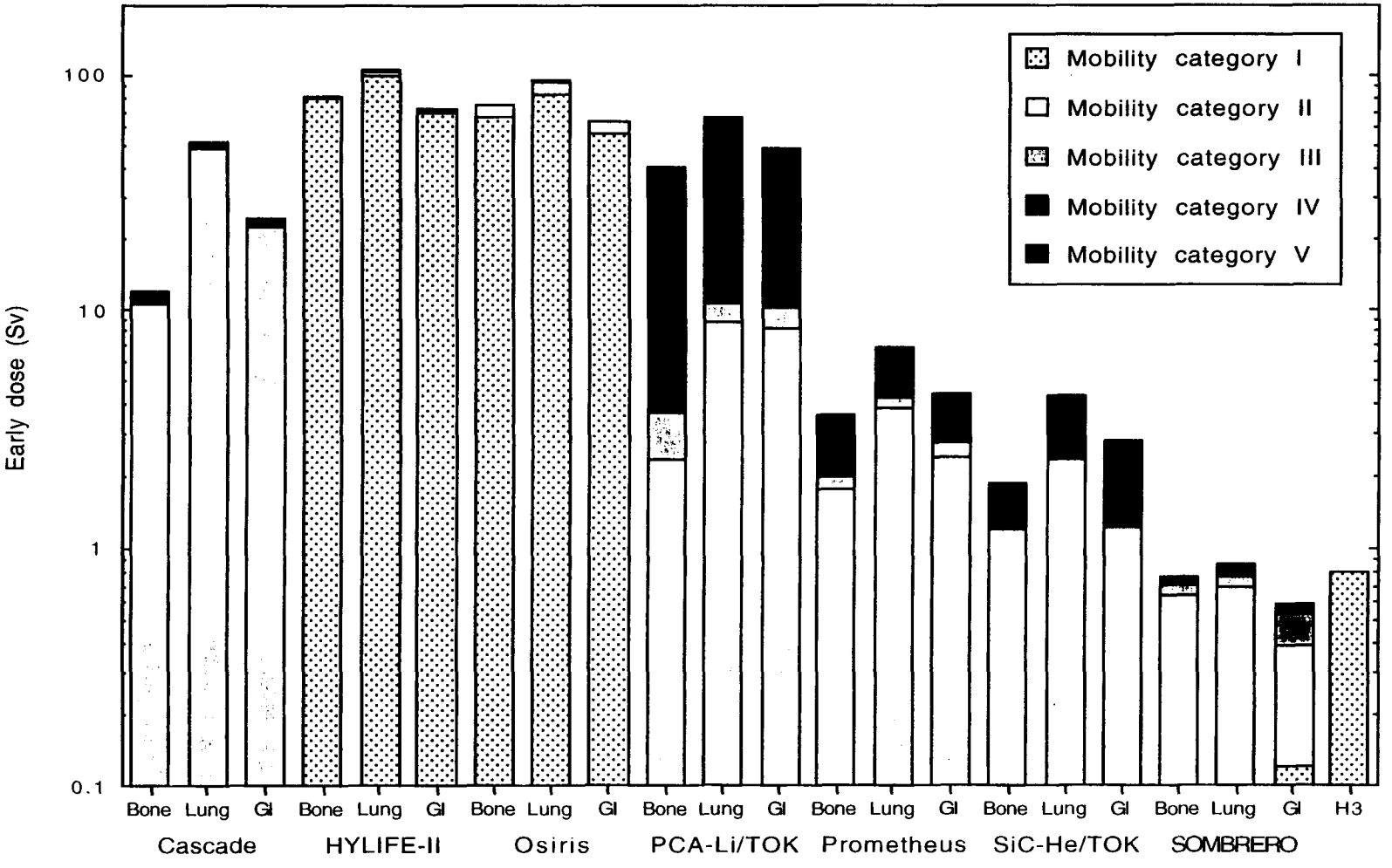

Figure 8.1.4. Early doses to the three organs are shown for each of the power plant designs. These results use the initial-case release fractions, in which chemical compounds, rather than elements, are classified into mobility categories according to their boiling points. Alkali metals, when minor constituents or impurities, are classified by their boiling points instead of being arbitrarily placed into the second mobility category. For comparison, a whole-body dose is also given for the release of 1 kg of tritium (as oxide).

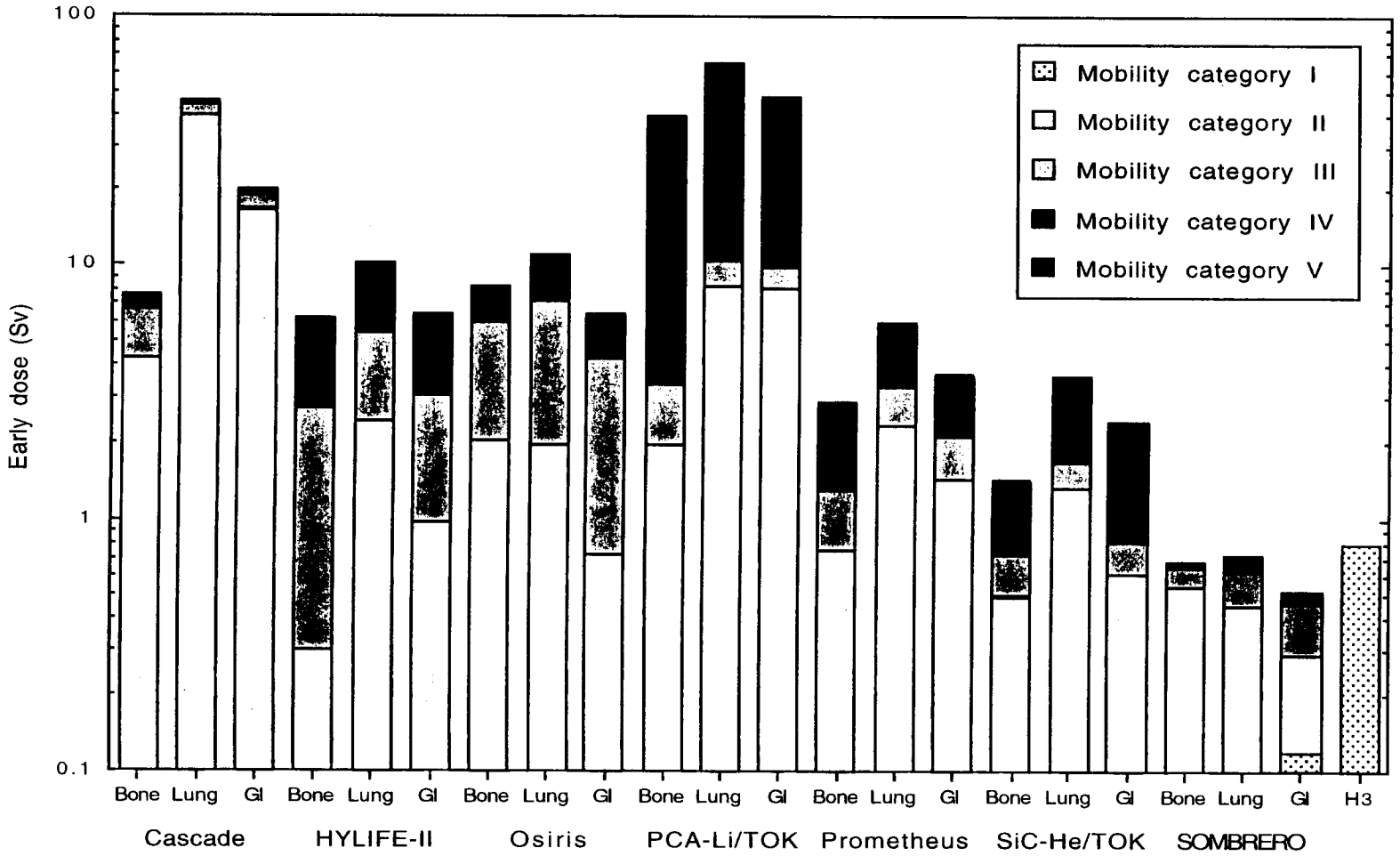

includes the dose commitment from inhaled, resuspended material during that residence time.

Doses that would result from the release of any of the candidate high-Z target materials are quite low and are not included in the figures. The worst of the candidate target materials would be pure mercury. Its early dose to the bone marrow would be 0.13 Sv. Pure tungsten would be the second worst with a dose of 0.12 Sv. The dose from tantalum would be 0.03 Sv, and the doses from pure and impure lead would be 0.001 and 0.002 Sv, respectively. Although these doses are quite low, it is likely that mercury and tungsten would have impurities which would pose a more serious hazard than that presented by the pure materials.

Figure 8.1.3 shows that early doses as high as 100 Sv would result from large release fractions. The HYLIFE-II and Osiris designs would have a large dose in the first mobility category due to the assumed release of the entire inventory of ^{18}F (around 10^{19} Bq in each case). The ^{18}F would be produced from fluorine in the Flibe used as coolant and breeding material. In reality, it is highly unlikely that such a large release of ^{18}F could be possible. The strong chemical bonds in LiF and BeF_2 preclude reactions with either air or steam and

make it doubtful that a significant fraction of the 2500 metric tons (1240 m^3) of Flibe could be released. The worst-case release fractions, however, assume that all fluorine-containing compounds react to form F_2 gas which would be readily released.

The PCA-Li/TOK doses would be dominated by the release of ^{56}Mn and ^{54}Mn in the fourth mobility category and ^{58}Co in the fifth mobility category. The calculated doses assume that 3% of the manganese and 1% of the cobalt is released from the first wall, blanket, manifold, and shield. While such a large release is unlikely, it cannot be entirely ruled out due to the large amount of afterheat that is available and the large chemical energy available in the lithium coolant.

The Cascade doses would be dominated by ^{24}Na and ^{76}As, which are both in the second mobility category. Much of the ^{24}Na would be created in $^{27}Al(n,\alpha)$ reactions in the $LiAlO_2$ breeder, the SiC-Al tendons, and the Al/water shield. The remaining ^{24}Na, however, would be produced via $^{23}Na(n,\gamma)$ reactions in the concrete shielding. This mode of ^{24}Na production may be significantly reduced through the addition of boron to the concrete, which would reduce the thermal neutron flux. The ^{76}As would be produced entirely within the

$LiAlO_2$ blanket from neutron capture reactions on the ^{75}As impurity (500 wppm). Simple changes in the design and impurity controls might reduce Cascade's worst- and initial-case doses by a factor of five or more.

The Prometheus-H doses would be dominated by ^{203}Pb, produced in the liquid-lead first-wall coolant, and ^{24}Na, produced via a two-step reaction on the silicon in the SiC. The ^{203}Pb is produced entirely via $^{204}Pb(n,2n)$ reactions. Production of ^{203}Pb may be avoided only through the isotopic removal of ^{204}Pb (1.4%) from natural lead -- a difficult and costly process.

Past studies, including the ESECOM report, have significantly underestimated the production of ^{24}Na from SiC. This has resulted from use of the ACTL cross-section library which underestimated the $^{28}Si(n,n'p)$ cross section [3]. This reaction produces stable ^{27}Al which, in turn, produces ^{24}Na in $^{27}Al(n,\alpha)$ reactions. Most currently accepted cross-section libraries have a $^{28}Si(n,n'p)$ cross section of 100-300 mb at neutron energies near 14 MeV. The ACTL library, now abandoned, had a value of only 0.64 mb. The reason for this discrepancy has not been identified.

Although the production of ^{24}Na from silicon cannot be avoided (apart from the continual removal of the aluminum produced in the first step), the threshold for the $^{28}Si(n,n'p)$ reaction is 12.0 MeV; thus, careful use of SiC could reduce the generation of ^{24}Na.

The worst- and initial-case doses from the SiC-He/TOK design would be dominated by ^{187}W and ^{24}Na. While the ^{24}Na would be produced in the SiC in the same manner as in the Prometheus-H design, the ^{187}W would be produced in the tungsten in the shield, which makes up 10.3%. The Prometheus-H doses assume that 3% of the tungsten would be released from the shield. Given the design's low afterheat and the large heat capacity of the shield, it is not clear how such a large release might occur.

SOMBRERO has the lowest worst- and initial-case doses of any of the designs. Even using quite conservative release fractions, SOMBRERO would not produce doses that would exceed any of the organ-dependent threshold doses for early fatalities. A total release, however, would result in some early fatalities as the TDRF for the bone marrow would be less than unity. The SOMBRERO doses are dominated by ^{32}P, which would be produced primarily in the concrete shielding.

The main difference between the worst-case and initial-case release fractions, and thus, between the doses shown in Figures 8.1.3 and 8.1.4, are in the release fractions assumed for Flibe and sodium. Since Flibe is composed of LiF, which falls into the fifth mobility category (1% release), and BeF_2, which falls into the third mobility category (10% release), an overall release fraction of 5.5% has been used for ^{18}F. The reclassification of sodium from the second mobility category to the third benefits all of the designs, in varying degrees (recall that Piet, et al. automatically placed the Group IA elements into the second mobility category due to their relatively high chemical reactivity). Doses that were dominated by ^{24}Na, such as those from Cascade and SiC-He/TOK, are as much as a factor of three lower with the new sodium classification.

Although materials such as $LiAlO_2$ have high boiling points that would result in their classification in the fifth mobility category, their activation products are frequently different elements such as sodium. For these materials, the initial-case results take no credit for the chemical reactivity of alternate elemental species. For example, due to its mobility category of five, the initial-case

results assume that only 1% of the $LiAlO_2$ would be released but still assume that 10% of the ^{24}Na activation product would be released.

It must be stressed that these calculations, like those of many past studies, have made no attempt to consider the possible energy sources that could conceivably lead to the assumed release fractions. Some of the assumed releases may not be energetically possible, yet, in the interest of conservatism, they have been assumed to occur.

8.1.5 Mechanistic-case early doses

This section gives details of the assumptions made to determine the mechanistic release fractions. The worst- and initial-case release fractions require little explanation as they depend solely upon the element or compound of interest. The mechanistic-case release fractions, however, depend upon the largest contributor to the initial-case dose and the energy available to drive its release.

In the Cascade design, the early and chronic doses would be dominated by the release of ^{76}As and ^{24}Na. The worst-case analysis assumed a 30% release fraction for ^{24}Na, while a 10% release

fraction was used in the initial-case analysis. Both analyses assumed a 30% release fraction for ^{76}As.

The carbon granules that would be used in the Cascade blanket could conceivably provide a large amount of energy for mobilization of ^{76}As and ^{24}Na from the $LiAlO_2$ granules: the combustion of carbon to form CO_2 gas releases 396 kJ per mole of carbon. The combustion of the entire carbon inventory (64,000 kg), if adequate oxygen were available, would release over 2100 GJ. This energy would be sufficient to melt nearly twice the total quantity of $LiAlO_2$ granules. Vaporization/decomposition data are unavailable for $LiAlO_2$, but it has been suggested that the granules would decompose before they would boil [4]. It is uncertain at what point during the combustion of the carbon granules and the heating of the $LiAlO_2$ granules the ^{76}As and ^{24}Na would be released. It is not clear whether the release could occur prior to melting, after melting, or following vaporization/ decomposition of the granules.

Although such high ^{76}As and ^{24}Na release fractions cannot be ruled out based upon energy considerations alone, the sources of the radionuclide inventories also should be considered. The ^{76}As would be produced entirely within the $LiAlO_2$ granules via the $^{75}As(n,\gamma)$

reaction. The BCSS Final Report claims that the composition of $LiAlO_2$ would include 500 wppm arsenic [5]. The BCSS composition has been used in the present work. Another reference, however, does not include arsenic in its list of $LiAlO_2$ impurities [6]. The amount of arsenic impurity in $LiAlO_2$ strongly affects the accident hazard posed by the Cascade design. Further analysis of $LiAlO_2$ impurities is required.

The majority (93%) of the ^{24}Na would be created outside of the $LiAlO_2$ granules. In fact, 68% of the ^{24}Na would be produced within the aluminum and concrete shielding. The quantity of ^{24}Na made in the concrete shield could be reduced by nearly 40% through the addition of one atom-percent boron. Additionally, it is unlikely that much, if any, of the ^{24}Na present in the concrete shielding would be mobilized even in a severe accident. In fact, even with the large amount of energy that could be available from combustion of the carbon granules, it is unlikely that any ^{24}Na, other than that found in the $LiAlO_2$ granules, first wall, and SiC-Al tendons, would be released. These assumptions can be combined to reduce the total releasable ^{24}Na inventory by more than 85%.

For the Cascade design, the mechanistic-case release fractions assume that only 15% of the calculated ^{24}Na inventory would be susceptible to release. Thus, the mechanistic-case release fractions are equal to those used in the initial-case analysis of Cascade. Rather than modifying the release fractions, credit has been taken for the relatively small fraction of ^{24}Na that would be susceptible to release. Although this process is believed to result in a more accurate representation of the hazard posed by the Cascade power plant, it must be noted that this methodology is not consistent with that used for the other power plant designs.

The worst-case and initial-case analyses indicate that an accident in the HYLIFE-II power plant would likely be dominated by the release of ^{18}F from the Flibe coolant. The worst-case analysis assumed that the LiF and BeF_2 would react (in an unspecified reaction) to convert all of the ^{18}F into F_2 gas, all of which would be released. The initial-case analysis assumed an overall ^{18}F release fraction of 5.5% (1% of the ^{18}F in LiF, due to its 1760 °C boiling point, and 10% of the ^{18}F in BeF_2 due to the 800 °C sublimation point of solid BeF_2). Since ^{18}F dominates the doses resulting from both

cases, the mechanistic-case release fractions analysis focussed on this radionuclide.

Several possible Flibe release mechanisms exist. Flibe may be vaporized during the fusion yield, it may be vaporized in a thin film from activated-steel components, it may boil under its own afterheat, it may undergo exothermic reactions (some of which may produce F_2 gas), it may be boiled by the energy released in exothermic oxidation reactions in steel, and, finally, it may be mobilized by other means such as a pump fire or the archetypical airplane crash. These release mechanisms are discussed in the following paragraphs.

Dolan and Longhurst estimate that approximately 8.8 kg of Flibe would be vaporized in a 350 MJ fusion yield [7]. Here, a conservative value of 10 kg is assumed. Flibe would not boil under its own afterheat even if adiabatic conditions are assumed. During the first year following an accident, Flibe would heat up by only 2.9 °C. Since its normal operating temperature would be about 650 °C, this temperature rise would be insufficient to mobilize any Flibe (BeF_2 sublimes at 800 °C). Flibe does not undergo any exothermic reactions with oxygen. The oxidation of LiF requires an energy input of 627

kJ/mole; that of BeF_2 requires 412 kJ/mole. Additionally, the kinetics of these reactions do not favor rapid forward reactions even when sufficient energy is provided.

Although a large quantity of energy could be released via the oxidation of steel (1000 GJ if all iron were oxidized to form FeO), the reaction kinetics do not appear to be favorable for the large-scale rapid oxidation of steel structures. INEL oxidation-driven mobilization experiments, for example, did not find internal heat generation resulting from the oxidation of samples -- no runaway oxidation reactions occur [8].

The release of ^{18}F would, most likely, be dominated by the vaporization of BeF_2 from the surface of hot, steel surfaces. The afterheat of the steel, although much lower than that from components in designs not utilizing thick-liquid protection schemes, is sufficient to boil 850,000 kg of BeF_2 during the first year. Of course, given the short (110 minute) half-life of ^{18}F, significant quantities of ^{18}F are released only during the first day of the accident. During this time, approximately 6600 kg of BeF_2 could be boiled. Consideration of possible losses of the thermal energy, such as conduction and radiation to surrounding structures, would

certainly lower the quantity of BeF_2 which could be released. The release of 6600 kg of BeF_2 would include approximately 0.033% of the initial ^{18}F inventory of about 1.1×10^{19} Bq -- substantially smaller release fractions than those assumed by either the worst-case or initial-case analyses.

Although the release of ^{18}F dominated the worst- and initial-case doses for HYLIFE-II, mechanistic-case release fractions have also been calculated for the SS304 structure. The SS304 has been approximated as PCA. These calculations assume that the steel in the first wall, blanket, and vacuum vessel is exposed to an oxidizing atmosphere for fifty hours at 1000 °C, assumptions consistent with ESECOM case 2, which was used "as a conservative approximation to what could be expected for the first-wall following a worst-case LOCA" [8]. Oxidation-driven mobilization data from INEL experiments are used as well.

Worst-case and initial-case results for the Osiris design also showed that ^{18}F, generated in liquid Flibe, would dominate the accident doses. The mechanistic-case analysis for Osiris is quite similar to that for HYLIFE-II. While Osiris would not have any structural components which would produce a large quantity of

afterheat, it would use a carbon composite first-wall and blanket structure which could release a large amount of chemical energy. The combustion of the entire chamber/blanket structure would release approximately 150 GJ -- enough to boil over 25,000 kg of Flibe. Assuming that the entire structure would burn during the first day of the accident, 5.6×10^{16} Bq of ^{18}F would be released -- approximately 0.6% of its total inventory at shutdown.

Simple energy conservation has been applied to calculate the mechanistic-case release fractions for the HYLIFE-II and Osiris designs. This method cannot be used for the PCA-Li/TOK design. The doses in the worst- and initial-case analyses would be dominated by radionuclides produced in the PCA steel. Unfortunately, simplifications similar to those used for Flibe do not exist for PCA. It is not clear how one can determine an upper bound for a release when it is limited by the reaction kinetics of the material. (That is, of course, without the use of chemical-reaction kinetics and a large materials database.) Thus, the mechanistic-case release fraction for PCA has been calculated from INEL experimental data for the oxidation-driven mobilization of PCA exposed to dry air [8]. The INEL data are used in conjunction with an assumed accident sequence

proposed by the ESECOM committee [1]. This accident corresponds "to a conservative assessment of first-wall temperatures produced by the combination of a lithium-air fire and decay heat" [1]. The accident assumes that the first-wall is exposed to temperatures of 1300 °C for the first ten hours and to 1000 °C for the next forty hours [1]. The quantity of material mobilized for each of nine elements is calculated using the INEL data [8]. These quantities, calculated for a PCA first-wall, are converted into elemental release fractions and are applied to the PCA-Li/TOK first-wall, blanket, and manifold.

The release fractions for elements for which INEL mobilization data are not available are based upon the mobility categories for each element -- these release fractions are the same as those used in the worst-case analyses. Table 8.1.4 shows the mobilization rates and the mechanistic-case release fractions for the nine elements for which INEL mobilization data was available.

The worst- and initial-case doses for Prometheus-H are dominated by radionuclides produced in the liquid-lead first wall. As was done for Flibe in the HYLIFE-II and Osiris designs, it is assumed that a thin film of liquid lead forms and is vaporized by the

afterheat of activated structural components. (Although lead does form several oxides in exothermic reactions, all but one decompose at temperatures below those of interest. The one, PbO, would not be produced rapidly due to unfavorable reaction kinetics.) All radionuclides produced within the lead are assumed to be released when the lead boils. Due to varying half-lives, the overall radionuclide release fractions range from 1.2 to 1.3 percent (all of the radionuclides have half-lives significantly greater than ^{18}F).

Table 8.1.4. Mobilization rates and mechanistic-case release fractions used for the PCA-Li/TOK first-wall, blanket, and manifold. The release fractions were calculated using INEL mobilization data for PCA [8]. Release fractions for the remaining elements are equal to those used for the worst-case analyses.

Element	Mobilization rate (g/m^2–h) 1000 °C	1300 °C	Overall release fraction
P	5.6E-2	5.4E-2	2.3E-1
Ti	8.3E-4	1.4E-3	1.8E-4
Cr	3.3E-2	1.6E-1	2.4E-4
Mn	4.3E-3	2.6E-2	3.2E-4
Fe	9.1E-2	3.3E-1	1.3E-4
Co	3.9E-5	1.3E-4	8.3E-5
Ni	3.2E-2	7.7E-2	1.5E-4
Cu	6.3E-4	4.5E-3	4.1E-3
Mo	2.8E-2	4.8E-1	3.6E-3

The SiC-He/TOK early doses for the initial-case release fractions are dominated by ^{187}W. Due to the possible production of

gaseous WO_3 in a highly exothermic reaction, simple energy arguments cannot be used to obtain a mechanistic-case release fraction for tungsten that is lower than those assumed in the worst- and initial-case results. The ESECOM report notes, however, that the production of WO_3 is kinetically unfavorable, and thus, is unlikely to produce the extreme temperatures that would be required to mobilize a significant fraction of the tungsten (ESECOM estimates that between ten and fifty hours at 2000 °C would be necessary to mobilize 10% of the tungsten) [1]. Afterheat and stored magnetic energy would prove insufficient to raise temperatures to this degree -- the total of approximately 110 GJ would cause an adiabatic temperature increase of only 417 °C.

In light of the apparent lack of energy from afterheat, magnetic, and chemical sources that would be required to mobilize significant fractions of the shield materials, the mechanistic-case results for SiC-He/TOK do not include the shield as a potential source-term. That is, only the first-wall, blanket, and manifold are considered for the mechanistic-case results. Although energy conservation cannot be used to argue for a decrease in release fractions, the neglect of radionuclide sources in the shield results in a considerable decrease

in the hazard posed by the SiC-He/TOK design. The mechanistic-case release fractions are the same as those used in the initial-case.

The SOMBRERO power plant design uses an unusually large quantity of carbon composite in its first-wall and blanket. If this carbon were to combust in an accident, nearly 20,000 GJ would be released. If this combustion took place over one day, the thermal power output would be over 200 MW. Due to this huge amount of energy that is available to cause the release of radionuclides, no argument can be made to decrease the mechanistic-case release fractions below those of the initial-case. Nor can an argument be made to exclude the shield inventory from the mechanistic-case results. The results presented for SOMBRERO for the mechanistic-case are identical to those presented for the initial-case.

Using the mechanistic-case release fractions, the early doses to the bone marrow, lung, and GI tract have been calculated for each of the power plant designs. The results of these calculations are presented in Figure 8.1.5.

Figure 8.1.5. Early doses to the three organs are shown for each of the power plant designs. These results use, where possible and appropriate, mechanistic-case release fractions for the component which dominated the early dose in the initial-case results. For other components, radionuclide release fractions are the same as those used in the initial-case. For comparison, a whole-body dose is also given for the release of 1 kg of tritium (as oxide).

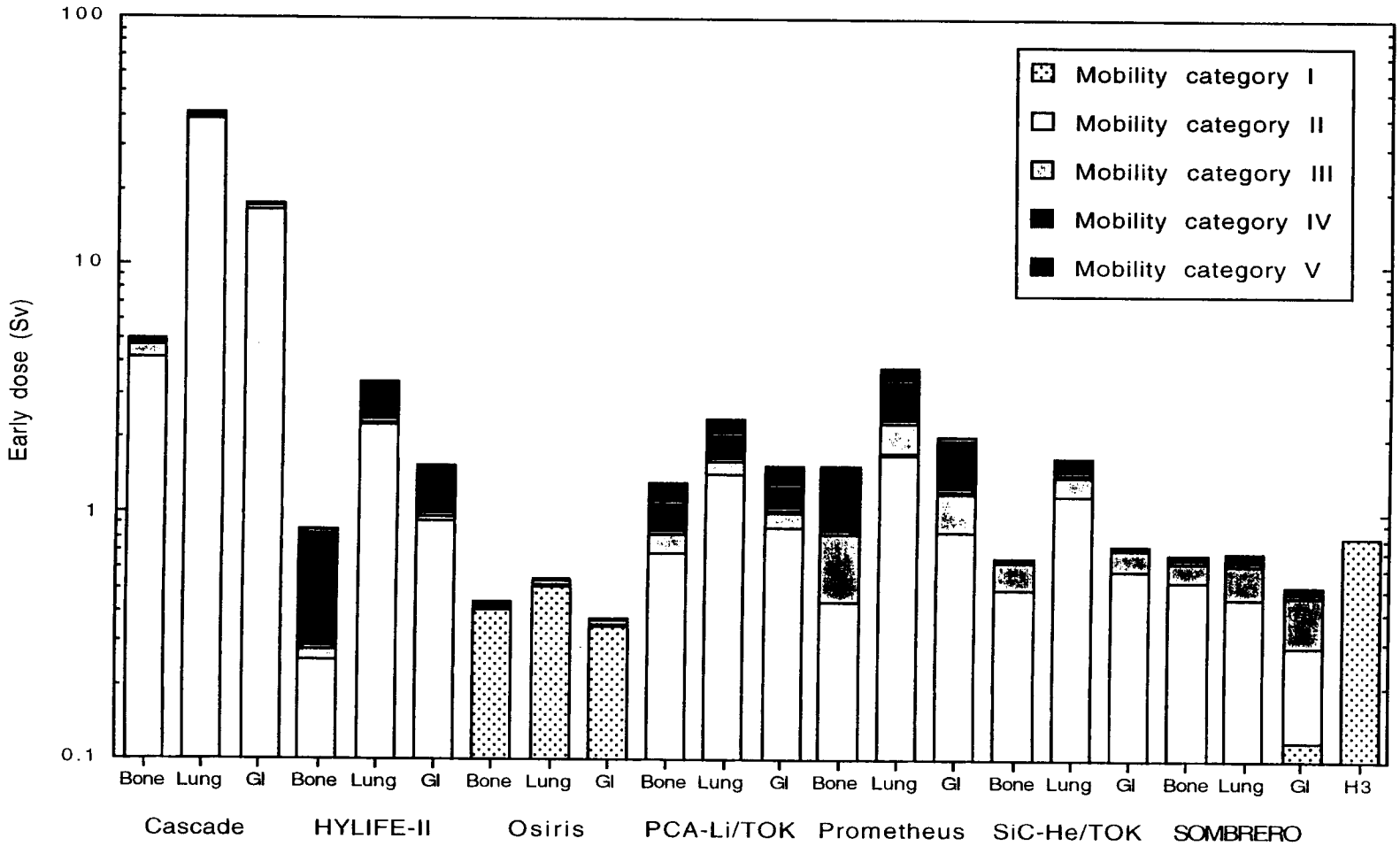

8.1.6 Chronic doses

As was done for early doses, chronic doses have been calculated for the worst-, initial-, and mechanistic-case release fractions. Figure 8.1.6 gives three sets of chronic doses at a distance of 10 km from each release. Results are given for each design and for 1 kg of tritium (released as oxide). As noted in Chapter 2, the chronic doses calculated in the present work include ingestion of food and water.

The chronic dose at 10 km resulting from the release of 1 kg of tritium (as oxide) is about five times higher than that reported by ESECOM [1]. About 80% of the chronic dose, however, is due to contributions from ingested food and water. The contributions from inhalation during plume passage and inhalation of resuspended material agree quite well with the ESECOM results.

The PCA-Li/TOK design has, by far, the highest chronic doses in the worst- and initial-cases, and the Cascade design has the highest mechanistic-case chronic dose. The SiC-He/TOK design has the lowest chronic doses in the worst- and initial-cases, but the SOMBRERO doses are only 25-50% higher. Osiris has the lowest mechanistic-case chronic dose. The worst-case chronic doses range from 0.16 Sv to 24.8 Sv. The initial-case chronic doses range from

Figure 8.1.6. Chronic doses, at a distance of 10 km from the site boundary, are shown for each of the power plant designs. Results are also given for 1 kg of tritium (released as HTO). Chronic doses are 50-year dose commitments including contribu-tions from ingestion of food and water. Case 1 results use worst-case release fractions, case 2 results use initial-case release fractions, and case 3 results use mechanistic-case release fractions.

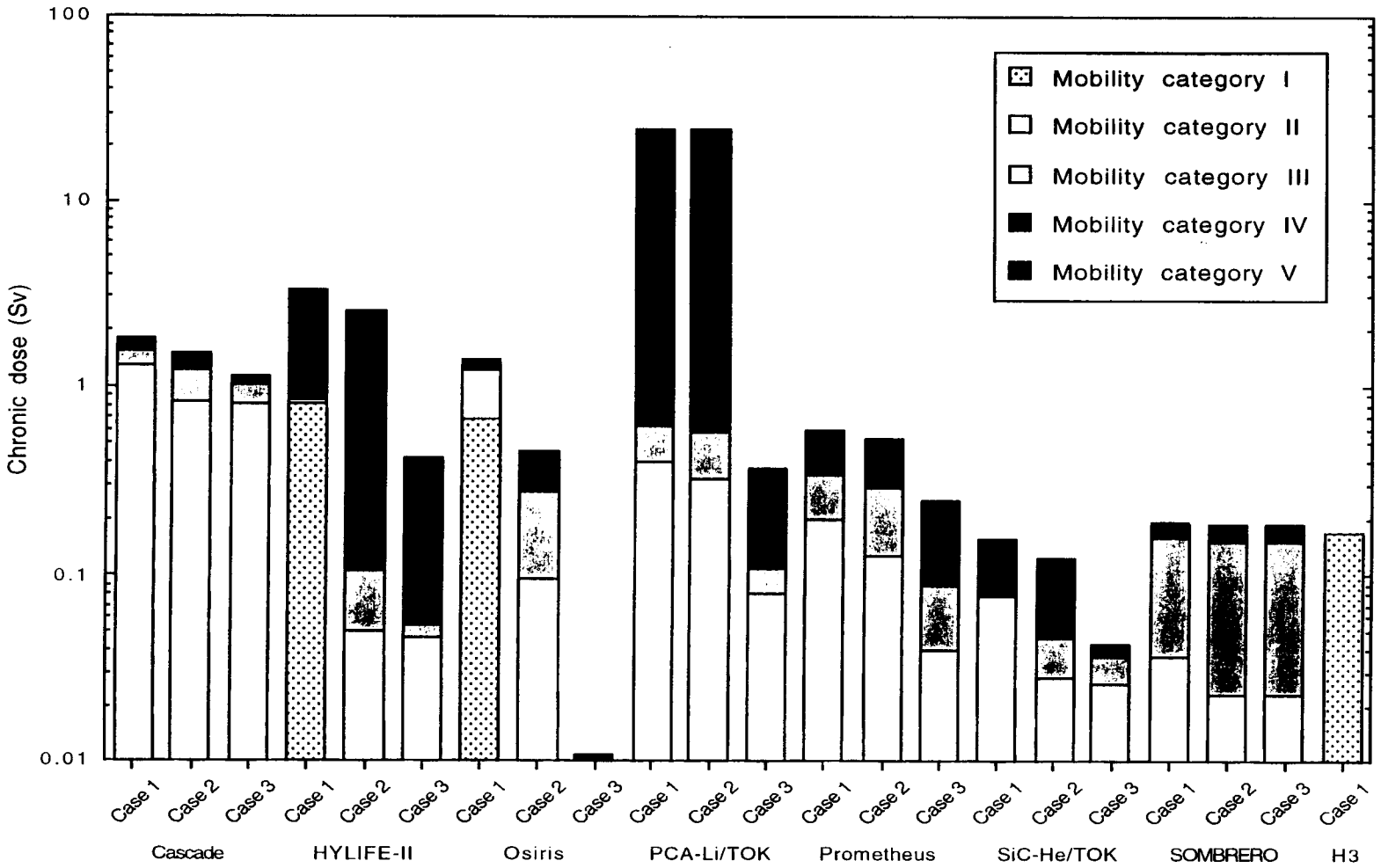

0.12 Sv to 24.7 Sv, and the mechanistic-case chronic doses range from just over 0.01 Sv to about 1.0 Sv.

Among the IFE designs only, the worst-case chronic doses at 10 km from the point of release range from 0.2 Sv (SOMBRERO) to 3.5 Sv (HYLIFE-II), the initial-case chronic doses range from 0.2 Sv (SOMBRERO) to 2.6 Sv (HYLIFE-II), and the mechanistic-case chronic doses range from 0.01 Sv (Osiris) to 1.1 Sv (Cascade).

The Cascade worst-case chronic doses are dominated by contributions from ^{76}As, ^{24}Na, and ^{65}Zn. Due to a reduction in the release fraction for ^{24}Na in the second case, ^{65}Zn becomes the second leading contributor to the chronic dose in the initial-case results. ^{76}As and ^{65}Zn are produced mostly from impurities in the $LiAlO_2$ pellets. Cascade's chronic dose changes little from the initial-case to the mechanistic-case as energy considerations cannot be used to limit the ^{76}As and ^{65}Zn release fractions.

^{60}Co and ^{18}F dominate the chronic dose from the HYLIFE-II design in the worst-case. ^{54}Mn becomes the second leading contributor in the initial-case due to the reduced ^{18}F release fraction. The ^{60}Co and ^{54}Mn would be produced entirely within the SS304 structures. The chronic dose from Osiris would be dominated by ^{18}F in the worst-

case and ^{24}Na in the initial-case. The ^{18}F would be produced in the Flibe coolant/breeder, while the ^{24}Na would be produced within the concrete shielding. Due to a lack of energy sources required for the large-scale mobilization of Flibe and the SS304 structures, the HYLIFE-II mechanistic-case chronic dose is about a factor of six lower than the initial-case dose. Similarly, the Osiris mechanistic-case chronic dose is much lower than the initial-case dose due to a reduction in the Flibe release fraction and the decision not to consider activation products in its shield.

The chronic dose for the PCA-Li/TOK design does not change from the worst-case to the initial-case. The dose is dominated by the release of ^{54}Mn and ^{60}Co. Due to the high afterheat of the steel structures (it would be more than 9 months before the afterheat would fall below 1 MW) and the high chemical reactivity of the Li coolant, release fractions in the 1-3% range cannot be immediately dismissed. Use of mechanistic-case release fractions for PCA, generated using INEL oxidation-driven mobilization data, however, results in a significant decrease in the chronic dose over that predicted by the worst- and initial-cases.

Chronic doses from the Prometheus-H design are dominated by ^{210}Po, ^{203}Hg, ^{203}Pb, and ^{207}Bi, which would be produced in the lead first-wall coolant. The ^{24}Na would contribute 13% of the chronic dose in the worst-case, so the initial-case dose is lower than the worst-case dose. The use of mechanistic-case release fractions for the lead coolant further reduce the chronic dose to about 0.25 Sv.

SiC-He/TOK worst- and initial-case chronic doses are dominated by ^{187}W, which would be produced from tungsten in the shield, and ^{24}Na and ^{28}Mg, which are produced in SiC structures. Even with the conservative release fractions used in the worst-case, the SiC-He/TOK design has a chronic dose of only 0.16 Sv. The mechanistic-case chronic dose neglects contributions from the shield, and thus, the dose drops to about 0.04 Sv.

The chronic doses for the SOMBRERO design are dominated by ^{133}Ba, produced in the special concrete shield (over 40% barium by weight). Other sizable contributors to SOMBRERO's chronic dose include ^{54}Mn (15%) and ^{32}P (11%). Due to the large chemical energy available in the blanket, the SOMBRERO mechanistic-case release fractions are identical to those used in the worst- and initial-cases.

Despite this, SOMBRERO's chronic dose would be only 0.2 Sv at 10 km from the point of release.

8.1.7 Early and cancer fatalities

Using the doses from the previous sections, estimates of the number of early and cancer fatalities that would result from accidental releases have been made. Figure 8.1.7 shows that even with the more conservative set of assumed release fractions, the SiC-He/TOK and SOMBRERO designs do not cause any early fatalities. The PCA-Li/TOK design, on the other hand, would cause about 270 early fatalities. Cascade would produce about 50 early fatalities, and HYLIFE-II and Osiris would each result in close to 200 early fatalities. The Prometheus-H design would result in only a single early fatality.

Unlike early fatalities, which are a threshold effect, cancer fatalities may result from a dose of any level. Each of the designs would produce some number of cancer fatalities, but the actual number varies widely from one design to another. For the worst-case release fractions and the resulting chronic doses, the SOMBRERO and

Figure 8.1.7. Estimated number of early and cancer fatalities resulting from the accidental release of radioactivity. These results use the worst-case release fractions which classify each element according to the lowest boiling point of the pure element or its oxides.

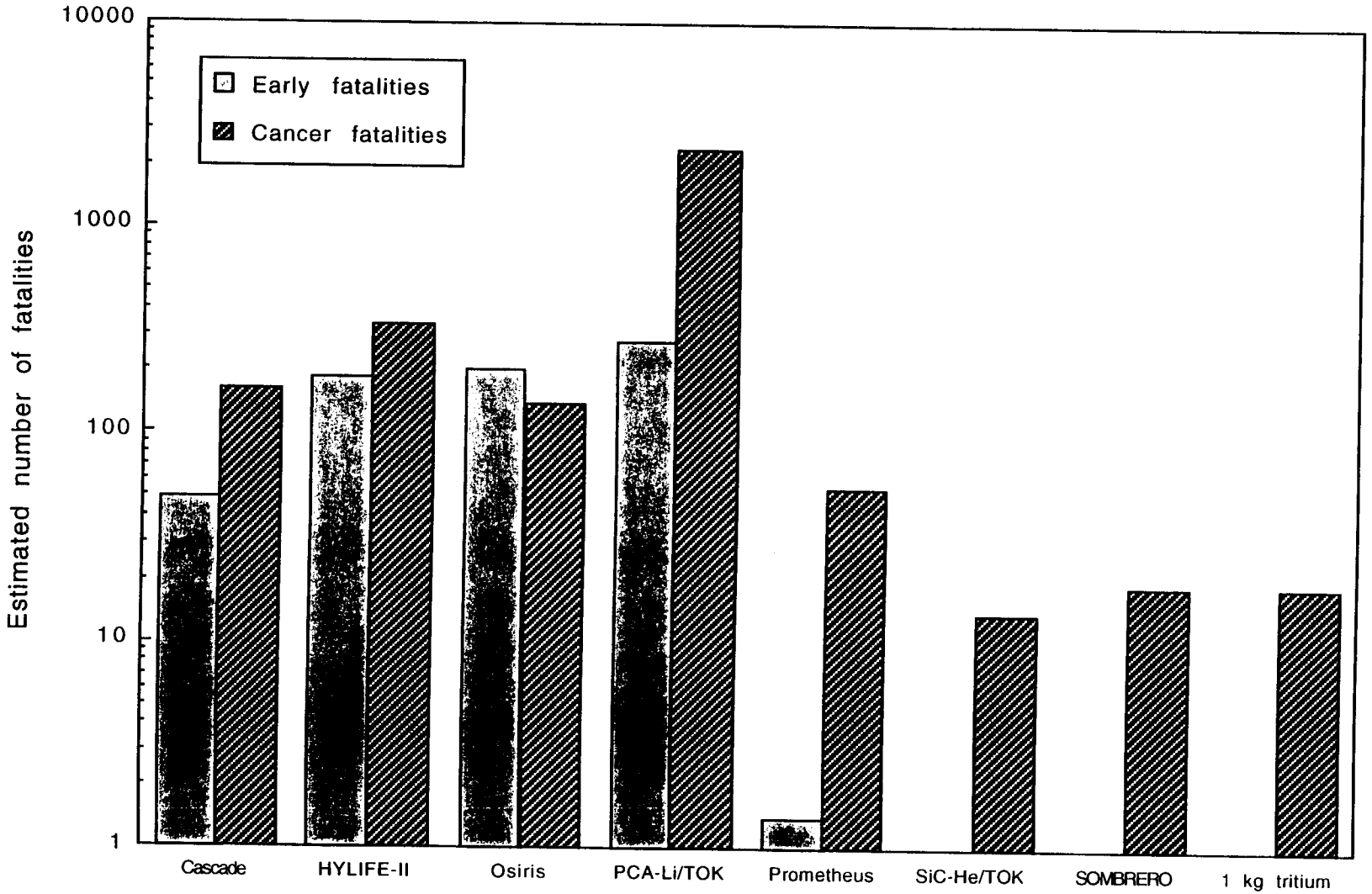

SiC-He/TOK designs would have the least effect; they each would result in about 20 cancer fatalities. Prometheus-H would produce about 50 cancer fatalities, while the Cascade and Osiris designs would each result in about 150 fatal cancers. The HYLIFE-II design would result in about 330 cancers. Finally, the PCA-Li/TOK design would be the worst with nearly 2400 cancer fatalities.

Figure 8.1.8 shows estimates of the number of early and cancer fatalities for the initial-case release fractions. The number of early fatalities produced by Cascade, HYLIFE-II, and Osiris drops significantly due to lower release fractions for ^{24}Na and ^{18}F. Cascade would produce about thirty early fatalities, while HYLIFE-II and Osiris would result in 10 and 20 early fatalities, respectively. Since elemental cobalt and manganese dominate the doses from the PCA-Li/TOK design and their release fractions do not change significantly, the number of early fatalities that it would produce remains around 270. The doses from Prometheus-H now fall below the early fatality thresholds, and thus, no early fatalities would be expected. The SOMBRERO and SiC-He/TOK designs still, of course, would not produce any early fatalities.

Figure 8.1.8. Estimated number of early and cancer fatalities resulting from the accidental release of radioactivity. These results use the initial-case release fractions which classify each material according to its boiling point. Possible oxidation reactions are not considered.

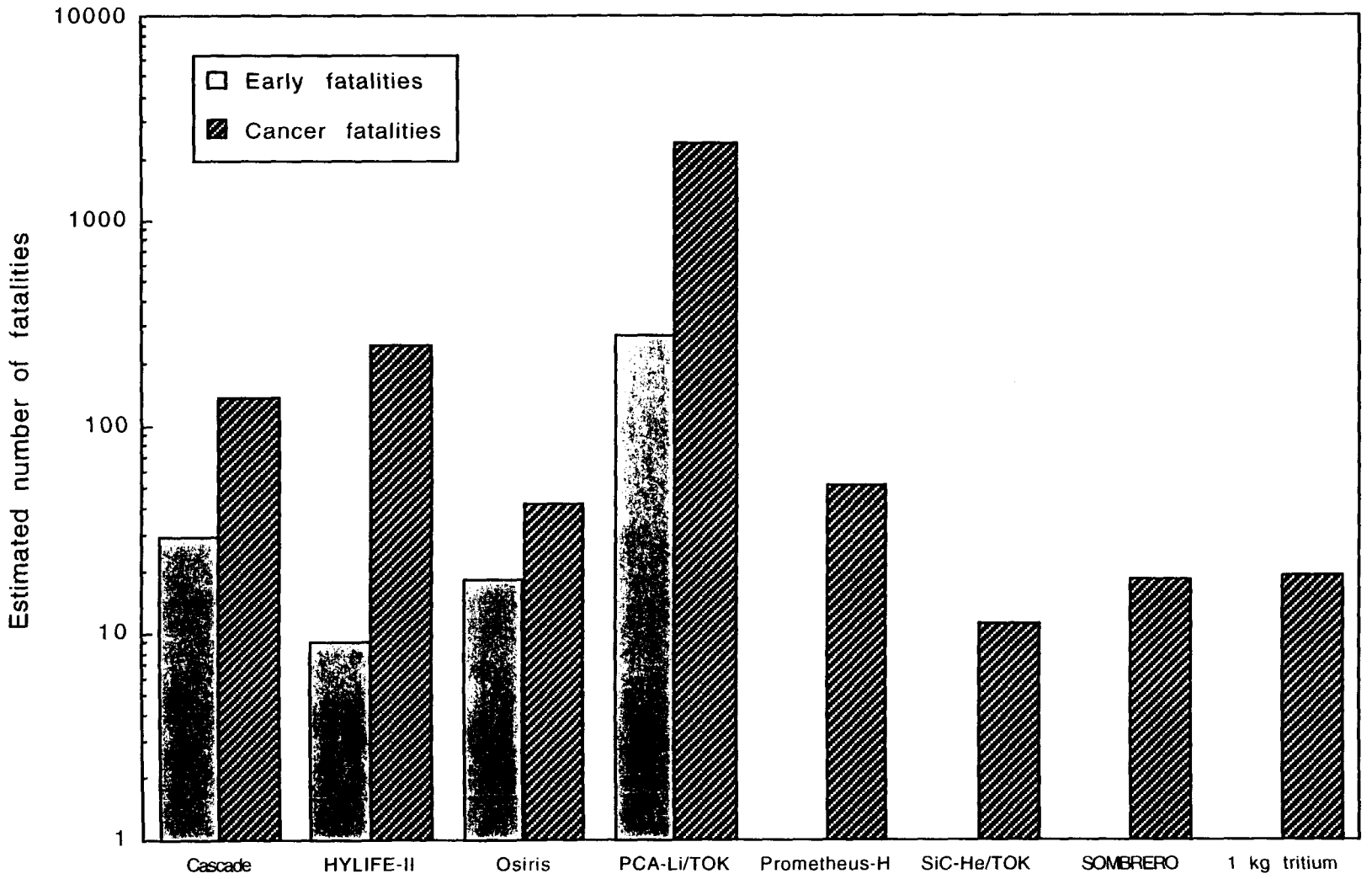

Because cancer fatalities are not a threshold effect, the impact of reducing the release fractions tends not to be as great as that for early fatalities. Nonetheless, the estimated number of cancer fatalities is somewhat lower than estimated from the first set of doses. The number of fatal cancers drops by 20-30% for the Cascade, HYLIFE-II, and SiC-He/TOK designs. Cascade results in about 140 fatal cancers. The HYLIFE-II and SiC-He/TOK designs produce 240 and 11 fatal cancers, respectively. Reductions in the overall release fractions of ^{18}F and ^{24}Na decrease the number of fatal cancers produced by Osiris from 150 to 50. The results for the PCA-Li/TOK, Prometheus-H, and SOMBRERO designs remain approximately constant, producing about 2400, 50, and 20 fatal cancers, respectively.

Utilizing the most realistic, mechanistic-case release fractions, Figure 8.1.9 shows that only the Cascade design would potentially produce any early fatalities. Further work in $LiAlO_2$ impurity analysis and arsenic release fractions would reduce the number of early fatalities resulting from an accident in Cascade. A factor of five reduction in the early doses (resulting from impurity control, small design modifications, and/or less conservatism in release

Figure 8.1.9. Estimated number of early and cancer fatalities resulting from the accidental release of radioactivity. These results use the mechanistic-case release fractions in which the release of the dominant contributor to the critical bone marrow dose (from the initial-case results) is bounded, where possible, according to the energy available to drive such a release.

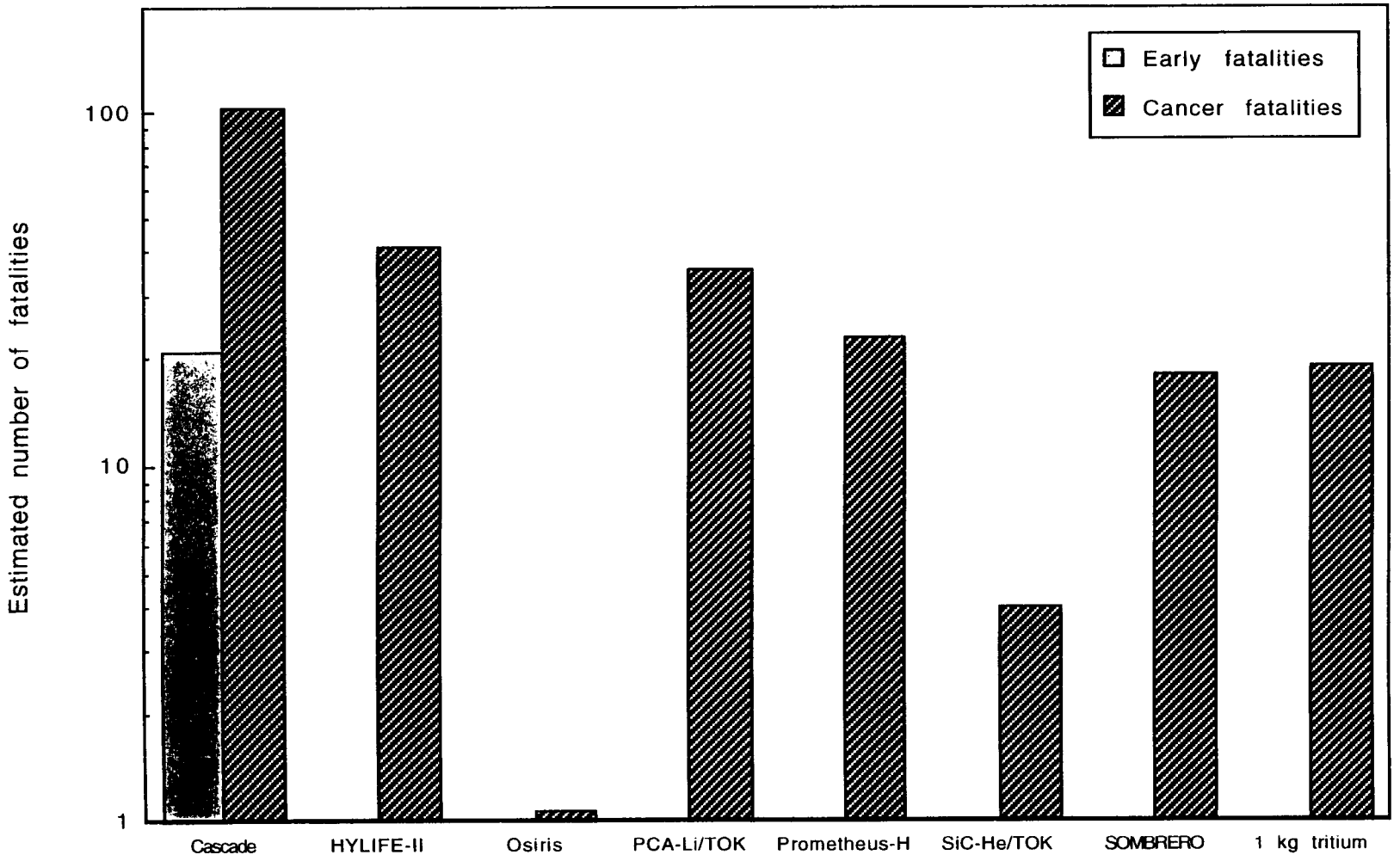

fractions) would eliminate the possibility of early fatalities from a Cascade accident.

Using the mechanistic-case chronic doses, the estimated number of cancer fatalities is reduced for each design (except for the SOMBRERO design, which uses the same release fractions for all three cases). The number of cancer fatalities would range from only one from Osiris to about 100 from Cascade. Among the four IFE for which mechanistic-case release fractions were possible, the number of cancer fatalities ranges from one (Osiris) to forty (HYLIFE-II).

8.2 Occupational and routine hazards

The hazards considered in this section include dose rates to personnel working on or near activated components as well as doses to the public resulting from the routine release of tritium and the more mobile activation products.

8.2.1 Contact dose rates

The dose rates which result from activation of irradiated materials may, in some cases, be high enough to preclude hands-on

maintenance of some components. Unrestricted occupational access is generally allowed to areas with dose rates below 0.025 mSv/h (on the assumption that 0.025 mSv/h would yield 1 mSv during a 40 hour work week and 50 mSv during a year) [1]. Components that have contact dose rates below 0.025 mSv/h within 100 years of irradiation may be eligible for hands-on recycling [9].

Table 8.2.1 gives the contact dose rates for the main components for each design. It must be noted that these contact dose rates are calculated using a semi-infinite medium approximation. That is, the dose rates are calculated at the surface of a semi-infinite medium that contains the activation products in the concentrations calculated for the finite components. Such an assumption greatly simplifies the calculation of dose rates, but it also tends to overestimate the results. Since the mean-free paths of energetic photons is 5-10 cm in most materials, components that are more than 30-cm-thick and 3-m-wide and high can usually be considered infinite [10]. Therefore, while the dose rates found in Table 8.2.1 are accurate for a meter of concrete, they are greatly overestimated for components such as a 1-cm-thick first-wall. Nevertheless, the use of contact dose rates provides useful information about the relative

Table 8.2.1. (Continued.)

	Contact dose rate (Sv/hour) vs time after shutdown													
	t = 0		1 hour		1 day		1 week		1 year		30 years		100 years	
Component	Dose rate	Main Isotope	Dose rate	Main Isotope	Dose rate	Main Isotope	Dose rate	Main Isotope	Dose rate	Main Isotope	Dose rate	Main Isotope	Dose rate	Main Isotope
PCA-Li/TOK														
PCA first wall	4.5E+8	^{58}Co	4.0E+8	^{58}Co	2.6E+8	^{58}Co	2.5E+8	^{58}Co	4.0E+7	^{54}Mn	2.9E+2	^{158}Tb	1.9E+2	^{158}Tb
PCA blanket	8.7E+7	^{58}Co	7.8E+7	^{58}Co	5.1E+7	^{58}Co	4.9E+7	^{58}Co	7.8E+6	^{54}Mn	6.8E+1	^{158}Tb	3.7E+1	^{158}Tb
PCA+ manifold	1.1E+5	^{58}Co	9.4E+4	^{58}Co	6.1E+4	^{58}Co	5.8E+4	^{58}Co	8.7E+3	^{54}Mn	2.1E-1	^{60}Co	7.9E-2	^{94}Nb
Li coolant	5.2E+1	^{6}He	1.1E+0	^{24}Na	4.1E-1	^{22}Na	2.4E-1	^{22}Na	1.6E-1	^{22}Na	3.1E-4	^{39}Ar	2.0E-4	^{39}Ar
FeCrV+ shield	2.1E+2	^{52}V	5.6E+1	^{56}Mn	6.8E+0	^{59}Fe	6.1E+0	^{59}Fe	2.9E-1	^{60}Co	5.1E-3	^{60}Co	5.3E-7	^{60}Co
Prometheus-H														
SiC first wall	4.2E+5	^{28}Al	3.0E+3	^{24}Na	1.0E+3	^{24}Na	2.7E+0	^{60}Co	4.8E-1	^{60}Co	9.2E-3	^{60}Co	5.8E-5	^{26}Al
Pb first wall coolant	3.2E+4	^{207m}Pb	6.7E+1	^{203}Pb	5.5E+1	^{203}Pb	2.3E+1	^{202}Tl	2.7E+0	^{207}Bi	1.4E+0	^{207}Bi	4.0E-1	^{207}Bi
SiC blanket	3.6E+4	^{28}Al	8.6E+1	^{24}Na	2.9E+1	^{24}Na	2.1E-1	^{60}Co	1.1E-1	^{60}Co	2.4E-3	^{60}Co	1.4E-6	^{26}Al
Li_2O blanket	5.0E+4	^{16}N	9.6E+0	^{56}Mn	1.5E+0	^{24}Na	1.6E-1	^{60}Co	8.8E-2	^{60}Co	1.8E-3	^{60}Co	7.0E-5	^{39}Ar
HT-9 vac. vessel	4.0E+4	^{56}Mn	3.2E+4	^{56}Mn	3.4E+3	^{54}Mn	1.6E+3	^{54}Mn	6.4E+2	^{54}Mn	1.3E-1	^{94}Nb	1.1E-1	^{94}Nb
Prometheus shield	2.5E+0	^{28}Al	2.1E-1	^{24}Na	7.1E-2	^{24}Na	1.1E-3	^{110m}Ag	4.7E-4	^{60}Co	1.7E-5	^{108m}Ag	7.2E-6	^{108m}Ag
SiC-He/TOK														
SiC first wall	3.8E+5	^{28}Al	1.3E+3	^{24}Na	4.7E+2	^{24}Na	1.6E+0	^{28}Al	8.6E-2	^{60}Co	1.2E-3	^{60}Co	1.2E-5	^{26}Al
SiC blanket	5.9E+4	^{28}Al	5.2E+1	^{24}Na	1.7E+1	^{24}Na	1.5E-1	^{28}Al	3.5E-2	^{60}Co	6.3E-4	^{60}Co	2.1E-7	^{26}Al
Li_2O blanket	3.8E+4	^{16}N	6.2E+0	^{56}Mn	7.8E-1	^{24}Na	7.2E-2	^{60}Co	2.9E-2	^{60}Co	5.3E-4	^{60}Co	1.6E-5	^{39}Ar
C+ manifold	3.3E+2	^{28}Al	2.9E-1	^{31}Si	4.0E-2	^{24}Na	1.3E-2	^{60}Co	1.1E-2	^{60}Co	2.4E-4	^{60}Co	2.7E-8	^{60}Co
SiC+ shield	2.5E+1	^{28}Al	6.4E+0	^{24}Na	2.0E+0	^{24}Na	2.1E-2	^{54}Mn	7.8E-3	^{54}Mn	2.6E-5	^{60}Co	2.4E-6	^{108m}Ag

Table 8.2.1. Contact dose rates from activated components.[a]

	Contact dose rate (Sv/hour) vs time after shutdown													
	t = 0		1 hour		1 day		1 week		1 year		30 years		100 years	
Component	Dose rate	Main Isotope	Dose rate	Main Isotope	Dose rate	Main Isotope	Dose rate	Main Isotope	Dose rate	Main Isotope	Dose rate	Main Isotope	Dose rate	Main Isotope
Cascade														
C granules	2.7E+0	^{207m}Pb	3.7E-1	^{24}Na	1.3E-1	^{24}Na	1.9E-2	^{46}Sc	1.2E-3	^{46}Sc	1.3E-5	^{39}Ar	7.2E-6	^{39}Ar
$LiAlO_2$ granules	8.0E+4	^{16}N	7.5E+2	^{76}As	4.6E+2	^{76}As	1.5E+2	^{124}Sb	3.0E+1	^{60}Co	4.0E-1	^{60}Co	8.7E-3	^{108m}Ag
SiC first wall	4.2E+3	^{28}Al	4.4E+0	^{31}Si	1.5E-1	^{28}Al	5.1E-3	^{60}Co	3.3E-3	^{60}Co	7.1E-5	^{60}Co	7.2E-9	^{60}Co
SiC/Al tendons	4.0E+4	^{28}Al	5.1E+3	^{56}Mn	5.5E+2	^{24}Na	2.7E+1	^{65}Zn	9.8E+0	^{65}Zn	3.2E-2	^{60}Co	1.6E-4	^{26}Al
Al/H_2O shield	1.6E+3	^{28}Al	1.8E+2	^{56}Mn	1.6E+1	^{24}Na	8.1E-1	^{65}Zn	2.9E-1	^{65}Zn	5.4E-4	^{60}Co	1.4E-5	^{26}Al
Al-5083 vac. vessel	1.8E+3	^{28}Al	5.5E+2	^{24}Na	1.4E+2	^{24}Na	1.9E+0	^{54}Mn	6.8E-1	^{65}Zn	6.8E-4	^{60}Co	1.8E-4	^{26}Al
Concrete shield	4.3E+1	^{28}Al	2.3E+1	^{24}Na	1.3E+1	^{46}Sc	7.6E+0	^{46}Sc	4.0E-1	^{46}Sc	2.8E-5	^{60}Co	2.6E-6	^{39}Ar
HYLIFE-II														
SS304 first wall	7.0E+3	^{56}Mn	5.4E+3	^{56}Mn	2.9E+3	^{60}Co	2.8E+3	^{60}Co	1.8E+3	^{60}Co	4.0E+1	^{60}Co	5.6E-3	^{60}Co
SS304 blanket	3.9E+1	^{60}Co	3.6E+1	^{60}Co	3.1E+1	^{60}Co	2.9E+1	^{60}Co	2.1E+1	^{60}Co	4.4E-1	^{60}Co	1.2E-4	^{108m}Ag
SS304 assorted	1.8E+3	^{60}Co	1.6E+3	^{60}Co	1.3E+3	^{60}Co	1.3E+3	^{60}Co	8.9E+2	^{60}Co	2.0E+1	^{60}Co	2.7E-3	^{60}Co
SS304 vac. vessel	4.2E+1	^{60}Co	3.9E+1	^{60}Co	3.4E+1	^{60}Co	3.2E+1	^{60}Co	2.1E+1	^{60}Co	4.6E-1	^{60}Co	1.2E-4	^{108m}Ag
Flibe	3.9E+4	^{16}N	6.7E+0	^{182}Ta	5.3E+0	^{182}Ta	4.9E+0	^{182}Ta	6.4E-1	^{182}Ta	1.8E-3	^{60}Co	3.6E-7	^{60}Co
Concrete shield	1.6E+0	^{56}Mn	1.1E+0	^{56}Mn	1.8E-1	^{24}Na	5.3E-2	^{59}Fe	4.0E-4	^{59}Fe	3.8E-6	^{60}Co	1.6E-8	^{26}Al
Osiris														
C/C first wall	4.5E+1	^{28}Al	4.6E+0	^{24}Na	1.6E+0	^{24}Na	8.0E-2	^{46}Sc	2.7E-3	^{46}Sc	1.2E-5	^{60}Co	5.7E-6	^{10}Be
C/C blanket	1.3E+1	^{28}Al	1.7E+0	^{24}Na	6.0E-1	^{24}Na	2.5E-2	^{46}Sc	9.1E-4	^{46}Sc	3.5E-6	^{60}Co	1.7E-6	^{10}Be
C/C vac. vessel	3.2E+0	^{24}Na	1.8E+0	^{24}Na	6.5E-1	^{24}Na	4.0E-2	^{46}Sc	4.2E-3	^{60}Co	5.4E-5	^{60}Co	2.1E-7	^{10}Be
Flibe	8.5E+4	^{16}N	8.1E+0	^{182}Ta	5.1E+0	^{182}Ta	4.5E+0	^{182}Ta	7.0E-1	^{182}Ta	4.6E-3	^{60}Co	8.2E-7	^{60}Co
Concrete shield	6.0E+1	^{56}Mn	4.7E+1	^{56}Mn	9.2E+0	^{24}Na	1.4E+0	^{59}Fe	2.3E-1	^{54}Mn	1.7E-4	^{60}Co	4.4E-7	^{26}Al

Table 8.2.1. (Continued.)

	Contact dose rate (Sv/hour) vs time after shutdown													
	t = 0		1 hour		1 day		1 week		1 year		30 years		100 years	
Component	Dose rate	Main Isotope	Dose rate	Main Isotope	Dose rate	Main Isotope	Dose rate	Main Isotope	Dose rate	Main Isotope	Dose rate	Main Isotope	Dose rate	Main Isotope
SOMBRERO														
C/C first wall	2.0E+1	^{28}Al	1.8E+0	^{24}Na	6.3E-1	^{24}Na	3.5E-2	^{46}Sc	1.4E-3	^{46}Sc	6.9E-6	^{10}Be	5.1E-6	^{10}Be
C/C blanket	5.6E-1	^{28}Al	9.7E-2	^{24}Na	3.4E-2	^{24}Na	1.0E-3	^{46}Sc	4.8E-5	^{46}Sc	1.8E-7	^{10}Be	1.2E-7	^{10}Be
Li_2O blanket	2.6E+3	^{16}N	7.5E-1	^{56}Mn	9.0E-2	^{24}Na	1.3E-2	^{60}Co	8.2E-3	^{60}Co	1.7E-4	^{60}Co	7.0E-6	^{39}Ar
Xe gas	2.7E+1	^{135m}Xe	9.6E+0	^{135}Xe	3.3E+0	^{127}Xe	1.7E+0	^{127}Xe	2.7E-1	^{137m}Ba	7.3E-2	^{137m}Ba	1.4E-2	^{137m}Ba
Ba-concrete shield	3.6E+1	^{56}Mn	2.4E+1	^{56}Mn	6.8E+0	^{54}Mn	6.6E+0	^{54}Mn	2.9E+0	^{54}Mn	1.9E-3	^{133}Ba	6.3E-4	^{94}Nb
High-Z Target Materials														
Tantalum	9.4E+6	^{178m}Hf	1.0E+4	^{182}Ta	9.1E+3	^{182}Ta	8.8E+3	^{182}Ta	1.0E+3	^{182}Ta	1.4E-7	^{174}Lu	1.9E-8	^{182}Ta
Tungsten	1.7E+6	^{183m}W	1.7E+3	^{187}W	9.3E+2	^{187}W	2.4E+2	^{182}Ta	2.6E+1	^{182}Ta	4.6E-6	^{186}Re	4.6E-6	^{186}Re
Mercury	1.2E+5	^{197m}Au	7.0E+3	^{199m}Hg	1.6E+2	^{203}Hg	9.8E+1	^{203}Hg	3.1E-1	^{203}Hg	6.5E-5	^{194}Au	6.0E-5	^{194}Au
Lead	9.7E+9	^{207m}Pb	3.5E+1	^{203}Pb	2.6E+1	^{203}Pb	6.2E+0	^{203}Pb	1.4E-2	^{207}Bi	8.0E-3	^{207}Bi	2.2E-3	^{207}Bi
Impure lead	9.7E+9	^{207m}Pb	2.1E+2	^{120m}Sb	1.1E+2	^{120m}Sb	5.0E+1	^{120m}Sb	4.1E+0	^{207}Bi	2.0E+0	^{207}Bi	6.8E-1	^{207}Bi

[a] Contact dose rates are following maximum irradiation of the indicated components (set according to radiation damage limit and rate for the given material). Main isotope means largest single contributor to the total dose rate. Al-5083 denotes the ASTM 5083 aluminum alloy; Flibe denotes a molten salt of two parts LiF and one part BeF_2; C/C denotes carbon-carbon composite; PCA+ means PCA plus FeCrV; FeCrV+ means FeCrV plus H_2O; Prometheus shield denotes a combination of SiC plus B_4C, Pb, H_2O, and Al; C+ means C plus SiC and BeO; SiC+ means SiC plus B_4C, Al, H_2O, W, and Pb. Impure lead includes 0.01 wt% Cu, 0.05 wt% Ag, 0.15 wt% Sb, and 0.20 wt% Bi.

hazard of components of similar dimensions. In addition, without detailed information about occupational access which might be required to specific components at specific times -- information accurate for a meter of concrete, they are greatly overestimated for components such as a 1-cm-thick first wall. Nevertheless, the use of contact dose rates provides useful information about the relative hazard of components of similar dimensions. In addition, without detailed information about the occupational access that might be required for specific components at specific times -- information that will not be available until fusion power plants have been operated for some time -- thorough time-and-motion analyses cannot be completed.

In the Cascade design, the $LiAlO_2$ granules, the SiC/Al tendons, and the Al-5083 vacuum vessel all fail to qualify for hands-on recycling. Each of these components, however, should be eligible for some form of remote recycling. High contact dose rates for the first wall and the SiC/Al tendons mean that first-wall changeout would need to be done remotely.

In the HYLIFE-II design, only the Flibe coolant and the concrete biological shield are able to qualify for hands-on recycling. All

stainless steel components should qualify for remote recycling. Although it qualifies for hands-on recycling within 100 years, the contact dose rate from Flibe will preclude maintenance of piping which is filled with coolant.

All components from the Osiris design qualify for hands-on recycling within 100 years. As in HYLIFE-II, maintenance of coolant pipes in Osiris would require prior drainage of Flibe.

In the PCA-Li/TOK power plant, only the biological shield qualifies for hands-on recycling within 100 years. The PCA first wall and blanket have contact dose rates of 190 and 37 Sv/h after 100 years of cooling, respectively. Worse still, these dose rates are dominated by ^{158}Tb, which has a 180 year half-life. Only the lithium coolant can qualify for remote recycling. All maintenance of PCA-Li/TOK components would need to be done remotely.

In Prometheus, the SiC blanket and composite shielding qualify for hands-on recycling. Personnel access near the HT-9 vacuum vessel would not be allowed, so all maintenance would need to be done remotely. The SiC first wall and Li_2O breeder should easily qualify for remote recycling.

All components from the SiC-He/TOK design would qualify for hands-on recycling within 100 years. This conclusion is different from that reached in the ESECOM study, however, ESECOM assumed that the first wall and blanket were irradiated for 6 years. The present work determined that radiation damage limits a SiC first wall to about 1 full-power-year of irradiation. SiC-He/TOK contact dose rates may allow some hands-on maintenance to be performed. The bulk of maintenance operations, however, would still need to be done remotely.

The SOMBRERO first wall, blanket, and breeder all would have acceptable contact dose rates for hands-on recycling with 100 years (the first wall and blanket can be recycled after only 30 years). The biological shield, which is high-density barium concrete, would have dose rates that would prohibit all hands-on maintenance near the shield or blanket. The xenon atmosphere, included in the design to avoid the use of potentially-activating beamtubes, also would have prohibitively high contact dose rates. The xenon contact dose rate is dominated by the decay of ^{137m}Ba which has a short half-life of only 2.6 minutes. Unfortunately, ^{137m}Ba would be produced continuously by the decay of ^{137}Cs, which has a 30 year half-life.

The contact dose rate from any of the high-Z target materials (pure or impure) would be quite high, especially early times such as one week after irradiation when they would be machined into the next generation of targets. Fortunately, contact dose rates are probably overestimated to the greatest degree for the high-Z materials. Even if a one-week inventory of high-Z material were assembled in one location, it still would not be accurately approximated by a semi-infinite medium. At any given time, far less than 1% of the total volume of high-Z material would be in a single location.

8.2.2 Routine emissions and effluents

While doses from activation products will almost certainly dominate the hazard from severe fusion power plant accidents, tritium will likely dominate hazard due to routine emissions and effluents. Depending upon the specific design of a given power plant, contributions from the more mobile activation products, such as those created in the reactor-building atmosphere, may also be significant. While accidental releases of tritium may contain large quantities of tritium in the water form (due to the high

temperatures that might be expected under accident conditions), routine releases will likely be mostly gaseous [11].

New estimates of routine releases of tritium and activation products have not been made in this work. Instead, previously published estimates have been collected and adjustments have been made in an attempt to present them upon equal footing. Estimates have been obtained from the actual design reports and other work that has summarized relevant designs. Unfortunately, not every design report gives a defensible estimate for routine releases. It is the author's belief that the most complete analysis for the routine release of tritium is presented in the Osiris/SOMBRERO report [12]. Although routine emissions will vary with the materials and other design details, the Osiris/SOMBRERO results should be indicative of tritium releases from other IFE power plants, and thus, those results are presented here.

Past analyses of tritium releases have calculated the 50-year dose commitment that results from exposure to one year of routine emissions of tritium as HT. This approach neglects contributions from ingestion of contaminated food and water, and thus, it does not portray the whole story. The dose that would result from the release

inventories from the Osiris/SOMBRERO analyses have been calculated including contributions from the ingestion of food and water. These calculations have been made possible by the generous assistance of Wolfgang Raskob [13]. Chronic doses and the number of cancer fatalities that would result from the estimated annual release of tritium are presented.

The Osiris/SOMBRERO report gives results for both indirect- (Osiris) and direct-drive (SOMBRERO) power plants. Although the contributions by system differ between the two designs, the total tritium emission rate is nearly the same at about 940 TBq/yr. This gives a chronic dose of 7×10^{-4} Sv at a downwind distance of 1 km. Approximately 8×10^{-3} cancer fatalities within a 100 km radius would result from this annual release.

The STARFIRE design estimated doses resulting from the routine release of not only tritium but also of activated atmosphere within the reactor building and of corrosion products that escape from the system [14]. Activated air and corrosion product estimates do not appear to be available for IFE designs. The STARFIRE results suggest that contributions from activated air are insignificant compared with those from tritium and corrosion products [14]. The STARFIRE

corrosion products contribute approximately 30% to the overall dose estimates [14]. It should be noted that the tritium contribution, estimated in the STARFIRE report, was estimated to be only about 25% of that estimated for the IFE designs. Although the rate of generation and release of corrosion products will be highly design-dependent, it would seem that their routine release is a minor contributor to the overall routine-release hazard.

8.3 Waste-disposal hazards

Each of the waste-disposal indices depends upon the assumed irradiation time of a given component. The composition of materials used in conjunction with calculated neutron fluxes, are given in Appendix A. This report assumes, as did the ESECOM report, that the blanket, manifold, and any solid breeding materials are replaced whenever the first wall is replaced.

Although the results for each of the waste-disposal indices are explained in the following sections, a summary of the main indices, including the component lifetimes, is given in Table 8.3.1. This table gives results for each component in each design. Results are also presented for the high-Z target material candidates.

Table 8.3.1. Waste-disposal indices from activated components.[a]

Component	Component lifetime (y)	Life-cycle waste volume (m^3)	Intruder dose (mSv)	Main Isotope	DDI (m^3)	AIHP ($Sv-m^3/y$)
			Waste-disposal indices			
			Cascade			
C granules	30	3.0E+1	8.4E-3	^{14}C	0.0E+0	8.4E-6
$LiAlO_2$ granules	1	5.1E+3	3.8E+0	^{108m}Ag	0.0E+0	6.5E-1
SiC first wall	15	2.6E+1	3.0E-6	^{14}C	0.0E+0	2.7E-9
SiC/Al tendons	30	7.8E+0	1.1E+0	^{26}Al	0.0E+0	2.7E-4
Al/H_2O shield	30	1.7E+2	8.0E-1	^{26}Al	0.0E+0	4.6E-3
Al-5083 vac. vessel	30	1.1E+2	1.1E+0	^{26}Al	0.0E+0	4.2E-3
			HYLIFE-II			
SS304 first wall	30	6.5E+0	1.6E+1	^{192s}Ir	2.1E+1	3.5E-3
SS304 blanket	30	1.6E+1	2.7E-1	^{108m}Ag	0.0E+0	1.5E-4
SS304 assorted	30	6.0E+0	7.6E+0	^{192s}Ir	9.1E+0	1.5E-3
SS304 vac. vessel	30	2.4E+0	3.7E-1	^{108m}Ag	0.0E+0	2.9E-5
Flibe	30	1.2E+3	1.6E-2	^{14}C	0.0E+0	6.5E-4
			Osiris			
C/C first wall	2.5	9.8E+0	9.1E-3	^{14}C	0.0E+0	3.0E-6
C/C blanket	2.5	2.3E+1	3.0E-3	^{14}C	0.0E+0	2.2E-6
C/C vac. vessel	30	2.2E+2	2.2E-2	^{14}C	0.0E+0	1.7E-4
Flibe	30	4.7E+2	6.7E-2	^{14}C	0.0E+0	1.0E-3
			PCA-Li/TOK			
PCA first wall	3	7.4E+1	6.1E+2	^{99}Tc	9.1E+3	1.5E+0
PCA blanket	3	2.0E+2	2.7E+2	^{99}Tc	1.1E+4	1.8E+0
PCA+ manifold	3	2.7E+3	4.6E+0	^{99}Tc	0.0E+0	4.1E-1
Li coolant	30	3.1E+2	1.4E-2	^{39}Ar	0.0E+0	1.5E-4
FeCrV shield	30	2.3E+2	7.4E-1	^{99}Tc	0.0E+0	5.6E-3
			Prometheus-H			
SiC first wall	2.5	6.7E+1	4.3E-1	^{26}Al	0.0E+0	9.6E-4
Pb first wall coolant	30	1.8E+1	3.1E+2	^{208}Bi	1.1E+3	1.8E-1
SiC blanket	2.5	2.3E+3	9.0E-3	^{26}Al	0.0E+0	6.9E-4
Li_2O blanket	2.5	1.1E+3	4.3E-2	^{14}C	0.0E+0	1.6E-3
HT-9 vac. vessel	30	3.2E+1	1.0E+2	^{99}Tc	6.4E+2	1.1E-1
			SiC-He/TOK			
SiC first wall	1	3.1E+2	8.6E-2	^{26}Al	0.0E+0	8.8E-4
SiC blanket	1	2.6E+3	1.1E-3	^{26}Al	0.0E+0	9.7E-5
Li_2O blanket	1	1.0E+4	1.1E-2	^{14}C	0.0E+0	3.8E-3
C+ manifold	1	5.4E+3	9.0E-5	^{14}C	0.0E+0	1.6E-5
SiC+ shield	30	1.5E+3	1.9E-2	^{108m}Ag	0.0E+0	9.0E-4

Table 8.3.1. (Continued.)

Component	Component lifetime (y)	Life-cycle waste volume (m^3)	Intruder dose (mSv)	Main Isotope	DDI (m^3)	AIHP ($Sv-m^3/y$)
			Waste-disposal indices			
			SOMBRERO			
C/C first wall	5	3.1E+1	8.2E-3	^{14}C	0.0E+0	8.4E-6
C/C blanket	5	2.1E+3	2.8E-4	^{14}C	0.0E+0	1.9E-5
Li_2O blanket	5	2.4E+3	5.3E-3	^{14}C	0.0E+0	4.2E-4
			High-Z Target Materials			
Tantalum	30	6.6E-2	1.5E-1	^{178s}Hf	0.0E+0	3.3E-7
Tungsten	30	6.6E-2	1.3E+0	^{186m}Re	0.0E+0	2.9E-6
Mercury	30	6.6E-2	1.1E+0	^{194}Hg	0.0E+0	2.4E-6
Lead	30	6.6E-2	3.5E+0	^{208}Bi	0.0E+0	7.7E-6
Impure lead	30	6.6E-2	2.3E+3	^{108m}Ag	3.1E+1	5.1E-3

[a] Material lifetimes are set according to estimated radiation damage limit and rate for the given component. Main isotope means largest single contributor to the total intruder dose. Al-5083 denotes the ASTM 5083 aluminum alloy; Flibe denotes a molten salt of two parts LiF and one part BeF_2; C/C denotes carbon-carbon composite; PCA+ means PCA plus FeCrV; Prometheus shield denotes a combination of SiC plus B_4C, Pb, H_2O, and Al; C+ means C plus SiC and BeO; SiC+ means SiC plus B_4C, Al, H_2O, W, and Pb. Impure lead includes 0.01 wt% Cu, 0.05 wt% Ag, 0.15 wt% Sb, and 0.20 wt% Bi.

8.3.1 Life-cycle waste volume

Once the lifetime of a given component is determined from the irradiation damage rate and the maximum number of DPA for a given material, the frequency with which components must be replaced is easily determined. Assuming that each power plant operates for thirty years at full power, the life-cycle waste volume may also be calculated. Figure 8.3.1 gives the life-cycle waste volumes for each of the designs.

Due to a short (1 year) lifetime of its first wall and blanket, the SiC-He/TOK design has, by far, the highest life-cycle waste volume at a total of nearly 20,000 m^3 (670 m^3 per year). Assuming a limit of 20 DPA for SiC, the first wall must be changed annually. If future work shows that the Li_2O breeder need not be replaced when the first wall and blanket are replaced, then the life-cycle waste volume would be reduced by 50%.

The Cascade design has the second highest waste volume. Cascade, however, is dominated by material that is replaced not for irradiation damage but from to burnup of ^6Li. (It is worth noting that an error was found in the Cascade final report. The report claims

Figure 8.3.1. The life-cycle waste volumes are the greatest for the SiC-He/TOK and Cascade designs. The SiC-He/TOK first-wall and blanket are limited to one year lifetimes due to irradiation damage. Cascade's $LiAlO_2$ granules are limited to one year of irradiation due to high burnup of ^6Li.

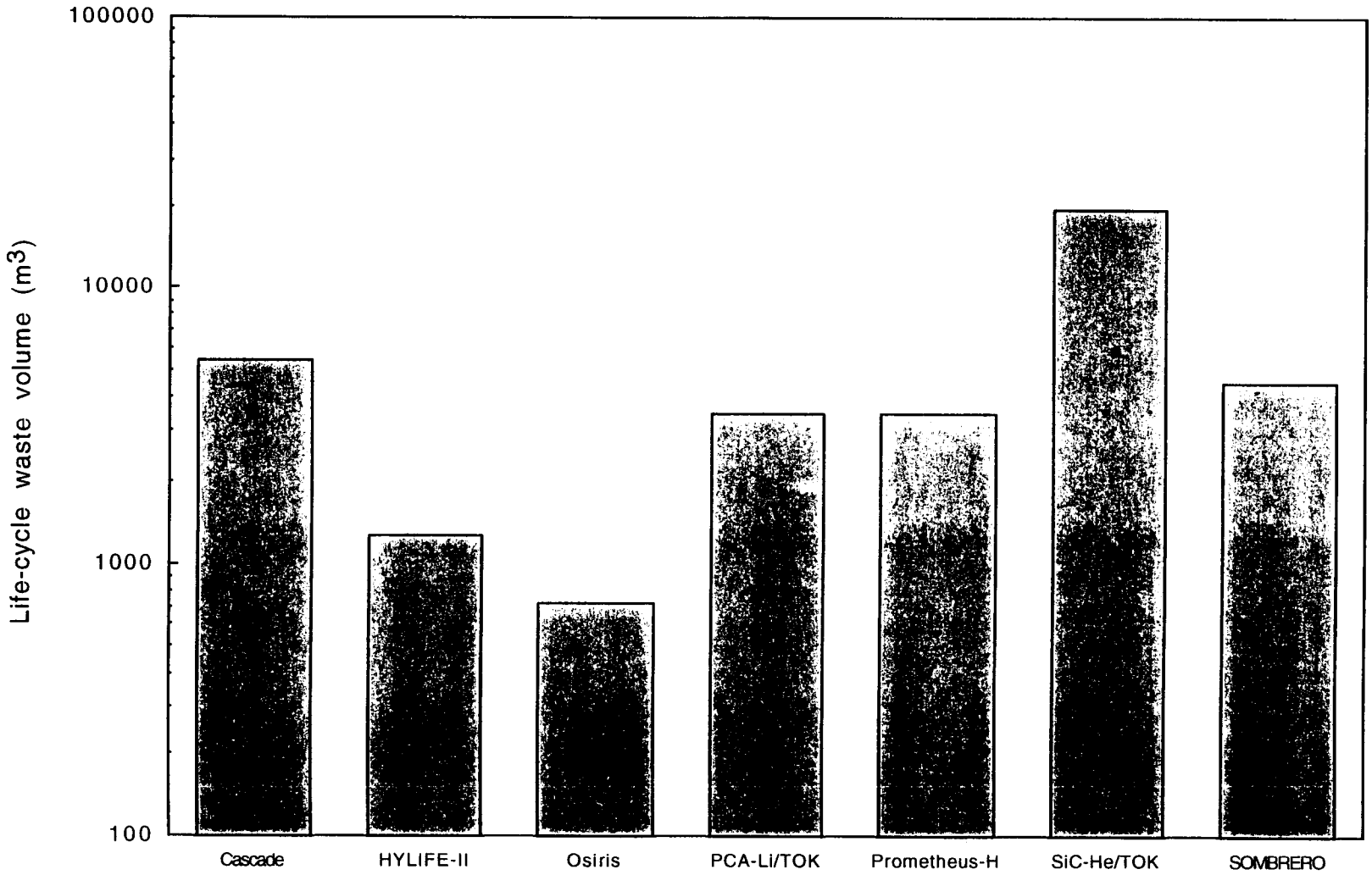

that ^{6}Li is burned up at a rate of 0.3 atom percent per year of operation at full power. The actual burnup rate, which has been calculated and verified with a simple atom balance, is nearly 3% per year). Design changes incorporating the use of more highly enriched lithium (the current design calls for lithium enriched to 15% ^{6}Li) or of a neutron multiplier might be able to reduce this waste volume.

The HYLIFE-II design, through use of a thick-liquid first-wall protection scheme, has a first wall that need not be replaced during the normal plant lifetime. The life-cycle waste volume is dominated by the 1240 m^3 of Flibe coolant. Similarly, although its first wall and blanket must be replaced every 2.5 years, the Osiris waste volume is dominated by 470 m^3 of Flibe. Osiris' carbon-composite vacuum vessel, although meant to last for the entire plant lifetime, contributes another 220 m^3. The total life-cycle waste volume for Osiris is the lowest of all of the designs at about 720 m^3 (24 m^3 per year).

The waste volume for the PCA-Li/TOK is dominated by PCA and FeCrV from the manifold. If removal of the first wall and blanket without the manifold is possible, the life-cycle waste volume could be reduced by 30% or more.

The Prometheus-H and SOMBRERO designs, like the SiC-He/TOK design, would benefit greatly from first-wall/blanket changeout without changeout of solid breeding material. Of the total life-cycle waste volumes of 3500 m^3 for Prometheus-H and 4500 m^3 for SOMBRERO, 31% and 53%, respectively, come from the solid Li_2O breeding material.

The life-cycle waste volume for any of the candidate high-Z target materials would be quite low. Assuming 5 Hz operation, weekly recycling of high-Z target materials, and a 40 μm thickness of high-Z material inside the hohlraum, the total life-cycle waste volume would be about 0.066 m^3 [15]. The total life-cycle waste volume would scale nearly linearly with the high-Z material thickness.

Those designs which use a thick-liquid protection scheme or minimize the volume of structural material in the blanket appear to achieve reduced life-cycle waste volumes.

8.3.2 BHP in water

The total BHP in water as a function of time after irradiation for each design is shown in Figure 8.3.2. Contributions from tritium are

not included in the design totals, but the BHP in water for 1 kg of tritium is shown for reference. As was the case for the BHP in air (section 8.1.2), the various designs differ by about a factor of fifty at early and late times after irradiation. The PCA-Li/TOK design has the highest BHP for about the first 100 years. At later times, the Osiris design becomes the worst offender. Its BHP is again dominated by ^{41}Ca, which is produced in the concrete shielding.

Although the BHP for HYLIFE-II is identical to that for the PCA-Li/TOK design at 100 years after irradiation, its value drops rapidly due to the decay of ^{63}Ni (100 y half-life), and, at 1000 years after irradiation, HYLIFE-II is tied with the SiC-He/TOK design for the lowest total BHP in water.

8.3.3 Intruder dose

The intruder doses are calculated using the specific activity limits proposed by Fetter, Cheng, and Mann [16]. The intruder doses for each component in each design are given in Table 8.3.1. An intruder dose above 5 mSv indicates that the given component would not qualify for shallow land burial as it is currently envisioned.

Figure 8.3.2. The biological hazard potential in water is the volume of water which would be contaminated to maximum acceptable levels if the entire radioactive inventory of each design was released to the environment. Results for each design do not include contributions from tritium, but values for 1 kg of tritium are given for reference.

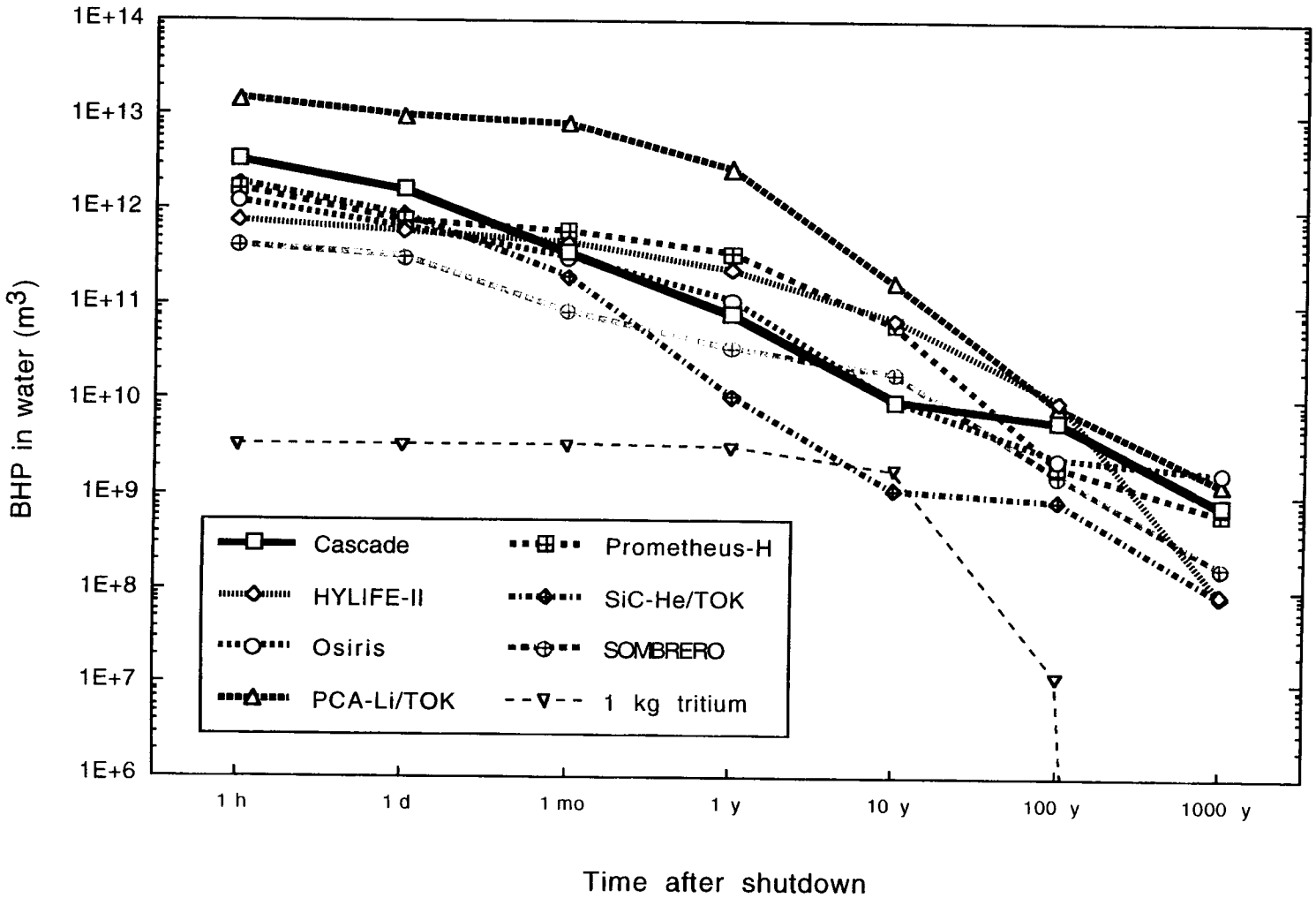

Each of the Cascade components would have an intruder dose below 5 mSv, and thus, all would qualify for shallow land burial. The $LiAlO_2$ granules would have the highest intruder dose at 3.8 mSv. If the granules were more highly enriched in ^6Li, which would allow their lifetime to be greater than one year, then they would fail to qualify for shallow land burial. Despite this, it may be advisable to opt for less volume that is high-level waste than for a large volume (5100 m^3) that is low-level waste. A detailed cost-benefit analysis would be required to decide upon the best option.

In the HYLIFE-II design, the SS304 blanket, vacuum vessel, and Flibe would all qualify for shallow land burial. The SS304 first wall and assorted SS304 components, which include the Flibe deflectors and trays, would fail to qualify. These components fail mainly due to the buildup of ^{192s}Ir which has a 240 year half-life. The lifetime of all components in HYLIFE-II would be thirty years -- the lifetime of the power plant itself. It is possible that, due to mechanical stresses, the deflectors would not survive the full thirty years. If they survive for twenty years or less, they would qualify for shallow land burial.

None of the components in the Osiris design would have any problem qualifying for shallow land burial. The highest intruder dose is from the Flibe coolant. At only 67 μSv, the Flibe is a factor of seventy-five away from the 5 mSv limit.

Even with component lifetimes of only three years, the PCA-Li/TOK first-wall and blanket would fail to qualify for shallow land burial, while the manifold (PCA and FeCrV mixed) would barely qualify. The intruder doses for all three components are dominated by ^{99}Tc, which is produced from the molybdenum constituent in the PCA. The intruder doses for the first wall, blanket, and manifold would be 610, 270, and 4.6 mSv, respectively. The lithium coolant and FeCrV/water shield would easily qualify for shallow land burial.

The SiC first-wall and blanket and the Li_2O breeder would all qualify for shallow land burial in the Prometheus-H design. The lead first-wall coolant, however, would not qualify for shallow land burial even if it only had a one year lifetime. The ^{208}Bi is responsible for nearly the entire intruder dose of 310 mSv. Due to ^{99}Tc, the HT-9 vacuum vessel fails to meet shallow land burial requirements by a factor of twenty.

All components for the SiC-He/TOK and SOMBRERO designs would easily qualify for shallow land burial. The SiC-He/TOK components are dominated by ^{26}Al, ^{14}C, and ^{108m}Ag, and are more than a factor of fifty from the 5 mSv limit. The SOMBRERO components are all dominated by ^{14}C, the worst of which falls a factor of six hundred below the limit.

As mentioned previously, impurities could not be obtained for all of the candidate high-Z target materials. Because a composition for lead was found, the intruder doses for impure as well as pure lead have been calculated. Of the pure target materials, tantalum would perform the best with an intruder dose of only 0.15 mSv. The pure tungsten, mercury, and lead would have intruder doses of 1.3, 1.1, and 3.5 mSv, respectively.

While impurities would make little difference in the accident-hazard indices, they would make a dramatic difference in the waste-disposal indices. The intruder dose for lead would increase from 3.5 mSv without impurities to 2.3 Sv with impurities. The intruder dose for impure lead would be dominated by ^{108m}Ag and ^{208}Bi which are produced from the silver and bismuth impurities, respectively. Because impurities are not available for the other high-Z target

material candidates, the conservative assumption that all of them would fail to meet the 5 mSv intruder dose limit was made. Thus, they would all have to be disposed of as high-level waste. Fortunately, the total volume of high-Z target materials would be only about 0.066 m^3.

8.3.4 Deep disposal index

Components that fail to meet intruder-dose guidelines for shallow land burial probably would require disposal as high-level radioactive waste in some type of deep geologic repository. The deep disposal index (DDI) characterizes the intensity and quantity of such wastes.

Since all components would fall below the 5 mSv intruder dose limit in the Cascade, Osiris, SiC-He/TOK, and SOMBRERO designs, these designs have DDIs of zero, by definition.

HYLIFE-II would have the lowest DDI of the designs that fail to qualify entirely for shallow land burial. The SS304 first wall, deflectors, and Flibe trays have a combined DDI of only 30 m^3. The PCA-Li/TOK design, on the other hand, would have the highest total DDI. The PCA first wall and blanket deep disposal ratings are

9.1×10^3 and 1.1×10^4 m^3, respectively. The lead coolant in the Prometheus-H design has a DDI of 1.1×10^3 m^3 and the DDI of the HT-9 vacuum vessel is 640 m^3.

Although any of the pure high-Z target materials have a DDI of zero, they probably would all require disposal as high-level waste once impurities are considered. The DDI for impure lead is 31 m^3.

8.3.5 Annualized intruder hazard potential

AIHPs for each component in each power plant design and for several candidate high-Z target materials were given in Table 8.3.1. The total AIHPs (including the average AIHP for the candidate target materials), which are simply a sum of the AIHPs for the individual components for each design, are shown in Figure 8.3.3. The total AIHPs vary from 4.5×10^{-4} Sv–m^3/yr for the SOMBRERO design to 3.8 Sv–m^3/yr for the PCA-Li/TOK design. The highest AIHP for an IFE design is about 0.65 Sv–m^3/yr for the $LiAlO_2$ granules in the Cascade design.

The contribution to the total AIHP from any of the pure target materials would be negligible (their AIHPs range from 3.3×10^{-7} Sv–m^3/yr for tantalum to 7.7×10^{-6} Sv–m^3/yr for lead). The AIHP for

Figure 8.3.3. The total AIHP is the highest for the PCA-Li/TOK and Cascade designs due to high-activation materials and large life-cycle waste volumes. The SOMBRERO design has the lowest AIHP due to its use of low-activation carbon composites and Li_2O breeder.

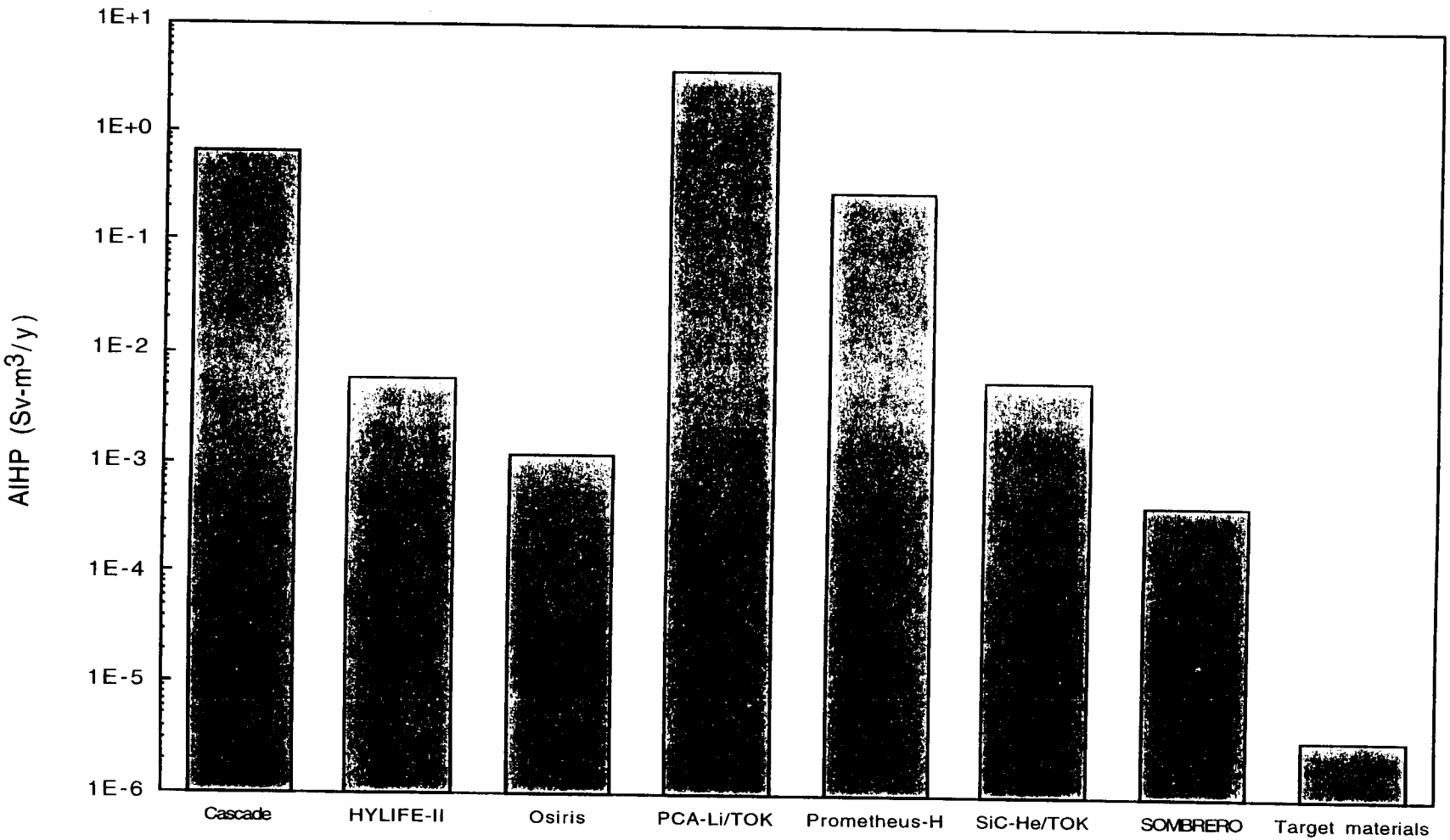

impure lead, however, would be approximately 5.1×10^{-3} Sv–m^3/yr. Thus, impure lead, if used as the high-Z target material, would dominate the total AIHP for Osiris design and double the total AIHP for the HYLIFE-II design.

It is likely that any of the high-Z target material candidates with impurities, would make a significant contribution to the total AIHP for the Osiris or HYLIFE-II designs but not for the Cascade, Prometheus-H, or SOMBRERO designs. Cascade's AIHP, which would be dominated by the large life-cycle waste volume of the $LiAlO_2$ granules, would be two orders of magnitude greater than the contribution from impure lead. Similarly, the total AIHP for Prometheus-H would be dominated by the large intruder dose from its liquid-lead first-wall coolant. SOMBRERO would use direct-drive targets, and thus, would not utilize any of the high-Z materials.

References for Chapter 8

1. J. P. Holdren, D. H. Berwald, R. J. Budnitz, J. G. Crocker, J. G. Delene, R. D. Endicott, M. S. Kazimi, R. A. Krakowski, B. G. Logan, and K. R. Schultz, "Report of the Senior Committee on Environmental, Safety, and Economic Aspects of Magnetic Fusion Energy," Lawrence Livermore National Laboratory, UCRL-53766, (September 1989).

2. A. P. Kinzig, J. P. Holdren, and P. J. Hibbard, "Safety and Environmental Comparisons of Stainless Steel with Alternative Structural Materials for Fusion Reactors," *Fusion Technology*, **26**, 79-104, (August 1994).

3. M. A. Gardner and R. J. Howerton, "ACTL: Evaluated Neutron Activation Cross Section Library -- Evaluation Techniques and Reaction Index," Lawrence Livermore National Laboratory, UCRL-50400, vol. 18, (1978).

4. D. R. Gardner, ed., "The Cascade Inertial Confinement Fusion Reactor Concept," Lawrence Livermore National Laboratory, UCRL-LR-104546, (December 1990).

5. D. L. Smith, G. D. Morgan, M. A. Abdou, C. C. Baker, D. H. Berwald, M. Billone, W. D. Bjorndahl, R. F. Bourque, D. A. Bowers, Y. S. Cha, E. T.

Cheng, R. Clemer, R. L. Creedon, C. F. Dahms, J. W. Davis, G. Deis, J. DeVan, D. Diercks, P. Finn, A. Fischer, J. Foley, K. Furuta, J. K. Garner, Y. Gohar, J. D. Gordon, C. Gung, A. Hassanein, G. Hollenberg, C. Johnson, J. Jung, T. Lechtenberg, J. D. Lee, R. Leonard, Y. Y. Liu, B. Loomis, S. Majumdar, R. C. Maninger, H. C. Mantz, R. F. Mattas, T. J. McCarville, R. Micich, B. Misra, R. W. Moir, W. S. Neef, Jr., B. Picologlou, S. Piet, D. E. Ruester, R. Ryder, K. R. Schultz, A. E. Sherwood, K. Shin, W. G. Steele, D. K. Sze, S.-W. Tam, A. Tobin, P. Tortorelli, L. Turner, D. Vasquez, S. Vogler, E. Vold, L. M. Waganer, K. Wenzel, F. W. Wiffen, C. P. C. Wong, L. Yang, S. Yang, M. Z. Youssef, "Blanket Comparison and Selection Study – Final Report," Argonne National Laboratory, ANL/FPP-84-1, (September 1984).

6. I. Maya, K. R. Schultz, R. F. Bourque, E. T. Cheng, R. L. Creedon, J. H. Norman, R. J. Price, J. Porter, H. L. Schuster, M. T. Simnad, D. L. Sonn, Ing Tang, and R. K. Wise, "Inertial Confinement Fusion Reaction Chamber and Power Conversion System Study," General Atomics Technologies, GA-A17842, (October 1985).

7. R. W. Moir, M. G. Adamson, R. O. Bangter, R. L. Bieri, R. H. Condit, C. W. Hartman, P. A. House, A. B. Langdon, B. G. Logan, C. D. Orth, R. W.

Petzoldt, J. H. Pitts, R. F. Post, R. A. Sacks, M. T. Tobin, W. H. Williams, T. J. Dolan, G. R. Longhurst, M. A. Hoffman, V. E. Schrock, P. F. Peterson, R. Y. Bai, X. M. Chen, J. C. Liu, D.-K. Sze, and W. R. Meier, "HYLIFE-II Progress Report," Lawrence Livermore National Laboratory, UCID-21816, (December 1991).

8. K. A. McCarthy, G. R. Smolik, and S. L. Harms, "A Summary and Assessment of Oxidation Driven Volatility Experiments at the INEL and Their Application to Fusion Reactor Safety Assessments," Idaho National Engineering Laboratory, EGG-FSP-11193, (September 1994).
9. J. Sanz, J. M. Perlado, A. S. Pérez, and D. Guerra, "Low activation structural materials for ICF reactors: differences with MCF environments," *Journal of Nuclear Materials*, **191-194**, 1450-1454, (1992).
10. S. A. Fetter, "Radiological Hazards of Fusion Reactors: Models and Comparisons," Doctoral Dissertation, University of California, Berkeley, Energy and Resources, (May 1985).
11. W. J. Hogan, ed., *Energy from Inertial Fusion*, Vienna, Austria: International Atomic Energy Agency, (1995).

12. W. R. Meier, R. L. Bieri, M. J. Monsler, C. D. Hendricks, P. Laybourne, K. R. Shillito, S. K. Ghose, L. M. Goldman, K. D. Auclair, C. Y. Pang, R. F. Bourque, L. D. Stewart, E. E. Bowles, E. L. Hubbard, C. W. von Rosenberg, Jr., M. W. McGeoch, I. N. Sviatoslavsky, R. R. Peterson, M. E. Sawan, H. Y. Khater, L. J. Wittenberg, G. L. Kulcinski, G. A. Moses, E. A. Mogahed, J. J. MacFarlane, S. Rutledge, S. Humphries, Jr., and E. T. Cheng, "Osiris and SOMBRERO Inertial Confinement Fusion Power Plant Designs," DOE/ER/54100-1, WJSA-92-01, W. J. Schafer Associates, Inc., Livermore, CA, (March 1992).

13. W. Raskob, Kernforschungszentrum Karlsruhe, private communication, (February 1996).

14. Argonne National Laboratory, McDonnell-Douglas Astronautics Co., General Atomics Co., and The Ralph M. Parsons Co., "STARFIRE: A Commercial Tokamak Fusion Power Plant Study," Argonne National Laboratory, Argonne, IL, ANL/FPP-80-1, (1980).

15. D. D.-M. Ho, Lawrence Livermore National Laboratory, private communication, (October 27, 1995).

16. S. A. Fetter, E. T. Cheng, and F. M. Mann, "Long-term radioactive waste from fusion reactors: Part II," *Fusion Engineering and Design*, **13**, 239-246, (November 1990).

9. Synthesis

Results from each of the three classes of hazard should not only be considered individually, but they should be integrated to form an overall view of the environmental and safety characteristics of a particular design. The present work has made no such attempt to quantify such integration, but it is discussed in a qualitative manner in the following sections.

9.1 Summary of hazards by design

Chapter 8 includes a thorough explanation of the results for each of the indices that have been calculated for the power plant designs. These indices include: activities, biological hazard potentials in air and water, critical and chronic threshold-dose release fractions, early doses, chronic doses, early and cancer fatalities, contact dose rates, life-cycle waste volumes, waste-disposal ratings, intruder doses, deep disposal indices, and annualized intruder hazard potentials.

Early doses are reported on the plume centerline at a distance of 1 km from the point of release. Adjustments are made to the early

doses to account for population that resides away from the plume centerline. The number of early fatalities is estimated from the early doses to three key organs: bone marrow, GI tract, and lungs. A two-parameter Weibull function is used for this estimation; see section 2.4.3 for more information.

Chronic doses are reported on the plume centerline at a distance of 10 km from the point of release. Chronic doses include contributions from ingestion of contaminated food and water. Adjustments are made to the chronic doses to account for population that resides away from the plume centerline, and the number of cancer fatalities are estimated. Cancer fatality estimates assume a linear dose-response function with no threshold and a rate of 3×10^{-2} cancer fatalities per person–Sv. This rate is the mean of the predicted range of 10^{-2}/person–Sv to 10^{-1}/person–Sv.

The following sections give a brief summary of results for accident, occupational, and waste-disposal hazards. For a more detailed explanation, the reader is directed to Chapter 8.

9.1.1 Cascade

Due primarily to activation of the $LiAlO_2$ granules and their arsenic impurity, the Cascade power plant design did not fare well compared to the other designs. Since arsenic reacts with oxygen in an exothermic reaction to produce oxides that are gaseous well below Cascade's normal operating temperatures, an argument could not be made for a reduction in the ^{76}As release fraction. As a result, Cascade could produce early doses in excess of the threshold doses for early fatalities associated with injuries to all three organs that have been considered in the present work. The mechanistic-case release fractions would lead to approximately twenty early fatalities.

The chronic dose from Cascade, using mechanistic-case release fractions, is the highest of the seven designs that have been analyzed. This chronic dose, which includes contributions from ingestion of contaminated food and water, would produce approximately 100 cancer fatalities within a 100 km radius of the accident.

The contact dose rates from Cascade components are quite average when compared with components from the other power plant

designs. As might be expected, the contact dose rates from the carbon granules and the SiC first-wall are the lowest. Those of the $LiAlO_2$ granules are dominated by contributions from activation products created from impurities. Finally, the contact dose rates from the vacuum vessel and the concrete shield suggest that some redesign would be required in order for limited access to be a possibility.

In terms of waste-disposal issues, Cascade ranks in the middle of the pack. Although it has the second largest life-cycle waste volume (resulting from the need to replace the entire inventory of $LiAlO_2$ granules on an annual basis), it would qualify entirely for shallow land burial after 30 years of operation. It must be noted, however, that if the lifetime of the $LiAlO_2$ granules were to be extended by 30%, they would not meet suggested intruder dose requirements for shallow land burial. Due primarily to its large waste stream, much of which would be close to the intruder dose limits, Cascade has the second highest AIHP.

9.1.2 HYLIFE-II

Once energy considerations were taken into account, the Flibe release fraction fell substantially, and early doses from HYLIFE-II fell below the thresholds for early fatalities. Apart from the rapid oxidation of the stainless steel structure or an energetic accident, such as an airplane crash, it is unreasonable to expect that a large quantity of Flibe could be mobilized. Although HYLIFE-II would not cause any early fatalities, it could produce as many as forty cancer fatalities in a population of over three million people within 100 km of the accident.

It is likely that the presence of ^{60}Co in activated steel components will preclude all but the most limited access to regions near the first-wall, blanket, and vacuum vessel. In addition, it appears that all Flibe coolant pipes would need to be drained prior to any maintenance. Once corrosion products are considered, this will become even more likely. Detailed γ-ray transport calculations would be required to determine if access within the concrete could be allowed.

Due to its first-wall and blanket being lifetime components, HYLIFE-II would have the second smallest life-cycle waste volume.

In fact, since the Flibe dominates the existing waste stream, it is conceivable that the life-cycle waste volume could be reduced to about 30 m^3 if the Flibe were reused in another such facility. This would give HYLIFE-II the smallest life-cycle waste volume by more than a factor of twenty. Although the first-wall, deflectors, and Flibe trays would not qualify separately for shallow land burial, it is conceivable that the first-wall, deflectors, Flibe trays, blanket, and perhaps, vacuum vessel could be considered to be of the same waste stream. If they were considered the same waste stream, then they could be mixed, and the entire mixture would qualify for shallow land burial. The AIHP from HYLIFE-II is approximately average among the seven designs.

9.1.3 Osiris

Despite a large quantity of stored chemical energy in the carbon composite chamber and blanket, it is unlikely that enough Flibe could be mobilized to cause any early fatalities in the Osiris design. For the mechanistic-case release fractions, Osiris has the lowest early doses of any of the designs. The bone marrow dose is more than a factor of three below the early fatality threshold, while the lung and

GI tract early doses are each a factor of twelve below their respective thresholds for early fatality. The chronic dose from Osiris is the lowest of all designs at just over 0.01 Sv. This chronic dose would cause only a single cancer among the surrounding population of more than three million.

Due to its use of low-activation carbon composites, the Osiris design offers a real opportunity for near-chamber hands-on maintenance. The contact dose rates from the Osiris first-wall, blanket, and vacuum vessel are, in fact, lower than those from the Flibe coolant and the concrete shielding. After one week of cooling, the contact dose rate from Osiris' blanket has fallen to about 25 mSv/hr. Once geometric effects are considered (the semi-infinite medium approximation significantly overestimates the true dose rate), limited access near the blanket may be allowed.

The Osiris life-cycle waste volume is only about 720 m^3 -- the lowest of any of the designs. As was true of HYLIFE-II, the majority of this waste volume would be from Flibe. If the Flibe were recycled in another facility, the life-cycle waste volume would drop to about 250 m^3. Not only would all components qualify for shallow land burial, but they would do so by a large margin -- the first-wall

lifetime could be extended by more than a factor of 500 before the intruder dose limit would be reached. Due to the combination of a low life-cycle waste volume and a low-activation material, Osiris has the second lowest AIHP among the seven designs.

9.1.4 PCA-Li/TOK

The mechanistic-case early doses for the PCA-Li/TOK design are nearly forty times lower than the initial-case early doses. Although they cannot easily be compared to one another due to different release assumptions, the PCA-Li/TOK early doses are lower than those calculated for Prometheus and Cascade. Using the mechanistic-case release fractions, the PCA-Li/TOK design would not cause any early fatalities. With respect to its chronic dose and cancer fatalities, the PCA-Li/TOK design performs better than Cascade and about the same as HYLIFE-II.

Due to extremely high contact dose rates, there is little chance that any PCA-Li/TOK components could be maintained manually. The PCA components, in particular, have contact dose rates greater than 50 Sv/hr, more than 30 years after irradiation ends. The contact dose rate from the PCA first-wall is more than ten orders of

magnitude greater than that from the Osiris first-wall. Once activated corrosion products are taken into account, access to the lithium coolant would no doubt also be prohibited.

The life-cycle waste volume for the PCA-Li/TOK design is average among the seven designs that were considered in the present work. The intensity of the wastes, however, would be much greater for the PCA-Li/TOK design than for the other designs. The PCA first-wall and blanket would exceed the intruder dose limit by more than a factor of 120 and 50, respectively. The manifold, composed of PCA and FeCrV, would have an intruder dose of 4.6 mSv and thus would just qualify for shallow land burial. The total deep disposal index for the PCA-Li/TOK design would be more than 2.0×10^4 m^3, which far exceeds the HYLIFE-II value of 30 m^3. Finally, the PCA-Li/TOK would have the highest total AIHP by about an order of magnitude.

9.1.5 Prometheus-H

Even if the worst-case release fractions were realized, the Prometheus-H design would produce only one to two early fatalities. Using the less conservative (and probably more accurate) initial-case or mechanistic-case release fractions, Prometheus-H would

not produce early fatalities. The chronic dose from Prometheus-H, although it would be nearly twenty times greater than that from Osiris, would still be lower than the doses from the Cascade, HYLIFE-II, and PCA-Li/TOK designs. Using the mechanistic-case release fractions, it has been estimated that Prometheus-H would produce twenty-five cancer fatalities.

Contact dose rates in Prometheus-H would be lower than those in the PCA-Li/TOK design, but they would still rule out much hands-on maintenance. The HT-9 vacuum vessel would be particularly problematic due to its contact dose rate of 640 Sv/hr even one year after irradiation ceases. Although dose rates near the first-wall and blanket would be lower due to use of SiC, the lead first-wall coolant would have a contact dose rate of 23 Sv/hr one week after shutdown. One day after irradiation, the contact dose rate of lead is dominated by activation products generated from the bismuth impurity. Similarly, the contact dose rates from SiC components are dominated by ^{60}Co produced from the iron and cobalt impurities.

The life-cycle waste volume from Prometheus-H would be about 3400 m^3. Most of this volume would be made up of used silicon carbide blankets. Due to a large inventory of ^{208}Bi, generated from

the bismuth impurity, the lead coolant would fail to qualify for shallow land burial by more than a factor of sixty. The HT-9 vacuum vessel would exceed the 5 mSv intruder dose limit by a factor of twenty. The total DDI for Prometheus-H would be about 1.7×10^3 m^3 -- a factor of sixty greater than HYLIFE-II and ten times lower than PCA-Li/TOK. The total AIHP for Prometheus-H would be the second highest among the IFE designs (third highest overall) at about 0.35 $Sv\text{-}m^3/yr$.

9.1.6 SiC-He/TOK

The SiC-He/TOK design would not produce any early fatalities even assuming the worst-case release fractions. The chronic dose would range from about 0.15 Sv for the worst-case release fractions to 0.04 Sv for the mechanistic-case release fractions. The estimated number of cancer fatalities ranges from fifteen to only four for the same range of release fractions.

Contact dose rates in the SiC-He/TOK design would be dominated by ^{24}Na at times of less than one week. For silicon carbide components, the long-term contact dose rates would be dominated by ^{60}Co generated from the iron and cobalt impurities. Despite

contact dose rates at one week in excess of 1 Sv/hr for the first-wall, some limited hands-on maintenance may be possible near the manifold where contact dose rates would be near 10 mSv/hr at the same time.

Even if the lifetime of the silicon carbide first-wall were extended from the calculated lifetime of one year to thirty years (the presumed lifetime of the power plant), it would qualify for shallow land burial by about a factor of two. Similarly, the remainder of the design would easily qualify for shallow land burial. The total life-cycle waste volume, however, is the highest by nearly a factor of four. The large waste volume results from the need to replace the entire first-wall and blanket structure after only one year of irradiation due to silicon carbide's relatively low radiation damage limit. Despite the large volume of waste, the low activity of the waste gives the SiC-He/TOK design a competitive total AIHP -- equal to that of HYLIFE-II -- and only Osiris and SOMBRERO would have lower totals.

9.1.7 SOMBRERO

The SOMBRERO design would be fairly benign with respect to accident consequences. Even assuming the worst-case release fractions, SOMBRERO would produce no early fatalities and only about twenty cancer fatalities. Only the SiC-He/TOK design had more favorable accident consequences for the worst-case release fractions. Due to materials composition and plentiful energy sources, however, the initial-case and mechanistic-case release fractions changed very little from the worst-case. Thus, both the early and chronic doses change little from one case to another. The early bone marrow dose, for example, drops only from 0.75 Sv in the worst case to about 0.70 Sv in the mechanistic-case results. The chronic dose remains at approximately 0.20 Sv for all three sets of radionuclide release fractions. Nonetheless, only SiC-He/TOK and Osiris would produce fewer cancer fatalities. SOMBRERO would cause approximately twenty fatal cancers.

9.2 Integration of the classes of hazard

The previous section compared the results for each design and each class of hazard individually, but to be meaningful, comparisons

must consider all three classes of hazard. The first step in this process is to rank each design within each of the classes of hazard. These rankings by class can then be used to draw qualitative conclusions regarding the overall attractiveness of a design with respect to its ES&H characteristics. Quantitative comparisons have not been attempted as they would require that some form of weighting function be applied to the rankings within each class of hazard -- a process that is inherently subjective.

The difficulties of creating such a weighting function are easily demonstrated. Some might consider accidents to be of the utmost importance and claim that early and cancer fatalities should be avoided at all costs. These people would probably give a high weight to the accident hazards, while giving relatively low weights to the occupational and waste disposal hazards. Others would claim that all three classes of hazards should be treated with equal importance. Still others could believe that the need for remote maintenance or the disposal of activated wastes should be given higher weights. Quantitative integration of the classes of hazard would be subjective and of questionable usefulness.

With regard to accident hazards, three designs seem to offer significant advantages over the others. The SiC-He/TOK and SOMBRERO designs would not produce any early fatalities even were the worst-case release fractions realized. Osiris, although it would produce early fatalities for worst-case and initial-case release fractions, would not produce any fatalities for the mechanistic-case release fractions. Since a large-scale release of Flibe seems highly unlikely, the mechanistic-case release fractions are probably the most representative of reality. The mechanistic-case release fractions would result in only a single cancer fatality from Osiris.

Following the first group of designs are the HYLIFE-II, Prometheus-H, and PCA-Li/TOK designs. Each of these designs would cause early fatalities for the worst-case release fractions, but none would cause any for the mechanistic-case release fractions. The three designs would cause 20-40 cancer fatalities. Although none of these three designs would produce early fatalities, early dose increases of 5-80% would put them beyond the early-fatality dose thresholds.

The Cascade design appears to have the worst accident performance of the seven designs. This poor performance is due

primarily to the production of ^{24}Na and ^{76}As in the $LiAlO_2$ granules and the inability to reduce plausible release fractions. Although Cascade appears to demonstrate the greatest potential to cause early and cancer fatalities, minor design changes and/or modifications in the assumptions made about the potential radionuclide releases from a Cascade-like power plant could significantly alter the early dose results. A factor of five reduction in the early doses would place Cascade near the average of the remaining designs. Thus, despite Cascade's poor performance with respect to accident hazards, its status may be altered with minor design changes.

For occupational hazards, the Osiris design appears to have an advantage over the other designs. Hands-on maintenance, even for the first-wall and blanket, is a possibility for Osiris.

The SiC-He/TOK, HYLIFE-II, and Cascade designs show possibilities of limited hands-on maintenance near the shield. SOMBRERO, in its current form, would require remote maintenance due to high contact dose rates from the shield and Xenon atmosphere. Redesign of the shield and removal of the Xenon atmosphere during

maintenance, however, could permit hands-on access to the first-wall and blanket at dose levels actually below those for Osiris.

Little hope exists for any hands-on maintenance for either the PCA-Li/TOK or Prometheus-H designs. The Prometheus-H lead first-wall and HT-9 vacuum vessel far exceed acceptable dose levels. All components in the PCA-Li/TOK design, with the possible exception of the lithium coolant, would have dose rates orders of magnitude too high for personnel access.

In waste-disposal hazards, as was the case in accident and occupational hazards, the Osiris design has a clear advantage over the other designs. Osiris would have the lowest total waste volume, and all of its waste would qualify easily for disposal via shallow land burial.

SOMBRERO would be the second most attractive design in terms of waste disposal. Its waste also would qualify entirely for shallow land burial, but it would have nearly an order of magnitude more waste than Osiris.

Following SOMBRERO, two designs would present about the same waste disposal hazard: HYLIFE-II and SiC-He/TOK. Although portions of HYLIFE-II would fail to qualify for disposal via shallow land

burial, if the first-wall and blanket were considered to be separate waste streams, it would have a small total life-cycle waste volume. On the opposite end of the spectrum, all components from the SiC-He/TOK design would easily qualify for shallow land burial, but the design would have a huge life-cycle waste volume. Interestingly, the two designs have nearly identical total AIHPs.

Cascade would follow HYLIFE-II and SiC-He/TOK due to its high life-cycle waste volume and relatively high total AIHP. If the $LiAlO_2$ granules are limited to a single year of irradiation (due to rapid ^6Li burnup), then all components would qualify for shallow land burial. An extension of the granule lifetime, however, would necessitate disposal by means other than shallow land burial.

The Prometheus-H and PCA-Li/TOK designs have, by far, the worst waste-disposal characteristics. Although each design is fairly average in terms of its life-cycle waste volume, both designs would require use of deep geologic disposal. Prometheus-H would have less volume by a factor of fifteen, but its intensity would be as high as the waste from PCA-Li/TOK.

Although quantitative integration of the classes of hazard is not attempted in the present work, some qualitative trends seem quite

obvious without the need for weighting of the classes of hazard. The Osiris design has the best overall performance as the best (or tied for best) performer in each of the classes of hazard. The PCA-Li/TOK and Prometheus-H designs appear at or near the bottom of each of the classes, and thus these are the worst overall performers. The remaining designs, Cascade, HYLIFE-II, SiC-He/TOK, and SOMBRERO are in the middle of the pack, and thus their overall performance depends on subjective decisions about the relative importance of the three classes of hazard. The biggest uncertainty is for the Cascade design: depending upon radionuclide release fractions, it could be either at the top or bottom of the middle of the pack.

Among only the IFE designs, Osiris shows the best overall potential performance. Prometheus-H is the worst overall performer. Cascade, HYLIFE-II, and SOMBRERO fall somewhere between Osiris and Prometheus-H.

9.3 Recommended design features

Three advantageous design features have become apparent through the present work. These features, where possible, should be

incorporated into new designs as well as into modified versions of any of the designs that have been analyzed.

The most obvious design feature that has proven to be advantageous is the use of low-activation materials such as composites and ceramics. In all cases, with the exception of ^{76}As from the $LiAlO_2$ granules, composites and ceramics have not contributed significantly to accident doses, occupational dose rates, or the need for deep geologic disposal. Such materials offer the possibility for avoiding the generation of many of the troublesome radionuclides that are generated in other materials. It should be noted, however, that composites and ceramics have made significant contributions to the life-cycle waste volumes of several of the designs. This potential drawback to their widespread use can be mitigated through the development of high-lifetime materials.

The second advantageous design feature is the use of a thick-liquid protection system. The attractiveness of this feature is evident when comparisons are made between the PCA-Li/TOK and HYLIFE-II designs. Although both designs use stainless steels that are fairly similar in composition (HYLIFE-II uses SS304 and PCA-Li/TOK uses PCA, which is a modified version of stainless steel type

316), the hazards associated with the first wall and blanket of each design are quite different.

Although similar assumptions were made for the two designs regarding the temperature and duration of a typical loss-of-coolant accident, such temperatures probably could not be achieved in HYLIFE-II due to the relatively low afterheat of its first wall and blanket. A reduction in the HYLIFE-II release fractions to account for the relatively small amount of afterheat would result in significantly lower early and chronic doses.

Although the HYLIFE-II contact dose rates are high enough to preclude near-chamber access, they are four to six orders of magnitude below those for the PCA-Li/TOK design.

Major advantages that can be achieved through the use of a thick-liquid blanket are readily demonstrated in the waste-disposal indices. Since the HYLIFE-II first wall is shielded from most of the damaging high-energy neutrons, it can easily last for the lifetime of the power plant. The PCA-Li/TOK first wall, however, must be changed-out about every three years due to excessive radiation damage. In terms of the quantity and intensity of waste that fails to qualify for shallow land burial, HYLIFE-II is superior to PCA-Li/TOK

by a factor of 670 or more (HYLIFE-II wastes, if mixed, would qualify entirely for shallow land burial). Finally, the total AIHP for HYLIFE-II is more than three orders of magnitude lower than that for PCA-Li/TOK.

The final design feature that leads to a significant advantage in the integrated hazard is the use of materials that need not be changed-out during the power plant lifetime. These “lifetime components” not only reduce the life-cycle waste volume of a given design, but they also can lead to significant economic savings. A power plant that does not need to be taken down every few years in order to change-out its first wall and/or blanket is likely to have a higher capacity factor. Plants with higher capacity factors will generate higher revenues. Additionally, the use of lifetime components suggests that a given power plant could be designed to make less use of remote maintenance equipment and require less hands-on access to activated equipment. Less remote maintenance equipment and less occupational exposure to radiation translate into cost savings. Although economics has not been considered in the present work, common sense suggests that lifetime components

have the potential to offer significant cost savings and/or increased revenues.

9.4 Directions for future research

The results of the present work suggest directions for future research. Such recommendations are based not only upon directions that could yield the best possible designs (and thus, enable fusion to achieve its full potential with respect to environmental and safety perspectives), but they are also based upon directions which have demonstrated the possibility of offering a large return for a given investment. That is, the issues with the highest leverage should be of the most interest to the fusion community.

The accident doses and the resulting early and cancer fatalities that were calculated for the three sets of radionuclide release fractions highlight the tremendously important task of obtaining accurate release fractions. Over the last decade, a series of experiments, performed at INEL, have measured oxidation-driven mobilization of materials as a function of temperature. These experiments have been performed for only a very limited set of materials (all of interest for the ITER) under a limited set of

conditions. Materials of potentially great importance to fusion power plants such as silicon carbide, carbon composites, lead, Flibe, concrete, sodium, and lithium have not been included in the experiments. A better understanding of release fractions requires that experiments such as those conducted at INEL be expanded to include many more materials. Such experiments would enable future comparative analyses like the present work to calculate release fractions using time-dependent temperature models.

Not only must the experiments be expanded to include additional materials, they also must include the mobilization of activation products. For example, if silicon carbide were to be tested, it should include some quantity of sodium to simulate the ^{22}Na and ^{24}Na that would be present in a component that has been activated. One possibility for conducting such simulations could be to simply use samples that have been exposed to 14 MeV neutrons. Potential problems with such a scheme are the generation of 14 MeV neutrons and the requirement to handle activated materials which would contaminate the experimental equipment.

Another possible method for simulating the mobilization of activated materials would be to use samples that have been doped

with trace quantities of stable isotopes. The addition of stable ^{23}Na to a silicon carbide sample, for example, could reveal valuable information regarding the mobilization of ^{22}Na and ^{24}Na.

Another high-leverage area of research is in the development and characterization of materials. Experiments with neutron irradiation of key fusion materials to fluences and DPA relevant to power plants will provide essential data. Structural materials must be irradiated and tested for changes in their strength, brittleness, and swelling. Accurate ES&H analyses require knowledge of the lifetime of each component that will be exposed to radiation. Not only are material lifetimes a function of integrated fluence and DPA, but they may depend upon dose rates effects as well. Irradiation of materials will also aid in the determination of impurity concentrations and can potentially lead to the development of high-lifetime low-activation materials. Finally, such experiments would supply information that could be used to validate data libraries such as those used for neutron transport and activation calculations.

The experimental verification of sequential charged-particle reactions would be quite beneficial to the fusion community. Such experiments could validate the PCROSS code and its data libraries

and also might aid in the determination of conditions under which sequential charged-particle reactions should be considered. Currently, without a method for determining the potential importance of (x,n) reactions in any given calculation, they must be included in all calculations. Related experiments have been planned for the Rotating Tritium Neutron Source (RTNS) at the University of California at Berkeley.

9.5 Improvements to the calculational methodology

The calculational methodology and the system of computer codes, RADSAFE, that have been used in the present work represent a significant advancement over previous work in the field. They do not, however, represent a complete set of methods and tools for the accurate assessment of radiological hazards -- a number of key improvements can and should be made.

The largest single improvement to the methodology can be made in the area of radionuclide release fractions. Although accurate release fractions will require much more experimental data than are currently available, significant advances could be made in this area through the use of two- and three-dimensional transient heat-

transfer calculations (even one-dimensional calculations would be of some use). Rather than making many assumptions about the chemical composition of a given material and about its mobility, a transient heat-transfer calculation, in conjunction with experimental mobilization data, could be used to estimate release fractions more accurately and thus to obtain a more accurate estimate of accident consequences. Even without additional mobilization data, transient heat-transfer calculations could improve the accuracy of estimated release fractions.

Once transient heat-transfer capabilities have been added to the methodology, some type of transient chemical-reaction kinetics package could be added as well. Such a package could provide time-dependent inventories of chemical compounds (such as potentially volatile oxides). This information could be used to further refine the estimated release fractions and could be used to distinguish between several sets of doses -- one for each chemical compound that a given radionuclide is likely to be found in during and after an accident.

Future work should strongly consider expansion of the dose library that was created with the MACCS2 code. Although the IDCF2

module used by MACCS2 includes nearly 400 radionuclides, only about 250 radionuclides were available in all of the libraries used by the code. Thus, early and chronic doses have been calculated for only about 250 radionuclides. Potentially important radionuclides such as ^{210}Po are not included in this subset of 250 radionuclides (doses for ^{210}Po and seven other radionuclides that were deemed to be of potential importance were scaled from previously published results). Expansion of the dose library would decrease the risk that a key radionuclide has been overlooked.

Finally, future work must consider economics. Ultimately, it is likely that trade-offs among designs and among hazard classes will be decided by economics. For example, a minor increase in accident consequences or waste-disposal burden might be deemed acceptable if the trade-off is a significant reduction in the cost of electricity. Cost-benefit analyses will almost certainly be used to ascertain which components and subcomponents should be replaced with more expensive but less hazardous materials (similar to ALARA practices used today). Costs must also be considered in areas such as waste disposal. One would not necessarily strive to make all components

disposable via shallow land burial if the cost savings per unit volume does not justify the cost of design changes.

Appendix A. Materials

All activation calculations that have been performed in the present work have had to specify materials compositions. The following tables, listed here in alphabetical order, give both the compositions that have been used as well as the source of these compositions. Each table lists the material, the reference from which the composition was taken, the density, and the material composition by weight percent.

Material: Ba-doped concrete

Source: Osiris/SOMBRERO Report [1]

Density: 3.8 g/cm^3

Element	Weight %	Element	Weight %
H	0.56	B	1.04
O	33.8	F	0.23
Na	1.21	Mg	0.23
Al	0.64	Si	3.31
S	9.15	K	0.0100
Ca	6.26	Mn	0.0200
Fe	2.19	Ni	1.32
Cu	0.22	Zn	0.66
Ba	40.13	Nb	0.0200
Mo	0.0800		

Material: Carbon/carbon composite

Source: Osiris/SOMBRERO Report [1]

Density: 1.7 g/cm^3

Element	Weight %	Element	Weight %
B	0.0002	C	99.999
Na	0.0010	Mg	0.0001
Al	0.0004	Si	0.0021
S	0.0001	Ca	0.0022
Ti	0.0001	V	0.0001
Fe	0.0003	Pb	0.0007

Material: Common lead

Source: HYLIFE-II Progress Report [2]

Density: 11.4 g/cm^3

Element	Weight %	Element	Weight %
Cu	0.01	Ag	0.05
Sb	0.15	Pb	99.59
Bi	0.20		

Material: Concrete

Source: Profio [3]

Density: 2.3 g/cm^3

Element	Weight %	Element	Weight %
H	1.0	C	0.1
O	52.7	Na	1.6
Mg	0.2	Al	3.4
Si	33.6	K	1.3
Ca	4.4	Sc	0.1
Ti	0.1	Fe	1.4
Ni	0.1		

Material: FeCrV

Source: ESECOM Report [4]

Density: 8.0 g/cm^3

Element	Weight %	Element	Weight %
C	0.11	N	0.015
Al	0.043	Si	0.3
P	0.007	S	0.015
Ti	0.003	V	1.5
Cr	2.4	Mn	0.3
Fe	95.13	Ni	0.05
Cu	0.04	Mo	0.02

Material: Flibe w/ 10 wppm tantalum impurity

Source: Toma [5]

Density: 2.0 g/cm^3

Element	Weight %	Element	Weight %
Li	14.1	Be	9.1
C	0.001	N	0.001
F	76.8	Na	0.0042
S	0.0005	Cr	0.0019
Fe	0.0166	Ni	0.0026
Ta	0.0010		

Material: $LiAlO_2$

Source: BCSS Final Report [6]

Density: 2.5 g/cm^3

Element	Weight %	Element	Weight %
Li	10.4842	Be	0.0010
B	0.0010	O	48.3423
Na	0.0050	Al	40.7585
P	0.0500	Cl	0.0100
K	0.0500	Ca	0.0030
Ti	0.0030	V	0.0030
Cr	0.0030	Mn	0.0010
Fe	0.0030	Co	0.0030
Ni	0.0020	Cu	0.0010
Zn	0.0500	As	0.0500
Sr	0.1000	Zr	0.0100
Mo	0.0030	Ag	0.0010
Cd	0.0100	Sn	0.0300
Sb	0.0100	Ba	0.0100
Pb	0.0010	Bi	0.0010

Material: LiO_2

Source: Osiris/SOMBRERO Report [1]

Density: 2.0 g/cm^3

Element	Weight %	Element	Weight %
^{6}Li	39.61991	^{7}Li	4.86447
Be	0.0001	B	0.0001
C	0.0100	N	0.0002
O	55.4649	F	0.0000001
Na	0.0060	Mg	0.0010
Al	0.0050	Si	0.0050
S	0.0000001	Cl	0.0010
K	0.0020	Ca	0.0100
Ti	0.0010	V	0.0001
Cr	0.0001	Mn	0.0001
Fe	0.0050	Co	0.0000002
Ni	0.0010	Cu	0.0010
Zn	0.0010	As	0.0000001
Br	0.0000001	Zr	0.0001
Mo	0.0000001	Cd	0.0000001
Sn	0.0001	Sb	0.0001
Ba	0.0005	Pb	0.0000001

Material: LiO_2

Source: ESECOM Report [4]

Density: 2.0 g/cm^3

Element	Weight %	Element	Weight %
Li	46.58	O	53.33
Na	0.005	Al	0.002
Si	0.001	Cl	0.01
K	0.037	Ca	0.021
Mn	0.002	Ni	0.002
Cu	0.0006	Pb	0.008

Material: Mild steel

Source: Osiris/SOMBRERO Report [1]

Density: 8.0 g/cm^3

Element	Weight %	Element	Weight %
C	0.0200	N	0.0070
Si	0.31	P	0.0160
S	0.0400	K	0.0004
Mn	0.52	Fe	98.747
Ni	0.0060	Cu	0.16
Ba	0.0002	Nb	0.0001
Mo	0.0003		

Material: PCA

Source: ESECOM Report [4]

Density: 8.0 g/cm^3

Element	Weight %	Element	Weight %
B	0.005	C	0.005
N	0.01	Al	0.03
Si	0.5	P	0.01
S	0.005	K	0.0003
Ti	0.3	V	0.1
Cr	14.	Mn	2.
Fe	64.88	Co	0.03
Ni	16.	Cu	0.02
As	0.02	Zr	0.005
Nb	0.03	Mo	2.
Ag	0.0001	Cd	0.0002
Sn	0.005	Sb	0.001
Ba	0.001	Tb	0.001
Ta	0.01	W	0.05
Ir	0.001	Pb	0.001
Bi	0.001		

Material: SiC

Source: ESECOM Report [4]

Density: 3.2 g/cm^3

Element	Weight %	Element	Weight %
C	29.95	Si	70.05
Fe	0.0011	Co	0.00003

Material: SS304

Source: J. D. Lee [7]

Density: 8.0 g/cm^3

Element	Weight %	Element	Weight %
B	0.005	C	0.2
N	0.06	Al	0.03
Si	0.4	P	0.04
S	0.016	V	0.005
Cr	19.	Fe	70.
Co	0.016	Ni	10.
Cu	0.03	Zn	0.003
As	0.02	Se	0.005
Zr	0.005	Ag	0.0001
Cd	0.0002	Sn	0.005
Sb	0.001	Ta	0.005
W	0.01	Pb	0.001
Bi	0.001		

References for Appendix A

1. W. R. Meier, R. L. Bieri, M. J. Monsler, C. D. Hendricks, P. Laybourne, K. R. Shillito, S. K. Ghose, L. M. Goldman, K. D. Auclair, C. Y. Pang, R. F. Bourque, L. D. Stewart, E. E. Bowles, E. L. Hubbard, C. W. von Rosenberg, Jr., M. W. McGeoch, I. N. Sviatoslavsky, R. R. Peterson, M. E. Sawan, H. Y. Khater, L. J. Wittenberg, G. L. Kulcinski, G. A. Moses, E. A. Mogahed, J. J. MacFarlane, S. Rutledge, S. Humphries, Jr., and E. T. Cheng, "Osiris and SOMBRERO Inertial Confinement Fusion Power Plant Designs," DOE/ER/54100-1, WJSA-92-01, W. J. Schafer Associates, Inc., Livermore, CA, (March 1992).
2. R. W. Moir, M. G. Adamson, R. O. Bangter, R. L. Bieri, R. H. Condit, C. W. Hartman, P. A. House, A. B. Langdon, B. G. Logan, C. D. Orth, R. W. Petzoldt, J. H. Pitts, R. F. Post, R. A. Sacks, M. T. Tobin, W. H. Williams, T. J. Dolan, G. R. Longhurst, M. A. Hoffman, V. E. Schrock, P. F. Peterson, R. Y. Bai, X. M. Chen, J. C. Liu, D.-K. Sze, and W. R. Meier, "HYLIFE-II Progress Report," Lawrence Livermore National Laboratory, UCID-21816, (December 1991).
3. E. A. Profio, *Radiation Shielding and Dosimetry*, New York: Wiley-Interscience, (1979).

4. J. P. Holdren, D. H. Berwald, R. J. Budnitz, J. G. Crocker, J. G. Delene, R. D. Endicott, M. S. Kazimi, R. A. Krakowski, B. G. Logan, and K. R. Schultz, “Report of the Senior Committee on Environmental, Safety, and Economic Aspects of Magnetic Fusion Energy,” Lawrence Livermore National Laboratory, UCRL-53766, (September 1989).
5. R. Toma, retired -- Oak Ridge National Laboratory, private communication to Ralph Moir, (April 5, 1995).
6. D. L. Smith, G. D. Morgan, M. A. Abdou, C. C. Baker, D. H. Berwald, M. Billone, W. D. Bjorndahl, R. F. Bourque, D. A. Bowers, Y. S. Cha, E. T. Cheng, R. Clemer, R. L. Creedon, C. F. Dahms, J. W. Davis, G. Deis, J. DeVan, D. Diercks, P. Finn, A. Fischer, J. Foley, K. Furuta, J. K. Garner, Y. Gohar, J. D. Gordon, C. Gung, A. Hassanein, G. Hollenberg, C. Johnson, J. Jung, T. Lechtenberg, J. D. Lee, R. Leonard, Y. Y. Liu, B. Loomis, S. Majumdar, R. C. Maninger, H. C. Mantz, R. F. Mattas, T. J. McCarville, R. Micich, B. Misra, R. W. Moir, W. S. Neef, Jr., B. Picologlou, S. Piet, D. E. Ruester, R. Ryder, K. R. Schultz, A. E. Sherwood, K. Shin, W. G. Steele, D. K. Sze, S.-W. Tam, A. Tobin, P. Tortorelli, L. Turner, D. Vasquez, S. Vogler, E. Vold, L. M. Waganer, K. Wenzel, F. W. Wiffen, C. P. C. Wong, L. Yang, S. Yang, M. Z.

Youssef, “Blanket Comparison and Selection Study – Final Report,” Argonne National Laboratory, ANL/FPP-84-1, (September 1984).

7. J. D. Lee, “Waste Disposal Assessment of HYLIFE-II Structure,” *Fusion Technology*, **26**, 74-78, (August 1994).

Technical Information Department • **Lawrence Livermore National Laboratory**
University of California • Livermore, California 94551